BOND CHARACTERISTICS OF HIGH STRENGTH CONCRETE

MEHDI ALAVI-FARD

Bond Characteristics of High Strength Concrete

by

©Mehdi Alavi-Fard, B.Sc., M.Sc., Ph.D.

A thesis submitted to the School of Graduate
Studies in partial fulfillment of the
Requirements for the degree of
Doctor of Philosophy

Faculty of Engineering and Applied Science
Memorial University of Newfoundland
St.John's, Nfld., Canada

January 1999

St.John's Newfoundland Canada

IN MEMORY OF MY FATHER
THE LOVE OF MY MOTHER
AND
THE SACRIFICES OF MY VERY DEAR SON,
KASRA

Those Who Love Never Go Away
They Walk Beside us,
Every Moment

Abstract

High strength concrete is used mostly in the construction of bridges, high rise buildings and marine structures. Bond strength between high strength concrete and rebar is an important factor in designing any reinforced concrete structures under various kinds of loadings. Therefore, this study is conducted to investigate the strength of bond between high strength concrete and reinforcement, to determine the internal distribution of stresses and strains along the rebar interface with high strength concrete.

In the experimental phase of this research a total of 150 specimens made of high strength concrete were cast to investigate the bond strength under monotonic and cyclic loading. The influences of load history, confining reinforcement, rebar diameter, concrete strength, rebar spacing, rate of pull out, and deformation pattern were investigated experimentally for reinforcement bars of 25 mm and 35 mm diameter. The internal concrete strains close to the contact surface and also the steel rebar strains were measured. The test set up, load application, instrumentation and measurement, test procedure, and type of materials were designed to measure accurate strains and deformations. Several specimens with different rebar diameters and rib geometries were tested. The range of the tested concrete compressive strengths was between 75 MPa and 95 MPa. The rib geometries were examined for rebar with nominal diameter of 25 mm and 35 mm.

The test results revealed that the maximum bond stress of high strength concrete is higher than the corresponding one for normal strength concrete. However, the behavior of high strength concrete is more noniinear-brittle and it must be considered in the bond model. The development of a new technique of strain measurement around the steel rebar was unique and it can be useful to identify the internal crack pattern and to predict possible failure modes. The area under the curve of the bond stress-slip curve can define the bond energy. The bond energy should be used to evaluate the bond behavior rather than the maximum bond stress. A new expression for calculating bond stress based on the cubic root of concrete strength is recommended and the results are compared with similar equations. Also, the influences of several parameters under cyclic loading condition are investigated.

In the numerical investigation, an attempt has been made to consider the effect of tension stiffening in the material model. The concepts of bond energy, fracture energy, tension softening and biaxial failure envelope of high strength concrete were applied in the development of a material model for high strength reinforced concrete. The improved model is implemented in the UMAT subroutine for use with the ABAQUS finite element program. In addition, three dimensional rebar element was added to the program in order that the new model will be able to analyze reinforced high strength concrete structures. The model has been checked against several standard problems. Further, A new parametric study based on the effect of bond energy on the fracture energy was introduced. Based on sensitivity analysis, the results were applied to analysis of slabs with low, moderate and high steel ratio. The modified model can be used to analyze reinforced high strength concrete members.

ACKNOWLEDGMENTS

The author wishes to thank Dr. Hesham Marzouk, Professor of Civil Engineering, for his generous support and guidance throughout the course of this investigation. I am also grateful for his supervision, support, and patience during my tenure, which helped me to complete this research investigation in time. In addition, my special thanks are directed to Prof. A.S.J. Swamidas for his useful and helpful comments and friendly encouragement as well as serving the examination committee. Also, I would like to thank you Prof. S. Adluri and Dr. G. Hoff for their time to read my dissertation, to make comments and for serving in the examination committee. I would also like to express my deep gratitude to the supervisory committee members, Professors M. Booton and K. Munaswamy.

Furthermore, many thanks are due to the office staff and technical staff of Faculty of Engineering and Applied Science who made their expertise available during the testing program and for the related technical support, especially Messrs. A. Bursey, C. Ward, D. Humphrey and R. O'Driscoll. I also thank the manager and staff of Center for Computer Aided Engineering for their support during the computational portion of this research.

The author is grateful to Dr. G. George, who provided comments on the English text. Furthermore, I would like to acknowledge the financial support provided by my supervisor, the school of graduate studies, and Faculty of Engineering and Applied Science for pursuing this research investigation.

In addition, I would like to extend my deep appreciation to Pastors W. Shannon Potter, Jeff Payne and P. Dean Brenton of Bethesda Pentecostal Church. I had a wonderful time under their ministry on Sundays. Also, I am so greatly appreciative of the friendship and social times I had with other wonderful Christian friends at Bethesda. They valued my friendship and in turn was helped by their faith in the goodness, power and glory of God.

I am also deeply indebted to Mr. Petten Newman, Mr. Keith Ireland and Mrs. Rose Ireland for their helpful suggestions, tremendous assistance and friendship.

I would like to take this opportunity to express my profound gratitude to all my family members for their kind support, continued encouragement and affection.

Although my very dear son, ***Kasra***, has lived far away from me since 1995, he has been in my thoughts constantly. He has been a source of great comfort and encouragement to me during the period of this research investigation and helped me to achieve my goals and dreams. I wish him a bright and prosperous future under the love, wisdom, peace and power of God so that in his own unique way he will contribute greatly to society.

Table of Contents

List of Tables

List of Figures

Nomenclature

Abbreviations

A_b : Area of contact zone (bond area)

A_s : Rebar Area, in^2

A_{tr} : Area of each stirrup or tie crossing the potential plane of splitting adjacent to the reinforcement being developed or spliced, in^2

A_{tw} : The smaller of the area of transverse reinforcement within a spacing "s" crossing the plane of splitting normal to the concrete surface

b : Intercepts of the best-fit lines relating $T_r/f_c'^{1/4}$ to Na_{tr}/n in Figs.5 and 6 or beam width, in.

c : $c_m + 0.5\ d_b$

C : Cover

c_b : Bottom cover of reinforcing bars, in.

c_M : Maximum value of c_s or c_b ($c_M/c_m <= 3.5$), in.

c_m : Minimum value of c_s or c_b ($c_M/c_m <= 3.5$), in.

c_{si} : Min. (c_{si}+0.25 in., c_{so}) or min (c_{si},c_{so}), in.

c_{so} : Side cover of reinforcing bars, in.

d : Beam effective depth, in.

d_b : Nominal bar diameter, in.

d_s : Stirrup diameter, in.

f_c' : Concrete compressive strength, in psi; $f_c'^{1/4}$ in psi

f_s : Steel stress at failure, psi

f_y : Yield strength of bars being spliced or developed, psi

f_{ytk} : Yield strength of transverse reinforcement, ksi

f_{yt} : Yield strength of transverse reinforcement, MPa

h : Beam depth, in.

H : Fourth order material tensor

I_1 : First invariant of stress tensor

J_2 : Second invariant of stress deviator tensor

J_3 : Third invariant of stress deviator tensor

K_{tr} : K_{tr}(conv.) = $34.5(0.72\ d_b+0.28)A_{tr}/sn$ for conventional reinforcement (average R_r=0.0727)
K_{tr} (new) = $53\ (0.72\ d_b+0.28)A_{tr}/sn$ for new reinforcement (average R_r=0.1275)

K_1 : Accounts the effect of the position of the rebar

K_2 : This factor varies with concrete cover, rebar diameter and clear distance between rebars

K_3 : This factor accounts the effect of transverse reinforcement
K_4 : This factor takes into account the effect of transverse compressive pressure
k_1 : Factor for the position of the rebar
k_2 : Factor for influence of concrete cover, rebar diameter and rebar space
k_3 : Factor for the effect of transverse reinforcement
k_4 : Factor for the effect of transverse compression pressure
k_5 : Factor for concrete cover
k_6 : Factor for position of the rebar
k_7 : Bar location factor
k_8 : Coating factor
k_9 : Concrete density factor
k_{10} : Rebar size factor
L : Bond length
l : Beam length, ft
l_c : Length of constant moment region, ft
l_d : Development of splice length, in.
l_s : Splice length, in.
M : Slope of the modified relationship
$M_{R_r=0.075}$: Value of M at R_r= 0.075
M_u : Moment at splice failure, kip-in.
m_s : Slopes of the best-fit lines relating $T_s/f_c'^{1/4}$ to Na_{tr}/n
m : Effect of study parameter
m_a : Friction parameter
m_1 : Modification factor for "Load History"
m_2 : Modification factor for "Confinement"
m_3 : Modification factor for "Bar Diameter"
m_4 : Modification factor for "Bar Spacing"
m_5 : Modification factor for "Rate of Pull-Out"
m_6 : Modification factor for "Deformation Pattern"
N : Number of transverse reinforcing bars (stirrups or ties) crossing l_d
n : Number of bars being developed or spliced along the plane of splitting
P :Total applied load at splice failure, kips
R_r : Ratio of projected rib area normal to rebar axis to the product of the nominal bar perimeter and the center-to-center rib spacing
s : Spacing of transverse reinforcement, in.
T_b : Total force in a rebar at splice failure, lb
T_c : Concrete contribution to total force in a bar at splice failure, lb
T_s : Confining steel contribution to total force in a bar at splice failure, lb
t_d : Term representing the effect of rebar size on T_s
t_r : Term representing the effect of relative rib area on T_s

α : Reinforcement location factor

β : Coating factor

ρ : The transverse compressive pressure in MPa, deviatoric stress (page 44)

γ : Reinforcement size factor

λ : Lightweight concrete factor

κ : Hardening parameter

σ : The mean normal stress

σ_t : The trial stress state

σ_n : Stress state

ε : Strain

$\dot{\varepsilon}_p$: Equivalent plastic strain rate

ϑ : Polar angle

Chapter 1

Introduction

1.1 High Strength Concrete and Bond

Engineers and material technologists were involved in perfecting concrete properties during the last 80 years. During the 30's Professor Hollister, the Past President of the American Concrete Institute (ACI), spoke of the future predicting a high strength concrete (HSC) with a compressive strength up to 70 MPa. In the fifties, 35 MPa concrete was used in construction and, by the end of the eighties, compressive strength reached 135 MPa.

The concept of high performance concrete as a technology emerged only about 15 years ago. The potential economic advantages of high performance concrete with high strength and improved durability for bridges, tall buildings and marine structures are very promising. In recent years, the use of high strength concrete in the construction of bridges, tall buildings, and marine structures has been receiving increasing attention.

Durability, economical construction and maintenance of high strength reinforced concrete structural members are of major worldwide concern now. High strength concrete is specified where reduced weight is important or where architectural considerations require smaller dimension of the member.

High strength concrete is being used in bridge decks for improved durability and longer life. It is being used to increase the span length of bridge girders to reduce the number of girders required in a given bridge or allow for the use of shallower sections and lighter superstructures. The use of high strength concrete promises to produce cost effective long range replacements for bridge components, and to reduce loss of prestress force because of lower creep deformation, while its high modulus of elasticity reduces the deflection of long span bridge members.

High strength concrete was used to built the 13 Km long Confederation Bridge in Canada, the world's longest high strength prestressed concrete box girder bridge, with 45 main spans of 250 m each that was designed for 100 years of service life. This bridge has been designed to withstand a harsh marine environment, destructive ice and high wind conditions. The massive high strength concrete components of this bridge were larger than those have been used on any other bridge in the world. All substructure and superstructure components for the main spans were precast and floated out and erected using a large floating crane. The majority of the concrete used for the superstructure has a compressive strength of 55 MPa and for some piers, the ice shields utilize concrete with a compressive strength of 80 MPa to resist abrasion damage. The concrete box girders were built in the controlled conditions of the precasting yards. Subsequently, the main girder

section measuring as long as 190 meters and weighing 8200 tonnes were erected on site. The construction phase started from October 1993 and the bridge was completed by May 1997. The Confederation Bridge represents one of the largest uses of high performance (high strength) concrete in a prestressed concrete bridge in North America.

High strength concrete is being used in columns of high rise buildings. As taller structures were being designed, the need for higher strengths and concrete columns were developed. High strength concrete helps achieve more efficient floor plans through smaller vertical members and has also often proven to be the most economical alternative to normal strength concrete, by reducing both the total volume of concrete and the amount of steel required for a load-bearing member. Also, formwork accounts for a large portion of the cost of constructing a column; smaller column sizes reduce the amount of formwork needed and result in cost savings. There has been a race regarding the record height of concrete structures. The highest concrete buildings that have been constructed recently utilizing high strength concrete include the Bay-Adelaide building in Toronto. The Kuala Lumpur City Center in Malaysia built in 1995 is considered to be the tallest concrete building in the world.

Marine and offshore structures are generally exposed to a harsh open ocean environment, where the use of high performance (high strength) concrete is very beneficial. Offshore concrete platforms for the recovery and processing of crude oil present some unique challenges in structural use of high strength concrete. These structures are designed to remain permanently or semi-permanently fixed to the seabed, or to remain afloat.

Hibernia is the first concrete gravity base structure (GBS) to be built in North America (1990-1997) made of high strength concrete under very harsh Atlantic weather conditions, and the first of such large-scale structures in the world that has been designed to resist the impact of icebergs. Located in the Grand Banks off Newfoundland in the North Atlantic Ocean, the structure sits in a water depth of 80 meters. It is designed to support topsides weighing 33,000 tonnes, and to store crude oil before it is off loaded to shuttle tankers. Troll, the tallest offshore concrete platform, was built in the North Sea and also constructed with high strength concrete.

In spite of the wide use of high strength concrete, more information is required on the material characteristics and the structural behavior of this relatively new material. The bond between reinforcement and concrete is one of the major properties that make high strength reinforced concrete an efficient material.

1-2 Scope of Research

This investigation was conducted to examine the strength of the bond between reinforcement and high strength concrete. The main objectives of this research are summarized as follows:

1. Determine the characteristics of the bond under different parameters.
2. Design a test set-up to examine the bond behavior.
3. Evaluate the influences of monotonic and reversed cyclic loading on the nature of the bond strength between steel reinforcement and high strength concrete.
4. Determine the internal strains of high strength concrete as well as steel reinforcement

strains close to the contact surface.

5. Analyze the output of the test results, define the bond stress-slip curve and evaluate the effect of individual parameters on the bond strength.
6. Identify the surface crack patterns and different modes of failure.
7. Develop a bond strength design formula suitable for high strength concrete design considering the effect of different parameters.
8. Implement the high strength concrete bond behavior results through a parametric study into a finite element analysis. Use a special concrete model developed for high strength concrete using UMAT subroutine and ABAQUS finite element program.

In this investigation about 150 specimens were tested. Among these, 100 specimens were subjected to monotonic loading, while the remaining specimens were subjected to cyclic loading to simulate the effect of cyclic loading. The main seven parameters considered in the investigation are: load history, confining reinforcement, rebar diameter, concrete strength, rebar spacing, rate of pull out, and steel reinforcement deformation patterns.

1-3 Research Significance

A clear understanding of the behavior of the bond between reinforcement and high strength concrete enables a designer to design safe, optimum, high strength concrete structures. The Canadian Building Code, CSA A23.3-1994 and ACI 318-1995 Building Code have conservative design provisions for calculating the tension development length and tension splice length, and no special provision for high strength concrete. The reason

is the lack of test results on the actual behavior of bond between rebar and high strength concrete. Therefore, this research is conducted to provide more information regarding the bond performance of reinforcement bars embedded in high strength concrete. Determination of the internal distribution of stress and strain along the steel bar and in the rebar and surrounding high strength concrete are one of the main objectives of this study. The influence of seven selected parameters on the bond resistance under monotonic and cyclic loading condition is investigated. The examination of cyclic loading is important for long span bridges, offshore dynamic loading and earthquake ground motions. The observed surface crack patterns are determined and the modes of failure are examined. Based on the test results of high strength concrete a new parametric evaluation to the tension stiffening is recommended. The new parametric factors were implemented in a UMAT subroutine that works with the ABAQUS finite element program.

1-4 Dissertation Outline

This dissertation consists of eight chapters. Chapter 1 contains a brief introduction on high strength concrete followed by the scope of research as well as significance of the research study. A general survey of literature is presented in the Chapter 2, while concepts of an applied finite element material model for high strength concrete are summarized in Chapter 3. Chapter 4 describes the experimental investigation, test program, test set up, instrumentation and preparation of high strength concrete specimens. The bond strength of high strength concrete is examined experimentally, with emphasis on the effects of load history, confinement, bar diameter,

spacing, rate of loading, concrete strength, and deformation patterns under monotonic and cyclic loading. The monotonic test results are discussed in Chapter 5 and cyclic effects are detailed in Chapter 6. One aspect of this dissertation that distinguishes it from most other investigations on reinforced high strength concrete, is the utilization of the concept of bond energy, the treatment of the influences of study parameters on the bond strength, the effects of earthquake loading on bond strength, and also the internal measurement of strains in high strength concrete and rebar. In addition, the contribution in the tension stiffening of high strength concrete make significance discriminates among other studies. Proper attention to detail and an understanding of possible failure mechanisms are given during the experimental program. The influences of study parameters on bond strength, bond energy, and fracture energy are treated in depth in the tension-stiffening correction by sensitivity factors of high strength reinforced concrete. It is an attempted to apply the results of the current experimental investigations as a base for the analytical formulation of the tension stiffening; this is covered in the Chapter 7. The thesis ends with a conclusion on the out come of the experimental and analytical investigation in Chapter 8. The conclusions are mostly focused on the key main points of the results. Some recommendations for improving the strength of bond in high strength concrete are given. Recommendations for future investigations are also made.

Chapter 2

Literature Review

2.1 Introduction

The compressive forces in a reinforced concrete member are resisted by concrete, while the steel rebar counteracts the tensile forces. This process dictates that there must be a force transfer or bond stress between the two materials. If the bond stress disappears, the rebar will pull out of the concrete and the member will fail under tensile loading. The reinforcement forces due to pullout are shown on Fig. 2.1.

The bond stress must be present whenever the stress in a reinforcing bar changes from point to point along the length of the rebar. The bond for a smooth rebar embedded in concrete is provided by adhesion and friction but when a deformed rebar is used the bond is provided by adhesion, friction, and bearing of the lugs against the concrete which is known as mechanical interlock. All major characteristics of the bond are classified under one of these three categories. There are two approaches for investigation of the behavior of the bond between rebar and concrete. Some investigators have studied the problem experimentally and others theoretically using numerical methods. The present

investigation mainly follows the first approach without sacrificing the theoretical concept of the problem. It is basically experimental and involves full-scale testing of high strength concrete specimens to investigate the influence of load history, rebar diameter, concrete strength, rebar spacing, the rate of loading and deformation pattern on the bond strength under monotonic and cyclic loading.

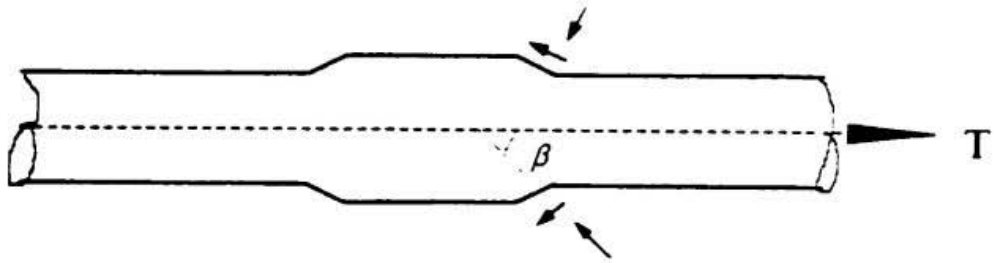

Fig. 2.1 A schematic illustration of pull out and reinforcement forces

2-2 Background

The bond failure and the influence of surface deformation have been examined for normal strength concrete for the past eighty years. Abrams (1913) conducted the earliest study with plain and deformed rebars in normal strength concrete. Glanville (1930) studied the effect of load history. It was concluded that in the case of axial compressive stress the effect of increasing rebar diameter causes an increase in the radial pressure. Since friction is dependent on radial pressure, bond failure occurs at a higher stress for a push-in test rather than in a pullout test.

Clark (1946) investigated the effect of rebar patterns by the pullout test method. The tests were based on an evaluation of the rib spacing and height of deformation pattern for

normal strength concrete. Clark's work (1946) showed that the ratio of the shearing area (rebar perimeter times distance between ribs) to the rib bearing area (projected rib area normal to the rebar axis) should be limited to a maximum of 10 for more efficient rib geometry. It was also suggested that the average spacing between deformations or ribs should not exceed 70 percent of the nominal diameter of the rebar to achieve maximum bond stress. Further, he determined a minimum height of deformations equal to 4 percent of the nominal rebar diameter for 13 mm rebar diameter and smaller, 4.5 percent of the nominal rebar diameter for 16 mm rebars diameter, and five percent for larger rebars.

Several experimental and theoretical investigations were conducted by Somayaji and Shah (1981), Jiang, Shah and Andonian (1984), Tianxi et al. (1992), Jiang, Shah and Ouyang (1992), Shah et al. (1994) and finally Li and Shah (1994), on the behavior of bond for normal strength concrete. Improved tools for measurement of local bond and local slip were introduced and applied. The observations of secondary cracks are reported, as well as the distribution of strain in concrete in the vicinity of the reinforcing bar. An analytical model for predicting the secondary cracks was developed. One-dimensional analysis was used by Jiang, Shah and Andonian (1984) to investigate the primary crack width and tension stiffening contribution between the crack and total elongation. However, the number of specimens was limited and no strain measurements were provided. Slip measurement was in terms of rebar movement and strains. The experiment was conducted under load control and bond stress was evaluated from the differences in readings between adjacent strain gauges.

The contact interface between concrete and steel was investigated by Mehlhorn and Kollegger (1985). Primary and secondary cracks were verified. The assumption of complete compatibility between steel and concrete based on steel stress, bond stress, and concrete stress have been determined and those stresses are illustrated in Fig. 2-2.

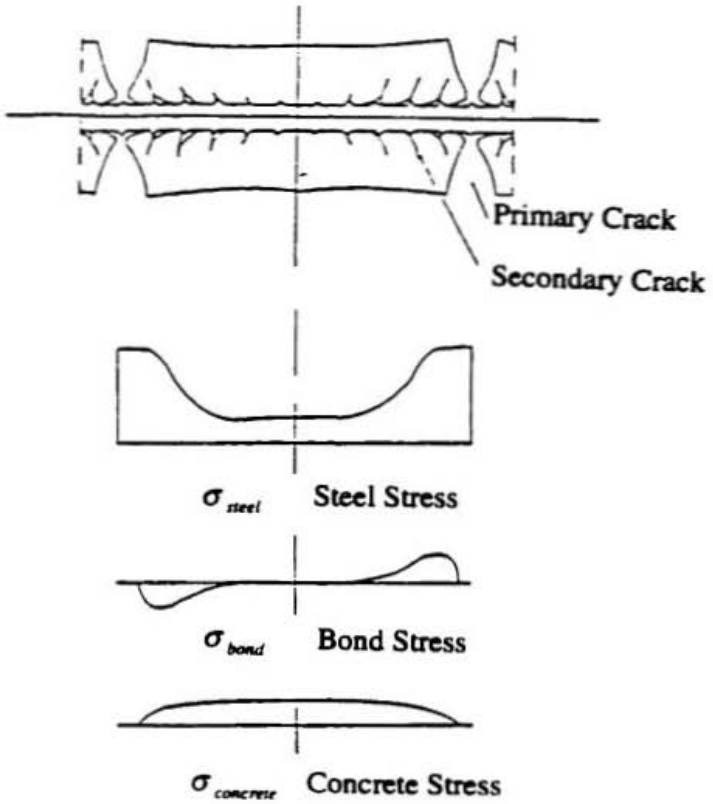

Fig. 2.2 Reinforced concrete in a cracked state
[Mehlhorn and Kollegger(1985]

Li and Shah (1994) conducted an investigation on the relationship between microcracking and macroscopic deformation of concrete material. Three groups of specimens were used and each group contained three specimens that were tested for plain concrete, steel fiber reinforced concrete, and polypropylene fiber reinforced concrete. The fracture process was the main objective of the study and uniaxial tensile tests were conducted. An interchangeably multiple-channel-control method was developed for testing the unnotched concrete specimens to obtain a stable post-peak response. Also, with Acoustic Emission measurement system microcrack was detected. Macroscopic deformation was measured by Linear Variable Differential Transducer (LVDT) and the test was run by displacement control. It is reported that the fracture process of an

unnotched concrete specimen under uniaxial tension can be classified into three stages: distributed damage during loading of the sample up to 80 percent of peak load, formation of microcrack localization during the loading up to 80 percent of the post peak descending load, and major crack propagation up to the load at maximum slip. The macro-deformation of the concrete specimen was largely influenced by micro cracks. Due to strain localization, the deformation of the concrete was a local rather than global phenomenon.

An analytical model to predict the cracking response and the tension-stiffening effect in a reinforced concrete member subjected to uniaxial tension was proposed by Somayaji and Shah (1981). The predicted composite stress-strain curves, crack spacing, crack width, and tension stiffening contribution from the matrix were close to the experimental data of this study. A total of 72 specimens with reinforced mortar type were tested to support the investigation. It was found that the theoretical local bond stress-slip relationship was nonlinear and not unique at every section along the member.

The mechanical behavior of concrete is largely affected by the properties of the interfacial zone between aggregate and cement paste as detailed by Shah et al. (1994). It was reported that the microstructure of the interfacial zone and thus the mechanical interfacial properties could be significantly improved by aggregate pretreatment and mixing methods. Mechanical properties such as stiffness, shear, bond strength and interfacial surface energy were obtained by analyzing the bond-slip relationship. The relationship between the microstructure of the interface and mechanical properties was analyzed. It was concluded that microstructure of the interface is the key factor that determines the mechanical behavior.

The bond of epoxy coated reinforcement was studied by Darwin and Graham (1993), Darwin, et al. (1995), Hadje-Ghaffaei, et al. (1994). These studies showed that

epoxy coating significantly reduces the strength of bond. It was also indicated that the development length modification factor could be reduced from 1.5 to 1.35 for all rebars; the relative bond strength of epoxy-coated reinforcement increase with increase in cover. It was found that the lack of vibration of concrete has a negative effect on the bond strength of both coated and uncoated reinforcement in high slump concrete.

Rehm (1961), and Sortz and Holzenbein (1979) showed that the influence of the geometry of rebar on the local bond stress-slip behavior can be expressed as a function of the relative rib area and it was followed by several other researchers.

Darwin and Graham (1993) investigated the effect of deformation pattern on rebar with nominal diameter of 25 mm. The investigation parameters were the effect of deformation heights between 1.27, 1.91, and 2.54 mm, and deformation spacing ranging from 6.7 to 56 mm. The study was based on relative rib area approach. This investigation concluded that relative rib area was dependent on bond strength and stiffness of the load-slip curve under all conditions of rebar confinement. Darwin and Graham (1993) showed that by providing additional confinement, in the form of transverse reinforcement or additional concrete, the bond strength increased with the increase of the relative rib area.

Hamad (1995), evaluated the effect of rebar deformation pattern considering rib face angle, rib spacing, and rib height for normal strength concrete. The tests included pullout specimens, and beam specimens under positive bending with two splices in the constant moment region at mid-span. The nominal rebar diameter was 25 mm, however after the rebar was machined, the actual net diameter was 20.6 mm. This study showed that the bond capacity depends on rib face angle, rib spacing, and rib height. The machined rebar with a rib face angle of 60° gave the highest ultimate bond strength and the best load-slip performance as compared with rebar with rib face angles of 30°, 45°, 75°, and 90°. Further, rib spacing of 10 mm (50 percent rebar diameter) and with a rib

height to rib spacing ratio of 0.15 developed the highest bond strength and the best bond slip performance, or lowest slip, for a given load. The study reported that the effect of rib parameter is independent of concrete strength. Finally, it was recommended that rebar deformation with a rib face angle of 60°, a rib spacing of 50 percent of the rebar diameter, and a rib height of 10 percent of the rebar diameter is the optimum rib geometry for achieving highest bond strength.

Esfahani and Rangan (1998) carried out a testing program on the effects of rebar face angle on bond capacity in high strength concrete. The results of the investigation indicated that the bond strength of the rebars with rib face angles between 23° and 27° was smaller than that of rebars with ribs face angles between 40° to 47°. Also, It was reported that bond strength u of tensile rebars based on Australian Standard AS 3600-1994 is calculated by:

$$u = \frac{\left(\frac{2a}{d_b} + 1\right)\sqrt{f_c'}}{K_{A1} K_{A2} \pi} \qquad (2\text{-}1)$$

In this equation, $2a$ is twice the cover to the rebar or the clear distance between adjacent parallel rebars developing stress, whichever is less, and d_b is the rebar diameter. K_{A1} is a correction factor for horizontal rebar diameter and K_{A2} is a correction factor for longitudinal rebars diameter. For a horizontal rebar with more than 300 mm of concrete cast below it, K_{A1}=1.25, and 1.0 for all other rebars. K_{A2}=1.7 for slabs, 2.2 for longitudinal rebars in beams and columns with fitments, and 2.4 for all other longitudinal rebars.

The following equation for calculation of the average bond stress, u, at ultimate for a deformed rebar in tension, is proposed by Esfahani and Rangan (1998):

$$u = \frac{0.5\sqrt{f_c'}}{K_1 K_2 K_3 K_4} \qquad (2\text{-}2)$$

However, the following expressions for calculation of the average bond stress, u, at ultimate for deformed rebar are recommended by ACI 318-1995 and Canadian Standard, CSA A23.3-1994, respectively. In chapter 5 a comparison between standards expressions, recommended expression and test result are performed and explained in details.

ACI-318M-1995:
$$u = \frac{25\sqrt{f_c'}}{48\alpha\beta\lambda} \qquad (2\text{-}3)$$

Canadian Standard, CSA A23.3-1994:
$$u = \frac{0.556\sqrt{f_c'}}{K_7 K_8 K_9 K_{10}} \qquad (2\text{-}4)$$

Darwin, et al. (1996) studied the splice strength of high relative rib area of reinforcing rebars. The effect of two different coarse aggregates on the bond was evaluated. The effect of relative rib area and rebar diameter on the increase in bond strength provided by confining reinforcement was studied. It was found that the splice strength of uncoated reinforcement confined by transverse reinforcement increased with an increase in the relative rib area and the rebar diameters of the spliced rebars. The results indicated that the maximum development length modification factor used for epoxy-coated reinforcement might be reduced by 20 percent. Esfahani and Rangan (1998) investigated the bond stress in splices in beams made of high strength concrete. In this study the bond stress distribution over the splice length was taken into account to develop an analytical model for the strength of tensile splices. The influence of the ratios between side cover, bottom cover, and spacing between the spliced rebars was included

in the model. It was concluded that the bond stress was a function of minimum cover, rebar diameter, tensile strength of concrete, and deformation properties of rebar.

Darwin, et al. (1995) studied the reliability-based strength reduction factor (ϕ) for bond. The formulation and calculation of (ϕ) for developed and spliced rebars was presented in this study. Conventional and high relative rib area rebars, both with and without coating reinforcement, were considered. The ϕ-factor they determined was statistically based.

Darwin, et al. (1995) studied development length criteria for conventional and high relative rib area reinforcing rebars. On the basis of a statically based expression, the development reinforcing rebars and splice strength of reinforcing rebars for concrete with strengths between 17 and 110 MPa, with and without confining reinforcement, was investigated. The effects of cover, rebar spacing, development/splice length, geometric properties of the development and spliced rebars were incorporated. The equation was developed for reduction in the development length of high relative rib area rebars confined by transverse reinforcement splice length of conventional/high relative rib area rebars as follows:

$$\frac{l_d}{d_b} = \frac{\frac{f_y}{f_c'^{1/4}} - 1900\left(0.1\frac{c_M}{c_m} + 0.9\right)}{72\left(\frac{c + K_{tr}}{d_b}\right)} \qquad (2\text{-}5)$$

which is based on the following equation:

$$\frac{A_s f_y}{f_c'^{1/4}} = \left\{\left[63 d l_d (c_m + 0.5 d_b) + 2130 A_s\right]\left(0.1\frac{c_M}{c_m} + 0.9\right) + 226 t_r t_d \frac{N A_{tr}}{n}\right\} \qquad (2\text{-}6)$$

It was also concluded that the quadratic root of concrete compressive strength, f_c, provides an accurate representation of the effect of concrete strength on bond strength for concrete with compressive strengths between 17 and 110 MPa.

Azizinamini, et al. (1993) and Azizinamini, Chisala and Ghosh (1994) examined bond performance of reinforcing bars and tension development length of reinforcing bars embedded in high strength concrete. The effects of concrete compressive strength, splice length, and casting position on bond strength of reinforcing bars have been studied and the failure hypothesis has been explained. It was concluded that in the case of high strength concrete, increasing the tension development length (or equivalent tension splices) was not an efficient way of increasing the bond capacity of deformed reinforcing bars, especially when the concrete cover is small. Furthermore, some modifications were suggested for design implementation. It has been indicated that when calculating for the tension development length of high strength concrete and tension splice some minimum stirrup should be provided over the splice region.

Tensile bond strength of deformed rebars embedded in high strength concrete has been investigated experimentally by Hwang, Leu and Hwang (1996). The equivalence between the tensile development length and the tensile splice length for high strength concrete was established and the effects of anchorage lengths on bond capacity have been discussed. Concrete strength, anchorage length, and the amount of transverse reinforcement have been measured. It was concluded that the bond performance of high strength concrete without silica fume was similar to that of the normal strength concrete and also the total confinement beyond the currently accepted limit was effective for the bond action of high strength concrete. The study also reported that the admixture of silica fume decreases the bond strength of the deformed rebar.

De Larrard, Schaller and Fuchs (1993) have investigated the effect of rebar diameter on bond strength in high performance concrete. It was concluded that bond capacity increases with the tensile strength of the concrete and at a higher rate with smaller reinforcement. It was also found that the bond is greater for smaller rebar diameters than for larger rebar diameters.

Eligehausen, Popov and Betero (1983) conducted one of the main investigations on the effect of rebar diameter embedded in normal strength concrete. It was concluded that the maximum bond capacity decreased slightly with the increasing rebar diameter. The frictional bond resistance was not influenced significantly by the different rebar diameter, lug spacing, or the related rib area.

2-3 Properties of High Strength Concrete

The direction of research in last two decades mostly has been concentreted in material and mixture development to ensure the highest possible strength of concrete. The properties of high strength concrete such as slump, density, air content, cohesion, creep, shrinkage, compressive strength, stress-strain behavior, permeability, flexural strength and chloride resistance, etc. have been investigated by several researchers in Europe and North America. Hoff (1985), Marzouk (1987), Malhotra (1988), Shah (1978) directed some comprehensive researches to investigate the properties of normal and lightweight high strength concrete.

Marzouk (1989) has conducted broad research to investigate properties of high strength concrete at Memorial University of Newfoundland. Different properties of high strength concrete such as the effect of low ocean temperature on strength and elasticity,

creep of high strength concrete at low temperatures, freezing and thawing resistance of high strength concrete have been investigated in details. A short summary of research investigation on the mix design of high strength concrete indicated that local materials with silica fume and fly ash can produce concrete with compressive strength greater than 70 MPa at 28 days, as recommended by Marzouk and Hussein (1990). The influence of low temperature was minor on strength, elasticity and stress-strain relationship of high strength concrete. The relation of creep to stress strength ratio at room temperature was found to be linear for concrete containing silica fume as was the case for ordinary Portland cement concrete, Marzouk (1992). The changes in weight, length, pulse velocity, resonant frequency, compressive strength, due to freezing and thawing were recorded for 458 cycles. As a result, high strength concrete made with local material and having about 3-5% air content is durable up to 458 cycles, Marzouk (1990). The stress strain relationships of high strength concrete under uniaxial compressive and tensile stresses recorded by Marzouk and Chen (1993) as well as an idealized stress strain curve of the steel reinforcement are shown in Fig. 2.5 and Fig. 2.6.

The properties of high strength lightweight concrete were investigated by Hoff (1992). The properties included stress-strain relationship, modules of elasticity, Poisson's ratio, tensile splitting strength, modulus of rupture, creep, shrinkage, aging, freezing and thawing, thermal properties and temperature development of high strength light weight concrete. It was found that strain at maximum stresses ranged from 0.0025 to 0.0035. The value of modulus of elasticity at 40 percent of ultimate stress ranged from 18 to 30 GPa for concrete having compressive strengths ranging from 55 to 82 MPa. The modulus of

elasticity for lightweight concrete was lower than normal weight concrete. Both aggregate volume and stiffness as well as aggregate types had a great effect on the compressive strength and modulus of elasticity of high strength lightweight concrete. The values for Poisson's ratio were in the range of 0.21 to 0.23 for moist cured and decreased to 0.16-0.17 when the concrete was exposed for additional air drying for concrete with compressive strengths 55 to 72 MPa. The value for tensile splitting strength of semi-(sand) lightweight concrete ranged from $0.43\sqrt{f_c}$ MPa ($5.15\sqrt{f_c}$ psi) downward: $0.49\sqrt{f_c}$ MPa ($5.87\sqrt{f_c}$ psi) or greater for moist cured concrete for compressive strengths ranged from 55 to 72 MPa.

Bilodeau, Malhotra and Hoff (1998) presented the mechanical properties of the lightweight and normal weight high strength with respect to hydrocarbon fire resistance incorporating polypropylene fires. It was concluded that the amount of deterioration in the concrete increased with the amount of lightweight aggregate in the concrete. The results demonstrated also the effectiveness of the polypropylene fibers to reduce the saplling of concrete during the hydrocarbon fire. The reduction of the saplling resulted in a reduction of the temperature rise in the concrete block during the fire test, and therefore to a better protection to the steel reinforcement.

The properties of fresh and hardened concrete made with the superplasticized cements, the effect of superplasticized with Portland cement clinker and gypsum on the fineness of the product, and on the water requirement and the compressive strength of the mortars made with the superplasticizer cement, were investigated by Bouzoubaa, Ahang, and Malhotra (1998). It was concluded that the integrinding of a given amount of a

naphthalene-based superplasticizer with Portland clinker and gypsum reduced the grinding time required for obtaining the same Blaine fineness as that of the control Portland cement without the superplasticizer.

The properties of high strength concrete play a significant role in the interface in strength enhancement of high strength concrete. The properties of concrete depend on the properties of its mixing material and the interactions between them and the presence of aggregates and weaker zones (interfaces) where crack growth begins. The difference in stiffness between aggregates and concrete matrix produces stress concentrations at the interface points. The stress concentration of material, multiple crack formation in mortar, concrete and aggregate particles can lead to propagating cracks to branch. In recent years, considerable attention has been given to the use of silica fume as a partial replacement for cement to produce high strength concrete. Silica fume improves concrete strength through physical and chemical modifications of the cement paste. It is reported by Goldman and Bentur (1989) that two effects should be considered when analyzing the effects of silica-fume: 1) the reduction in water requirement of the system, and 2) the pozzolanic reaction of the silica fume. Other chemical admixtures are also used in the mixture for increasing the strength of concrete such as 'superplasticizer' and 'retarder' which have been recently the focus of adequate research attention.

2-4 Bond and Fracture Energy

Failure of concrete is a process of crack formation and development. For some materials the risk of failure due to the growth of crack is treated as a fracture mechanics problem. Although fracture mechanics has been developed for brittle materials, the applicability of conventional concepts to concrete is not easy, due to the complex characteristics of the material, Giaccio et al. (1992). Concrete is a composite, multiphase

material; cracking itself is a heterogeneous process (initiation of cracks, slow stable crack growth, crack arrest, and unstable crack propagation); the surface area formed is many times larger than the effective fracture area (multiple crack formation occurs) and the energy-dissipating mechanism in concrete is not merely confined to surface energy. To characterize fracture in concrete, several nonlinear fracture-mechanics approaches have been proposed. These approaches can be categorized as "Cohesive Crack Models" (Hillerborg, Modeer and Petersson (1976); Hillerborg (1985); Marzouk and Chen (1995); Bazant and Oh (1983)); and effective (or equivalent elastic) crack models (Bazant (1984); Jenq and Shah (1985) and Bazant and Kazemi (1990). In these models, the behavior of the fracture process zone is not modeled through stress-strain relations. Instead, some adaptation of linear elastic fracture mechanics was introduced to approximately reflect the nonlinearity of fracture response. The cohesive crack models simulate the fracture process zone by a closing pressure that reduces the stress singularity at the crack tip. The effective crack models characterize the fracture process zone by an effective crack length that can be determined from an additional instability condition.

Developing a constitutive model that contains the material characteristics for every conceivable load history for high strength concrete is essential. This constitutive model has to cover the entire spectrum of triaxial strength, stiffness as well as fragility in tension when brittle-ductile materials such as high strength concrete are considered.

The fracture toughness concept of concrete by means of fracture energy "G_f" was indicated by Hillerborg (1976). It is indicated that the fracture process zone may be more than 100mm long at maximum load and the stress within this zone decreases as the load increases. Hence, the formation of a crack should be analyzed for high strength concrete. The most direct way of determining G_f is by means of a uniaxial tensile test, where the complete stress-deformation response is measured. It is established that the

direct tensile test is the only test that gives all the relevant information for numerical analysis.

A general description of the stress-deformation properties of concrete can be given by means of two curves: the stress-strain curve, including branches; and the stress-deformation curve for the additional deformation "w" within the damage zone.

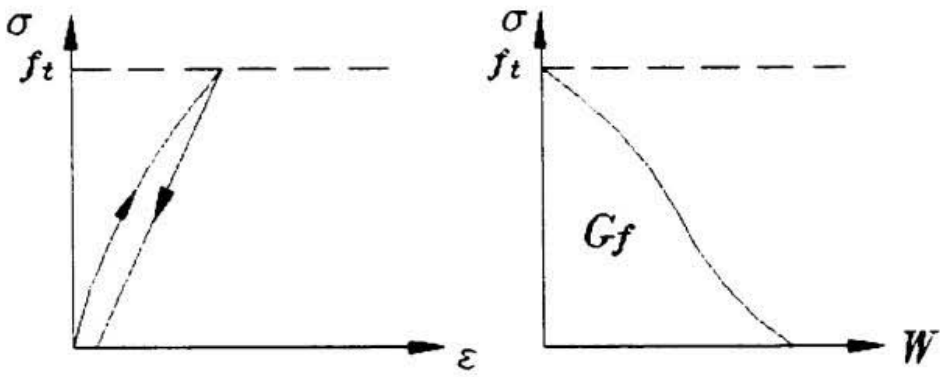

Fig. 2.3 Description of the tensile behavior by means of two curves. σ–ε Curve for the whole volume and one σ-w curve for additional deformation within the damage zone

Another method for analyzing crack formation and crack growth in concrete by means of fracture mechanics was developed by Hillerborg, Modeer and Petersson (1976). In this model stresses are assumed to act across a crack as long as it is narrow. This assumption may be regarded as a way of expressing the energy absorption, G_f in the energy balance approach, but it is also in agreement with results of tension tests. The crack is assumed to propagate when the stress at crack tip reaches the tensile strength. When the crack opens the stress decreases with increasing crack width ω. In

other words, the model counts for the observed response that stress continues to be transferred across a developing crack after the material's tensile strength has been reached. The transfer region is the fracture process zone. Using the fictitious crack model, the fracture process zone is defined as the region in which the strain corresponding to the tensile strength, has been exceeded (resulting in the formation of a physical crack) but the material can carry a tensile stress. As the crack continues to open, the ability of the concrete to resist the tensile stress decreases, finally reaching zero at a crack width of w_o.

Using fracture mechanics to predict the size effect was conducted by Tianxi, Shah and Ouyang (1992). It has been found that the strength of concrete structures generally decreases with increasing structural size before reaching a limiting value. The two-parameter fracture model is used to predict the size effect of three-point bend beams. The effect of different widths of load distribution on strength of concrete structures was also discussed.

Darwin, et al. (1993) performed a finite element fracture analysis of steel-concrete bond. It is inferred that the reason for using fracture mechanics concepts for modeling failure of the beam specimens is the nature of the splitting crack, where fracture surfaces are displaced symmetrically perpendicular to one another in opposite directions. Due to nonlinearity at the tip of the crack, a nonlinear fracture mechanics approach is used.

Energy is absorbed as displacements across the crack increase from 0 to w_o. The area under the stress-displacement curve represents the total energy absorbed per unit area of the crack surface, known as the fracture energy, G_f and is calculated as:

$$G_f = \int_0^{w_o} \sigma d\omega \qquad (2\text{-}7)$$

σ is tensile stress at the crack, ω is the crack width and ω_o is the displacement at which the tensile stress in the concrete becomes zero. The researchers applied the

fictitious crack model to the finite element analysis to represent the crack that forms along the centerline of the beam-end specimens. In the model, the crack is predefined along the specimen centerline and the stress across the crack, σ is transferred using rod elements oriented perpendicular to the crack plane. The rod elements have two nodes with each node having one degree of freedom parallel to the element, a unit length and the total area equal to the tributary area of the concrete elements attached to the same node.

In general, the investigation improved the development characteristics of reinforcing rebars. The effects of the deformation pattern on bond strength were investigated experimentally and analytically. The influences of deformation pattern on the bond of reinforcing rebars to concrete were examined. A nonlinear finite element analysis was employed to study the bond mechanism.

The load deformation behavior of plain high strength concrete under direct uniaxial tension, including post cracking or softening response, was investigated in detail by Marzouk and Chen (1995). The complete tension softening model of high strength concrete is shown in Figure 2.7. The tensile-softening response, strains in cracking process zone and elongation for various gauge lengths were measured. The recorded results from direct tension, splitting-tension, and modulus of rupture test procedures for high strength concrete in tension were compared. The research revealed that high strength concrete exhibits a more brittle and stiffer behavior with a large initial modulus of elasticity. It is estimated that the fracture energy of high strength concrete is about five times the area under the ascending portion of the stress-deformation curve, compared to a corresponding value of 10 estimated for normal strength concrete. A constitutive relationship was recommended for the behavior of high strength concrete in tension, including post peak softening response.

2-5 Constitutive Modeling

In order to simulate experimentally the observed behavior of reinforced concrete under multiaxial loading, a suitable constitutive relationship must be established. Hence, the relation between stress and strain under various stages of loading has to be verified. The constitutive relations may vary from simple equilibrium methods to the more general relations between stresses and strains such as a) linear elasticity theory b) nonlinear elasticity theory c) work hardening plasticity theory d) endochronic theory.

Elwi and Murray (1979) proposed a nonlinear three dimensional (axisymmetric) stress-strain relationship for concrete. The proposed material model was based on a hypoelastic orthotropic approach and incremental stress-strain equations. The model presented the assumed form of the incremental constitutive equations and established the shear stiffness in terms of some material constants. Secondly, a technique was introduced for expressing this incremental relationship in terms of incremental uniaxial strains. Finally, the relationship between equivalent uniaxial strain and stress was introduced and the incremental elastic model was derived in terms of strain parameters. A comparison of the proposed theory with two sets of experimental data indicated reasonable agreement, for both tensile and compressive responses.

Cervenka (1985) studied a constitutive model for cracked reinforced concrete. The relationship between stress and strain was in terms of the tensile resistance of concrete normal to cracks (also called tension stiffening), represented the tension stiffness of concrete between cracks activated through bond between concrete and reinforcement. Further, the material stiffness matrix was derived and a constitutive equation in an incremental form was proposed. The computation of the stress-strain curve was achieved by incremental loading, with iteration at each step based on the initial stress method.

Different types of stiffness were used for each component of concrete in a single iteration. The tangent stiffness was used for compression, zero stiffness for tension and secant stiffness for the shear. The solution within a load step is repeated until the material laws and stress equilibrium is satisfied. The material parameters were determined from experimental testing. A 3-D concrete constitutive model which was implemented in a computer program by Buyukozturk and Shareff (1985) incorporated nonlinear material properties, based on isotropic elastic, orthotropic elastic, and plasticity formulations, cracking in concrete, shear transfer in cracked reinforced concrete sections, and time dependent effects such as creep, shrinkage, and transient temperature distributions. Cracking, load-displacement response and ultimate strength prediction were achieved with adequate accuracy. In addition, some comparison between predictions with different constitutive models and between predictions and test results was made.

Pramono and Willam (1989) developed a comprehensive constitutive model for the triaxial behavior of plain concrete with emphasis on the material formulation of concrete failure in tension and compression including calibration of the underlying constitutive parameters from laboratory experiments. It was reported that the fracture energy release approach describes the degradation of triaxial strength below the transition point of brittle-ductile fracture due to debonding and decohesion in tension and low confined compression.

Sankarasubramanian and Rajasekaran (1996) studied the concept of neural network principle for compressive and tensile meridians of the surface. A nonlinear hypoelastic constitutive relationship was proposed to analyze plane and axisymmetric reinforced concrete structures. The proposed model assumed concrete to be orthotropic and the equivalent uniaxial strain concept was used along with an incremental formulation based on hypoelasticity.

An excellent investigation was performed by Hussain (1998) to develop a constitutive model for high strength concrete based on test results of a biaxial loading conditions to enable the numerical prediction, through the finite element method. A plasticity based model based on Etse and Willam's (1994) original model was adopted. The numerical implementation of plasticity was carried out through the elastic-predictor plastic-corrector method. The material model was calibrated for high strength concrete using the data obtained from the experiment. The validity of the proposed model was studied by comparing experimental results, which showed an excellent agreement.

2-6 Numerical Analysis of Bond-Slip Behavior

A mechanical model for bond between concrete and reinforcement has been developed by Plauk and Hees (1981). The mechanical model took into account the nonlinear properties of material, progressive cracking and local failure. It was concluded that the true state of stress and strain as well as the actual crack pattern and deflections of a reinforced concrete beam can only be obtained from analysis. The moment-curvature relation obtained from analytical results shows furthermore the significant influence of bond on internal deformations which cannot be neglected without essential loss of accuracy.

Investigation of bond via the concept of nonlinear contact problems was initiated by Mehlhorn, Kollegger (1985). The application of the element with different contact models was shown in this study. Slip occurred in the longitudinal direction while lateral pressure as well as gapping may occur normal to the rebar surface. The bond stress-slip relation that is derived from Doerr's tests (1981) was explained. The strength of concrete in the bond zone near the rebar surface, the position of the rebars during casting, the geometry of the rebar surface, transverse pressure or gapping, and local damage of

concrete were considered in the relationship. The application of the developed element is restricted to static problems in this study.

An incremental hypoelastic plane stress material model for reinforced concrete was developed by Massicotte (1988). The suggested material model for concrete allows for strain softening after cracking and crushing and includes fixed and rotating crack models. A rational tension stiffening relationship was introduced, in which the post cracking stress strain response is described in terms of the reinforcement ratios and the angle of the crack to the reinforcement. Several verification examples have been solved with use of the proposed model.

Lucie (1992) derived a model to predict the ultimate bond stress as a function of the concrete cover on the steel rebar, the concrete quality and the temperature. It was shown that the magnitude of the ultimate bond stress of deformed rebars depends upon the failure mode of concrete. This study used a thick-walled cylinder model subjected to an internal pressure in order to determine the ultimate bond stress theoretically. Using Coulomb's failure criterion, the maximum shear stress is calculated at the maximum internal pressure.

Budan and Murray (1994) proposed a distributed discrete concrete cracking model for the finite element analysis of reinforced concrete structures. Their investigation considered discrete cracking, longitudinal splitting cracking, interface behavior, and identification of local crushing and progression of these mechanisms at different stages during the loading history. The bond stress and the bond slip were evaluated within intervals referenced to the position of the lug on the reinforcing surface and the correlation between splitting mechanisms and bond variables was examined. It was reported that longitudinal splitting has an important influence on the bond. A numerical analysis indicated that for maximum crack spacing, the concrete interface progressively

lifts up from the rebar surface. It was found that at any fixed point, the bond slip increases suddenly, and the bond stress decreases suddenly as the longitudinal splitting crack propagates past the point.

Shear forces applied by the lugs to surrounding concrete cause vertical concrete cracks located at, or close to, the center of the crack spacing, to grow slowly and steadily. The bond-slip increases linearly with increase of steel stresses. It seems that more extensive comparison with tests and correlation with experimental measurements, and improvements in modeling of longitudinal cracking, are necessary.

2-7 Bond and Cyclic Loading

One of the major sources of failure in reinforced concrete members is the sudden loss of bond between the rebar and concrete in anchorage zones, which has been the cause of damage and even collapse of several structures during earthquakes. It was also proven that the bond-slip for rebars anchored within connections, influences the stiffness and ductility of reinforced concrete structures subject to intense seismic loading. Therefore, accurate knowledge of the load-slip characteristics, and on anchorage requirements for such rebars, is essential for the realistic modeling of the seismic response of concrete structures.

The effects of tensile versus compressive loading, amount of confinement reinforcement, rebar diameter, concrete strength, rebar spacing, transverse pressure and rate of pull out of the bond behavior for normal strength concrete under monotonic and cyclic loading were investigated by Popov (1984). A local bond stress-slip relationship was developed and an analytical approach for the analysis of the deteriorating cyclic behavior of beam-column joints was discussed.

The behavior of compression lap splices of normal reinforced concrete members subjected to high level repeated cyclic loads was studied by Panahshahi, et al. (1992). The force transfer mechanisms in compression lap splices were obtained by implementing the result of experimental observation into an inelastic finite element model. A design method for resistance of compression lap splices for concrete members subjected to earthquake loading was proposed.

Failure due to shearing of the concrete between the ribs by pulling the rebars out of specimens with large concrete cover was studied by Rehm and Eligehausen (1979). The effect of maximum load, load amplitude, rebar diameter, concrete quality and bond length were investigated. It was reported that the slip at the free rebar end considerably increased during the cyclic loading and the upper load and the bond length mainly influenced the increase. Hawkins, Lin and Ueda (1987) demonstrated a computer model and the results of inelastic reversed cyclic loading tests on deformed rebars anchored in idealized models of exterior beam-column connections.

Hawkins, et al. (1982), studied local bond strength of concrete for cyclic reversed loading both experimentally and analytically. This study demonstrated that the load-slip response of an inelastically and reverse cyclically-loaded rebar can be modeled by integration of: 1) the local bond-slip relationship; 2) the stress-strain relationship and; 3) the conditions for continuity of forces and displacements along the rebar. Three stages of behavior for the local bond stress-slip response were ascertained as: 1) the development of internal cracks radiating from the lug; 2) the coalescence of those cracks into a failure cylinder surrounding the rebar; and 3) the movement of one lug under loading into a position occupied previously by an adjacent lug. For cyclic loading local bond stress-slip envelope was found to be similar to that of monotonic loading prior to attainment of the maximum capacity.

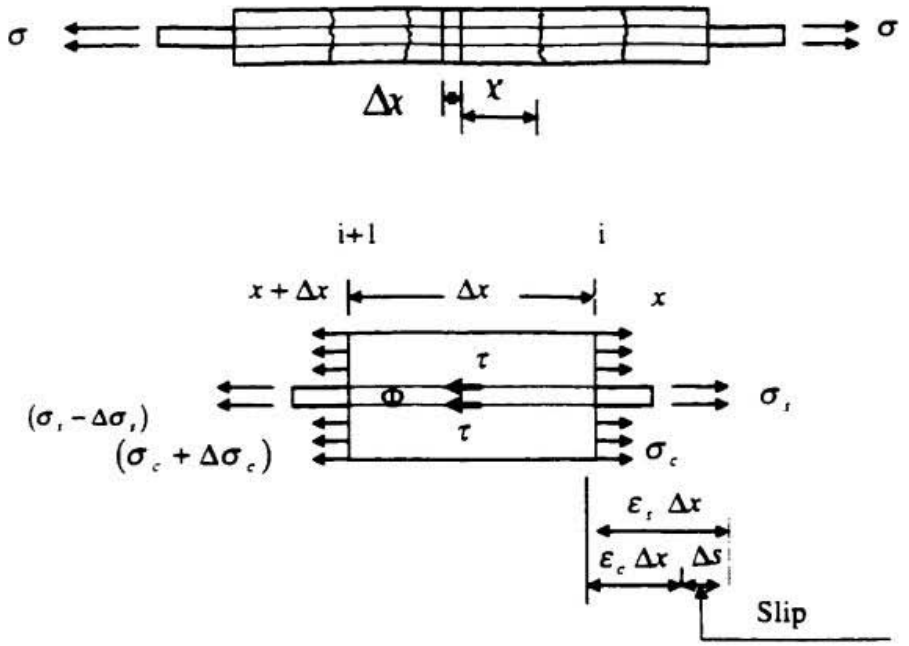

Fig. 2.4 Stresses and strains on a reinforced concrete element of a finite length in tension specimen

Tassios T.P.. and Yannopoulos P.J. (1981)

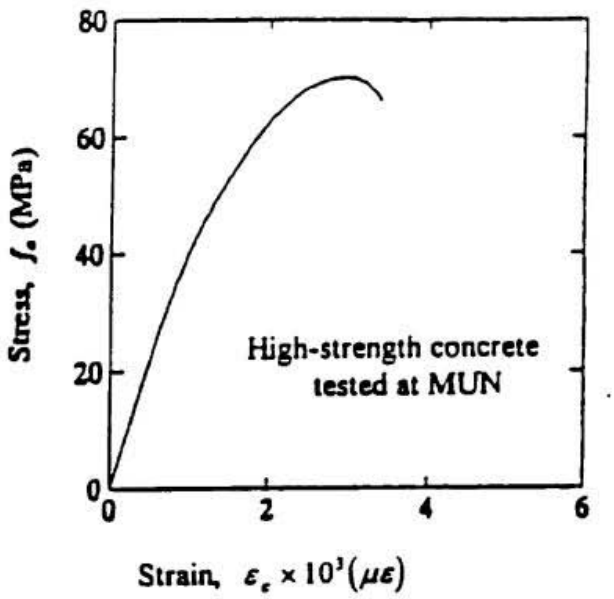

Fig.2.5 Uniaxial compressive stress-strain curve for high-strength concrete

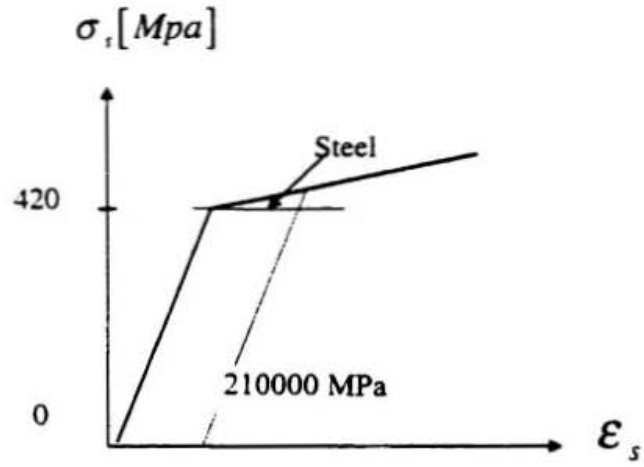

Fig.2.6 Idealized stress-strain curve of the steel bar

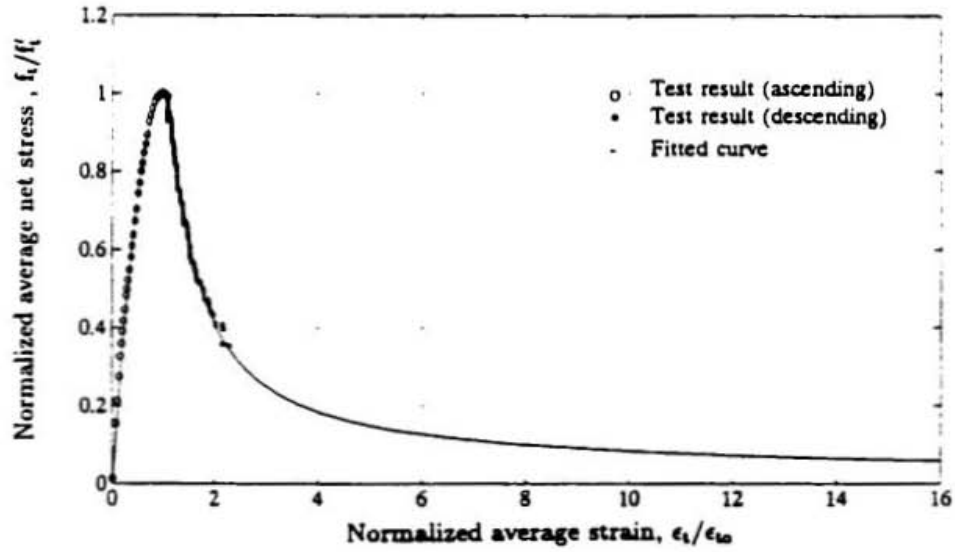

Fig. 2.7 Complete tension softening model of high strength concrete [Marzouk and Chen (1993)]

Chapter 3

High Strength Concrete Constitutive Model

3.1 Introduction

The continuum theory of solid mechanics deals with the mathematical theories of elasticity, plasticity, a basic set of equilibrium equations, condition of geometry or strain compatibility and displacement and material constitutive law or stress-strain relation. Clearly, both the equations of equilibrium and the equations of compatibility are independent of the characteristics of the material. The main feature of various material behaviors is accounted for in the material constitutive relationship. The constitutive model idealizes the behavior of the actual material.

The equations that model the behavior of a material are called "constitutive equations." A constitutive equation is a mathematical model that can permit production of the observed response of a continuous medium. Establishment of constitutive equations in engineering can be based on the experimental observations at a macroscopic

level, taking into account the principles of mechanics. Physics provides the fundamental basis and mathematics the concise way to express the physical phenomena.

The material model used in this study is largely based on Etse and Willam (1994). That particular model was chosen because it possesses different characteristics that make it attractive for use in concrete material with finite element analysis. Compatibility of displacements across the element boundaries is satisfied identically and force equilibrium is satisfied approximately. The stiffness matrix for each individual element is constructed using the energy approach. The complete finite element equations are then determined to solve for unknown nodal displacements, element strains, and stresses.

The fundamentals of the constitutive model used to define high strength concrete behavior are presented in this chapter. The relationship between stress and strain for a material, yield surface, hardening behavior, non-associated flow rule and softening behavior characterize the concrete model which is presented in the subsequent sections.

3.2 The Assumptions for Flow Theory of Plasticity

The flow theory of plasticity is based on three assumptions:

- Decomposition of total strain rate into an elastic recoverable, $\dot{\varepsilon}_e$ and a plastic irrecoverable, $\dot{\varepsilon}_p$ part, so that the tangential material law is recovered for loading, and the initial elastic modulus governs the unloading response. Decomposition of elastic and inelastic strain rates can be expressed as follows:

$$\dot{\varepsilon} = \dot{\varepsilon}_e + \dot{\varepsilon}_p \tag{3-1}$$

This assumption is normally justified for small or infinitesimal deformation.

- Yield criterion that delimits the elastic portion of the material response under combined state of stress. The yield criterion is generally expressed as a function of the state of stress σ and the internal variables q, Lubliner (1990). The internal variables q, in vector form, are used to describe the past history of the state of stress. Thus, the general form of the yield function can be written as

$$F(\sigma, q) = 0 \tag{3-2}$$

For the case of isotropic behavior, the yield surface can be expressed in terms of the principal stresses or in terms of the invariants of the stress tensor.

- The flow rule describes the evolution of the plastic strain rate when the material undergoes plastic deformation. The plastic flow equation takes the form:

$$\dot{\varepsilon}_p = \dot{\lambda} \frac{\partial Q}{\partial \sigma} = \dot{\lambda}\, m \tag{3-3}$$

where, Q designate the plastic potential, m describes the direction of the plastic flow, and $\dot{\lambda}$ is a positive scalar factor called the plastic multiplier. The value of $\dot{\lambda}$ is non-zero only when plastic deformations occur. When the plastic potential and the yield surface coincide $Q = F$, this leads to associated plastic flow. For pressure-sensitive materials, it is widely accepted that the use of an associated flow results in the prediction of too much dilatancy, Vermeer and Borst (1984). Consequently, the non-associated flow is used.

- The material stability postulates: many material stability postulates were proposed by different researchers, for example, Hill (1950), Ilyushin (1948) and Drucker (1959). However, Bazant (1984) proved that those postulates are neither necessary nor sufficient for stability. As a result no stability postulate is used in the applied model.

3.2.1 Numerical Computation of Plasticity

The elastic-predictor plastic-corrector method is used here. It is based simply on an assumed trial stress vector (elastic-predictor) and a correcting procedure (plastic-corrector) in case the trial vector violates the yield condition. In general, the initial values σ, ε, q are known at time $t = t_n$, in the procedure, then an increment of stress $\Delta\sigma$ is applied and it is required to find the new state of stress and strain.

3.2.2 Elastic-Predictor Step

The plastic-predictor defines the trial stress state as:

$$\sigma_t = \sigma_n + E\Delta\varepsilon \tag{3-4}$$

where

σ_n : Stress state

E : Young's modulus

$\Delta\varepsilon$: Strain increment

From this step, the stress point that represents the stress state in principal stress space causes one of three situations to arise. It is either elastic loading: $F(\sigma_t, q_n) < 0$, neutral loading: $F(\sigma_t, q_n) = 0$ or plastic loading: $F(\sigma_t, q_n) > 0$. The case of elastic loading and neutral loading is handled within the elastic constitutive relation. In the case of plastic loading, a plastic-corrector will be required as presented in the next section.

3.2.3 Plastic-Corrector Step

When the state of stress exceeds the elastic limit, the stresses cross the yield surface. The purpose of the plastic-corrector is to return the trial stress vector σ_t to the

yield surface. In order to obtain an efficient return strategy, the stress state σ_{n+1} must be on the loading surface and the constitutive law for hardening/softening must be satisfied. For the case of plastic loading the elastic-predictor step is followed by a plastic-corrector step. This can be expressed as:

$$\Delta\sigma = \Delta\sigma_e - \Delta\sigma_p \tag{3-5}$$

The elastic stress and the plastic stress, as mentioned before, are expressed as

$$\Delta\sigma = E\Delta\varepsilon_e \tag{3-6}$$

$$\Delta\varepsilon_p = \Delta\lambda m \tag{3-7}$$

Thus, Equation 3-5 can be written as

$$\Delta\sigma = E\Delta\varepsilon - E\Delta\lambda m \tag{3-8}$$

3.2.4 Crossing the Yield Surface

The integration procedure used here requires the location of the integration of the elastic stress vector with the yield surface. In such circumstances, we have

$$f(\sigma_x + \alpha\Delta\sigma_e) = 0 \tag{3-9}$$

where the original stresses, σ are such that

$$f(\sigma_x) = f_x < 0 \tag{3-10}$$

while, with $\alpha = 1$, the elastic stresses $\sigma_x + \sigma_e$ give

$$f(\sigma_B) = f(\sigma + \Delta\sigma_e) > 0 \tag{3-11}$$

For some yield surfaces, this problem can be solved exactly. In the current work, an iterative scheme is used to determine the point of intersection with the yield surface. A scheme is needed to return the stresses to the yield surface following an initial predictor. Numerical solution schemes for most material models will include the numerical integration of some kind of rate equations. There are two schemes, which are well known for numerical integration. The Forward-Euler integration scheme is called explicit, as information at some future time $t > t_n$ is used to advance the numerical solution. The Backward-Euler integration scheme is called implicit, as information at some future time $t > t_n$ is used to advance the numerical solution from station t_n. The procedure used in the current work is a standard predictor in the form of a Forward-Euler procedure, as shown in Figure 3-1, such that

$$\Delta\sigma = E\Delta\varepsilon - \Delta\lambda E\frac{\partial f}{\partial\sigma} = \Delta\sigma_e - \Delta\lambda E\frac{\partial f}{\partial\sigma} \tag{3-12}$$

Moving from the intersection point A (Fig. 3.1), $\Delta\sigma_e$ is now the elastic increment after reaching the yield surface, i.e. $(1-\alpha)$ times the $\Delta\sigma_e$. In relation to Figure 3.1

$$\sigma_c = \sigma_A + \Delta\sigma_e - \Delta\lambda E\frac{\partial f}{\partial\sigma} = \sigma_B - \Delta\lambda\frac{\partial f}{\partial\sigma} \tag{3-13}$$

The step can be interpreted as giving an elastic step from the intersection point A to B followed by a plastic return that is orthogonal to the yield surface at A.

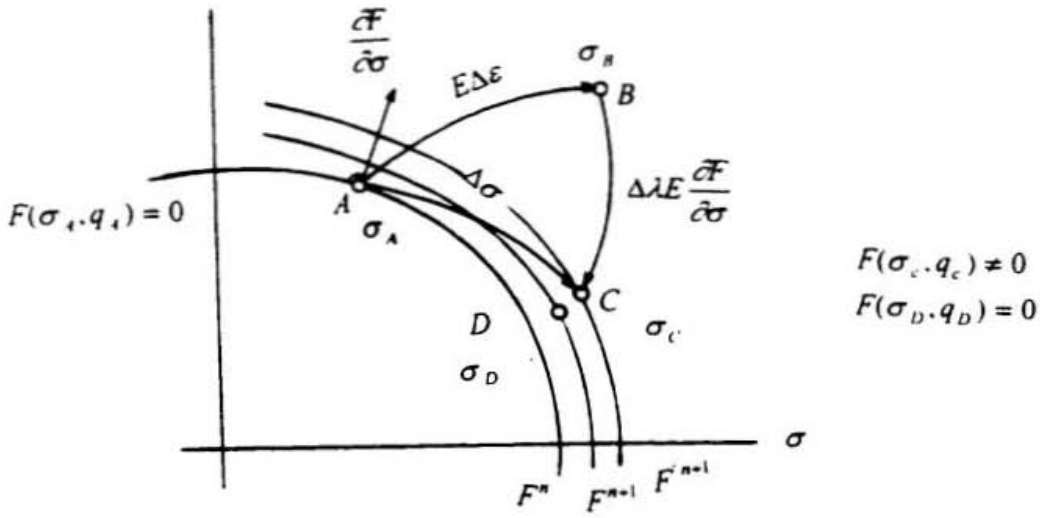

Fig. 3.1 Forward-Euler integration scheme

[NAFEMS, Introduction to Nonlinear Finite Element Analysis, ed. E. Hinton, 1991]

3.2.5 Plastic Multiplier

The linearized consistency condition is derived by expanding the yield criterion into a first order truncated Taylor series around the previous converged state.

$$F_{n+1} = F_n + \frac{\partial F}{\partial \sigma}(\sigma_{n+1} - \sigma_n) + \frac{\partial F}{\partial q}(q_{n+1} - q_n) = 0 \qquad (3\text{-}14)$$

This assumes that the previous stress state $F_n = 0$ is satisfied. The classical linearized consistency condition can be written as: it can be seen that the full consistency condition is not satisfied since $F_{n+1} \neq F_n + \Delta F_n$ except for linear yield surfaces and hardening/softening rules. In case of isotropic softening/hardening the internal variables degenerate into a single variable function of the plastic strain and are expressed as:

$$\Delta F = \frac{\partial F}{\partial \sigma} \Delta \sigma + \frac{\partial F}{\partial q} \Delta q_{n+1} = 0 \tag{3-15}$$

where:

$$\Delta q = \sqrt{tr(\Delta \varepsilon_p)^2} = \Delta \lambda \left| m \right| \tag{3-16}$$

Therefore, the plastic multiplier $\Delta\lambda$ can be expressed in an explicit form as:

$$|m| = \left[tr(m)^2 \right]^{1/2} = \left[tr(\frac{\partial Q}{\partial \sigma})^2 \right]^{1/2} \tag{3-17}$$

$$\Delta \lambda = \frac{tr(nE:\Delta \varepsilon)}{-\frac{\partial F}{\partial q} \left| m \right| + tr(nEm)} \tag{3-18}$$

3.2.6 Returning to the Yield Surface

In general, the previous method produces stresses that lie outside the yield surface. It is possible to simply scale the stresses at C, Figure 3.1 by a factor r until the yield surface f becomes zero, Ortiz and Popov (1985). However, this technique will generally involve an elastic component and thus it is not encouraged to use it. An alternative technique Ortiz and Simo (1986) suggests that the total strains are kept fixed while additional plastic strains are introduced in order to relax the stresses to the yield surface. Consequently Equation 3-13 can be repeated at point C, Figure 3.1 so that

$$\sigma_D = \sigma_C - \Delta \lambda E \frac{\partial f}{\partial \sigma} \Big|_C \tag{3-19}$$

If the resulting yield function at D, Figure 3.1, is insufficiently small, further relaxation can be applied.

3.3 Leon's Triaxial Strength Failure Criterion

The failure criterion proposed by Leon (1935) was for the shear strength of concrete under combined tension-compression. The extension of this failure criterion is widely used in the field of rock mechanics, where it is known under the names of Hook and Brown (1980). This strength formula combines the two-parameter Mohr-Coulomb friction law and the one-parameter tension cut-off condition of Rankine. Hook and Brown (1980) developed the isotropic failure criterion in terms of the major and minor principal stresses as:

$$F(\sigma_1, \sigma_3) = (\frac{\sigma_1 - \sigma_3}{f_c'})^2 + m_{hb} \frac{\sigma_1}{f_c'} - c_{hb} = 0 \qquad (3\text{-}20)$$

in which σ is the principal stress vector. It is clear that the influence of the intermediate principal stress is omitted, similar to the Tresca and Coulomb conditions of maximum shear. The triaxial failure criteria in Equation 3-20 are characterized by the uniaxial compressive strength f_c' , the frictional parameter m_{hb}, and the cohesion parameter c_{hb}. At failure, c_{hb} has a value of 1.0.

The friction parameter m_{hb} is calibrated in terms of the uniaxial tensiie strength, which has an important role in the fracture energy formulation. A uniaxial state of stress ($\sigma_3 = 0, \sigma_1 = f_t'$) results in

$$m_{hb} = \frac{c_{hb} f_c'^2 - f_t'^2}{f_c' f_t'} \qquad (3\text{-}21)$$

The triaxial failure surface proposed by Leon was used by Pramono and Willam(1988) and is depicted in Figure 3.2.

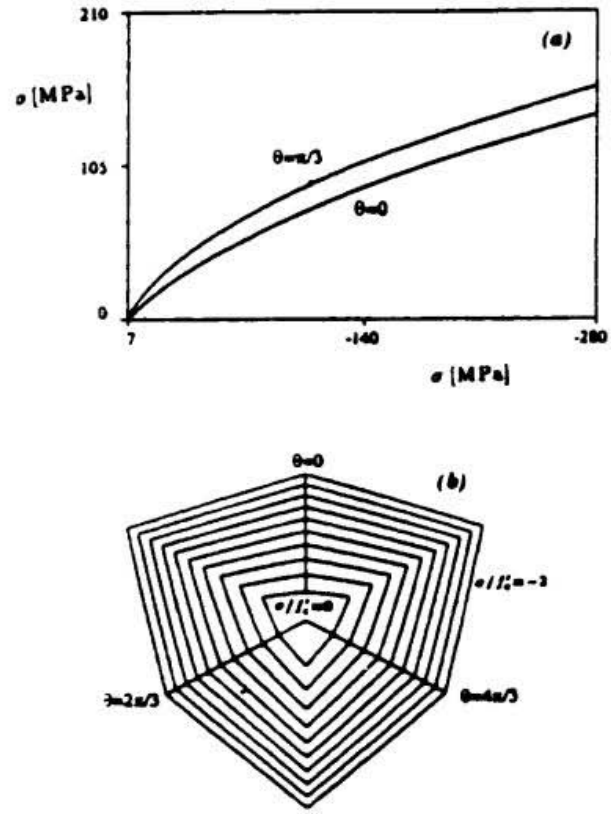

Fig. 3.2 Triaxial Failure Envelope of Leon (also used by Pramono and Willam (1988))

3.4 Extended Leon's Triaxial Strength Failure Criterion

The Extended Leon Model (ELM) combines the Leon-Pramono characterization, Pramono and Willam (1989) with the five-parameter model of Willam and Wranke (1975). That produces an elliptical approximation of the failure surface. Consequently, the corners in the deviatoric trace are eliminated. As a result, a C^1- Continuous failure surface is produced. There are several reasons for selecting these criteria such as

accuracy, simplicity, providing continuous transition between failure in direct tension and triaxial compression, and reducing calibration of the failure criterion to two strength parameters that are readily available from uniaxial-tension and uniaxial-compression data. Further, Hussein (1998) developed a new model for plain high strength concrete, which is based on the biaxial failure curves. The failure surface was defined in the finite element program. In addition, the ductility parameters A_h, B_h *and* C_h of Equation 3-35 are also calibrated from laboratory experiments at Memorial University of Newfoundland by Hussein (1998).

Using the three scalar invariant σ, the mean normal stress, ρ, the deviatoric stress, and the polar angle ϑ,

$$\begin{aligned} \sigma &= \frac{I_1}{3} \\ \rho &= \sqrt{2J_2} \\ \cos 3\vartheta &= \frac{\sqrt{27}J_3}{2J_2^{3/2}} \end{aligned} \qquad (3\text{-}22)$$

where

I_1 : first invariant of stress tensor,

J_2 : second invariant of stress deviator tensor

J_3 : third invariant of stress deviator tensor.

the relationship between the principal stresses and the Haigh-Westergaard coordinates can be given by:

$$\begin{Bmatrix}\sigma_1\\ \sigma_2\\ \sigma_3\end{Bmatrix} = \sigma\begin{Bmatrix}1\\ 1\\ 1\end{Bmatrix} + \sqrt{\frac{2}{3}}\rho\begin{Bmatrix}\cos\vartheta\\ \cos(\vartheta-\frac{2\pi}{3})\\ \cos(\vartheta+\frac{2\pi}{3})\end{Bmatrix} \tag{3-23}$$

this relationship is valid for $0 \le \vartheta \le \frac{\pi}{3}$ and consequently for $\sigma_1 \ge \sigma_2 \ge \sigma_3$. Substituting the principal stresses into Eq. (3-20) leads to

$$F(\sigma,\rho,\vartheta)=\left[\sqrt{2}\frac{\rho}{f_c}\sin(\vartheta+\frac{\pi}{3})\right]^2+m_o\left[\sqrt{\frac{2}{3}}\frac{\rho}{f_c}\cos\vartheta+\frac{\sigma}{f_c}\right]-c_o=0 \tag{3-24}$$

Introducing the following approximations into Equation 3-24

$$\sqrt{2}\sin(\vartheta+\frac{\pi}{3}) \approx \sqrt{1.5}r(\vartheta) \tag{3-25}$$

$$\sqrt{\frac{2}{3}}\cos(\vartheta) \approx \sqrt{\frac{1}{6}}r(\vartheta) \tag{3-26}$$

leads to the failure criteria of the ELM:

$$F(\sigma,\rho,\vartheta)=\frac{3}{2}\left[\frac{\rho r(\vartheta)}{f_c}\right]^2+\frac{m_o}{f_c}\left[\sigma+\frac{\rho r(\vartheta)}{\sqrt{6}}\right]-c_o=0 \tag{3-27}$$

This yield surface is a function of the three scalar invariant σ, the mean normal stress, ρ, the deviatoric stress, and the polar angle ϑ.

The elliptic variation of the five-parameter model $r(\vartheta)$ is given by the following equation:

$$r(\vartheta)=\frac{4(1-e^2)\cos^2\vartheta+(2e-1)^2}{2(1-e^2\cos(\vartheta)+(2e-1)\sqrt{4(1-e^2\cos^2\vartheta+5e^2-4e)}} \tag{3-28}$$

The eccentricity e is defined by the ratio ρ_t / ρ_c. The values of ρ_t and ρ_c can be found by considering the tensile ($\vartheta = 0$), and compressive meridians ($\vartheta = \pi / 3$) in Equation 3-27.

3.5 Isotropic Hardening Model for Pre-Peak Behavior

The hardening rule defines the motion of the subsequent yield surfaces during plastic loading. The expansion of the yield surface is called hardening, conversely a contracting yield surface denotes softening, and a stationary yield surface designates perfect plasticity. The hardening rule can be expressed in a general form as:

$$\dot{\varepsilon}_p = \dot{\lambda} H : \qquad \dot{q} = H \tag{3-29}$$

where H is a fourth order material tensor, $\dot{q}$ is normal vector to plastic potential surface in stress space and $\dot{\varepsilon}_p$ is equivalent plastic strain rate. The hardening rule can be expressed as:

- Work-hardening: $\dot{q}_w = tr(\sigma \dot{\varepsilon}_p)$

- Strain-hardening: $\dot{q}_c = tr(\dot{\varepsilon}_p)^{1/2}$

A number of hardening rules has been proposed such as isotropic hardening, kinematic hardening, and mixed hardening rules Chen (1982). Among these three hardening rules, the assumption of isotropic hardening is the simplest one to formulate mathematically

and it is used in this model. The isotropic rule requires only one parameter κ to define the subsequent yield surface after plastic deformation occurs. This hardening rule assumes that the yield surface expands uniformly without distortion as plastic deformation occurs. It should be noted that the isotropic hardening rule is adequate in modeling the behavior of concrete under monotonically loading conditions.

The isotropic hardening mechanism involves, in this case, an initial loading surface that expands uniformly when a hardening parameter, κ, increases monotonically from an initial value $\kappa = \kappa_o > 0$ to a final value at peak $\kappa = \kappa_p = 1$

$$F(\sigma, \rho, \vartheta, \kappa, c) = \left\{(1-\kappa)\left[\frac{\sigma}{f_c} + \frac{\rho^r(\vartheta)}{\sqrt{6} f_c}\right]^2 + \sqrt{\frac{3}{2}}\frac{\rho^r(\vartheta)}{f_c}\right\}^2 + \frac{\kappa^2 m}{f_c}\left[\sigma + \frac{\rho^r(\vartheta)}{\sqrt{6}}\right] - \kappa^2 c = 0 \tag{3-30}$$

The constitutive model assumes that the material is initially isotropic and remains isotropic during the entire deformation history irrespective of the orientation and magnitude of the principal stress components and inelastic deformations. The total stress increment can thus be decomposed into independent elastic and plastic components:

$$d\varepsilon = d\varepsilon_e + d\varepsilon_p \tag{3-31}$$

The elastic or recoverable response is governed by the linear isotropic material parameter, E.

$$\Delta\sigma = E d\varepsilon_e \tag{3-32}$$

3.6 Nonlinear Hardening Response

The strain-hardening hypothesis describes the current state of the inelastic deformation process in terms of a scalar-valued kinematic variable, ε_p, which defines the length of the plastic strain trajectory. During progressive plastic deformations, the value of the hardening parameter increases according to an elliptical function of ε_p. The influence of confinement on the rate of hardening is introduced in terms of a ductility measure X_p, which defines the accumulated plastic strain at peak in terms of the lateral confinement. As a result, the hardening parameter $\kappa = \kappa(\varepsilon_p, X_p)$ is expressed as a monotonically increasing elliptic function of the plastic strain:

$$\kappa = \kappa_o + \frac{1+\kappa}{\varepsilon_p}\sqrt{2\varepsilon_p X_p - \varepsilon_p^2} \tag{3-33}$$

The equivalent plastic strain rate is defined as the Euclidean norm of the plastic strain increment:

$$d\varepsilon_p = \sqrt{d\bar{\varepsilon}_p' : d\bar{\varepsilon}_p} \tag{3-34}$$

where $d\bar{\varepsilon}_p$ is the vector of principal plastic strain increments. The ductility measure X_p introduces the effect of confining pressure on the rate of hardening in terms of a quadratic polynomial of the mean normal stress, σ,

$$X_p = X_p(\sigma) = A_h\left(\frac{\sigma}{f_c'}\right)^2 + B_h\left(\frac{\sigma}{f_c'}\right) + C_h \tag{3-35}$$

The ductility parameters A_h, B_h *and* C_h are dimensionless deformation parameters that are

calibrated from laboratory experiments. Hussein (1998) has done the calibration of these parameters for high strength concrete.

3.7 Nonassociated flow rule

When the concrete deforms plastically, it is convenient to assume that, based on the normality condition, the incremental plastic strain, $d\varepsilon_p$, can be related to a plastic potential function, Q, by the following equation

$$d\varepsilon_p = d\lambda \frac{\partial Q}{\partial \sigma} \tag{3-36}$$

where $d\lambda$ is a plastic multiplier, and it is a positive scalar factor that may vary through the hardening process. It has a non-zero value only when plastic deformation occurs. The gradient of the potential surface, m= $\partial Q / \partial \sigma$, defines the direction of the incremental plastic strain vector $d\varepsilon_p$, and the length is determined by the factor $d\lambda$. Because the vector $\partial Q / \partial \sigma$ is normal to the potential surface, the plastic strain is also normal to the surface defined by the plastic potential function, Q. This condition is referred to as the normality law. In the simplest case when the plastic potential function and the yield function coincide ($Q = F$), then

$$d\varepsilon_p = d\lambda \frac{\partial F}{\partial \sigma} = d\lambda \frac{\partial Q}{\partial \sigma} \tag{3-37}$$

this equation is called the associated flow rule because the incremental plastic strains are associated with the yield function. If $Q \neq F$ then Equation 3-37 is termed a nonassociated flow rule. Generally, for pressure-sensitive materials, it is widely accepted

that the use of an associated flow results in the prediction of too much dilatancy. Thus, the associated flow rule does not hold for the whole range of response spectrum of concrete and it sometimes leads to great discrepancies between predicted and measured response, as well as load carrying capacities.

Etse and Willam (1994) applied a nonassociated flow rule, which defines the plastic strain rate as:

$$d\bar{\varepsilon}_p = d\lambda \, m \qquad \text{with} \qquad m = \frac{\partial Q}{\partial \sigma} \tag{3-38}$$

The plastic potential for nonassociated flow is based on a modification of the loading surface as

$$Q(\sigma, \rho, \vartheta, \kappa, c, m_q) = \left\{ (1-\kappa) \left[\frac{\sigma}{f_c} + \frac{\rho r(\vartheta)}{\sqrt{6} f_c} \right]^2 + \sqrt{\frac{3}{2}} \frac{\rho r(\vartheta)}{f_c} \right\}^2 + \frac{\kappa^2}{f_c} \left[m_Q + m \frac{\rho r(\vartheta)}{\sqrt{6}} \right] - \kappa^2 c = 0 \tag{3-39}$$

The friction parameter $m \rightarrow m_Q(\sigma)$ which is redefined in terms of its gradient

$$\frac{\partial m_Q}{\partial \sigma} = D \exp(E x^2) + G \qquad \text{where} \qquad x = \frac{-\sigma + f_l' / 3}{f_c'} \tag{3-40}$$

The material parameters $D, E,$ and G are calibrated from test results. The gradient of the plastic potential is evaluated by the chain rule of differentiation

$$m = \frac{\partial Q}{\partial \sigma} = \frac{\partial Q}{\partial \sigma}\frac{\partial \sigma}{\partial \sigma_{ij}} + \frac{\partial Q}{\partial \rho}\frac{\partial \rho}{\partial \sigma_{ij}} + \frac{\partial Q}{\partial \vartheta}\frac{\partial \vartheta}{\partial \sigma_{ij}} \qquad (3\text{-}41)$$

where

$$\frac{\partial Q}{\partial \sigma} = \frac{\partial F}{\partial \sigma} = \frac{\kappa^2}{f_c'}\left(\frac{\partial m_Q}{\partial \sigma} - m\right); \qquad \frac{\partial Q}{\partial \rho} = \frac{\partial F}{\partial \rho}; \qquad \frac{\partial Q}{\partial \vartheta} = \frac{\partial F}{\partial \vartheta} \qquad (3\text{-}42)$$

3.8 Tension Softening Behavior

Various types of tension softening models have been proposed for plain concrete in uniaxial tension: linear, bilinear, exponential, rational, etc., which are available in literature (Bazant and Oh (1983); Massicotte et al. (1990); Scanlon (1972); Lin and Scordelis (1975); Cope (1984)).

The softening response is initiated when the concrete starts cracking, due to increasing loading, in tension or low confined compression in triaxial tests. In direct tension, (Mode I type cracking), the fracture process is based on the fictitious crack model by Hillerborg, Modeer and Petersson (1976). This failure concept will be extended to model Mode II (shear) type of failure in chapter 7, since the cracking and post-cracking behavior is a very important feature of high strength concrete. The tension softening model is significant for any accurate nonlinear analysis of high strength concrete structural members.

3.9 Summary

A plasticity model that previously was developed for describing the response of plain high strength concrete is described. The model is required for strength degradation due to cracking, strength enhancement due to confinement, pre- and post- peak stress-strain response in tension or compression and other study parameters. The extended five-parameter material model of Etse and Willam (1994) was found to be an ideal model for considering the effect of tension stiffening of high strength concrete. The modification proposed by Hussein (1998) to implement the model for high strength concrete is examined. A brief explanation is given, concerning the characterized parameters of concrete model such as yield surface, hardening behavior, non-associated flow rule and softening behavior in compact form are discussed.

Chapter 4

Experimental Investigation on the Bond Behavior of High Strength Concrete

4.1 Introduction

High strength concrete is used mostly in construction of bridges, tall buildings and marine structures. Bond strength between high strength concrete and rebar is an important factor for the strength and stability of these reinforced concrete structural elements. The behavior of bond under increasing pull out load can be described by the initiation of inclined cracks at contact points between the steel lugs and concrete at relatively low stresses, crushing of concrete in front of the lugs, and shearing-off of an increasingly larger part of concrete keys between the lugs until the keys are fully sheared off. The results of the experimental studies reported by Eligehausen, Popov and Betero (1983) indicated that the key factors determining local bond stress-slip characteristics of deformed bars embedded in concrete are: the effect of load history, confining reinforcement, rebar diameter, concrete strength, rebar spacing, rate of pull out, and

deformation pattern. Further investigation showed that several other parameters such as casting position, size of cover, specimen dimension, transverse pressure, crack width, aggregate size, reinforcement coating and creep can affect the bond strength.

This chapter will provide a summary of the experimental program conducted at the structural laboratory of Memorial University of Newfoundland to investigate the behavior of bond of high strength concrete. The test set-up, load application, instrumentation, measurement, the procedure of test, and type of materials are the main subjects of discussion in this chapter.

4.2 Selection of Test Set-up

Several methods of testing can be considered for pursuing experimentally the bond strength between rebar and high strength concrete. These methods include pull out test, single span beam test and beam-column connection as reported by early experimental studies. Several investigators used the method of pull out testing. It includes a short length of a rebar embedded in a cube or cylindrical concrete taking into consideration the other parameters in order to idealize reinforced concrete joints. The single span beam method was considered to study the bond strength by applying a concentrated load on a beam. Since the method of testing must not affect the result of the research investigation, the pull out method has been considered for the present study. The availability of laboratory equipment is another factor for choosing the test method.

4.3 Experimental Program

The experimental phase of this investigation was designed to test the confined region of a joint in a high strength concrete structure in order to study the behavior of the bond between rebar and high strength concrete. A total of 150 specimens were tested under monotonic and cyclic loading. The load history, confining reinforcement, rebar diameter, concrete strength, rebar spacing, rate of pull out, and deformation pattern were considered as the main study parameters. The study parameters were evaluated under monotonic loading in tension and compression, cyclic loading (full cycles), and cyclic loading at selected peak slip values. The internal strain in concrete close to the contact surface area was measured.

A summary of the test program is presented in Tables 4.1 to 4.5. The tests are subdivided into seven series for the 25 mm rebar diameter as well as seven series for 35 mm rebar diameter. Only one parameter has been changed at a time, while all other parameters were kept constant. The influence of study parameters on the bond behavior under monotonic and cyclic loading was examined.

4.3.1 Load History

The test for examining the influence of load history was run under monotonic loading in tension and compression. The adopted standard rate of pull out, 1.50 mm displacement per minute, was chosen mainly for practical reasons to complete a test in a reasonable time. It is about twelve times faster than the loading rate for the load controlled pull out rate used by Eligehausen, Popov and Betero (1983). During an

earthquake motion the rebar is normally subjected to a larger strain rate. Therefore, the rate of pull out is increased to 75 mm slip per minute.

4.3.2 Confining reinforcement

It is understood that the force in the contact surface of rebar and high strength concrete has two components. One is parallel to the axis of rebar and the other is radial component that is perpendicular to the axis of rebar. The radial forces can cause extra stresses in the concrete. These are normally the source of the crack and ultimate crushing of concrete. In order to prevent the failure of concrete some extra reinforcement as confinement is necessary. The failure of high strength concrete without confinement is accompanied by the release of a huge amount of energy, which is extremely harmful to the structure. The bond behavior of high strength concrete under radial confining stress around the concrete specimen, together with bond stress and slip was considered in this investigation. Different sizes of rebars were used as confinement for the specimen in this experimental investigation. In addition, some specimens were tested without confining reinforcement.

4.3.3 Rebar Diameter

The rebar diameters were changed and the influence of rebar diameter was investigated. The rebar diameters were varied from 20, 25 and 35 mm. The diameters of 20 and 25 mm are mostly used in the construction of buildings and bridges while the rebar diameter of 35 mm and higher is normally used in offshore structures.

4.3.4 Concrete Strength

According to the American Concrete Institute (ACI), high strength is defined as concrete with ultimate compressive strength over 42 MPa. Different values of concrete including nominal f_c' = 50 MPa, 75 MPa, 100 MPa were tested and the results are reported.

4.3.5 Rate of Loading

It is commonly understood that excessively rapid loading can cause a notable increase in the strength of steel and concrete members. For structures having a small period of vibration and a high ductility demand, the strain rates are surprisingly high and may result in significant strength increase of the materials. Since most of the structures are designed to resist against dynamic loading such as seismic loading, it is important to examine the bond behavior of high strength concrete under different rates of loading. For this purpose, the rates of loading were changed from 0.0151, 1.51, to 75 mm/min to achieve the influence of this parameter.

4.3.6 Spacing

Undoubtedly for reinforced concrete elements the distance between rebars is extremely important. The effect of spacing was examined, taking into consideration two different spacings. The first one was equivalent to the rebar diameter and the second one was equal to twice the rebar diameter.

4.3.7 Deformation Pattern

Clark (1946), Darwin and Graham (1993), Hamad (1995), Tholen and Darwin (1998), Esfahani and Rangan (1998) studied the effect of the deformation pattern for normal and high strength concrete. The effect of deformation pattern on the bond behavior in the previous studies was given a high degree of importance. In this investigation the influence of different rib geometries on the bond of high strength concrete are examined and the results are evaluated. The details of rib geometries are illustrated in Table 4.6.

4.4 Test specimens

The test specimen represented the confined region of a joint in high strength concrete structures. The reinforced high strength concrete specimen was confined by secondary reinforcement representing the joint reinforcement. Extra top and bottom stirrups were added to the specimens to ensure good confinement of the rebars.

A typical illustration of the test specimen that was considered in this investigation is shown schematically in Figure 4.1. A test specimen before casting the concrete is shown in Figure 4.2. The designed specimen represents the local bond behavior of deformed bars in a confined region of a beam-column connection of high strength concrete. A short length of the deformed rebar was embedded in the high strength concrete block as well as secondary reinforcement was provided with top and bottom stirrups. The embedment lengths of rebar diameters of 25 and 35 mm were taken as 75 and 100 mm, respectively. This embedment length is short enough to result in a fairly

uniform bond stress when the rebar is pulled-out, but not long enough to reduce the scatter usually observed in test results when a very short bonded length is used. The bond length was positioned in the middle of the specimen at the confined concrete region.

The arrangement of bond position was designed such that the bond length was located at the middle of the specimen and the other two ends of the rebar were enclosed in a tube to eliminate bond. The tubes were made of (P.V.C.) material and were neither restrained by the slip of the bar nor affected by the transfer of bar forces to the total length of the specimens.

4.5 Material

High strength concrete was made with the same basic ingredients as normal strength concrete plus mineral and chemical admixtures. It was the result of optimization of the characteristics of the cementing medium, characteristics of the aggregate interaction, proportions of the paste, paste-aggregate interaction, mixing and consolidating and curing, and testing procedures.

High strength concrete is being used in structures, which are located in harsh environments. These structures are subjected to tremendous forces from wave loading and impacts from wave-tossed debris in offshore and marine structures. In addition, the influences of wetting and drying, freezing and thawing, abrasion by ice and other debris, chemical attack or mineral depletion by water it is in, salt accumulations, and attack by marine organisms are important. Therefore, in last decades several researchers including

Hoff (1989), Marzouk (1987), Malhotra (1988) in North America as well as other researchers in Europe investigated the material characteristics of high strength concrete.

Broad research has been directed to develop the best mixing proportions and mixing procedure to produce high strength concrete using local Newfoundland aggregates and cement at the structural laboratory of the faculty of Engineering and Applied Science of Memorial University of Newfoundland, St. John's, Canada. In addition, various other aspects of this new material, such as the effect of low ocean temperature on strength and elasticity, creep of high strength concrete at low temperatures, freezing and thawing resistance of high strength concrete have been investigated in detail. Local test results indicated that local materials can be used with silica fume and fly ash to provide a strength of 70 MPa and higher at 28 days curing, Marzouk and Hussein (1990). The effect of low temperature has a minor effect on strength, elasticity and stress-strain relationship as detailed by Marzouk and Hussein (1990). The relation of creep to stress strength ratio at room temperature was found to be linear for silica fume concrete, as was the case for ordinary Portland cement concrete as reported by Marzouk (1992). The changes in weight, length, pulse velocity, resonant frequency, compressive strength, due to freezing and thawing were recorded for 458 cycles. As a result, high strength concrete made with local material and having about 3-5% air content is durable up to 458 cycles, Marzouk (1990).

Hoff (1991) investigated the advantages of supplementary cementing materials in offshore and marine concrete structures. The ability of concrete to resist the influences of the environment while performing its desired function was called durability. The need of

durable concrete for construction of offshore and marine structures was predicted and recommendations for improving the quality of high strength concrete have been made. Furthermore, Hoff (1998) presented some information about material characteristics of high strength concrete such as creep and shrinkage, air void parameters, permeability, and chloride-ion permeability used in the Hibernia offshore platform. In this section the material used for high strength concrete mixture is explained.

4.5.1 Cement

Producing high strength concrete depends on the quality of the cement paste. Selection of a Portland cement for high strength concrete should be based on comparative strength tests of concrete at 28 and 90 days. Cement that yields the highest compressive strength at the later age (90 days) is preferable. The high strength concrete mixture for this investigation contained normal Portland cement. Normal Portland cement Type 10, Canadian Standards Association (CSA); CSA3-AS5 as produced in Newfoundland, Canada was used for all test specimens. About 10 percent replacement by silica fume (pozzolanic materials) in a powder form of a total cementatious product was used on the basis of weight. The silica fume has a specific gravity of 2.30 and surface area equal to 200,000 cm^2/gm, which is about 50 times finer than most Portland cements.

4.5.2 Mineral Admixtures

Silica fume played an important role in the development of high strength concrete. Silica fume is a mineral admixture added to concrete to improve plastic or hardening properties of Portland cement concrete. Silica fume used for concrete must

meet the requirement of ASTM C1240-88. The addition of silica fume increases the cohesiveness, viscosity, and water demand of fresh concrete. However, the increased strength remains the main reason for using silica fume in most high strength concrete applications.

Hoff (1991) reported that the effect of silica fume on concrete depends both on its fineness and its pozzolanic activity. The fineness creates more hydration for cement and produces a denser microstructure of the hydration product than without such dispersion. Thus, it reduces the size of capillary porosity and provides a greater probability of discontinuous porosity without affecting total porosity. The pozzolanic activity increases the amount of gel porosity. Both effects decrease the number of gel pores in the hydrated cement, in turn reduce water that freezes in winter ambient conditions. The probability then, of creating concrete with more dense gel, is greater for concrete containing silica fume than without dense gel. The greater discontinuity of porosity decreases permeability. It can be used as either an addition to or replacement for cement usually at dosage rates up to 15 percent. Air entertainment (4 to 6 percent) of concrete containing silica fume or other pozzolans has been shown to be essential for resistance to freezing and thawing.

4.5.3 Chemical Admixtures

The admixtures consisted of superplasticizer based on a pure naphthalene sulphonate mixed in combination with retarder with catalysts promoting more cement hydration to obtain greater compressive strengths. The superplasticizer significantly reduces the amount of water required, but it often increases slump loss, making it difficult

to place the concrete properly even though true setting time is extended slightly. The high rate of slump loss is overcome by the addition of the water-reducing retarder, which extends the time of set and permits the placement of a very low water-cement ratio concrete. Both chemical admixtures should meet the requirement of ASTM C 494-86.

4.5.4 Coarse Aggregate

The largest fraction of the volume of concrete consists of coarse aggregate. The characteristics of the aggregate significantly influence the properties of the concrete, including strength. The strength of the aggregate, the bond or adhesion between the cement paste and aggregate, and the absorption characteristics of the aggregate are very important for the design of high strength concrete mix. There is a practical value for determining the optimum size of coarse aggregate for different concrete strength levels. The optimum size depends on such factors as: relative strength of the cement paste, cement-aggregate bond, and strength of the aggregate particles. Standard tests are not readily available to measure these factors adequately. The chemical content of the aggregate and the mineral content does lend some insight into predicting the interaction between cement paste and aggregate particles. Still, trial batches provide the most practical information for choosing the best aggregate for a concrete mixture. For this investigation a normal weight local coarse aggregate was used in the mixture and it was mostly crushed granite with a maximum nominal size of 20 mm. Sieve analysis of the aggregates was conducted according to ASTM C135-86. The results of sieve analysis are given in Table 4.7. The specific gravity and absorption percentage were determined in

accordance with ASTM C127-88 and ASTM C128-88, the specific gravity of coarse aggregate was 2 65 and absorption 0.48%, respectively.

4.5.5 Fine Aggregate

The shape and surface texture of fine aggregate has a greater influence on water demand of concrete than that of coarse aggregate since fine aggregates contain a much higher surface area for a given weight. The grading of fine aggregate within typical specification limits is not highly critical except that slightly coarse sand probably would be more beneficial if available and not economically prohibitive. Sieve analysis of the aggregates was conducted according to ASTM C135-86. The results of sieve analysis are given in Table 4.8. The specific gravity of fine aggregate was 2.73 and absorption 0.42%.

4.5.6 Mixing Water

The mixing water in the mixture was clear and about 4 ^{0}C. The ratios of water to cement for concrete with compressive strength of 50 MPa, 75 MPa, 100 MPa were 0.35, 0.29, 0.26, respectively.

4.5.7 Concrete Mixture Design

The high strength concrete mixture contained a normal Portland cement, type 10 in accordance with Canadian Standards Association (CSA), and content of silica fume used on the basis of weight. Local aggregates were used as explained in the above sections. The coarse aggregate were mostly crushed quartzite sandstone with a maximum

nominal size of 20 mm. The fine aggregate was identical in composition to the coarse aggregate with a minor percentage of siltstone and shale. A non-chloride water-reducing agent and retarder and superplasticizer of sulphonated naphthalene formaldehyde base were also used in the mixture for high strength concrete. Table 4.8 gives the mix proportions of the concrete used. The batching of the concrete was done in a 0.1 m^3 laboratory mixer. A drum type (Turbine) mixer was used for mixing the concrete batch. The mixer was used for 90 to 120 seconds at a rate of 18 rpm. The mix was sticky and cohesive. At least three concrete cylinders, 152x304 mm, were taken from each batch and used to determine the concrete compressive strength f'_c. The mix design was tried several times and concrete cylinders were cast in a plastic or cardboard molds in accordance to ASTM C192-88. The test specimens were cured under polyethylene sheets in the form and dispersed by water for an average one week. The cylinders were cured for four weeks and tested.

The slump values were 100 mm and the density of the high strength concrete was 2400 kg/m^3 in average. The strains at maximum stresses ranged from 0.0025 to 0.0035. A soil test machine was used for the loading of cylinder specimens using a hydraulic compressive ram capable of providing a maximum compression of 2670 kN. (600.000 lbs.). The value of modulus of elasticity ranged from 26.0 to 27.5 GPa.

4.5.8 Rebar

The reinforcing rebars were Grade 400 steel conforming to CAN/CSA-G40.20-M92. Two samples of each rebar size with diameter of 10, 25, and 35 mm were tested for tensile strength. T-Olsen hydraulic machine was used to apply load and electrical strain

gauges were used to measure the strain up to the yielding and Linear Potential Differential Transducers (LPDT) were used to measure the elongation up to the failure. The properties of the steel reinforcement are given in Table 4.9. All deformation patterns for rebars of Series M7 were machined. The nominal diameters were 25 mm and 35 mm. The details of rib geometry for series M7 are illustrated in Table 4.6, while the standard deformation pattern was used for rest of the experiments.

All rebars were cut to the desired length. One side of the rebars was threaded for 50 mm and 75 mm in the case of monotonic tests for rebar with diameter of 25 and 35 mm, respectively. In the case of cyclic tests the length of threaded rebars were 135 and 165 mm for rebars 25 and 35 mm, respectively.

4.6 Fabrication of Test Specimens

Two sets of forms were prepared for casting the bond specimens. The first set was for specimens with rebar diameter of 25 mm and concrete dimensions of 375x250x150 mm. The second set was used for the specimens with reinforcement 35 mm and concrete dimensions of 525x250x175 mm. The casting position was from the side of the form as shown in Figures 4.3 & 4.4. All reinforcements have been machined to fit in the test set-up and depend on the study parameters; some strain gauges were installed as necessary as shown in Figure 4.4. In order to examine the behavior of concrete around the rebar, some strain gauges were installed inside the concrete, close to the contact surface, to measure internal concrete strain as shown in Figure 4.4.

4.7 Test Set-up

A test frame was designed to carry out this experimental program and some extra parts were designed and fitted to facilitate the bond strength investigation. Figure 4.8 schematically shows the test set-up and Figure 4.11 shows a photograph of the test set-up with a specimen mounted. The vertical loading frame consisted of two main vertical W-shape columns connected by two horizontal cross channels. The channels were braced together by means of several plates. The vertical columns were bolted to two inclined wide flanged steel columns that acted as a horizontal brace to the frame. To increase the stiffness of the loading frame two solid vertical 50 mm rods were bolted to the horizontal beam and few steel plates were added.

4.8 Instrumentation

An electrohydraulically controlled testing actuator with capacity 1350 kN was used to apply monotonic tensile and compression load as well as for cyclic loading. The general arrangement of the closed-loop test scheme and associated instrumentation is shown in the block diagram, Figure 4.10. The load cell attached to the actuator measured the load. The load cell was connected to an internal amplifier via the controller. The output voltage from the controller was feed into the input channel of the data acquisition system. The test was run under displacement control. The displacement was measured at the loaded rebar end by using the built in Linear Variable Differential Transducer (LVDT) in the actuator and by an external Linear Potential Differential Transducer (LPDT) mounted at the unloaded end of the rebar. In order to minimize the friction

between specimen and the upper head of the test set-up, a teflon sheet was used between the specimen and the bearing plate. The slip was controlled at a rate of 1.51 mm/min for deformed reinforcement. It adjusted by Servo-valve Controller in the Laboratory. Concrete strain gauges were located close to the contact surface of the rebar and concrete. The concrete strain gauges were placed around the bond area in a proper position. The steel strain in the middle of the bond area as well as outside the bond area was measured by strain gauges. A load cell situated in the actuator measured the applied force. The output of strain gauges together with load and displacement data were continuously scanned and recorded by use of a data acquisition system and constantly displayed through a computer. The slip was measured as the relative displacement between the reinforcement with respect to high strength concrete minus the elongation of the rebar outside of the bond area. The bond length is located at the middle of the specimen. It was assumed that the stress distribution is uniform.

4.9 Data Acquisition System

The data acquisition system was used to record the test results and analyze the data. The data acquisition system has six basic subsystems which include the controller, the signal conditioner, the multiplexed amplifier, the analog-to-digital converter, the storage or memory unit, and the readout devices. The controller is a microprocessor that serves as the interface between the operator and the data-acquisition system. The signal conditioner consists of the power supply, the bridges, and the terminals used to connect a large number of gauges in turn to the multiplexer. Usually, several bridges are contained

on a plug-in circuit board, which can be modified by adding or deleting fixed resistors to provide for quarter, half, or full-bridge arrangements. The multiplexer portion of the signal conditioner-scanner subassembly consists of two parts: (1) A bank of switches serves to switch the two output leads and the cable shield from the bridge to the differential amplifier. (2) The multiplexer also contains the circuits that control the switching sequence as programmed in the controller. The amplified analog signal is converted into a digital signal by using an analog-to-digital converter. The data is output from the interface unit on a parallel wired data bus. Usually it is stored temporarily in the random-access memory on a first-in first-out basis. The data can be processed in real time on a host computer. The disks provide the input data, in digital format, to an off-line computer where the data is processed. Gen 200 software is used to assist the organization of data files and the transfer of data files to spreadsheets for subsequent processing.

4.10 Strain Gauge

Several types of strain gauges were available for measuring strain such as mechanical, optical, electrical, acoustical strain gauges; electrical strain gauges have been used in this investigation. The length of the electrical strain gauge was 10-mm, 120 Ω resistance with a gauge factor of 2.04 ± %0.5. The excitation range for strain gauges was checked, this range was between 2.5 to 10 volts. Generally, the characteristics of a strain gauge include the gauge length, accuracy or precision, range (the maximum strain that can be recorded without rezeroing or replacing the strain gauge), sensitivity of the gauge due to the smallest value of strain that can be read on the scale associated with the strain

gauge. These characteristics along with budget limitation were evaluated for choosing the most suitable type of the gauges for the test.

4.11 Installation of Strain Gauge

The small concrete prisms were selected and strain gauges were glued to measure the internal concrete strain as described previously. The electrical strain gauges also were used to measure steel strain. In order to install a strain gauge on the surface of rebar or on the precast concrete prism, the surface was prepared. This preparation consisted of sanding away any rust, dust or paint to obtain a smooth but not highly polished surface. Next, solvents were employed to remove all traces of oil and the surface was etched with an appropriate acid. Finally, the clean, sanded, degreased, and etched surface was neutralized (treated with a basic solution) to give it the proper chemical affinity for the adhesive. The gauge location was then marked on the specimen and the gauge was positioned by using a rigid transparent tape. The tape maintains the position and orientation of the gauge as the adhesive is applied and as the gauge is pressed into place by squeezing out the excess adhesive. After the gauge was installed, the adhesive was exposed to a proper combination of pressure and temperature for a suitable length of time to ensure a complete curing. For protection against any possible water damage during casting, water proofing such as M-coat D kind of chemical material including Flammable toluene 50% and rubber splicing tape were applied for coating as shown in Figures 4.5 and 4.6.

4.12 Summary

A total of 150 specimens made of high strength concrete were cast to investigate the bond strength under monotonic and cyclic loading. The influences of load history, confining reinforcement, rebar diameter, concrete strength, rebar spacing, rate of pull out, and deformation pattern were investigated experimentally. The internal concrete close to the contact surface and also in the steel rebar was measured. The test set up, load application, instrumentation and measurement, test procedure, and type of materials are reported.

Table 4.1- Experimental Program for Monotonic Test (M1, M2, M3, M4, M5)

Series	Investigation Parameter	Loading History	Specimen Notation	Rebar Diameter	Concrete Strength f'c	Vertical Confinig Rebar	Slip Rate	Type of Deformation Pattern
				mm	MPa	mm	mm/min	
M1	**Load History**	Monotonic in Tension	1HNM-19-1	35	85.00	10	1.51	Canadian Standard
			1HNM-19-1A	35	81.00			
			1HNM-19-1B	35	81.00			
			1HNM-19-1C	35	81.00			
		Monotonic in Compression	1HNM-19-2A	35	81.00			
			1HNM-19-2B	35	85.12			
			1HNM-19-2C	35	83.16			
		Monotonic in Tension	1HNM-19-1	**25**	81.70	10	1.51	Canadian Standard
			1HNM-19-1A	**25**	86.00			
			1HNM-19-1B	**25**	85.12			
			1HNM-19-1C	**25**	85.12			
		Monotonic in Compression	1HNM-19-2	**25**	83.60			
			1HNM-19-2A	**25**	83.67			
			1HNM-19-2B	**25**	83.67			
			1HNM-19-2C	**25**	83.67			
M2	**Confining Reinforce.**	Monotonic in Tension	2HNM-8-1	35	85.00	No Conf.	1.51	Canadian Standard
			2HNM-8-2	35	85.00	10		
			2HNM-8-3	35	85.00	20		
			2HNM-8-4	35	85.00	25		
		Monotonic in Tension	2HNM-8-1	**25**	81.70	No Conf.	1.51	Canadian Standard
			2HNM-8-2	**25**	81.70	10		
			2HNM-8-3	**25**	85.00	20		
			2HNM-8-4	**25**	85.00	25		
		Monotonic in Compression	2HNM-8-1	**25**	81.70	No Conf.	1.51	Canadian Standard
			2HNM-8-2	**25**	81.70	10		
			2HNM-8-3	**25**	85.00	20		
			2HNM-8-4	**25**	85.00	25		
M3	**Rebar Diameter**	Monotonic in Tension	3HNM-12-1	20	78.00	10	1.51	Canadian Standard
			3HNM-12-2	25	90.30			
			3HNM-12-3	35	87.45			
M4	**Concrete Strength**	Monotonic in Tension	4HNM-12-1	35	50.61	10	1.51	Canadian Standard
			4HNM-12-2	35	87.45			
			4HNM-12-3	35	91.45			
			4HNM-12-4	35	92.70			
			4HNM-12-1	**25**	50.61	10	1.51	Canadian Standard
			4HNM-12-2	**25**	86.00			
			4HNM-12-3	**25**	92.61			
			4HNM-12-4	**25**	94.96			
M5	**Bar Spacing** (1db) (2db)	Monotonic in Tension	5HNM-4-1	35	86.59	10	1.51	Canadian Standard
			5HNM-4-2	35	94.64			
			5HNM-4-1	**25**	90.30	10	1.51	Canadian Standard
			5HNM-4-2	**25**	92.61			

Table 4.2- Experimental Program for Monotonic Test (M6, M7)

Series	Investigation Parameter	Loading History	Specimen Notation	Rebar Diameter	Concrete Strength f'c	Vertical Confinig Rebar	Slip Rate	Type of Deformation Pattern
				mm	MPa	mm	mm/min	
M6	**Rate of Loading**	Monotonic in Tension	6HNM-6-1	35	89.00	10	1.5100	Canadian Standard
			6HNM-6-2	35	87.45		0.0151	
			6HNM-6-3	35	78.00		75.0000	
			6HNM-6-1	25	83.30	10	1.5100	Canadian Standard
			6HNM-6-2	25	83.67		0.0151	
			6HNM-6-3	25	83.30		75.0000	
M7	**Rebar Deformation Pattern**	Monotonic in Tension	7HNM-14-1	35	83.15	10	1.51	See Table 4.6
			7HNM-14-2	35	83.15			
			7HNM-14-3	35	83.15			
			7HNM-14-4	35	83.15			
			7HNM-14-5	35	82.93			
			7HNM-14-6	35	82.93			
			7HNM-14-7	35	82.56			
			7HNM-14-8	35	82.56			
			7HNM-14-9	35	89.52			
			7HNM-14-10	35	89.52			
			7HNM-14-11	35	86.23			
			7HNM-14-12	35	86.23			
			7HNM-14-13	35	74.75			Plain
			7HNM-14-14	35	81.00			Standard
			7HNM-10-1	25	94.64	10	1.51	See Table 4.6
			7HNM-10-2	25	94.64			
			7HNM-10-3	25	92.00			
			7HNM-10-4	25	86.70			
			7HNM-10-5	25	86.00			
			7HNM-10-6	25	86.00			
			7HNM-10-7	25	86.70			
			7HNM-10-8	25	88.79			
			7HNM-10-9	25	86.00			Standard
			7HNM-10-10	25	90.26			Plain

Table 4.3- Experimental Program for Cyclic Test (M1, M2)

Series	Investigation Parameter	Loading History	Specimen Notation	Rebar Diameter	Concrete Strength f'c	Vertical Confinig Rebar	Min. Number of Cycle	Rate of Loading		Type of Deformation Pattern
									Last Cycle	
				mm	MPa	mm		S=+/-(mm)	S=+/-(mm)	
M1	Load History	Cyclic	1HND-19-3	35	93.67	10	10	3.00	6.10	Canadian Standard
			1HND-19-4	35	93.67			3.75	7.50	
			1HND-19-5	35	93.67			3.75	7.50	
			1HND-19-6	35	93.67			3.75	8.00	
			1HND-19-7	35	86.00			4.20	4.20	
			1HND-19-8	35	86.00			4.20	4.20	
			1HND-19-3	25	81.00	10	10	-	-	Canadian Standard
			1HND-19-4	25	81.00			3.00	18.50	
			1HND-19-5	25	81.00			3.75	3.75	
			1HND-19-6	25	81.00			3.75	18.50	
			1HND-19-7	25	81.00			4.25	19.00	
M2	Confining Reinforce.	Cyclic	2HND-8-5	35	89.00	10	10	3.10	6.20	Canadian Standard
			2HND-8-6	35	86.20	No Conf.		3.10	6.40	
			2HND-8-7	35	86.20	20		4.00	9.00	
			2HND-8-8	35	86.20	25		5.50	5.50	
			2HND-8-5	25	88.10	No Conf.	10	2.50	2.50	Canadian Standard
			2HND-8-6	25	88.62	10		2.50	2.50	
			2HND-8-7	25	88.62	20		4.30	6.25	
			2HND-8-8	25	88.62	25		5.50	10.00	
			2HND-8-9	25	88.62	No Conf.		5.50	5.50	

Note S displacement

Table 4.4- Experimental Program for Cyclic Test (M3, M4)

Series	Investigation Parameter	Loading History	Specimen Notation	Rebar Diameter	Concrete Strength f'c	Vertical Confinig Rebar	Min. Number of Cycle	Rate of Loading		Type of Deformation Pattern
									Last Cycle	
				mm	MPa	mm		S=+/-(mm)	S=+/-(mm)	
M3	**Rebar Diameter**	Cyclic	3HND-12-5	20	87.45	10	10	3.75	3.75	Canadian Standard
			3HND-12-6	25	94.64			3.75	12.00	
			3HND-12-7	30	93.31			3.75	12.00	
			3HND-12-8	35	85.17			2.40	7.50	
			3HND-12-9	20	87.45			5.00	5.00	
			3HND-12-10	25	89.52			5.00	5.00	
			3HND-12-11	30	87.45			5.00	18.50	
			3HND-12-12	35	85.17			5.00	5.00	
M4	**Concrete Strength**	Cyclic	4HND-12-5	35	50.61	10	10	3.75	7.50	Canadian Standard
			4HND-12-6	35	83.3			3.75	7.50	
			4HND-12-7	35	92.65			3.75	7.50	
			4HND-12-8	35	90.00			4.00	19.00	
			4HND-12-9	35	50.61			-	-	
			4HND-12-10	35	88.62			5.00	10.00	
			4HND-12-11	35	92.65			4.00	10.00	
			4HND-12-12	35	90.12			5.00	5.00	
			4HND-12-5	25	50.61	10		3.75	3.75	Canadian Standard
			4HND-12-6	25	78.00			3.75	12.50	
			4HND-12-7	25	92.65			3.75	7.50	
			4HND-12-8	25	95.00			3.75	7.50	
			4HND-12-9	25	50.61			5.00	5.00	
			4HND-12-10	25	85.17			4.00	4.00	
			4HND-12-11	25	92.65			4.00	4.00	
			4HND-12-12	25	95.00			4.00	4.00	

Note : S displacement

Table 4.5- Experimental Program for Cyclic Test (M5, M6)

Series	Investigation Parameter	Loading History	Specimen Notation	Rebar Diameter	Concrete Strength f'c	Vertical Confinig Rebar	Min. Number of Cycle	Rate of Loading		Type of Deformation Pattern
									Last Cycle	
				mm	MPa	mm		S=+/-(mm)	S=+/-(mm)	
M5	**Bar Spacing**	Cyclic	5HND-4-3	35	94.64	10	10	4.00	4.00	Canadian Standard
			5HND-4-4	35	94.64			-	-	
			5HND-4-3	25	93.40			4.00	4.00	Canadian Standard
			5HND-4-4	25	93.40	10	10	4.00	4.00	
M6	**Rate of Loading**	Cyclic	6HND-6-4	35	86.59	10	10	4.00	8.00	Canadian Standard
			6HND-6-5	35	94.64			4.00	8.00	
			6HND-6-6	35	94.64			4.00	8.00	
			6HND-6-4	25	94.64	10	10	-	-	Canadian Standard
			6HND-6-5	25	94.64			4.00	4.00	
			6HND-6-6	25	94.64			2.00	2.00	

Note: S: displacement

Table 4.6- Details of Tested Rib Geometries

Group	Specimen Notation	Rib Geometry							Relative rib area
		Rebar Diameter		Area	A*	B**	Height	Rib Spacing	
		Nominal	Actual						
		mm	mm	mm2	mm	mm	mm	mm	
M7	7HNM-14-1	35	26.88	620	2.29	9.40	3.56	16.26	0.196
	7HNM-14-2	35	26.88	620	2.29	9.40	3.56	19.05	0.167
	7HNM-14-3	35	26.88	620	2.29	9.40	3.56	25.4	0.125
	7HNM-14-4	35	26.88	620	2.29	9.40	3.56	31.75	0.100
	7HNM-14-5	35	27.91	660	2.29	8.38	3.05	16.26	0.171
	7HNM-14-6	35	27.91	660	2.29	8.38	3.05	19.05	0.146
	7HNM-14-7	35	27.91	660	2.29	8.38	3.05	25.40	0.109
	7HNM-14-8	35	27.91	660	2.29	8.38	3.05	31.75	0.102
	7HNM-14-9	35	29.41	705	2.29	6.86	2.29	16.26	0.131
	7HNM-14-10	35	29.41	705	2.29	6.86	2.29	19.05	0.112
	7HNM-14-11	35	29.41	705	2.29	6.86	2.29	25.4	0.084
	7HNM-14-12	35	29.41	705	2.29	6.86	2.29	31.75	0.067
	7HNM-14-13	35	34.00	908	-	-	-	-	-
	7HNM-14-14	35	35.70	1000	S	S	S	S	0.163
	7HNM-10-1	25	22.00	380	2.03	5.08	1.52	16.26	0.087
	7HNM-10-2	25	21.60	366	2.03	5.08	1.52	19.05	0.074
	7HNM-10-3	25	21.40	360	2.03	5.08	1.52	25.40	0.056
	7HNM-10-4	25	21.80	373	2.03	5.08	1.52	31.75	0.045
	7HNM-10-5	25	22.00	380	2.03	6.6	2.29	16.26	0.126
	7HNM-10-6	25	21.20	353	2.03	6.6	2.29	19.05	0.107
	7HNM-10-7	25	21.70	370	2.03	6.6	2.29	25.40	0.081
	7HNM-10-8	25	21.90	376	2.03	6.6	2.29	31.75	0.065
	7HNM-10-9	25	25.00	500	S	S	S	S	0.101
	7HNM-10-10	25	23.00	415	-	-	-	-	-

A* : Rib width at the face
B** : Rib width at depth
S : Canadian Standard

Table 4.7 Aggregate grading

Sieve size		Cumulative percentage retained	
Metric	Imperial	Coarse	Fine
mm	(US units)	Aggregate	Aggregate
12.7	1/2	-	-
11.2	7/16	0	-
9.6	3/8	2	-
6.3	1/4	36	-
4.76	No. 4	71	0
2.36	No. 8	92	22
1.18	No. 16	-	38
600 µm	No. 30	-	65
300 µm	No. 50	-	81
150 µm	No. 100	-	92

Table 4.8- Properties of Concrete Mixture for 0.1 cubic meter

Constituent	Unite	Normal Strength Mix	High Strength Mix
Cement	Kg	31	42
Silica Fume	Kg	-	5
Fine aggregate	Kg	65	65
Coarse aggregate	Kg	107	107
Retarder	ml	-	2200
Superplasticizer	ml	-	5500
Water Cement Ratio	-	0.55	0.29
Mix Density	Kg/m3	2392	2410
Expected Compressive Strength	MPa	50	75

Table 4.9- Properties of the Steel Reinforcement

Rebar Size	Diameter	Area	Yield Yield	Mean Yield Stress	Mean Ultimate Stress	Elastic Modulus
	mm	mm2	mm/mm	MPa	MPa	GPa
M-10	11.3	100	0.00235	450	660	191
M-20	19.5	300	0.00225	435	670	193
M-25	25.0	500	0.00220	445	670	192
M-35	35.7	1000	0.00237	448	665	191

Fig. 4.3 Preparation for steel reinforcement

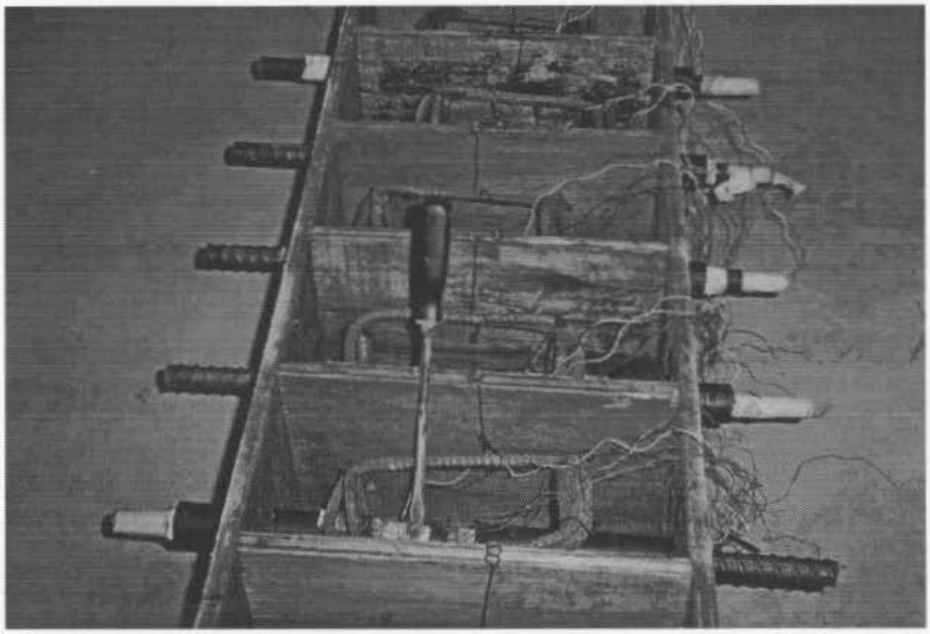

Fig. 4.4 Concrete strain gauges glued around rebar prior to casting

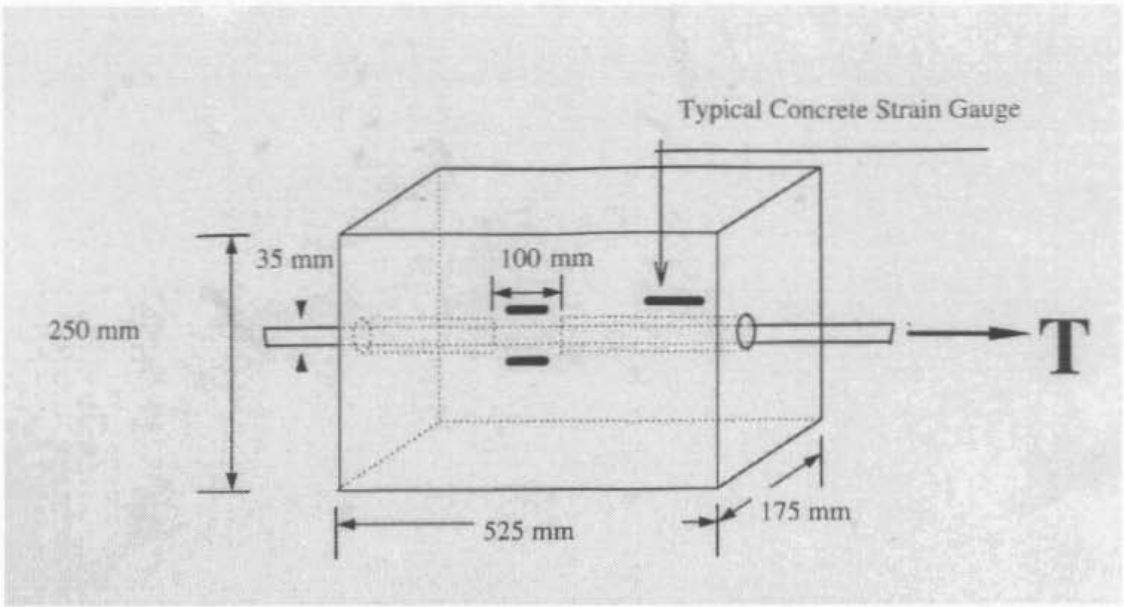

Fig. 4.1 Typical high strength concrete specimens with the position of concrete strain gauges

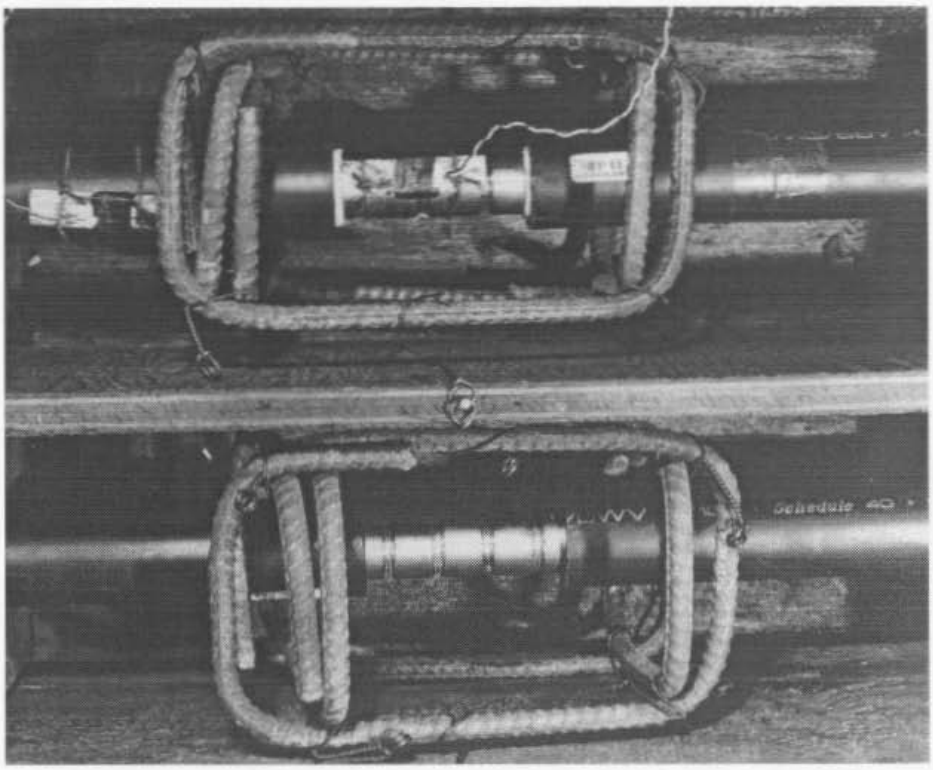

Fig. 4.2 Specimens before casting

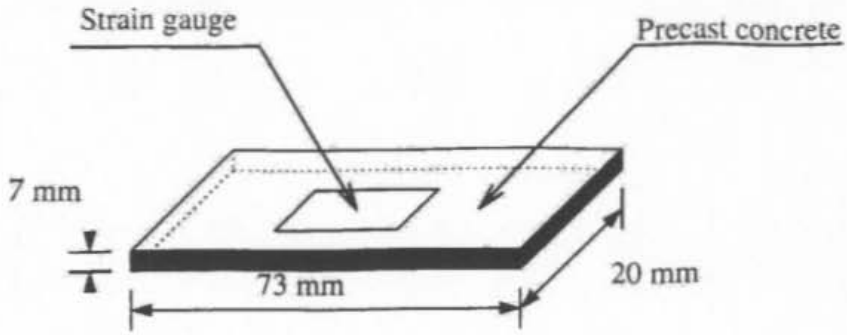

Fig. 4.5 Typical precast concrete with strain gauge

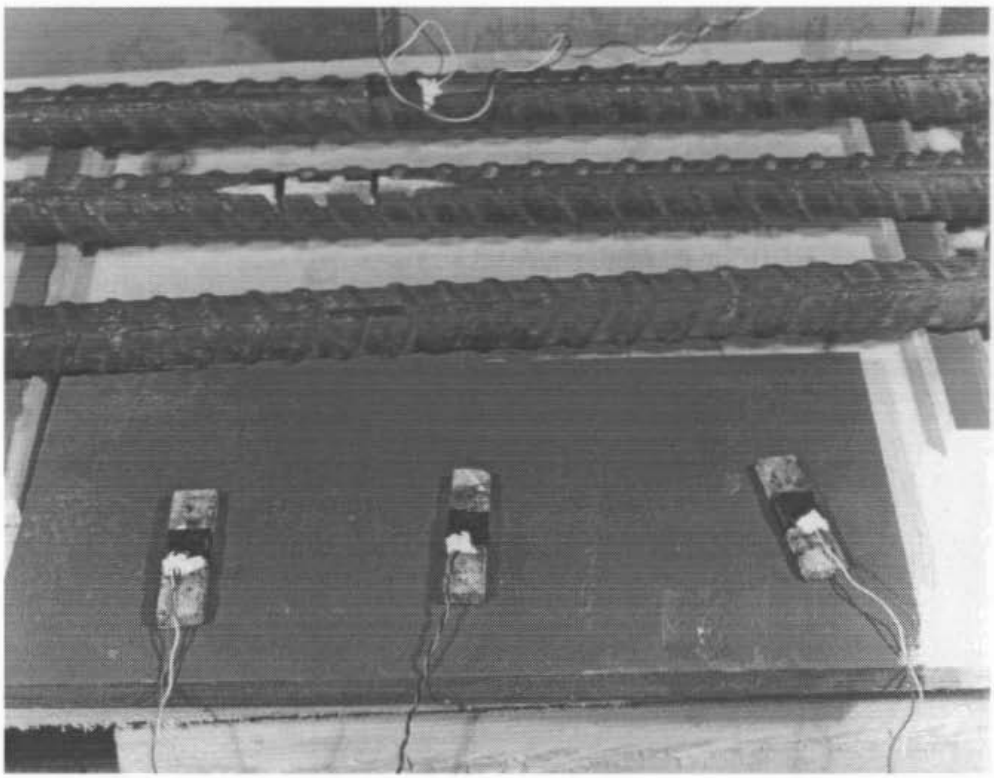

Fig. 4.6 Strain gages on concrete and rebar

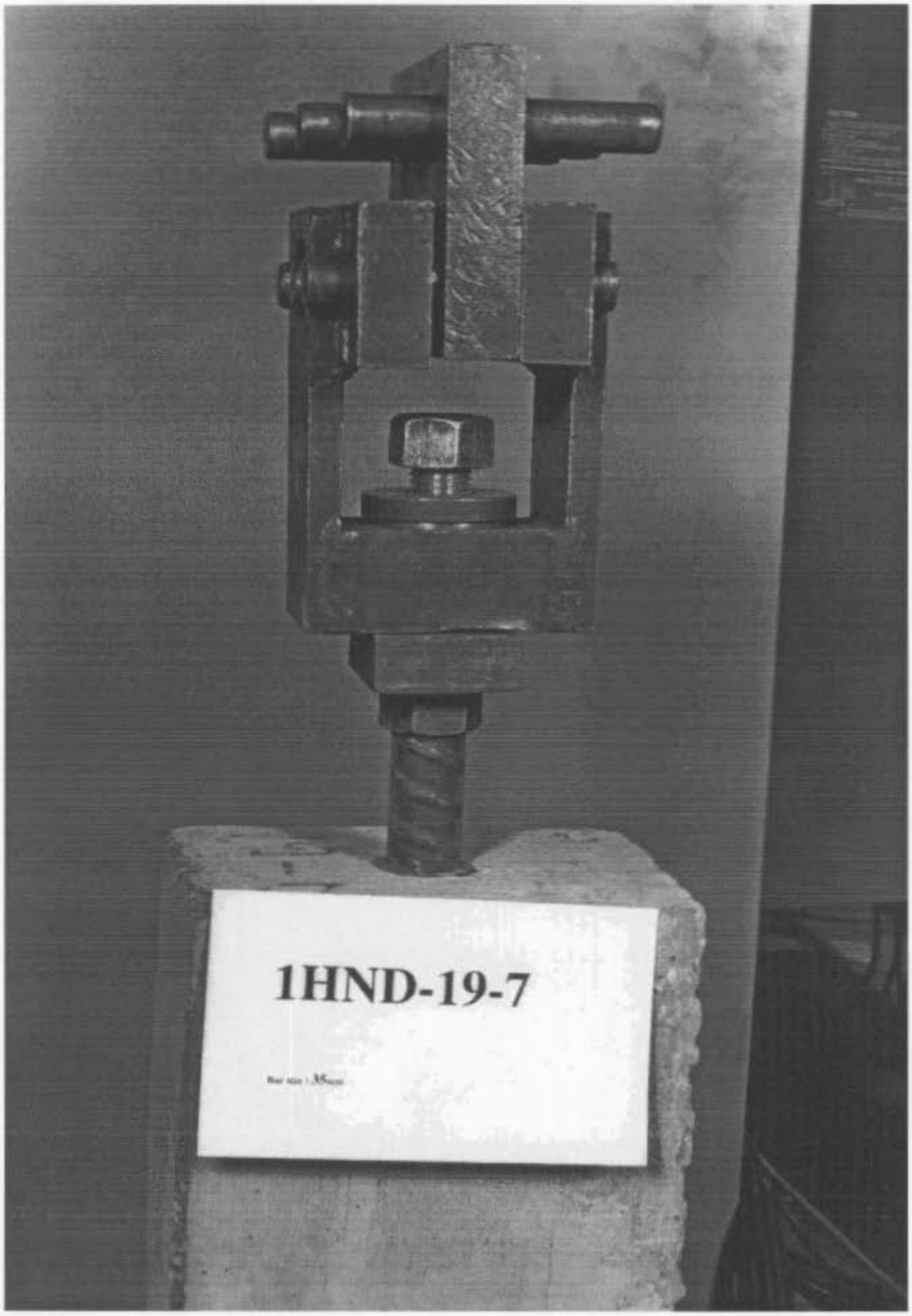

Fig. 4.7 Cyclic specimen after testing

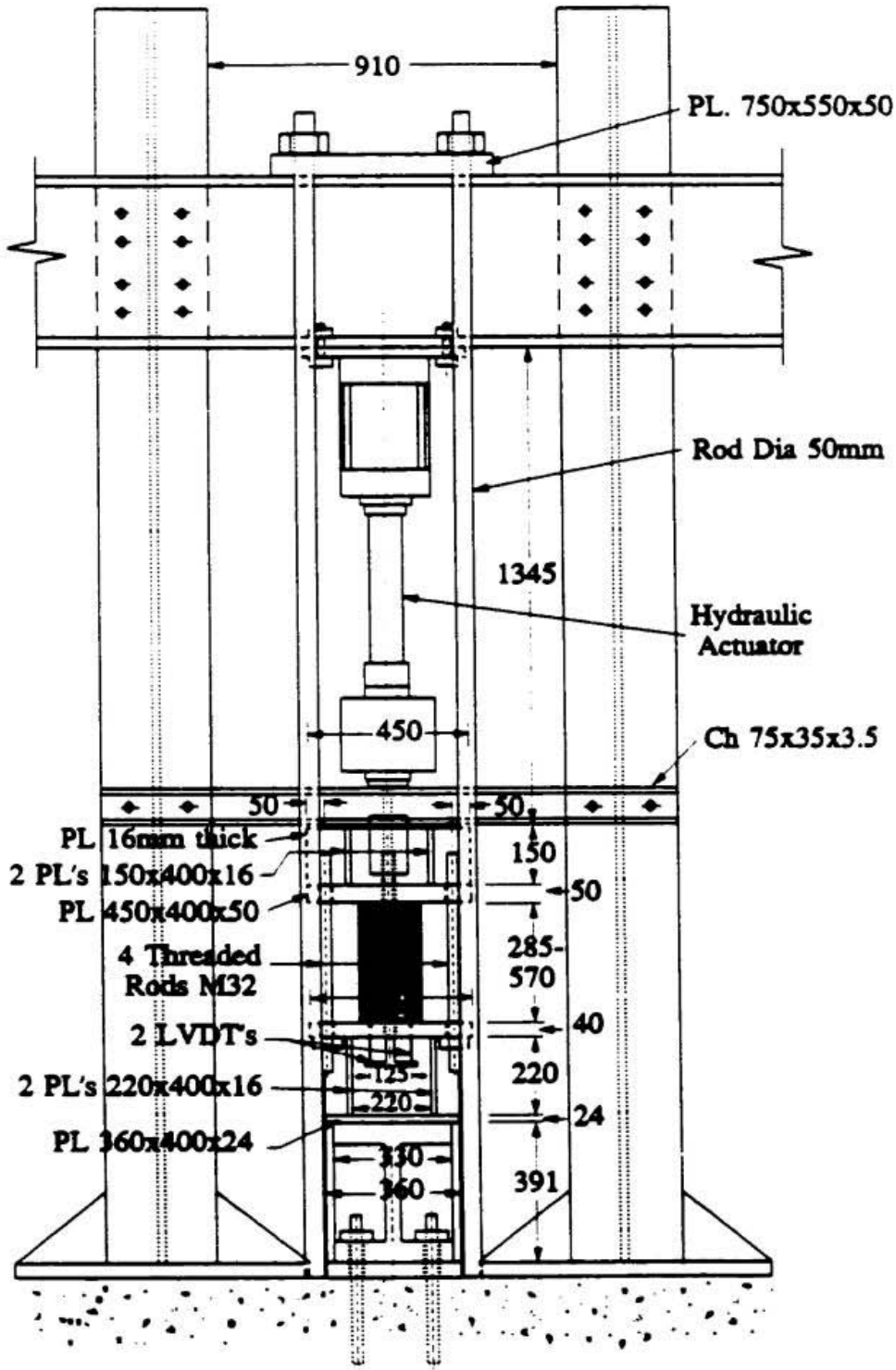

Fig. 4.8 Steel test frame

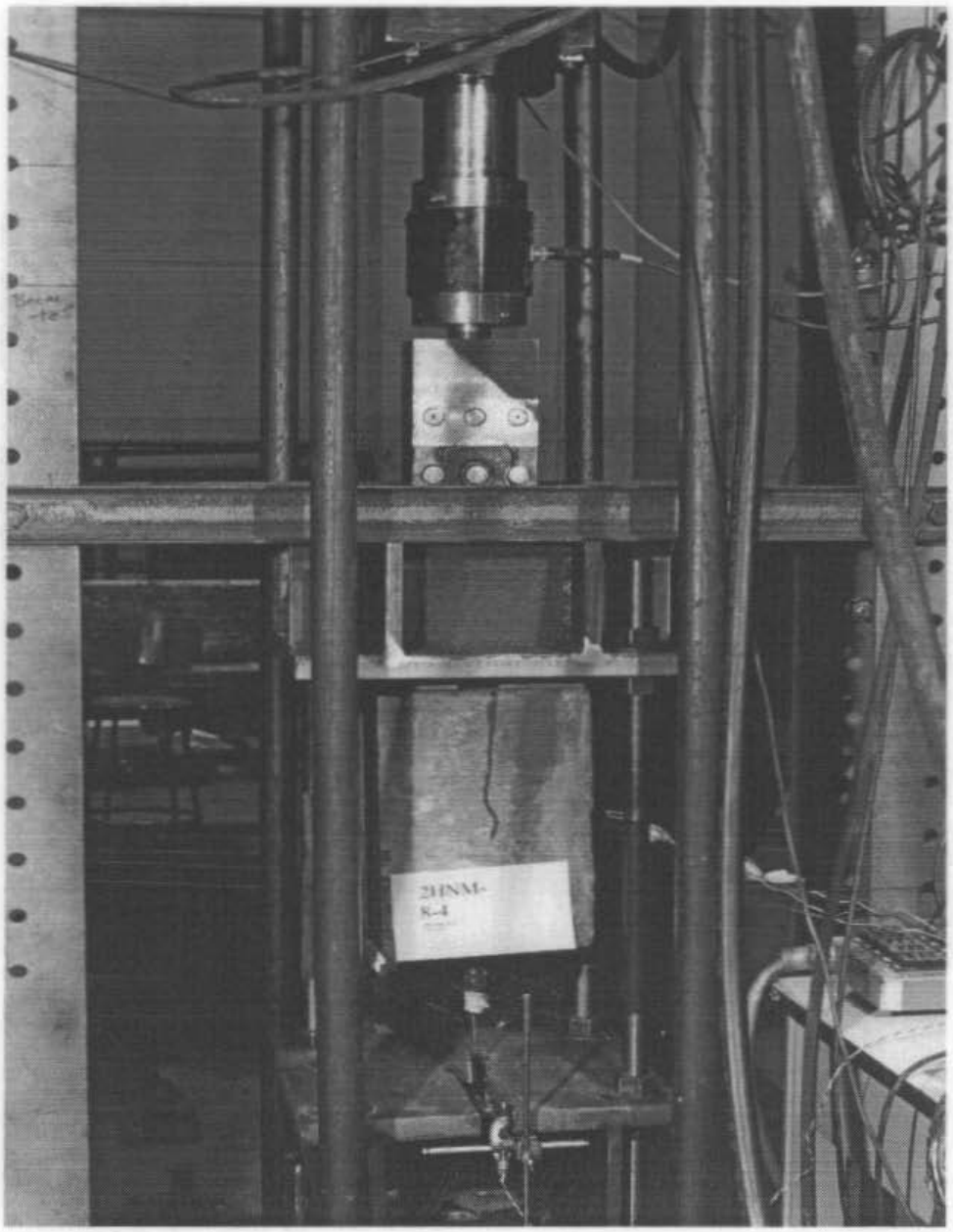

Fig. 4.9 Specimen during testing

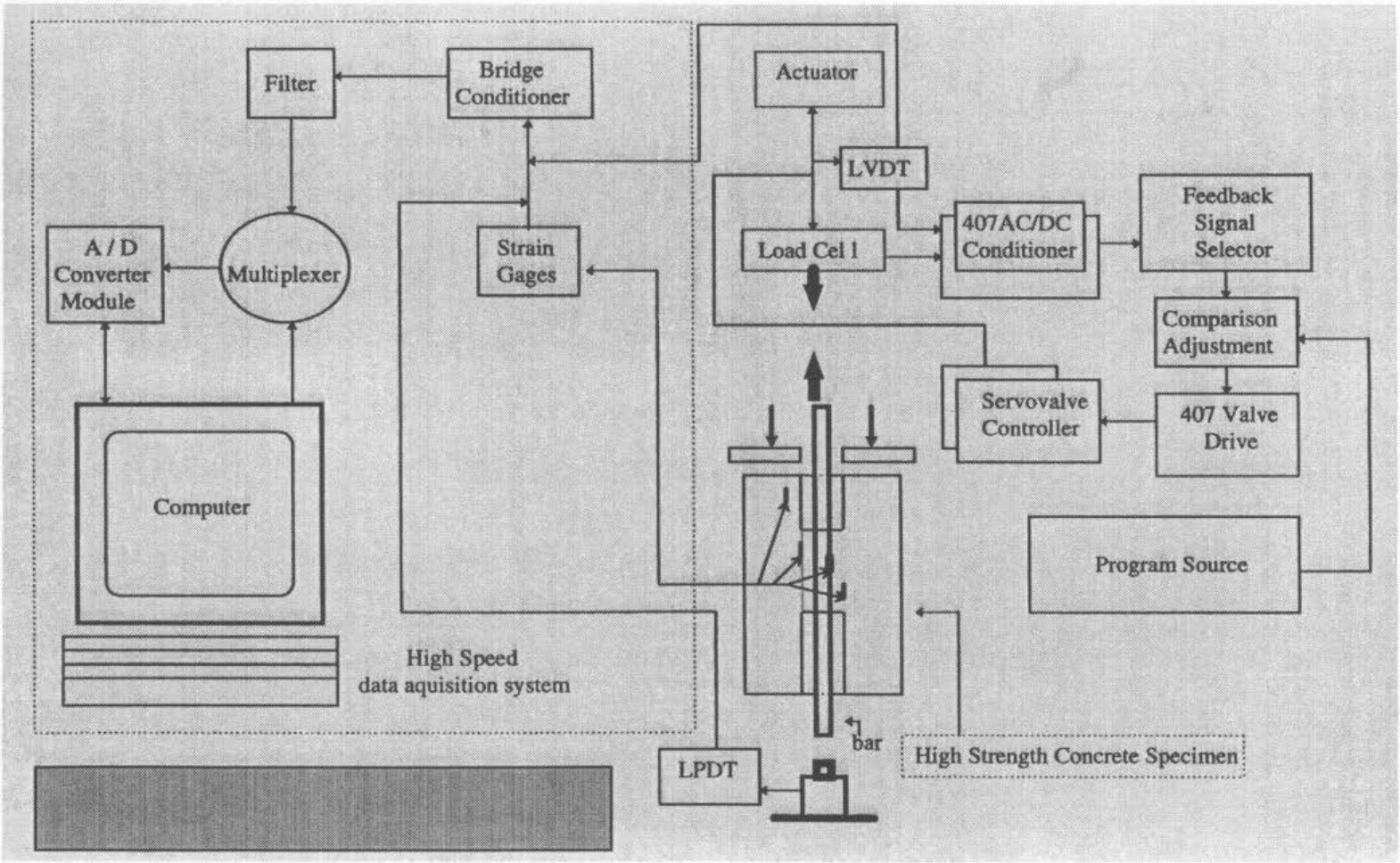

Fig. 4.10 Test instrumentation and close-loop scheme

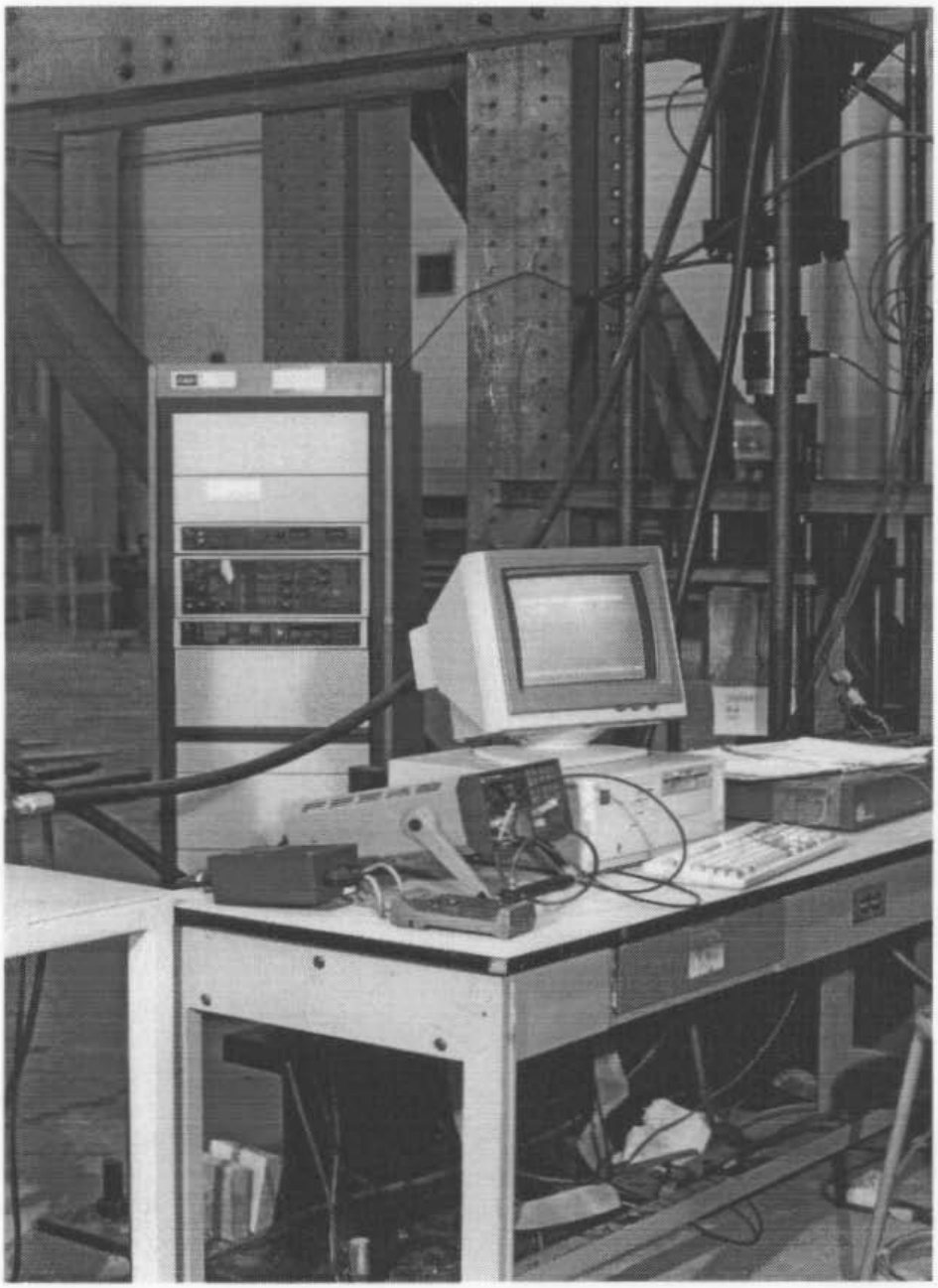

Fig. 4.11 Test set-up and instrumentation

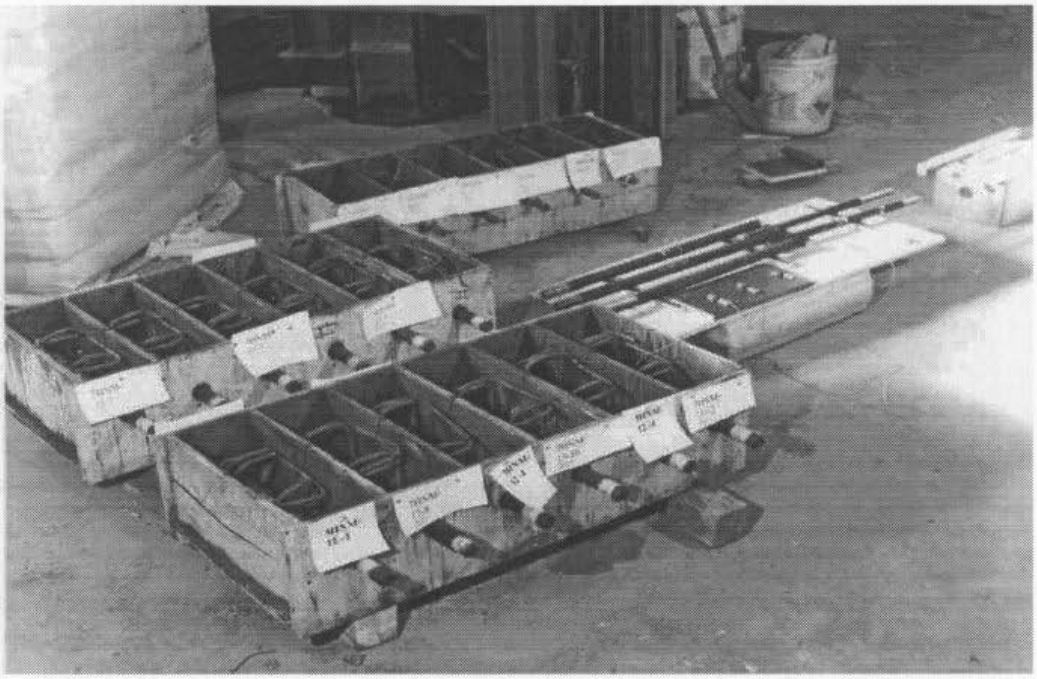

Fig. 4.12 Specimens prior to casting

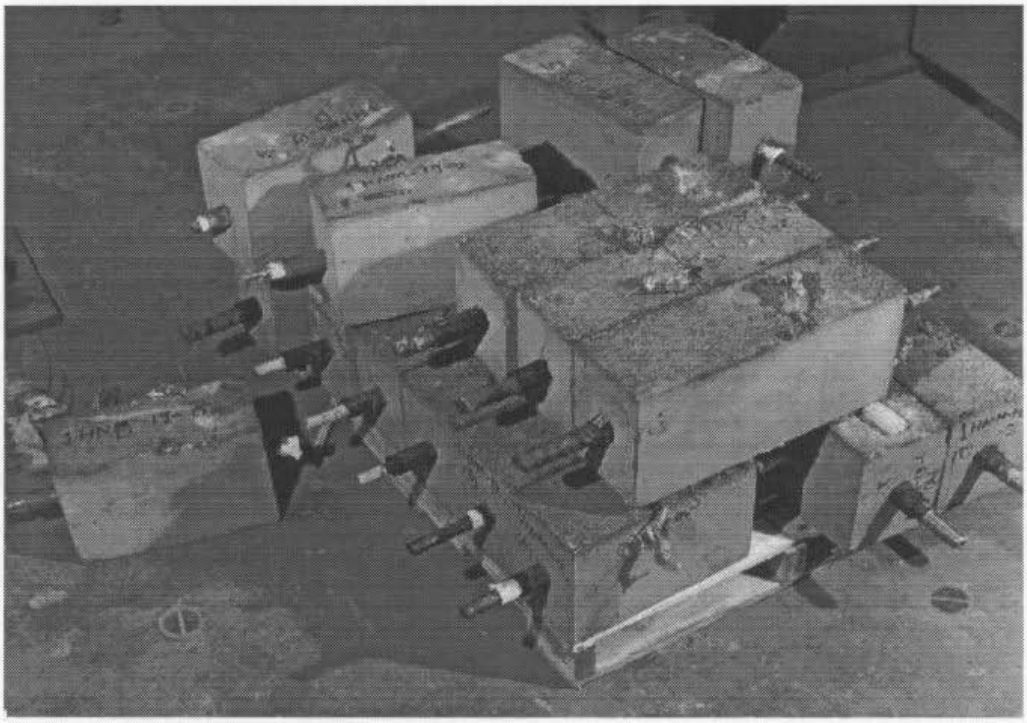

Fig. 4.13 High strength concrete specimens before testing

Fig. 4.14 Tested specimens

Chapter 5

Bond Strength of High Strength Concrete under Monotonic Loading

5.1 Introduction

The success of analytical design describing the bond behavior depends on the characteristics of the stress-deformation response of the element being analyzed, such as ultimate stress, stiffness and deformability, and also the mode of anticipated failure. Therefore, this chapter reflects the results and observation of the experimental investigation of the bond resistance between rebar and high strength concrete under monotonic loading condition. The behavior of high strength concrete bond is not well known. Therefore, this experimental investigation was focused on the influence of load history, confining reinforcement, rebar spacing, rate of pull-out, rebar diameter, concrete strength and rebar deformation patterns in conjunction with high strength concrete. A total of 100 specimens were tested for this part of investigation. The tests were examined for rebar with nominal diameter of 25 mm and 35 mm. The range of the tested concrete

compressive strengths was between 75 MPa and 95 MPa. A Series of tests were devoted to investigate the influence of rib geometry on the bond characteristics. Different deformation patterns were realized by machining the standard rebar. The internal concrete strain and steel strain to some degree of accuracy have been measured during testing. The surface crack patterns have been plotted and the modes of failures and test results were recorded. A new empirical expression for a bond stress-slip curve has been suggested to represent the experimental results. Finally, a new expression for the bond strength of high strength concrete based on the cubic root of concrete strength is developed and recommended.

5.2 Test Results and Observations

5.2.1 General Behavior

A bond stress versus slip curve, for high strength concrete as recorded in this investigation, is illustrated in Figure 5.1. The measured slip is recorded by the built in Linear Variable Differential Transducer (LVDT) actuator from the loaded side of reinforcement. The elongation of reinforcement was deducted from the value of LVDT to provide the net slip value. This curve demonstrates the actual behavior of high strength reinforced concrete bond. The typical stress-slip curve can be characterized into three main sections. Firstly, an ascending portion represents the increase of stress for about 20% of the total slip. In addition, some nonlinearity can be observed at the beginning of the ascending portion of the curve and close to peak bond stress. Secondly, there is a

sharp drop in the level of the stress in the beginning of the descending portion of the curve as a result of losing adhesion between high strength concrete and reinforcement. Finally, there is some complex behavior at point "c" of the descending portion of the curve, which could be the result of changing state of the stress. The bond stress will decrease nonlinearly and gradually with the increase of slip throughout the remaining 75% of the total slip. This indicates that the effects of friction and mechanical interlock are completed. The path of the curve from point "d" to point "e" is the result ofrecovery the effect of the yield stress in rebar. In general, the above three stages of the bond stress-slip curve fairly describe the process of stress transfer from rib to concrete that invariably occurs by cracking and crushing of the surrounding concrete. Therefore, in the case of using a fracture mechanics approach for numerical modeling the complete curve or area under the curve as bond energy should be considered for a complete bond model.

5.2.2 Load-deflection relationship

The average equivalent bond stress for experimental phase of this investigation is calculated as follow

$$\tau_b = \frac{q}{2\pi r l_b} \tag{5-1}$$

where

τ_b: Bond stress
q: Tension/compression force
l_b: Bond length

The slip is calculated as the difference between the reading of the Linear Variable Differential Transducer (LVDT) and elongation of steel bar. Therefore, the measured slip represents the local slip in the middle of embeded length with sufficient accuracy. Since the bond location is situated at the middle of the specimen, it is possible to assume that the stress distribution is uniform.

5.3 Effect of Investigation Parameters

5.3.1 Loading History

A total of fifteen specimens were tested for determining the effect of loading history under monotonic condition in tension as well as compression for bars with diameter 25 mm and 35 mm. All graphs are normalized on the basis of maximum bond stress in vertical direction and the maximum displacement (slip) in horizontal direction. The detail of the test specimen under monotonic loading can be found in Table 5.1. The maximum magnitude of load, bond stress, and slip for each specimen are shown in Table 5.16. The comparison of results for four specimens under pullout test with an embeded rebar diameter of 35 mm and 25 mm each are plotted in Figure 5.2 and Figure 5.3, respectively. The bond stress and slip curve for push-in tests has been plotted on the graphs, Figure 5.4, to facilitate the comparisón between pullout and push-in tests. Among each group of tests, a few have been selected for general evaluation. The comparison of normalized bond stress-displacement response for five specimens due to pullout and push-in tests with an embeded bar diameter of 25 mm and 35 mm is given in Figure 5.5. Although the main cracks developed in the longitudinal direction, some cracks also are

developed in a transverse direction. The test results indicate that nonlinearity of the bond stress-slip in the ascending section of the curve, especially close to peak stress, is evident. All results confirmed the sudden drop of the stress level at the beginning of the descending section of the curve and followed by the gradual decrease of stress. The bond strength for a rebar with large diameter is less than that of a smaller rebar diameter. The slope of the curves in the ascending section in case of the push-in is higher than the pullout test. Hence, the total capacity of bearing load in compression is slightly higher than in the pullout test. In addition, the area under the curve for the push-in test is slightly less than the pullout tested. However, this difference is not large enough to provide a distinct difference between the two behaviors. In order to approximate the area under the curve for this study parameter, the magnitude of maximum slip is useful. The magnitude of maximum slip can be approximated by five times the magnitude of slip corresponding to maximum bond stress. In order to study the bond behavior under loading, the level of stress has to be kept to less than the yield stress of the rebar. A typical specimen 1HNM-19-2S with special cross section shown in Fig. 5.5 indicated that the cross section of rebar or surface area of the rebar has significant effects on the bond strength. The major difference in this series of tests with the previous test result of normal strength concrete Eligehausen, Popov and Bertero (1983) is the instantaneous drop of the curve located at the beginning of the descending part.

The steel strain and internal concrete strain for a typical specimen (1HNM-19-2B) with embeded bar diameter 35 mm is plotted in Figure 5.6. The specimen is tested under push-in load. The two strain gauges STC1 and STC2 are installed in the bond area and

the strain gauge STC3 is far from the bond area, as shown schematically in the graph. There are differences between the magnitudes of concrete strain reading of STC1 and STC2 due to the location of the strain gauges and the distance from the bond surface. The strain reading of STC3 is not very significant, since it is very far from the location of the bond failure. Figure 5.7 shows the measured steel strain for the specimen. The location of this strain gauge was at the middle of the bond length. The curve demonstrates the increase of steel strain proportional to the load and the decrease of the strain at the beginning of the descending portion of the bond stress-slip curve. The result shows that when secondary cracks started to open. the steel strain gauges were damaged.

5.3.2 Confining Reinforcement

The influence of different rebar diameters as confinement on local bond behavior of deformed rebars was investigated in Series M2. The specification of each tested specimen is shown in Table 5.2. The normalized bond stress-displacement curves for different size of confining reinforcement for embeded bar diameter of 25 mm and 35 mm are presented in Figures 5.8 to 5.10, respectively. Table 5.9 presents the measured values of bond strength, peak load and slip at peak load.

When no reinforcement was provided as confinement, the bond stresses vanished as soon as the longitudinal crack developed through the cover. The failure mode was of a splitting type. In addition, huge energy was released when the specimen was splitting. Figure 5.28 shows the photograph of the unconfined specimen after splitting. However, when confinement was provided, the total area of the bond energy curve for specimens with confinement rebar diameter of 10 mm and 20 mm were higher than rebar diameter

of 25 mm. A 10 mm diameter stirrups was used for confinement of 25 mm and 35 mm rebar diameters efficiently. Also, the failure mode for specimens with confinement was based on pulling out rebar from concrete. Therefore for high strength concrete specimen the following aspect ratio is suggested for selecting an efficient rebar as confinement:

$$0.3 < \frac{d_s}{d_b} < 0.6 \tag{5-2}$$

where

d_s : Diameter of confining reinforcement

d_b : Bar diameter

The mechanism of the influence of confining reinforcement can be explained as follows: When the tensile load is increased until it reaches the ultimate load, the splitting crack will develop in the plane of the longitudinal axis of the main rebar, then the horizontal stirrups will be activated to resist against the splitting failure. The slip corresponding to the maximum bond stress was lower for reinforcement with diameter of 25 mm as confinement, compared to confining reinforcement with diameter of 20 mm. Finally, the bond slip at peak bond stress will be increased for specimens with larger diameter of reinforcement as confinement compared to specimens with smaller diameter of reinforcement as confinement as well as specimen without confinement, as shown in Figure 5.10. The ultimate bond stress for confined and unconfined specimens was approximately the same.

5.3.3 Varying Rebar Diameters

The effect of varying rebar diameter on the bond strength is illustrated in Figure 5.11. The details of the test specimens are shown in Table 5.2. The test results of the 20

mm, 25 mm and 35 mm rebar diameters are shown in Table 5.9 and the results are compared with analytical expressions as well as different codes. All curves of this figure are normalized with respect to maximum bond stress and maximum displacement of a 25mm bar diameter (specimen 3HNM-12-2). The bond resistance of the 20 mm rebar diameter is greater than the tensile capacity of the rebar cross section area. Therefore, the rebar is broken and this curve does not demonstrate the whole behavior. The ascending slope of the curve for a 20 mm rebar diameter is much steeper than for the 25 mm and 35 mm rebar diameters. Further, comparison between the areas under the curves shows that the area under the curve for the rebar with a diameter of 35 mm is less than for the rebar diameters of 20 mm and 25 mm. Hence, the bond resistance is higher for the smaller diameter than that for larger diameter rebar.

In this series of tests the effect of losing adhesion at the beginning of the descending portion of the curve is evident. From the results of these tests it can be deduced that the strength of the bond can be improved by choosing a smaller size rebar for designing reinforced concrete structures. In general, the results of this series agree with the findings of Eligehausen, Popov and Bertero (1983), using a similar test set-up for normal strength concrete. However, there are some differences in the magnitudes and the shape of the curves that are attributed to the characteristics of the high strength concrete.

The measured concrete strains for the specimen 3HNM-12-4 with a bond length of 100 mm and an embeded bar diameter of 35 mm are plotted in Figure 5.12. The distribution of concrete strains is changed along the embeded length of the rebar as well

as along the surrounding high strength concrete. Figure 5.12a shows the concrete strain in high strength concrete close to the contact surface. Figure 5.12b shows the variation of strain in the steel rebar. The concrete strain will increase with respect to the increase of bond stress until it reaches the maximum value; it decreases due to the decrease of bond stress. These values for the strain gauges clearly confirm that the behavior of high strength concrete corresponds to the bond-slip curve. The high strength concrete bond-slip has a sharp drop at the beginning of the descending portion of the curve.

5.3.4 Rebar Spacing

Results of an experimental investigation conducted to study the influence of rebar spacing are presented in this section. A total of four specimens were used in this investigation. Two specimens were tested with rebar diameter of 25 mm and spacing of 25 and 50 mm and the other two specimens were tested with rebar diameter of 35 mm and rebar spacing of 35 and 50 mm. The detailed information about each specimen is summarized in Table 5.3. Table 5.10 shows the slip at peak, ultimate load and stresses for the tested specimen. The normalized bond stress and displacement curves for the two specimens with rebar diameter of 25 mm are shown in Fig 5.14. Curve one is for a specimen with 25 mm bar spacing and curve two is for a specimen with 50 mm spacing. Figure 5.15 shows a comparison of normalized bond stress-displacement response of the two specimens with rebar spacing of 35 and 50 mm for embeded bar diameter of 35 mm.

In the case of rebar diameter of 25 mm there was no significant difference between the two in the ascending portion, while in the descending portion there was a small difference. The ultimate bond stress for specimen with bar spacing of 25 mm was

about 20 percent less than for a specimen with 50 mm bar spacing.

The test results for the specimen with rebar diameter of 35 mm shows that the increase in rebar spacing had more influence on the bond resistance of the initial part of the bond stress-slip relationship than on the maximum bond resistance. The bond strength is improved with the increase of rebar spacing. The result of observation and comparison between ultimate bond stresses for this series of tests showed a difference of 20% between the ultimate bond stresses of chosen rebar spacing. This result can be explained by the fact that the ultimate failure load was caused by pulling out the rebar from concrete and the effect of the restraining reinforcement can control only the growth of the splitting cracks. In the case when less restraining reinforcement is provided, the ultimate failure can be due to the splitting cracks, and a more significant influence of rebar spacing would be expected.

5.3.5 Rate of Pull out

This section presents the experimental results from the testing of three specimens tested under different rates of loading: 75, 0.0151 and 1.51 mm/min. Figure 5.16 shows a comparison of normalized bond stress-displacement response to LVDT for the three specimens with different rate of loading with rebar diameter of 35 mm. The results show that the ultimate load for different rates of loading for 35 mm rebar are approximately the same as presented in Table 5.10. Although at the initial stage of loading there was a noticeable difference for the specimen with rate of loading of 1.51 mm/min, in general there are no significant differences between all of the different rates of loading.

5.3.6 Concrete Strength

The results of the tests for different types of concrete strength for the rebars with diameter 35 and 25 mm, respectively are demonstrated on Figure 5.13. The different concrete strengths included in this series were 51, 86, 93, and 95 MPa. The details of the test specimens are shown in Table 5.4. The comparison of test results with analytical expressions as well as codes is shown in Table 5.10. In principal, the results of this series of tests agree with the previous study for normal concrete strengths of 30 MPa and 55 MPa, Eligehausen, Popov and Bertero (1983). The instantaneous drop of the curve at the beginning of the descending branch of the curves, as a result of losing adhesion, is well illustrated in this series of tests especially for concrete with higher strength. The results of all tests in this series confirmed the nonlinear-brittle behavior of the bond for high strength concrete. In the case of high strength concrete the capacity of bond stress is higher than the normal one, however, the impact of the instantaneous drop of the high strength concrete curve must be recognized. The test results revealed that the bond resistance is strongly dependent on concrete strength and this parameter has a direct effect on bond resistance. In addition, the results of strain gauge readings for a typical specimen with an embeded bar diameter 35 mm and bond length 100 mm indicate that strain will increase as a result of the increasing the tension load and will decrease as a result of dropping the load. These strains show tensile stresses in high strength concrete at the area surrounding the rebar due to bond stress and normally will lead to deformations and cracks. The cracks will result in pulling the concrete away from the rebar.

5.3.7 Different Rebar Deformation Patterns

The results of the investigation into the influences of different deformation patterns on the bond resistance for reinforced high strength concrete are presented in this section. A total of 14 specimens with different rib geometries of nominal 35 mm rebar diameter and 10 specimens with 25 mm rebar diameter were tested. The varying parameters were the rib spacing and rib height. The detail of the test specimens is shown in Table 5.4. The maximum pullout load, maximum bond stress, and slip at maximum load for each specimen are given in Table 5.17. The test results are compared with analytical expressions and different codes. Detailed information on the rib geometries for each specimen is presented in Table 4.6

The first four specimens with a nominal bar diameter of 35 mm and rib height of 3.56 mm are designed to examine the effect of different rib spacing of 16.26, 19.05, 25.40 and 31.75 mm. The results are reported and it is evident that the bond stress of specimen 7HNM-14-1 is higher than that of specimens 7HNM-14-2, 3 & 4 as shown in Figure 5.17. However, when the total bond energy is calculated based on the area under the bond stress-slip curve considering both of the ascending and descending portions, it is clear that specimen 7HNM-14-1 with a 25.4 mm rib spacing (72% of the nominal bar diameter) gives the best results. Therefore, the bond stress-slip curve of this specimen is considered more suitable than other specimen and test results are shown in Figure 5.18.

The effects of different rib heights of 3.56, 3.05, 2.29, 1.86 mm correspond to 0.102, 0.0871, 0.0654, 0.0531 of the 35 mm nominal rebar diameter, respectively, are considered in the investigation. In addition, the rebar with standard rib geometry and a

plain rebar without rib is tested, and the bond stress-slip curves are compared. All of the deformed bars were tested at a rate of 1.51 mm/min, while for plain rebars, the rate was 0.0151 mm/min. The ultimate loads and relative rib areas for selected specimens with a nominal bar diameter of 35 mm are shown in Table 5.6.

The test results indicate that the rebar geometries or deformation patterns have a significant effect on the bond resistance in reinforced high strength concrete. The comparison of the test results for rebar with diameter of 35 mm is shown in Figure 5.18. All curves of this figure are normalized with respect to maximum bond stress and maximum displacement of the results for specimen 7HNM-14-14. The comparison of the results shows that the deformation pattern corresponding to curve 3 of Figure 5.18 has the highest magnitude for bond stress. While taking into consideration the bond energy and the behavior of the bond in descending portion, the geometries of the rebar represented by the curve 7 gives the most effective rib geometry among all the tested specimens.

In addition, curve 3 of Figure 5.18 represents a rebar with a relative rib area of 0.125, ultimate bond stress of 21.62 MPa and area of 620 mm^2, while curve 14 of the same figure, represents a rebar with a relative rib area of 0.163, ultimate bond stress of 19.47 MPa and rebar area of 1000 mm^2. It is clear that the relative rib area and the cross section area of curve 14 are higher but the bond stress is relatively lower.

It can be drawn out of this study that the evaluation of rib geometries by rib face angle, rib height and rib spacing approach are more suitable than the relative rib area approach. Soretz and Holzenbe (1979) define the relative rib area used in this study, as follows:

$$R_r = \frac{\textit{projected rib area normal to bar axis}}{\textit{Nominal rebar perimeter} \times \textit{Center to center rib spacing}} \qquad (5\text{-}3)$$

This formula is suitable for evaluating the effect of ribs in the ascending portion of the bond stress-slip curve and in the mean time, the German specification Din 488 (1986) recommended the same approach for relative rib area. It will not cover the descending portion of the bond stress-slip curve. It is recommended to develop a formula which describes the effect of the rib on both the ascending and descending portions of the curve using the concept of bond energy and fracture energy.

The results of the tests for 10 specimens with a nominal embeded bar diameter of 25 mm are presented in Figure 5.19. The curves of this figure are normalized with respect to maximum bond stress and maximum displacement of the results for specimen 7HNM-10-5. The details for the rib geometries and other test specifications are shown in Table 5.4 and Table 5.17. The Canadian standard deformation pattern for the 25 mm rebar diameter with a cross section area of 500 mm^2 is plotted as shown in curve 9. The test results are provided in Table 5.7. The most effective deformation pattern belongs to curve 9, representing the Canadian standard deformation pattern.

5.4 Proposed Bond Model for High Strength Concrete

The force required to pull a deformed reinforcing bar out of a block of concrete will obviously increase as the length of the bar cast into the block (the embedment length) increases. When the embedment length becomes long enough the bar will yield in tension before it pulls out of the block. The minimum embedment length required to develop the

yield force of the bar is called the development length. This development length, l_d , is used in North American Codes as an indicator of the bond characteristics of the reinforcing bar.

If a bar subjected to its yield force is embeded for a length equal to the development length, then the average bond stress, u, on the surface of the bar is:

$$u = \frac{A_b f_y}{\pi d_b l_d} = \frac{\pi d_b^2 f_y}{4\pi d_b l_d} = \frac{d_b f_y}{4 l_d} \tag{5-5}$$

where

A_b : Bar area
d_b : Bar diameter
f_y : Yield stress
l_d : Development length
u : The average bond stress

An expression for calculating development length is available in each code It contains several modification factors to account for different conditions surrounding the bar. In this section a comparative study has been done to select the best expression for calculating average bond stress for high strength concrete.

The bond strengths are calculated based on the equations that are collected in Table 5.16 with the use of the above relationship. The results are compared and recorded in Table 5.5 through Table 5.8. It is highly recommended for more information about the modification factors of the following equations to use the references.

Table 5.1 Comparison of different code equations for test results

Equation Notation	Bond stress/ Normalized Bond stress	Source
RBE	$u_R = \frac{1.285(f_c')^{1/3}}{\sum_{i=1}^{7} m_i}$	Recommended bond expression
E&R	$u_3 = \frac{0.5\sqrt{f_c'}}{k_1 k_2 k_3 k_4}$	Esfahani & Rangan (1998)
AUS	$u_4 = \frac{(\frac{2C_d}{d_b} + 1)\sqrt{f_c'}}{k_5 k_6 \pi}$	Australian standard, AS3600
ACI	$u_5 = \frac{0.651\sqrt{f_c'}}{\alpha\beta\lambda}$	ACI-318-1995
CSA	$u_6 = \frac{0.556\sqrt{f_c'}}{k_7 k_8 k_9 k_{10}}$	Canadian standard, CSA A23.3-1994
Dar	$u_7 = \frac{33.75 f_y}{\frac{f_y}{\sqrt[4]{f'_c}} - 1900}$	Darwin et al. (1995)

The best agreement with experimental results, was based on the cubic root of compressive strength of concrete as follows:

$$u = \frac{1.285(f_c')^{1/3}}{\sum_{i=1}^{7} m_i} \qquad (5\text{-}6)$$

in this equation "u" is the bond stress in high strength concrete, $m_1 = 0.08$, the effect of load history, $m_2 = 0.05$, the effect of confining reinforcement, $m_3 = 0.14$, the effect of

rebar diameter, $m_4 = 0.10$, the effect of concrete strength, $m_5 = 0.20$, the effect of rebar spacing, $m_6 = 0.10$, the effect of rate of loading, $m_7 = 0.33$, the effect of deformation pattern. These values are determined through a parametric study as detailed in Chapter 7.

In addition, Tables 5.12 through 5.15 show comparison results of proposed bond strength expression with previous study and different expression. It is indicated that the proposed expression better correlates with the Code method. Therefore, the Canadian Building Code, CSA A23.3-(1994) and ACI 318-(1995), American Building Code, need special consideration for high strength concrete based on this investigation to calculate the development length. The proposed modification is to replace the current $\sqrt{f_c}$ limitation stated in clause 12.2.3 of the Canadian Standard Code to another expression including $\sqrt[3]{f_c}$ after taking into consideration some modification factor response to main study parameters, to ensure that structural members designed using development or tension length of the code would reach adequate levels of ductility before failing.

5.5 Bond Mechanisms

Goto (1971) carried out a study to investigate experimentally the bond action between concrete and deformed steel bars. The test specimens were axially loaded tensile specimens, each a single bar embeded concentrically in a long concrete prism. The pulling load was applied through the exposed ends of the bar. The cracking of concrete was indicated by ink from special injecting holes. Afterwards the prisms were cut axially

and the ink colored cracks became visible, Figure 5.22. It is widely accepted that the physical-chemical interaction between the interface of concrete and rebar that make the bond stress are due to adhesion, friction and mechanical interlock forces. The process of stress transfer from rib to concrete occurs by cracking and crushing of the surrounding concrete. Figure 5.23 shows separation of concrete near a primary crack for deformed bars, as it is shown some of tension in the concrete is lost when a primary crack opens near surface of the rebar. The deformation mechanisms that contribute to bond-slip is classified into four types i.e., elastic deformations, secondary cracking (cone shaped), longitudinal splitting cracking (radial), and crushing in front of the ribs. Of those, it is commonly assumed that secondary and longitudinal cracking are the most important contributions. The influence of confining reinforcement improves the condition of failure. When the concrete is well confined, the propagation and the width of splitting cracks are kept small so that the ultimate failure is caused by rebar pullout.

5.6 Bond Mechanisms of High versus Normal Strength Concrete

The bond resistance mechanism for confined concrete near the rebar end loaded in tension has been described in Figure 5.24, Eligehausen, Popov and Bertero (1983). This mechanism reflected the behavior of normal strength concrete and under monotonic loading condition. It is indicated that the bond behavior under increasing pull-out forces follows the initiation of inclined cracks at contact points between the steel lugs and concrete at relatively low stresses which is known as an elastic deformation process. A secondary crack is formed when crushing of concrete in front of the lugs has started. Shearing-off of an increasingly larger part of concrete keys between the lugs takes place

until the keys are fully sheared off, Figure 5.24(c). After some frictional bond resistance is left, the gradual shearing off of the concrete keys is possible only in well confined concrete, where excessive growth of the splitting cracks can be prevented. It is commonly accepted that secondary and longitudinal cracking are the most important causes to failure of bond resistance.

The results of this investigation indicate that for specimens subjected to monotonic axial loading, the behavior of the bond stress-slip would be nonlinear and more brittle for high strength concrete. The recorded value for maximum pull-out force, slip at maximum pull-out force, bond stress and normalized test results with respect to $\sqrt[3]{f_c}$ for each tested high strength concrete specimen are shown in Tables 5.16 to 5.17. Figure 5.25 shows clearly that the bond stress-slip curve for high strength concrete is characterized by a sharp drop at the beginning of the descending portion of the curve. It would be reasonable to assume that the ascending branch of the curve represents strong cooperation between adhesion, friction and mechanical interlock forces. Meanwhile, at ultimate load, before the lugs cause crushing of concrete, adhesion in the interface loses its strength rapidly. This will be reflected by a sharp drop at the beginning of the descending portion, which can be estimated by approximately thirty percentage of ultimate load. Then, friction and mechanical interlock forces will resist against the force of rebar. In this step, the bond stress gradually decreases and crushing of concrete in front of the lugs will increase. The magnitude of the maximum slip at failure was estimated by five times that of the slip corresponding to maximum bond stress for high strength concrete. The behavior of the model explained above would confirm the ACI 318-(1995)

assumption of uniform bond stress distribution close to the ultimate bond stress in reinforced concrete. Further the failure that caused the rebar to pull out, happened at steel stress below yield strength.

5.7 Mode of Failure

The failure bond mechanism of deformed reinforcement embeded in high strength concrete is presented in this section. There are two types of failure mechanisms that are known for the pullout test. The first type is splitting of the concrete cover and the second type is pullout of the bar by shearing, leaving a smooth surface, provided the concrete cover is thick enough. There are several parameters which govern the mode of failure such as: type of loading, confining reinforcement, concrete cover, rebar spacing, rate of pull out, rebar diameter, concrete strength and deformation patterns.

The results of this investigation under a confinement condition and a monotonic increase of the load revealed that for high strength reinforced concrete the behavior of the bond stress-slip was nonlinear-brittle. Also, the magnitude of the maximum slip at failure of the bond resistance for high strength concrete was estimated to be five times that of the slip corresponding to maximum bond stress. Therefore, the primary cracks have been developed and surface cracks were observed in most of the tested specimens.

The longitudinal crack at the surface of the specimen appeared approximately at the ultimate load and the rebar failed by pulling out from the concrete. The role of rib angle was significant. When the rib angle was small and the surface was smooth, the slip can occur along the face of the rib, and the rib tended to push the concrete away from the rebar. This wedging action can be a major cause of longitudinal splitting along the rebar,

as illustrated in Figure 5.26. Failure mechanisms at the ribs of deformed rebars are shown in Figure 5.27. The wedging action had a higher percentage of contribution in the failure of the bond mechanism. Also, the result for the plain rebar test showed that the rebar fails by pulling out from concrete. In addition, in the case of the unconfined condition, failure occured in the plane of longitudinal axis of the rebar by splitting the concrete into two parts and at the same time a huge amount of energy was released.

5.8 Summary and Conclusion

The test results revealed that the maximum bond stress for high strength concrete is higher than the corresponding one for normal strength concrete. However, the behavior of high strength concrete is more nonlinear-brittle and it must be considered in modeling. The predicted value for the maximum slip which leads to complete failure of the bond resistance would indicate that the value is estimated by five times the value of the slip corresponding to the maximum bond stress. The internal concrete strain to some degree of accuracy has been measured. The surface crack patterns have been plotted and the mode of failures has been identified. The development of a new technique of strain measurement around the steel rebar is unique and it can be useful to identify the internal crack pattern and to predict possible failure modes.

The bond resistance of high strength concrete subject to the effects of the rebar diameter and deformation patterns was examined. Several specimens with different rebar diameters and rib geometries were tested. The range of the tested concrete compressive strengths was between 78 MPa and 95 MPa. The deformation patterns were examined for rebar with nominal diameter of 25 mm and 35 mm. All deformations for rebars of Series

M7 were machined. An examination of the test data reveals the following:

1. The bond stress-slip curve of high strength concrete is characterized by a sharp drop of the level of stress at the beginning of the descending portion of the bond stress-slip curve.
2. The area under the curve of the bond stress-slip curve can define the bond energy. The bond energy should be used to evaluate the bond behavior rather than the maximum bond stress.
3. The influence of confinement on bond is significant, especially after reaching the ultimate bond strength. A method for selecting a suitable size of rebar confinement is suggested.
4. The result of tests examining the effect of varying rebar diameter embeded in high strength concrete indicates that the bond is higher for the smaller rebar diameter than for the bigger one. The ultimate bond strength for 25 mm rebar diameter is approximately 15 percent higher than 35 mm rebar diameter. A sharp drop of bond stress at the beginning of the descending portion of the bond stress-slip curve for high strength concrete is confirmed for all rebar diameters. The level of bond stress decreases by about 30 percent of total bond stress-slip at the beginning of the descending branch of the bond stress-slip curve.
5. Results of the investigation regarding the influence of rebar spacing revealed that the bond strength could improve by selecting a proper rebar spacing.
6. An investigation into the bond resistance subjected to the effect of the concrete strength concluded that the ultimate bond stress for high strength concrete is higher

than the corresponding one for normal strength concrete. However, the behavior of high strength concrete is more nonlinear and brittle, and it must be reflected in the bond model.

7. The bond resistance increased approximately proportional to $\sqrt[3]{f_c}$.

8. In the case of high strength concrete the capacity of bond stress is higher than the normal one. Also, the strength of bond depends on the concrete strength.

9. The relative rib area approach determines only the effect of the rib in the ascending portion of the bond stress-slip curve and more attention should be given to the descending portion. The rib face angle, rib height and rib spacing combined with the area under the curve approach are more suitable to express the effect of rib on the bond behavior.

10. It is recommended to consider the total behavior of the bond stress-slip curve for evaluating the bond resistance of the high strength concrete with respect to deformation pattern. In this case the effect of concrete strength will be considered automatically.

11. The most effective deformation pattern for 25 mm rebar diameter and smaller is the standard deformation pattern adopted by the Canadian code. For rebar diameters higher than 25 mm a new deformation pattern is recommended for high strength concrete.

12. A new expression for calculating bond stress based on the cubic root of concrete strength is suggested and the results are compared with similar equations of different codes.

Table 5.2- Detail of the test specimens under monotonic loading (M1)

Group	Investigatio Parameter	Loading History	Specimen Notation	Rebar				Cover	Embedded Length	Rate of Loading	Confining rebar	Concrete Strength		Yield Stress	Steel Stress
				Diam. Nominal	Diam. Actual	Area	Perim.			Displ.Con.	diameter	Compr. f'_c	Tensile f'_{ct}	f_y	f_s
				mm	mm	mm2	mm	mm	mm	mm/min	mm	MPa	MPa	MPa	MPa
M1	Load History	Monotonic in Tension	1HNM-19-1	35	35.7	860	112	70	100	1.51	10	85.00	5.07	448	323.26
			1HNM-19-1A	35	35.7	860	112	70	100	1.51	10	81.00	4.95	448	253.49
			1HNM-19-1B	35	35.7	860	112	70	100	1.51	10	81.00	4.95	448	195.12
			1HNM-19-1C	35	35.7	860	112	70	100	1.51	10	81.00	4.95	448	244.59
		Monotonic in Compression	1HNM-19-2A	35	35.7	860	112	70	100	1.51	10	81.00	4.95	448	254.24
			1HNM-19-2B	35	35.7	860	112	70	100	1.51	10	85.12	5.07	448	252.95
			1HNM-19-2C	35	35.7	860	112	70	100	1.51	10	83.16	5.02	448	222.19
		Monotonic in Tension	1HNM-19-1	25	25.2	410	79	75	73	1.51	10	81.70	4.97	445	439.36
			1HNM-19-1A	25	25.2	410	79	75	73	1.51	10	86.00	5.11	445	335.19
			1HNM-19-1B	25	25.2	410	79	75	73	1.51	10	85.12	5.07	445	335.19
			1HNM-19-1C	25	25.2	410	79	75	73	1.51	10	85.12	5.07	445	356.65
		Monotonic in Compression	1HNM-19-2	25	25.2	410	79	75	73	1.51	10	83.6	5.03	445	331.49
			1HNM-19-2A	25	25.2	410	79	75	73	1.51	10	83.67	5.03	445	339.21
			1HNM-19-2B	25	25.2	410	79	75	73	1.51	10	83.67	5.03	445	367.49
			1HNM-19-2C	25	25.2	410	79	75	73	1.51	10	83.67	5.03	445	435.07

Table 5.3- Detail of the test specimens under monotonic loading (M2, M3)

Group	Investigation Parameter	Loading History	Specimen Notation	Rebar				Cover	Embedded Length	Rate of Loading	Confining rebar	Concrete Strength		Yield Stress	Steel Stress
				Diam. Nominal	Diam. Actual	Area	Perim.			Displ.Con.	diameter	Compr.	Tensile		
				mm	mm	mm2	mm	mm	mm	mm/min	mm	f'c MPa	f'ct MPa	fy MPa	fs MPa
M2	Confinnng Reinf.	Monotonic in Tension	2HNM-8-1	35	35.7	860	112	70	100	1.51	-	85.00	5.07	448	314.69
			2HNM-8-2	35	35.7	860	112	70	100	1.51	10	85.00	5.07	448	294.45
			2HNM-8-3	35	35.7	860	112	70	100	1.51	20	85.00	5.07	448	316.91
			2HNM-8-4	35	35.7	860	112	70	100	1.51	25	85.00	5.07	448	221.12
			2HNM-8-1	25	25.2	410	79	75	73	1.51	-	81.70	4.97	445	411.68
			2HNM-8-2	25	25.2	410	79	75	73	1.51	10	81.70	4.97	445	417.63
			2HNM-8-3	25	25.2	410	79	75	73	1.51	20	85.00	5.07	445	410.32
			2HNM-8-4	25	25.2	410	79	75	73	1.51	25	85.00	5.07	445	-
		Monotonic in Compr.	2HNM-8-1	25	25.2	410	79	75	73	1.51	-	81.70	4.97	445	472.78
			2HNM-8-2	25	25.2	410	79	75	73	1.51	10	81.70	4.97	445	452.54
			2HNM-8-3	25	25.2	410	79	75	73	1.51	20	85.00	5.07	445	454.56
			2HNM-8-4	25	25.2	410	79	75	73	1.51	25	85.00	5.07	445	281.19
M3	Rebar Diameter	Monotonic in tension	3HNM-12-1	20	19.5	220	61	77.75	73	1.51	10	78.00	4.86	435	853.54
			3HNM-12-2	25	25.2	410	79	75	73	1.51	10	90.30	5.23	445	350.12
			3HNM-12-3	35	35.7	860	112	70	100	1.51	10	87.45	5.14	448	256.58

Table 5.4- Detail of the test specimens under monotonic loading (M4, M5, M6)

Group	Investigation Parameter	Loading History	Specimen Notation	Rebar				Cover	Embedded Length	Rate of Loading	Confining rebar	Concrete Strength		Yield Stress	Steel Stress
				Diam. Nominal	Diam. Actual	Area	Perim.			Displ. Con.	diameter	Compr. f'_c	Tensile f'_{ct}	f_y	f_s
				mm	mm	mm2	mm	mm	mm	mm/min	mm	MPa	MPa	MPa	MPa
M4	Concrete Strength	Monotonic in Tension	4HNM-12-1	35	35.7	860	112	70	100	1.51	10	**50.61**	3.91	448	79.69
			4HNM-12-2	35	35.7	860	112	70	100	1.51	10	**87.45**	5.14	448	289.48
			4HNM-12-3	35	35.7	860	112	70	100	1.51	10	**91.45**	5.26	448	289.36
			4HNM-12-4	35	35.7	860	112	70	100	1.51	10	**92.70**	5.29	448	317.65
			4HNM-12-1	25	25.2	410	79	75	73	1.51	10	**50.61**	3.91	448	344.37
			4HNM-12-2	25	25.2	410	79	75	73	1.51	10	**86.00**	5.11	448	384.51
			4HNM-12-3	25	25.2	410	79	75	73	1.51	10	**92.61**	5.29	448	384.51
			4HNM-12-4	25	25.2	410	79	75	73	1.51	10	**94.96**	5.36	448	407.9
M5	Bar Spacing	Monotonic in Tension	5HNM-4-1	35	35.7	860	112	70	100	1.51	10	86.59	5.12	448	236.80
			5HNM-4-2	35	35.7	860	112	70	100	1.51	10	94.640	5.350	448	284.66
			5HNM-4-1	25	25.2	410	79	75	73	1.51	10	90.30	5.23	445	350.11
			5HNM-4-2	25	25.2	410	79	75	73	1.51	10	92.61	5.29	445	407.91
M6	Rate of Pull-out	Monotonic in Tension	6HNM-6-1	35	35.7	860	112	70	100	**75.00**	10	89.00	5.19	448	275.27
			6HNM-6-2	35	35.7	860	112	70	100	**1.510**	10	87.45	5.14	448	289.48
			6HNM-6-3	35	35.7	860	112	70	100	**0.0151**	10	78.00	4.86	448	264.73
			6HNM-6-1	25	25.2	410	79	75	73	**75.000**	10	83.30	5.02	445	68.91
			6HNM-6-2	25	25.2	410	79	75	73	**1.510**	10	83.67	5.03	445	366.73
			6HNM-6-3	25	25.2	410	79	75	73	**0.0151**	10	83.30	5.02	445	260.71

Table 5.5- Details of the test specimens under monotonic loading (M7)

Group	Investigation Parameter	Loading History	Specimen Notation	Rebar				Cover	Relative Rib Area	Embedded Length	Rate of Loading	Confining rebar	Concrete Strength		Yield Stress	Steel Stress
				Diam. Nominal	Diam. Actual	Area	Perim.				Displ.Con.	diameter	Compr. f'_c	Tensile f'_{ct}	fy	fs
				mm	mm	mm2	mm	mm		mm	mm/min	mm	MPa	MPa	MPa	MPa
M7	Rebar Deformation Pattern	Monotonic in tension	7HNM-14-1	35	26.88	620.00	84.45	74.00	0.196	100	1.51	10	83.15	5.02	448	435.94
			7HNM-14-2	35	26.88	620.00	84.45	74.00	0.167	100	1.51	10	83.15	5.02	448	378.57
			7HNM-14-3	35	26.88	620.00	84.45	74.00	0.125	100	1.51	10	83.15	5.02	448	306.94
			7HNM-14-4	35	26.88	620.00	84.45	74.00	0.100	100	1.51	10	83.15	5.02	448	289.27
			7HNM-14-5	35	27.91	660.00	87.68	73.54	0.171	100	1.51	10	82.93	5.01	448	298.49
			7HNM-14-6	35	27.91	660.00	87.68	73.54	0.146	100	1.51	10	82.93	5.01	448	327.61
			7HNM-14-7	35	27.91	660.00	87.68	73.54	0.109	100	1.51	10	82.56	5.00	448	276.31
			7HNM-14-8	35	27.91	660.00	87.68	73.54	0.102	100	1.51	10	82.56	5.00	448	251.87
			7HNM-14-9	35	29.41	705.00	92.39	72.79	0.131	100	1.51	10	89.52	5.20	448	357.11
			7HNM-14-10	35	29.41	705.00	92.39	72.79	0.112	100	1.51	10	89.52	5.20	448	366.84
			7HNM-14-11	35	29.41	705.00	92.39	72.79	0.084	100	1.51	10	86.23	5.10	448	293.21
			7HNM-14-12	35	29.41	705.00	92.39	72.79	0.067	100	1.51	10	86.23	5.10	448	237.98
			7HNM-14-13	35	34.00	860.00	106.81	70.51	-	100	1.51	10	74.75	4.76	448	96.72
			7HNM-14-14	35	35.70	860.00	112.00	70.00	0.163	100	1.51	10	81.00	4.95	448	253.49
			7HNM-10-1	25	22.00	380.00	69.12	76.50	0.087	73	1.51	10	94.64	5.35	445	175.03
			7HNM-10-2	25	21.60	366.00	67.86	76.70	0.074	73	1.51	10	94.64	5.35	445	209.85
			7HNM-10-3	25	21.40	360.00	67.23	76.80	0.056	73	1.51	10	92.00	5.28	445	275.34
			7HNM-10-4	25	21.80	373.00	68.49	76.60	0.045	73	1.51	10	86.70	5.12	445	238.52
			7HNM-10-5	25	22.00	380.00	69.12	76.50	0.126	73	1.51	10	86.00	5.10	445	299.24
			7HNM-10-6	25	21.20	353.00	66.60	76.90	0.107	73	1.51	10	86.00	5.10	445	-
			7HNM-10-7	25	21.70	370.00	68.17	76.65	0.081	73	1.51	10	86.70	5.12	445	203.32
			7HNM-10-8	25	21.90	376.00	68.81	76.55	0.065	73	1.51	10	88.79	5.18	445	262.36
			7HNM-10-9	25	25.00	410.00	78.54	75.00	0.101	73	1.51	10	86.00	5.10	445	384.51
			7HNM-10-10	25	23.00	410.00	72.26	76.00	-	73	1.51	10	90.26	5.23	445	91.92

Table 5.6-Comparison of results for rebar with nominal diameter 35 mm

Curve Number	Specimen Notation	Rib Geometry							Relative rib area
		Rebar Area	Concrete Strength f'c	Peak Load Pmax	Bond Stress U'max	Slip at Peak S	Height	Rib Spacing	
		mm2	MPa	kN	MPa	mm	mm	mm	
3	7HNM-14-3	620	83.15	190.30	21.62	7.46	3.56	25.40	0.125
7	7HNM-14-7	660	82.56	182.36	19.99	5.17	3.05	25.40	0.109
12	7HNM-14-12	705	86.23	167.78	17.80	5.64	2.29	31.75	0.067
14	7HNM-14-14	1000	81.00	218.00	19.47	6.53	S	S	0.163
13	7HNM-14-13	908	74.75	83.18	7.76	3.07	-	-	-

S Canadian Standard

Table 5.7- Comparison of results for rebar with nominal diameter 25 mm

Curve Number	Specimen Notation	Rib Geometry							Relative rib area
		Rebar Area	Concrete Strength f'c	Peak Load Pmax	Bond Stress U'max	Slip at Peak S	Rib		
							Height	Spacing	
		mm2	MPa	kN	MPa	mm	mm	mm	
3	7HNM-10-3	360	92.00	99.12	20.12	4.12	1.52	25.40	0.056
5	7HNM-10-5	380	86.00	113.71	22.55	4.21	2.29	16.26	0.126
9	7HNM-10-9	500	86.00	157.65	27.34	6.53	S	S	0.101
10	7HNM-10-10	415	90.26	37.68	7.08	2.49	-	-	-

S Canadian Standard

Table 5.8- Comparison of different expressions for bond strength (M1)

Group	Investigation Parameter	Loading History	Specimen Notation	Comparison of Bond Stress					
				Suggessted (RBE)	Esfahani& Rangan (E&R)	AS3600 (AUS)	ACI-95 (ACI)	CSA94 (CSA)	Darwin et al. (DAR)
				MPa	MPa	MPa	MPa	MPa	MPa
M1	Load History	Monotonic in Tension	1HNM-19-1	5.649	5.388	6.017	6.002	5.126	3.545
			1HNM-19-1A	5.559	5.257	5.874	5.859	5.004	3.484
			1HNM-19-1B	5.559	5.257	5.874	5.859	5.004	3.484
			1HNM-19-1C	5.559	5.257	5.874	5.859	5.004	3.484
		Monotonic in Compression	1HNM-19-2A	5.559	5.257	5.874	5.859	5.004	3.484
			1HNM-19-2B	5.653	5.389	6.021	6.006	5.129	3.547
			1HNM-19-2C	5.609	5.327	5.952	6.006	5.129	3.517
		Monotonic in Tension	1HNM-19-1	5.576	6.419	8.339	5.884	5.025	3.505
			1HNM-19-1A	5.672	6.586	8.551	6.037	5.156	3.571
			1HNM-19-1B	5.653	6.552	8.507	6.006	5.129	3.557
			1HNM-19-1C	5.653	6.552	8.507	6.006	5.129	3.557
		Monotonic in Compression	1HNM-19-2	5.621	6.494	8.434	5.935	5.086	3.534
			1HNM-19-2A	5.621	6.497	8.434	5.955	5.086	3.534
			1HNM-19-2B	5.621	6.497	8.434	5.955	5.086	3.534
			1HNM-19-2C	5.621	6.497	8.434	5.955	5.086	3.534

Table 5.9- Comparison of different expressions for bond strength (M2, M3)

Group	Investigation Parameter	Loading History	Specimen Notation	Comparison of Bond Stress					
				Suggessted (RBE)	Esfahani & Rangan (E&R)	AS3600 (AUS)	ACI-95 (ACI)	CSA94 (CSA)	Darwin et al. (DAR)
				MPa	MPa	MPa	MPa	MPa	MPa
M2	Confining Reinf.	Monotonic in Tension	2HNM-8-1	5.649	5.385	6.017	6.002	5.126	3.541
			2HNM-8-2	5.649	5.385	6.017	6.002	5.126	3.541
			2HNM-8-3	5.649	5.385	6.017	6.002	5.126	3.541
			2HNM-8-4	5.649	5.385	6.017	6.002	5.126	3.541
			2HNM-8-1	5.576	6.419	8.334	5.884	5.025	3.512
			2HNM-8-2	5.576	6.419	8.334	5.884	5.025	3.512
			2HNM-8-3	5.649	6.548	8.501	6.002	5.126	3.565
			2HNM-8-4	5.649	6.548	8.501	6.002	5.126	3.565
		Monotonic in Compression	2HNM-8-1	5.576	6.419	8.334	5.884	5.025	3.512
			2HNM-8-2	5.576	6.419	8.334	5.884	5.025	3.512
			2HNM-8-3	5.649	6.585	8.501	6.002	5.126	3.565
			2HNM-8-4	5.649	6.585	8.501	6.002	5.126	3.565
M3	Rebar Diameter	Monotonic in tension	3HNM-12-1	5.491	6.308	10.511	5.749	4.909	3.481
			3HNM-12-2	5.765	6.749	8.762	6.186	5.283	3.632
			3HNM-12-3	5.704	5.462	6.103	6.087	5.198	3.381

Table 5.10- Comparison of different expressions for bond strength (M4, M5, M6)

Group	Investigation Parameter	Loading History	Specimen Notation	Comparison of Bond Stress					
				Suggessted (RBE)	Esfahani& Rangan (E&R)	AS3600 (AUS)	ACI-95 (ACI)	CSA-94 (CSA)	Darwin et al. (DAR)
				MPa	MPa	MPa	MPa	MPa	MPa
M4	Concrete Strength	Monotonic in Tension	4HNM-12-1	4.753	4.155	4.643	4.631	3.954	2.954
			4HNM-12-2	5.704	5.462	6.103	6.087	5.198	3.581
			4HNM-12-3	5.789	5.586	6.241	6.225	5.316	3.641
			4HNM-12-4	5.816	5.624	6.284	6.267	5.352	3.658
			4HNM-12-1	4.753	5.053	6.559	4.631	3.954	2.961
			4HNM-12-2	5.672	6.586	8.551	6.037	5.156	3.571
			4HNM-12-3	5.814	6.835	8.873	6.265	5.351	3.668
			4HNM-12-4	5.863	6.921	8.985	6.344	5.418	3.702
M5	Bar Spacing	Monotonic in Tension	5HNM-4-1	5.685	5.435	6.073	6.058	5.174	3.569
			5HNM-4-2	5.856	5.682	6.349	6.333	5.408	3.686
			5HNM-4-1	5.765	6.749	8.762	6.186	5.283	3.635
			5HNM-4-2	5.814	6.835	8.873	6.265	5.351	3.668
M6	Rate of Pull-out	Monotonic in Tension	6HNM-6-1	5.737	5.511	6.157	6.141	5.244	3.604
			6HNM-6-2	5.703	5 462	6.103	6.087	5.198	3.581
			6HNM-6-3	5.491	5.159	5.764	5.749	4.909	3.437
			6HNM-6-1	5.612	6.482	8.415	5.941	5.074	3.529
			6HNM-6-2	5.521	6.496	8.434	5.954	5.085	3.535
			6HNM-6-3	5.612	6.482	8.415	5.941	5.074	3.535

Table 5.11- Comparison of different expressions for bond strength (M7)

Group	Investigation Parameter	Loading History	Specimen Notation	Comparison of Bond Stress					
				Suggessted (RBE) MPa	Esfahani & Rangan (E&R) MPa	AS3600 (AUS) MPa	ACI-95 (ACI MPa	CSA-94 (CSA) MPa	Darwin et al. (DAR) MPa
M7	Rebar Deformation Pattern	Monotonic in tension	7HNM-14-1	5.609	6.186	7.868	5.936	5.069	3.517
			7HNM-14-2	5.609	6.186	7.868	5.936	5.069	3.517
			7HNM-14-3	5.609	6.186	7.868	5.936	5.069	3.517
			7HNM-14-4	5.609	6.186	7.868	5.936	5.069	3.517
			7HNM-14-5	5.604	6.039	7.572	5.928	5.062	3.513
			7HNM-14-6	5.604	6.039	7.572	5.928	5.062	3.513
			7HNM-14-7	5.595	6.039	7.555	5.915	5.051	3.513
			7HNM-14-8	5.595	6.039	7.555	5.915	5.051	3.513
			7HNM-14-9	5.748	6.073	7.466	6.159	5.259	3.612
			7HNM-14-10	5.748	6.073	7.466	6.159	5.259	3.612
			7HNM-14-11	5.677	5.960	7.328	6.045	5.162	3.612
			7HNM-14-12	5.677	5.960	7.328	6.045	5.162	3.612
			7HNM-14-13	5.413	5.152	5.903	5.628	4.806	3.385
			7HNM-14-14	5.559	5.257	5.874	5.859	5.003	3.484
			7HNM-10-1	5.856	6.949	10.263	6.333	5.408	3.698
			7HNM-10-2	5.856	6.949	10.454	6.333	5.408	3.698
			7HNM-10-3	5.801	6.851	10.402	6.244	5.332	3.659
			7HNM-10-4	5.687	6.651	9.914	6.061	5.176	3.581
			7HNM-10-5	5.672	6.624	9.783	6.037	5.156	3.571
			7HNM-10-6	5.672	6.624	10.152	6.037	5.156	3.571
			7HNM-10-7	5.687	6.651	9.958	6.062	5.177	3.581
			7HNM-10-8	5.732	6.731	9.987	6.131	5.236	3.612
			7HNM-10-9	5.672	6.624	8.551	6.037	5.156	3.571
			7HNM-10-10	5.764	6.786	9.586	6.185	5.282	3.634

Table 5.12- Comparison of normalized bond stress with other bond stress expressions

Group	Investigation Parameter	Loading History	Specimen Notation	Test* / RBE	Test* / E&R	Test* / AUS	Test* / ACI	Test* / CSA	Test* / DAR
M1	Load History	Monotonic in Tension	1HNM-19-1	0.966	1.013	0.907	0.909	1.065	1.540
			1HNM-19-1A	0.809	0.856	0.766	0.768	0.899	1.291
			1HNM-19-1B	0.623	0.659	0.589	0.591	0.692	0.994
			1HNM-19-1C	0.781	0.826	0.739	0.741	0.868	1.246
		Monotonic in Compression	1HNM-19-2A	0.811	0.858	0.768	0.770	0.901	1.295
			1HNM-19-2B	0.781	0.819	0.733	0.735	0.861	1.245
			1HNM-19-2C	0.697	0.734	0.657	0.651	0.762	1.111
		Monotonic in Tension	1HNM-19-1	1.248	1.084	0.834	1.183	1.385	1.985
			1HNM-19-1A	1.092	0.940	0.724	1.026	1.201	1.735
			1HNM-19-1B	0.958	0.826	0.637	0.902	1.056	1.522
			1HNM-19-1C	1.019	0.880	0.677	0.960	1.124	1.620
		Monotonic in Compression	1HNM-19-2	0.953	0.825	0.635	0.902	1.053	1.516
			1HNM-19-2A	0.978	0.846	0.652	0.923	1.081	1.556
			1HNM-19-2B	1.053	0.911	0.702	0.994	1.164	1.675
			1HNM-19-2C	1.258	1.089	0.839	1.188	1.390	2.001

Note. * refer to Normalized bond stress of test result, RBE refer to Recommended bond expression

E&R refer to Esfahani and Rangan, AUS refer to Australian Code, AS 3600

ACI refer to ACI 318-1995, CSA refer to CSA A23.3-1994, DAR refer to Darwin et al (1995) Expression

Table 5.13- Comparison of normalized bond stress with other bond stress expressions (M2,M3)

Group	Investigation Parameter	Loading History	Specimen Notation	Test* / RBE	Test* / E&R	Test* / AUS	Test* / ACI	Test* / CSA	Test* / DAR
M2	Confining Reinf.	Monotonic in Tension	2HNM-8-1	0.960	1.007	0.901	0.903	1.058	1.531
			2HNM-8-2	0.910	0.955	0.855	0.857	1.003	1.452
			2HNM-8-3	0.980	1.028	0.920	0.922	1.080	1.563
			2HNM-8-4	0.684	0.717	0.642	0.643	0.753	1.091
			2HNM-8-1	1.204	1.046	0.806	1.141	1.337	1.912
			2HNM-8-2	1.225	1.064	0.820	1.161	1.360	1.946
			2HNM-8-3	1.173	1.012	0.780	1.104	1.293	1.859
			2HNM-8-4	-	-	-	-	-	-
		Monotonic in Compression	2HNM-8-1	1.383	1.201	0.925	1.310	1.534	2.195
			2HNM-8-2	1.325	1.151	0.886	1.255	1.470	2.103
			2HNM-8-3	1.285	1.103	0.854	1.210	1.417	2.037
			2HNM-8-4	0.802	0.688	0.533	0.754	0.883	1.270
M3	Rebar Diameter	Monotonic in tension	3HNM-12-1	1.061	0.923	0.554	1.013	1.187	1.673
			3HNM-12-2	0.960	0.820	0.632	0.895	1.048	1.525
			3HNM-12-3	0.778	0.812	0.727	0.729	0.853	1.312

Note: * refer to Normalized bond stress, RBE refer to Recommended bond expression

E&R refer to Esfahani and Rangan, AUS refer to Australian Code, AS 3600

ACI refer to ACI 318-1995, CSA refer to CSA A23.3-1994, DAR refer to Darwin et al (1995) Expression

Table 5.14- Comparison of normalized bond stress with other bond expressions (M4, M5, M6)

Group	Investigation Parameter	Loading History	Specimen Notation	Test* / RBE	Test* / E&R	Test* / AUS	Test* / ACI	Test* / CSA	Test* / DAR
M4	Concrete Strength	Monotonic in Tension	4HNM-12-1	0.856	0.979	0.876	0.879	1.029	1.377
			4HNM-12-2	0.878	0.917	0.821	0.823	0.963	1.398
			4HNM-12-3	0.852	0.883	0.791	0.793	0.928	1.355
			4HNM-12-4	0.927	0.958	0.858	0.860	1.007	1.473
			4HNM-12-1	1.390	1.308	1.008	1.427	1.671	2.232
			4HNM-12-2	1.092	0.940	0.724	1.026	1.201	1.735
			4HNM-12-3	1.101	0.937	0.721	1.022	1.196	1.745
			4HNM-12-4	0.914	0.774	0.596	0.845	0.989	1.448
M5	Bar Spacing	Monotonic in Tension	5HNM-4-1	0.723	0.756	0.677	0.678	0.794	1.151
			5HNM-4-2	0.819	0.844	0.755	0.757	0.887	1.301
			5HNM-4-1	0.961	0.821	0.632	0.895	1.048	1.524
			5HNM-4-2	1.101	0.937	0.721	1.022	1.196	1.745
M6	Rate of Pull-out	Monotonic in Tension	6HNM-6-1	0.821	0.855	0.765	0.767	0.898	1.307
			6HNM-6-2	0.878	0.917	0.821	0.823	0.963	1.398
			6HNM-6-3	0.866	0.922	0.825	0.827	0.969	1.384
			6HNM-6-1	0.199	0.172	0.133	0.188	0.220	0.317
			6HNM-6-2	1.072	0.911	0.702	0.994	1.164	1.674
			6HNM-6-3	0.756	0.655	0.504	0.714	0.836	1.200

Note: * refer to Normalized bond stress, RBE refer to Recommended bond expression

E&R refer to Esfahani and Rangan, AUS refer to Australian Code, AS 3600

ACI refer to ACI 318-1995, CSA refer to CSA A23.3-1994, DAR refer to Darwin et al (1995) Expression

Table 5.15- Comparison of normalized bond stress with other bond stress expressions (M7)

Group	Investigation Parameter	Loading History	Specimen Notation	Test* / RBE	Test* / E&R	Test* / AUS	Test* / ACI	Test* / CSA	Test* / DAR
M7	Rebar Deformation Pattern	Monotonic in tension	7HNM-14-1	1.256	1.139	0.895	1.187	1.390	2.003
			7HNM-14-2	1.091	0.989	0.778	1.031	1.207	1.740
			7HNM-14-3	0.883	0.801	0.630	0.834	0.977	1.408
			7HNM-14-4	0.832	0.755	0.593	0.787	0.921	1.328
			7HNM-14-5	0.885	0.821	0.655	0.836	0.979	1.411
			7HNM-14-6	0.971	0.901	0.719	0.918	1.075	1.549
			7HNM-14-7	0.821	0.760	0.608	0.776	0.909	1.307
			7HNM-14-8	0.747	0.692	0.554	0.707	0.828	1.190
			7HNM-14-9	1.039	0.983	0.800	0.969	1.135	1.653
			7HNM-14-10	1.068	1.010	0.822	0.996	1.167	1.699
			7HNM-14-11	0.872	0.831	0.676	0.819	0.959	1.371
			7HNM-14-12	0.710	0.676	0.550	0.667	0.781	1.115
			7HNM-14-13	0.340	0.358	0.312	0.327	0.383	0.544
			7HNM-14-14	0.809	0.856	0.766	0.768	0.899	1.291
			7HNM-10-1	0.494	0.416	0.282	0.457	0.535	0.782
			7HNM-10-2	0.580	0.489	0.325	0.536	0.628	0.919
			7HNM-10-3	0.769	0.651	0.429	0.714	0.836	1.219
			7HNM-10-4	0.707	0.605	0.406	0.664	0.777	1.123
			7HNM-10-5	0.901	0.771	0.522	0.846	0.991	1.431
			7HNM-10-6	-	-	-	-	-	-
			7HNM-10-7	0.599	0.513	0.342	0.562	0.658	0.952
			7HNM-10-8	0.767	0.653	0.440	0.717	0.839	1.217
			7HNM-10-9	1.092	0.935	0.724	1.026	1.201	1.735
			7HNM-10-10	0.274	0.233	0.165	0.255	0.299	0.434

Note. * refer to Normalized bond stress, RBE refer to Recommended bond expression
E&R refer to Esfahani and Rangan, AUS refer to Australian Code, AS 3600
ACI refer to ACI 318-1995, CSA refer to CSA A23.3-1994, DAR refer to Darwin et al (1995) Expression

Table 5.16- Slip, load and bond stress of tested specimens (M1, M2, M3, M4)

Group	Investigation Parameter	Loading History	Specimen Notation	Slip at Peak S mm	Peak Load Pmax kN	Test Result MPa	Normalized Test Result*
M1	Load History	Monotonic in Tension	1HNM-19-1	7.71	278.00	24.800	5.458
			1HNM-19-1A	6.53	218.00	19.470	4.499
			1HNM-19-1B	5.24	167.80	14.980	3.462
			1HNM-19-1C	6.06	210.35	18.780	4.341
		Monotonic in Compression	1HNM-19-2A	6.71	218.65	19.520	4.511
			1HNM-19-2B	6.69	217.54	19.420	4.415
			1HNM-19-2C	5.72	191.08	17.060	3.908
		Monotonic in Tension	1HNM-19-1	8.19	180.14	30.190	6.958
			1HNM-19-1A	9.67	157.65	27.340	6.194
			1HNM-19-1B	5.92	137.43	23.820	5.415
			1HNM-19-1C	5.08	146.23	25.350	5.763
		Monotonic in Compression	1HNM-19-2	5.52	135.91	23.420	5.356
			1HNM-19-2A	5.12	139.08	24.050	5.498
			1HNM-19-2B	3.86	150.67	25.890	5.919
			1HNM-19-2C	5.29	178.38	30.930	7.072
M2	Confining Reinf.	Monotonic in Tension	2HNM-8-1	7.01	270.64	23.84	5.422
			2HNM-8-2	6.43	253.23	22.61	5.142
			2HNM-8-3	17.54	272.54	24.34	5.536
			2HNM-8-4	5.14	190.16	16.98	3.862
			2HNM-8-1	8.71	168.79	29.14	6.716
			2HNM-8-2	8.41	171.23	29.65	6.833
			2HNM-8-3	8.48	168.23	29.14	6.628
			2HNM-8-4	-	-	-	-
		Monotonic in Compr.	2HNM-8-1	6.83	193.84	33.45	7.709
			2HNM-8-2	3.23	185.54	32.05	7.386
			2HNM-8-3	5.94	186.37	31.93	7.261
			2HNM-8-4	2.32	115.29	19.91	4.528
M3	Rebar Diameter	Monotonic in tension	3HNM-12-1	7.29	112.67	24.89	5.825
			3HNM-12-2	6.84	143.55	24.84	5.537
			3HNM-12-3	6.82	220.66	19.69	4.436
M4	Concrete Strength	Monotonic in Tension	4HNM-12-1	6.89	68.530	6.120	4.069
			4HNM-12-2	6.95	248.950	22.230	5.008
			4HNM-12-3	6.38	248.850	22.220	4.934
			4HNM-12-4	8.06	273.180	24.390	5.389
			4HNM-12-1	6.72	141.190	24.450	6.609
			4HNM-12-2	9.38	157.650	27.340	6.194
			4HNM-12-3	6.92	167.240	28.960	6.401
			4HNM-12-4	8.83	141.210	24.450	5.359

* Normalized test results with respect to $\sqrt{f_c}$

Table 5.17- Slip, load and bond stress of tested specimens (M5, M6, M7)

Group	Investigation Parameter	Loading History	Specimen Notation	Slip at Peak S	Peak Load P_{max}	Test Result	Normalized Test Result*
				mm	kN	MPa	
M5	Bar Spacing	Monotonic in Tension	5HNM-4-1	5.80	203.650	18.180	4.109
			5HNM-4-2	8.78	244.810	21.856	4.796
			5HNM-4-1	6.83	143.540	24.850	5.539
			5HNM-4-2	7.19	167.240	28.960	6.401
M6	Rate of Pull-out	Monotonic in Tension	6HNM-6-1	6.85	236.730	21.030	4.711
			6HNM-6-2	6.96	248.950	22.230	5.008
			6HNM-6-3	5.98	227.670	20.320	4.756
			6HNM-6-1	5.54	28.250	4.880	1.117
			6HNM-6-2	5.29	150.360	25.890	5.919
			6HNM-6-3	7.19	106.890	18.530	4.243
M7	Rebar Deformation Pattern	Monotonic in tension	7HNM-14-1	7.42	270.28	30.750	7.045
			7HNM-14-2	7.63	234.71	26.710	6.119
			7HNM-14-3	7.46	190.30	21.620	4.953
			7HNM-14-4	5.91	179.35	20.380	4.669
			7HNM-14-5	4.64	197.00	21.620	4.958
			7HNM-14-6	5.23	216.22	23.730	5.442
			7HNM-14-7	5.17	182.36	19.990	4.591
			7HNM-14-8	6.08	166.24	18.210	4.182
			7HNM-14-9	7.93	251.76	26.710	5.971
			7HNM-14-10	7.92	258.62	27.450	6.136
			7HNM-14-11	5.13	206.71	21.870	4.951
			7HNM-14-12	5.64	167.78	17.800	4.029
			7HNM-14-13	3.07	83.18	7.760	1.842
			7HNM-14-14	6.53	218.00	19.470	4.499
			7HNM-10-1	4.79	66.51	13.180	2.892
			7HNM-10-2	4.24	76.82	15.480	3.397
			7HNM-10-3	4.12	99.12	20.120	4.46
			7HNM-10-4	5.15	89.01	17.800	4.022
			7HNM-10-5	4.21	113.71	22.550	5.109
			7HNM-10-6	-	-	-	-
			7HNM-10-7	5.07	75.23	15.090	3.409
			7HNM-10-8	4.02	98.65	19.610	4.395
			7HNM-10-9	6.53	157.65	27.340	6.194
			7HNM-10-10	2.49	37.68	7.080	1.578

* Normalized test results with respect to $\sqrt{f'_c}$

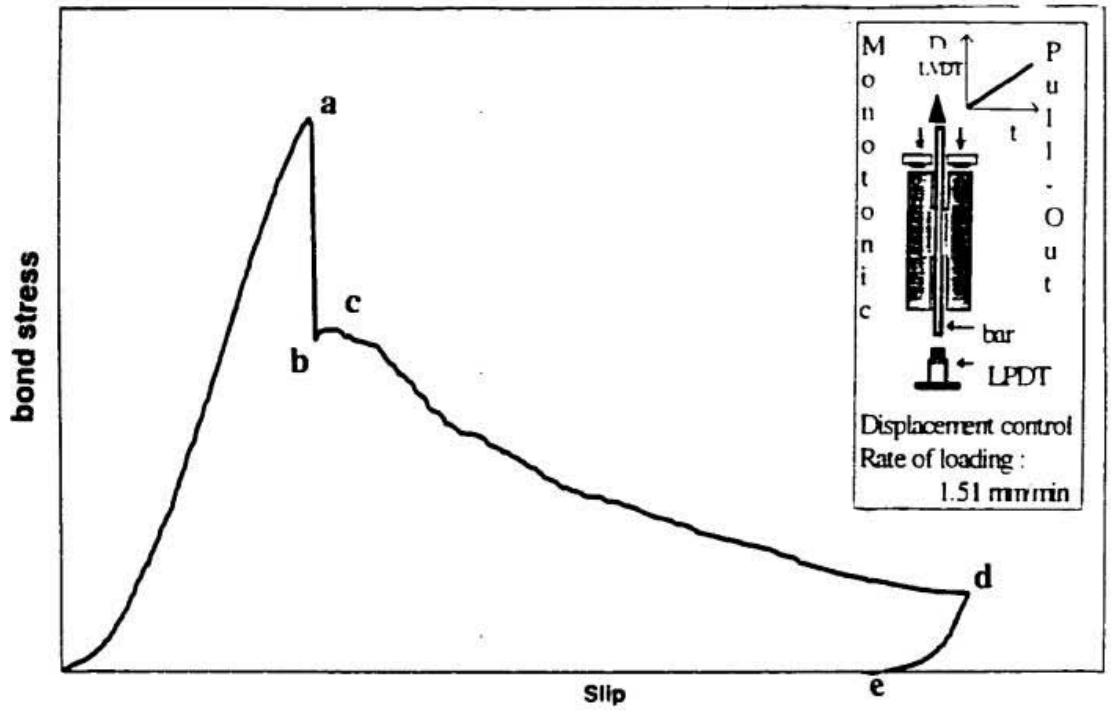

Fig. 5.1 Typical bond stress-slip relationship for high-strength concrete under monotonic load

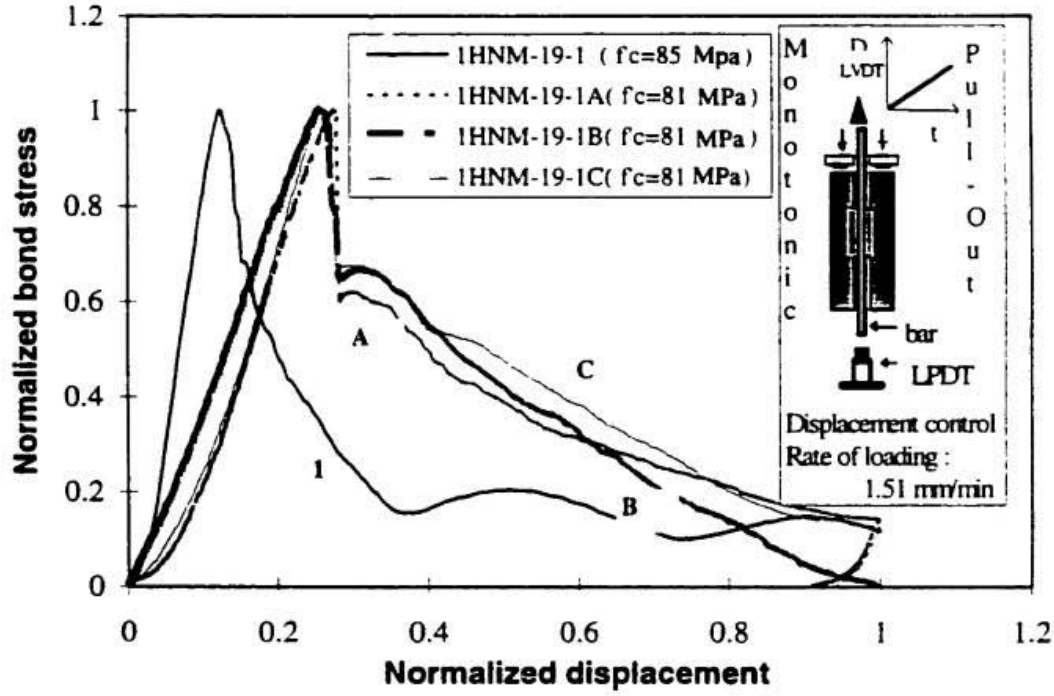

Fig. 5.2 Comparison of normalized bond stress-displacement response for four specimens due to pull-out test with an embedded bar diameter of 35 mm each

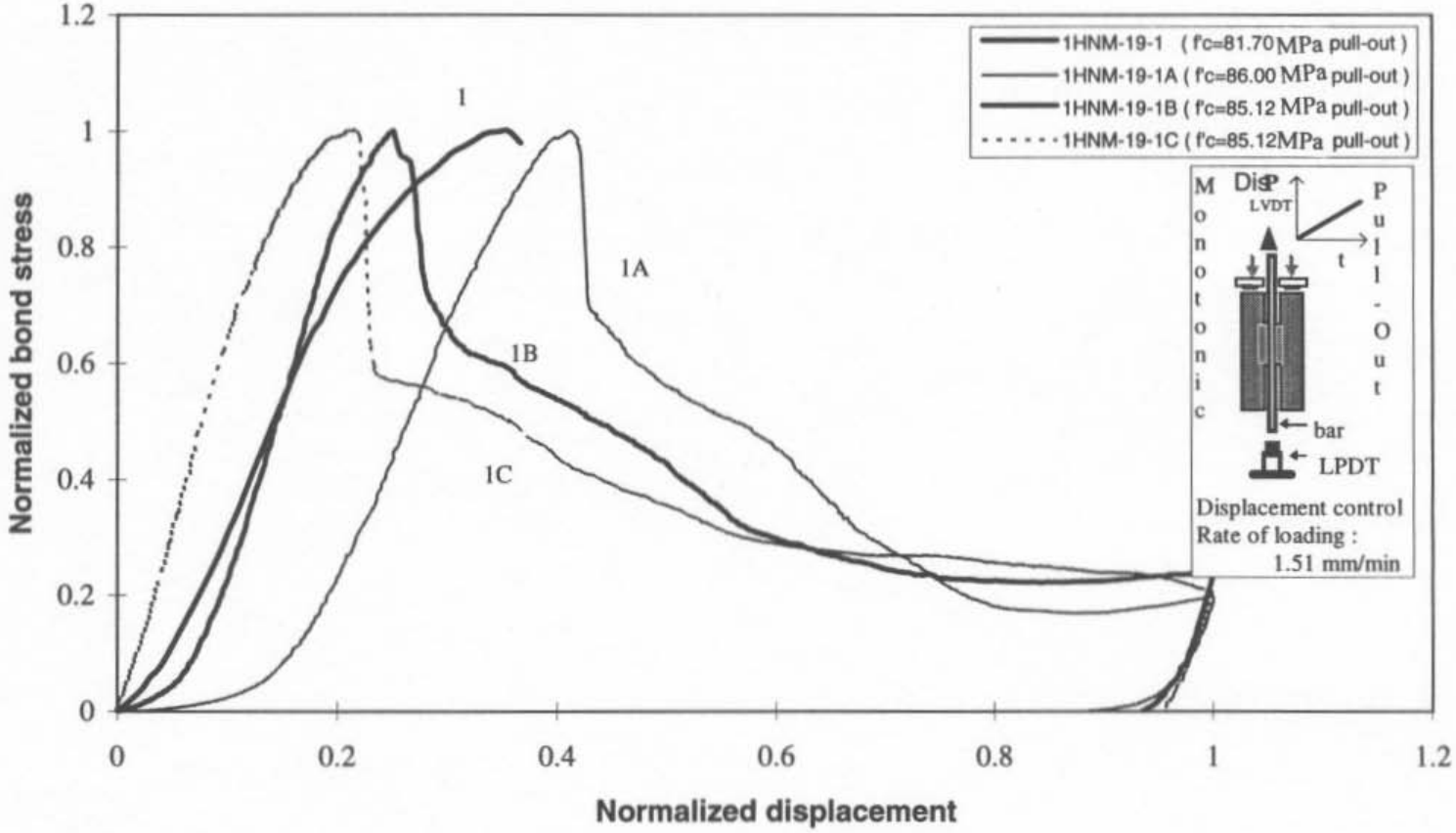

Fig. 5.3 Comparison of normalized bond stress-displacement response for four specimens due to pull-out test with an embedded bar diameter of 25 mm

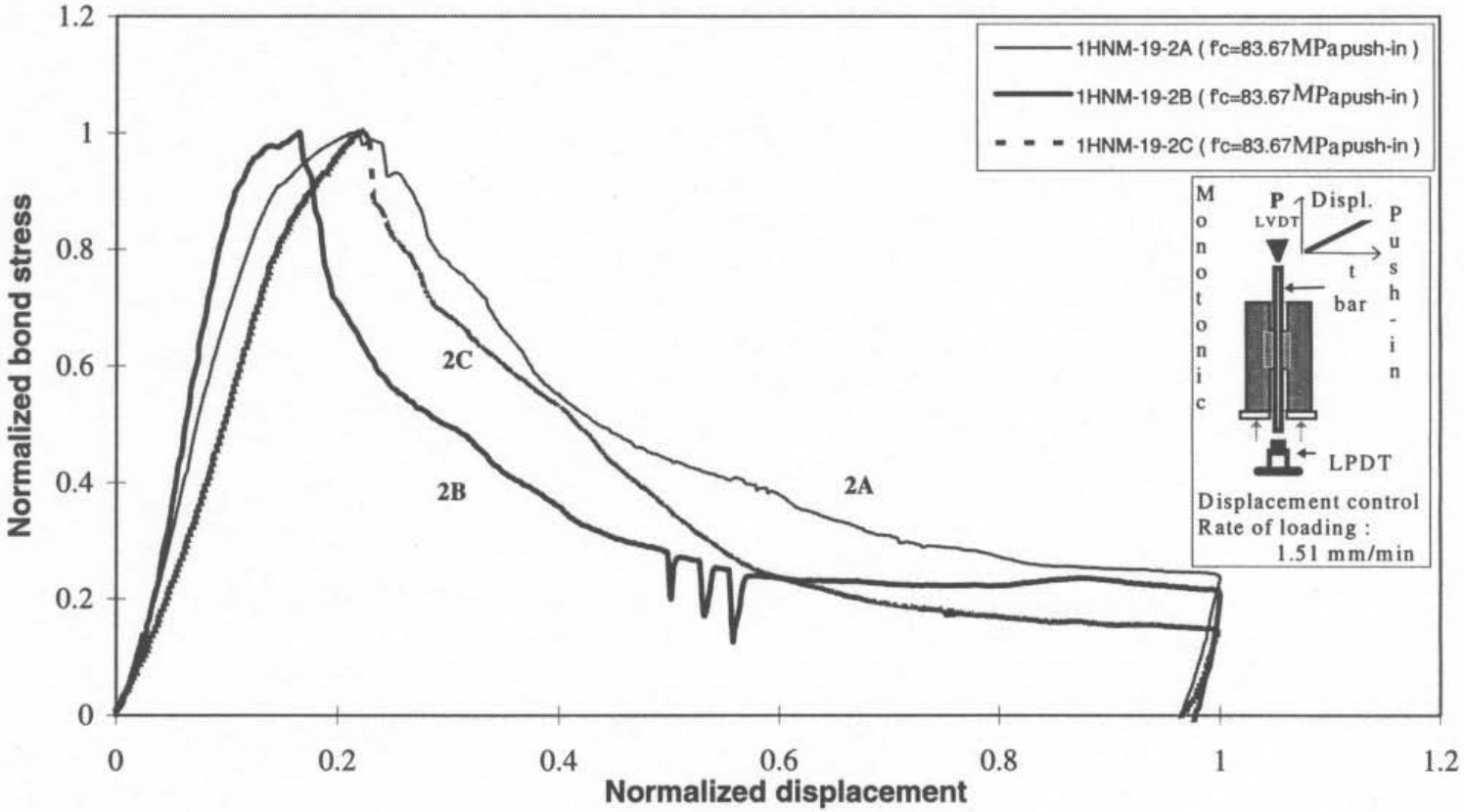

Fig. 5.4 Comparison of normalized bond stress-displacement response for three specimens due to push-in test with an embedded bar diameter of 25 mm

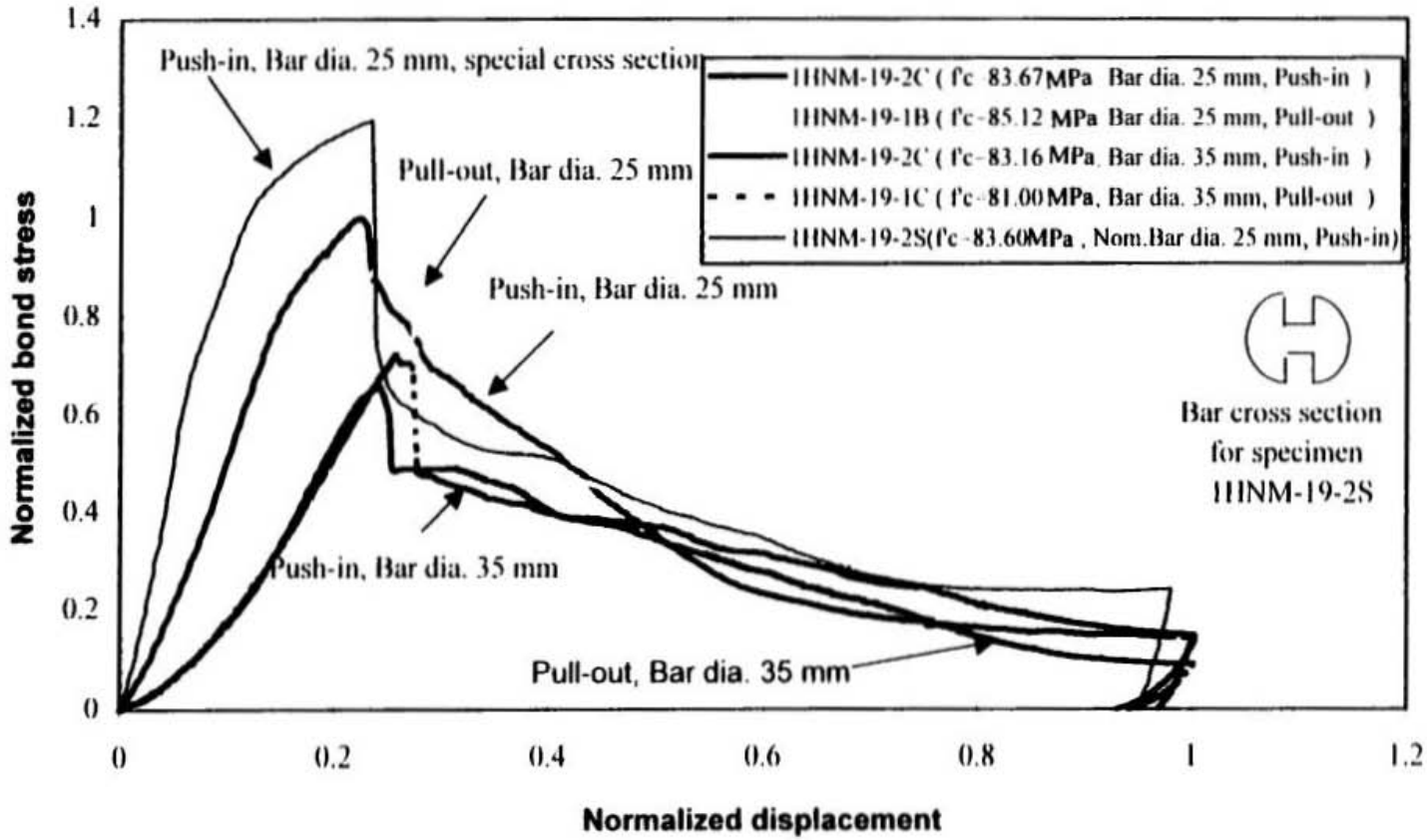

Fig.5.5 Comparison of normalized bond stress-displacement response for typical specimens due to pull-out and push-in test with an embedded bar diameter of 35 mm and 25 mm

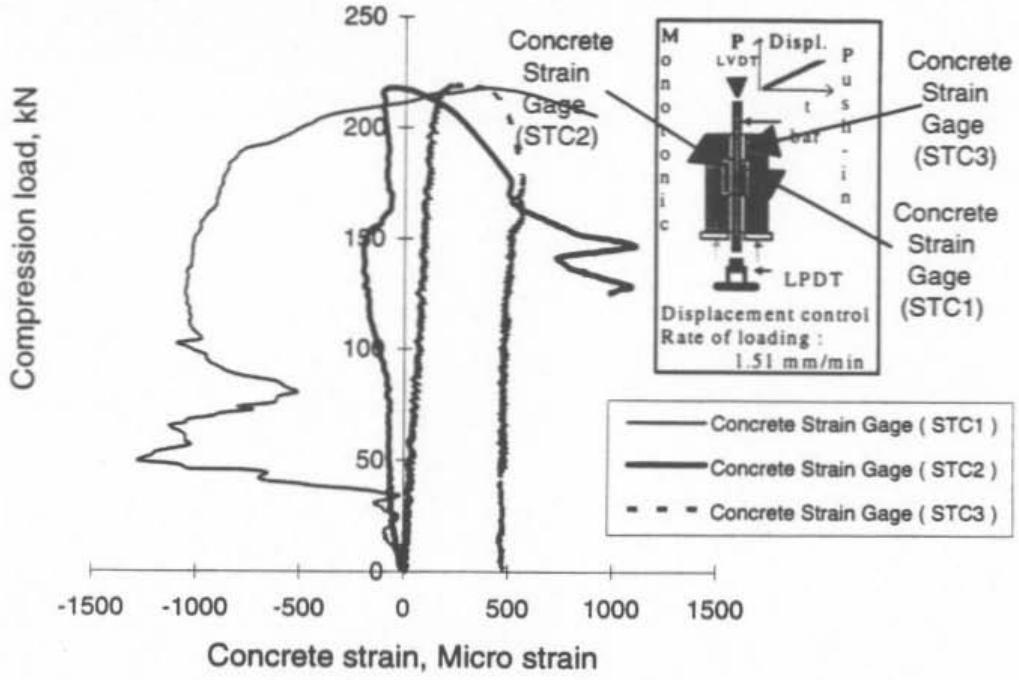

Fig. 5.6- Bond force-internal concrete strain for specimen 1HNM-19-2B with bond length 100 mm and embedded bar diameter of 35 mm

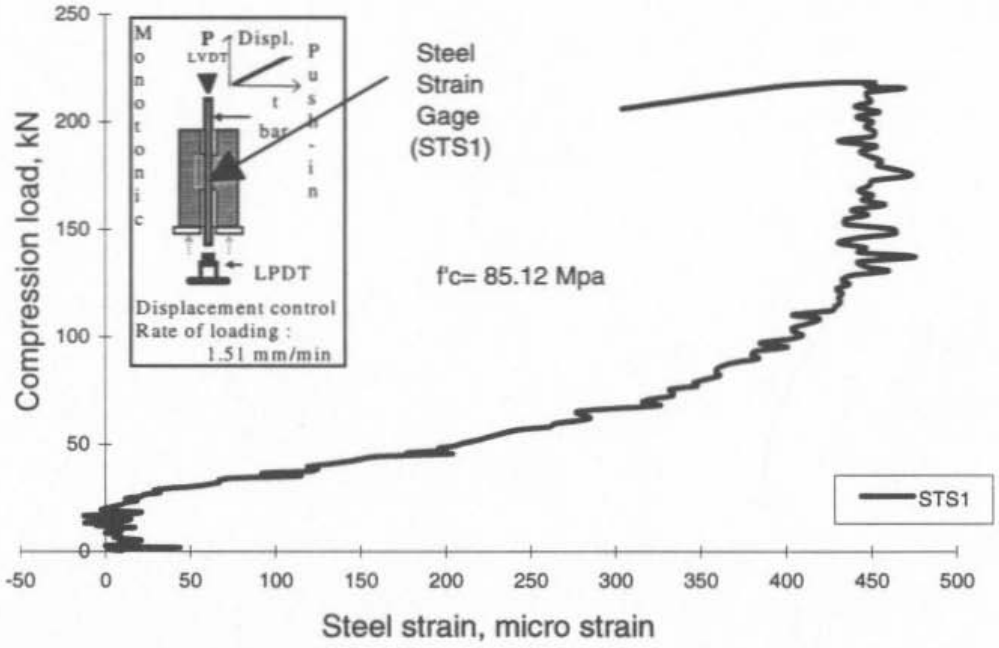

Fig. 5.7- Bond force-steel strain (STS1) for specimen 1HNM-19-2B with bond length 100 mm and embedded bar diameter of 35 mm

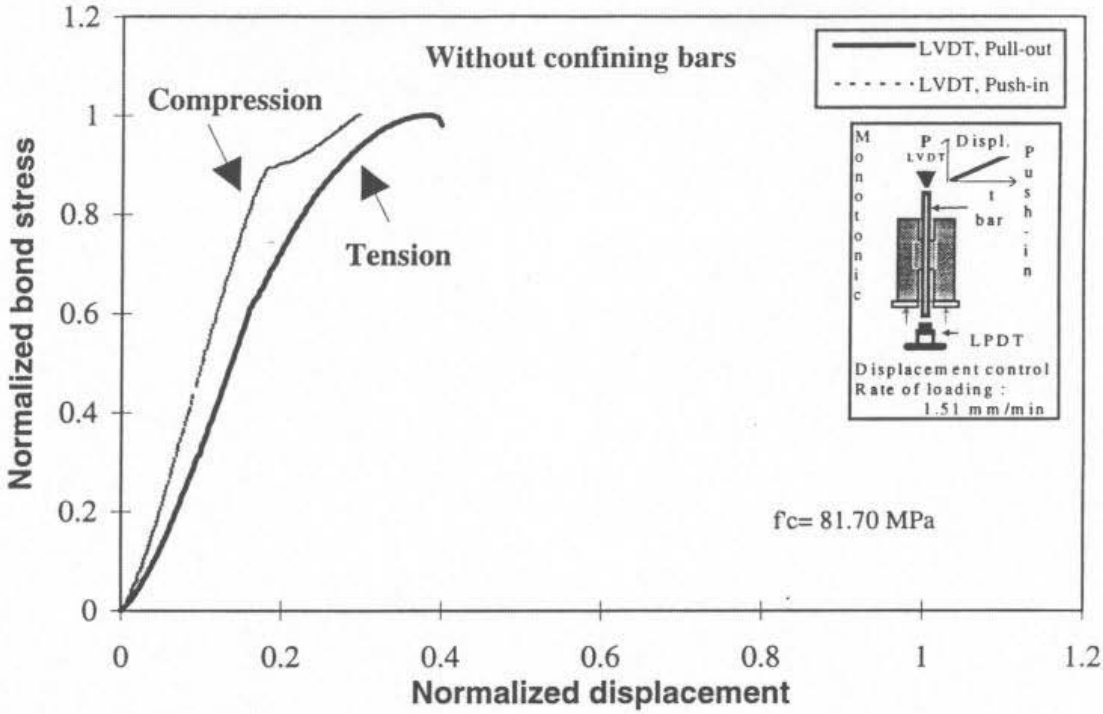

Fig. 5.8 Normalized bond stress-displacement response to LVDT for specimen 2HNM-8-1 with an embedded bar diameter of 25 mm under the tension and compression loading

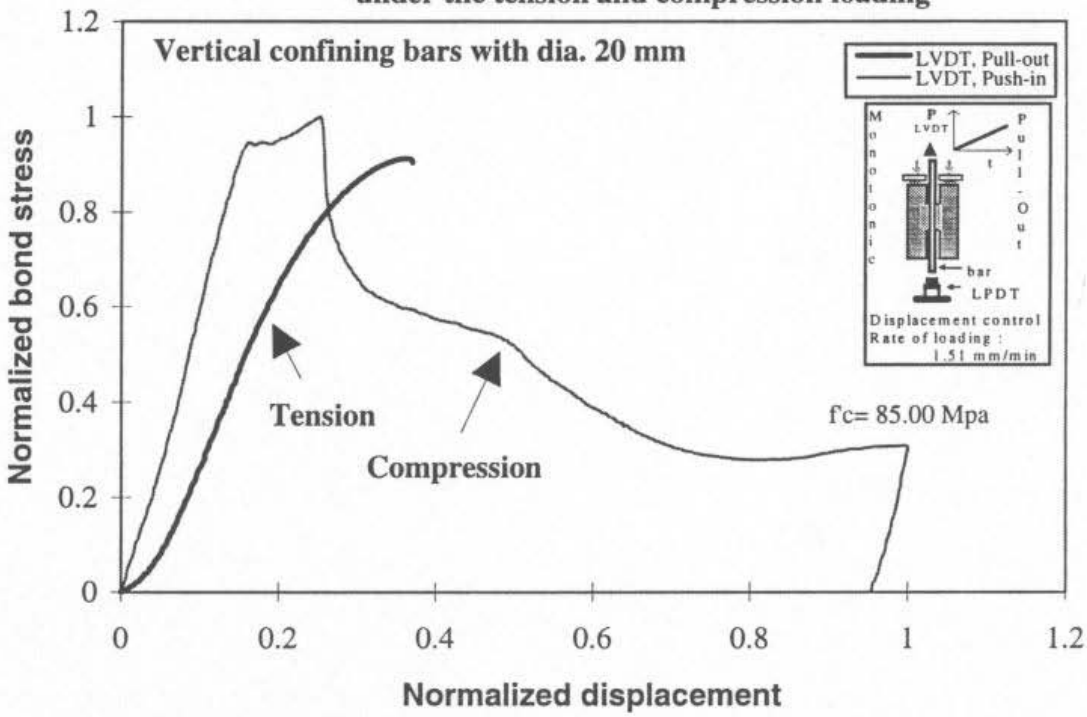

Fig. 5.9 Comparison of normalized bond stress-displacement response to LVDT for specimen 2HNM-8-3 with an embedded bar diameter of 25 mm under the tension and compression loading

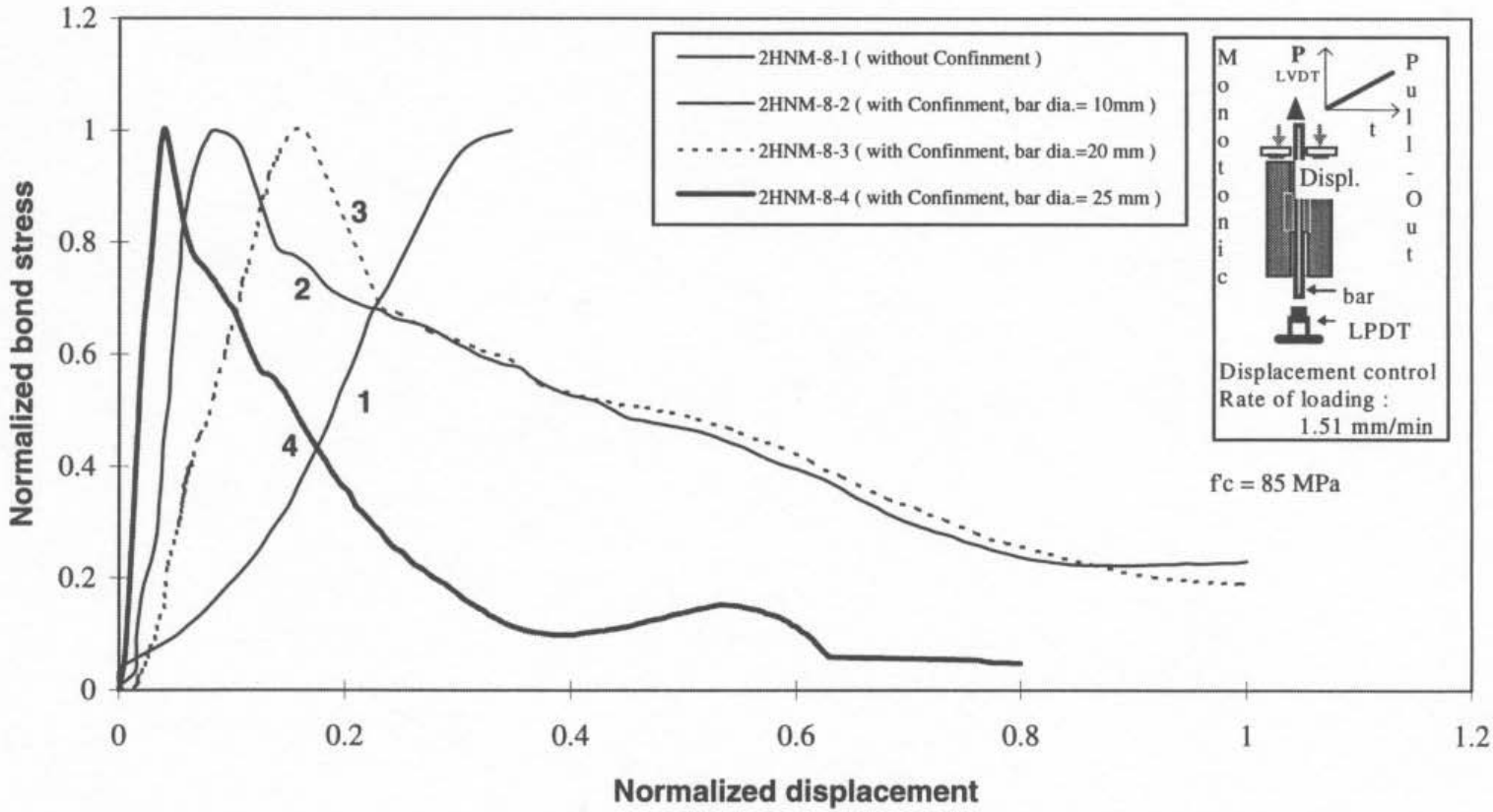

Fig. 5.10 Comparison of normalized bond stress-displacement response to four specimens with different confining bars with an embedded bar diameter of 35 mm

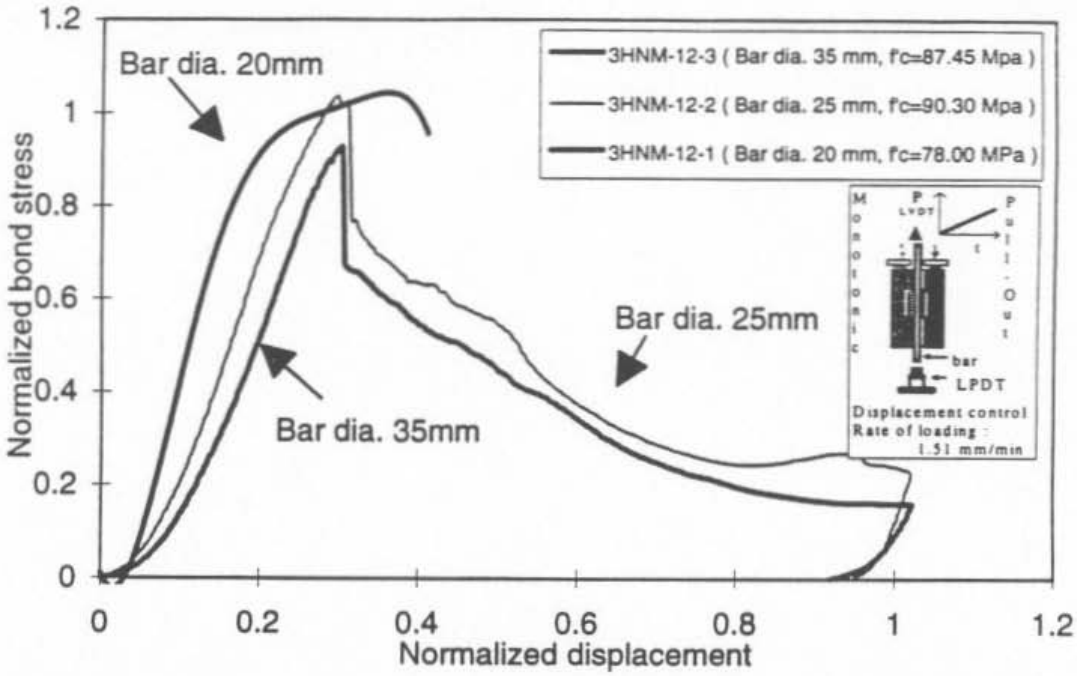

Fig. 5.11- Compression of normalized bond stress-displacement response to three specimens with different rebar diameter for high-strength concrete

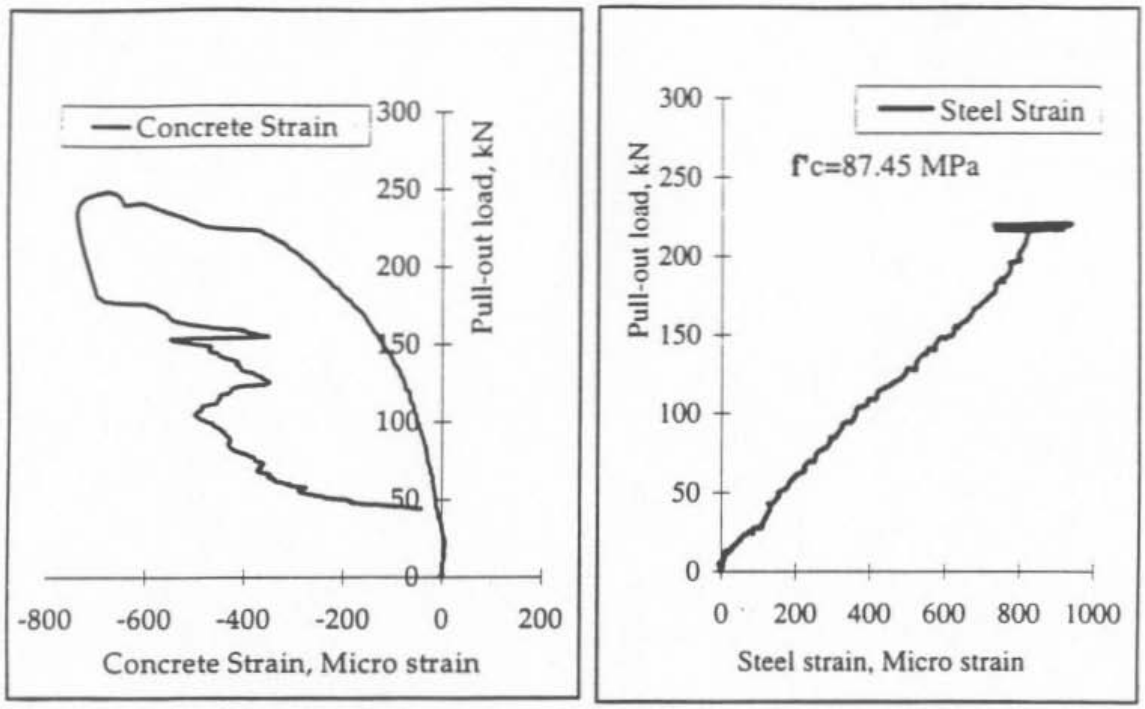

Fig. 5.12a & b- Bond force-internal concrete and steel strain (STC1)&(STS1) for specimen 3HNM-12-4 with bond length 100 mm and embedded bar diameter of 35 mm

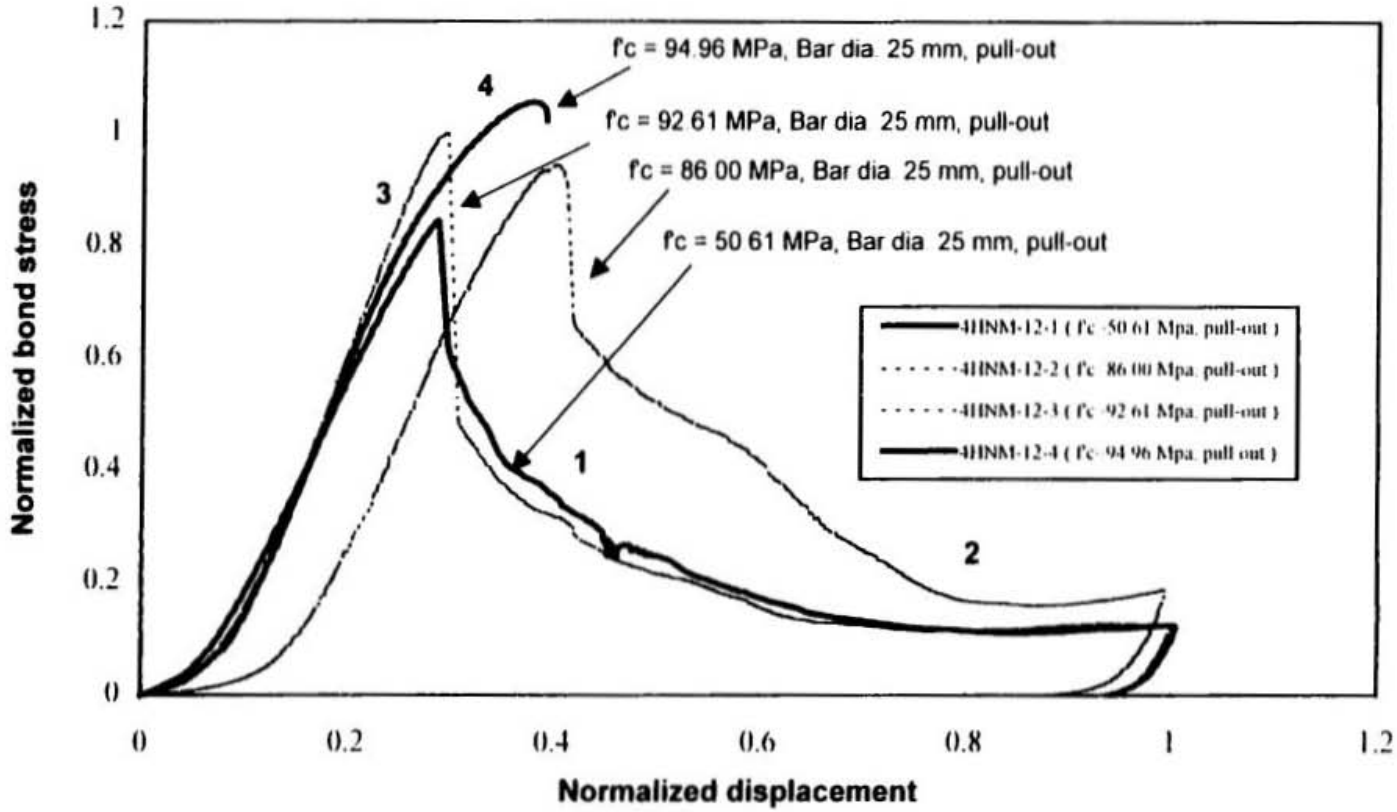

Fig. 5.13- Compression of normalized bond stress-displacement for response for four specimens with different type of concrete strength with an embedded bar diameter of 25 mm

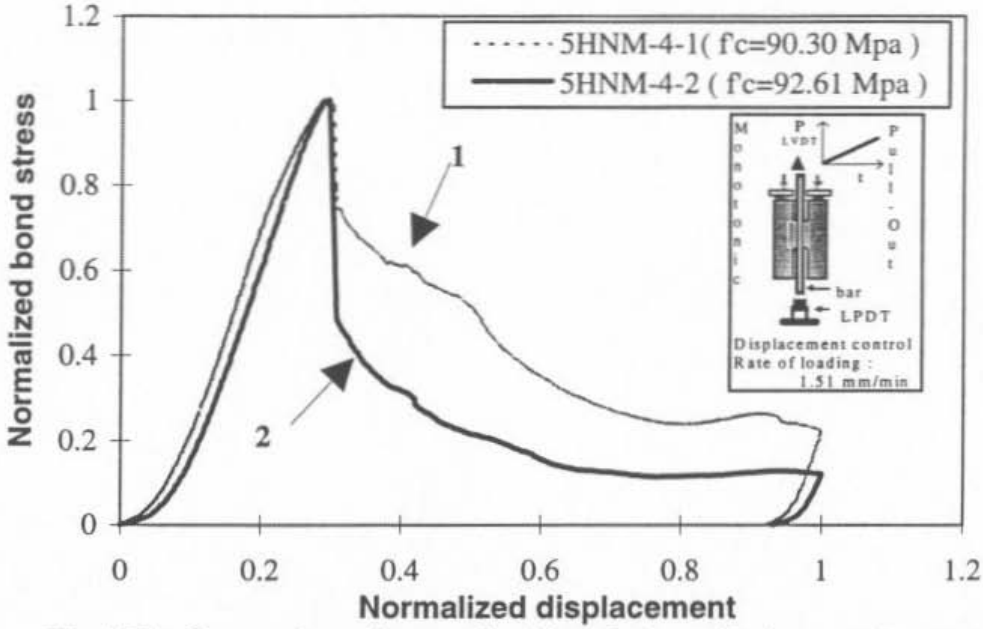

Fig. 5.14 Comparison of normalized bond stress-displacement response to two specimens with different bar spacing with an embedded bar diameter 25 mm

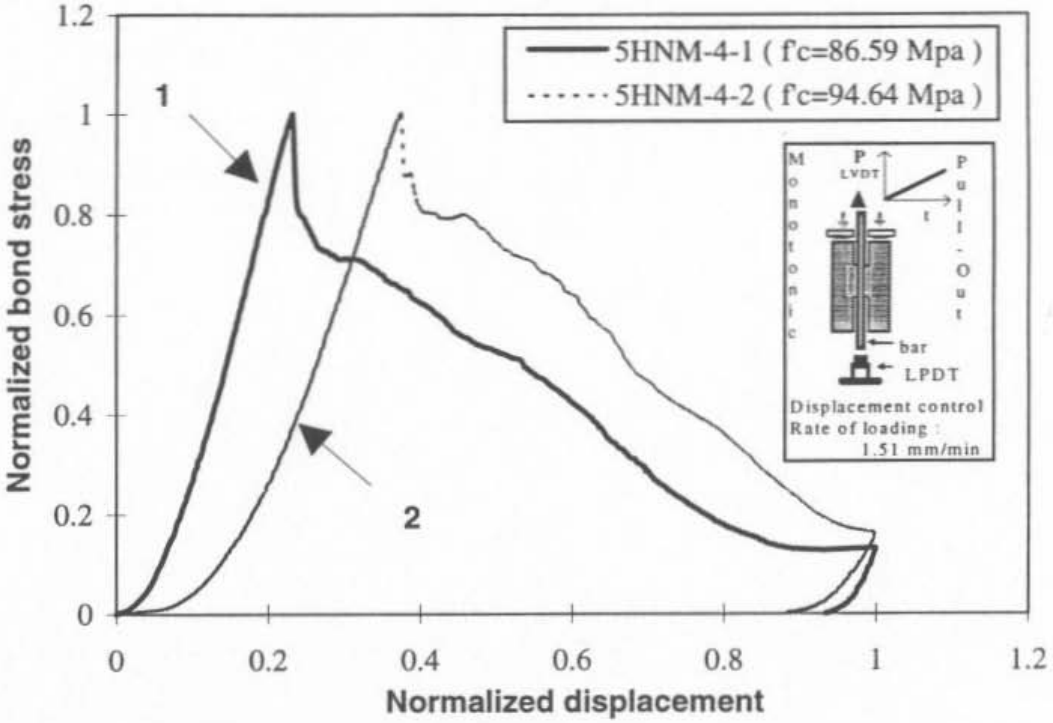

Fig. 5.15 Comparison of normalized bond stress-displacement response for two specimens with different bar spacing with an embedded bar diameter of 35 mm

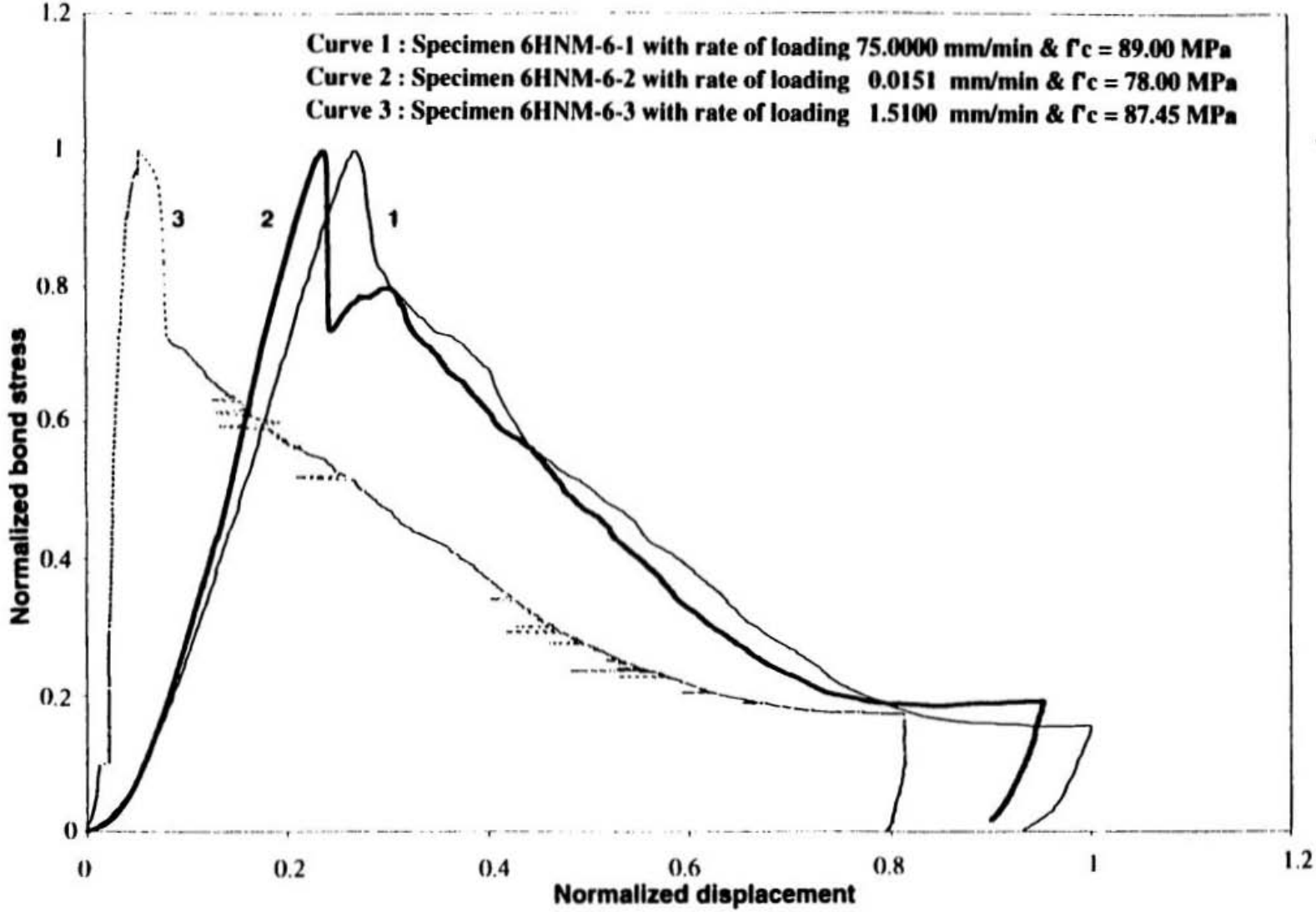

Fig. 5.16 Comparison of normalized bond stress-displacement response to LVDT for three specimens with different rate of loading with embedded bar diameter of 35 mm

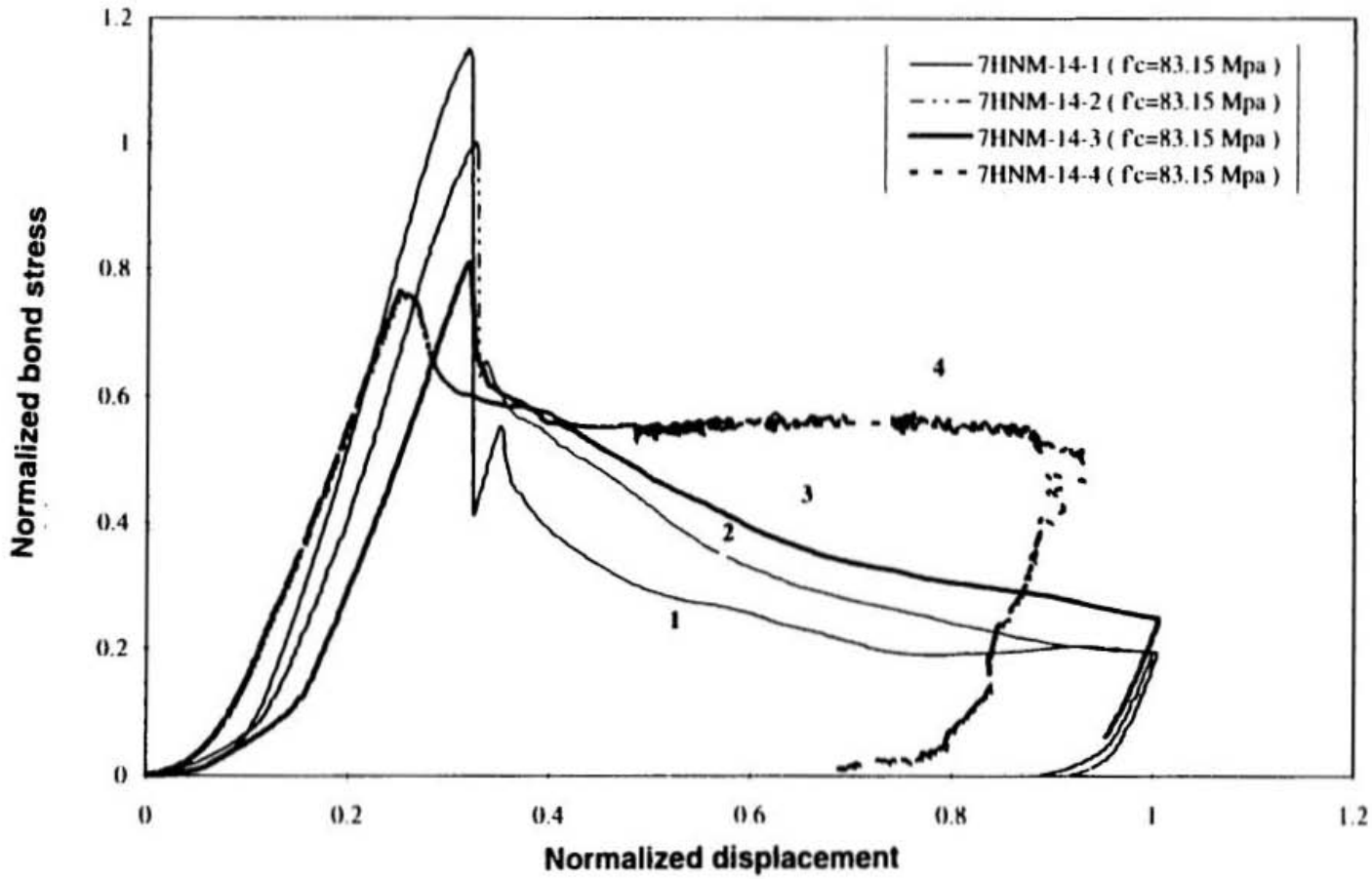

Fig. 5.17 Comparison of normalized bond stress-displacement with respect to curve number 2 for specimens 7HNM-14-1, 7HNM-14-2, 7HNM-14-3, 7HNM-14-4 with nominal bar diameter 35 mm

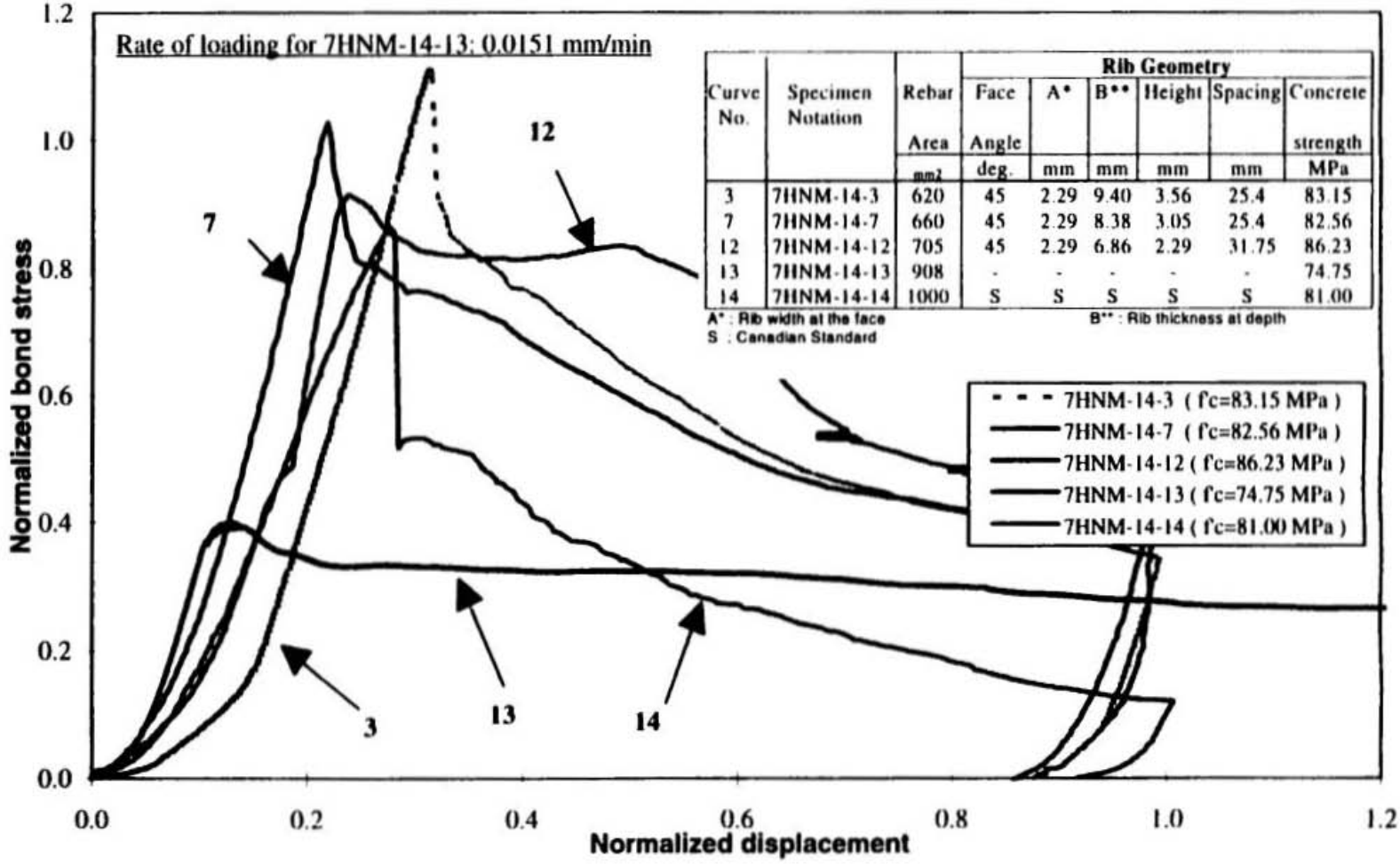

Curve No.	Specimen Notation	Rebar Area	Rib Geometry					
			Face Angle	A*	B**	Height	Spacing	Concrete strength
		mm²	deg.	mm	mm	mm	mm	MPa
3	7HNM-14-3	620	45	2.29	9.40	3.56	25.4	83.15
7	7HNM-14-7	660	45	2.29	8.38	3.05	25.4	82.56
12	7HNM-14-12	705	45	2.29	6.86	2.29	31.75	86.23
13	7HNM-14-13	908	-	-	-	-	-	74.75
14	7HNM-14-14	1000	S	S	S	S	S	81.00

A* : Rib width at the face
S : Canadian Standard
B** : Rib thickness at depth

Fig. 5.18- Compression of normalized bond stress-displacement response to five different deformation patterns with bar diameter of 35 mm

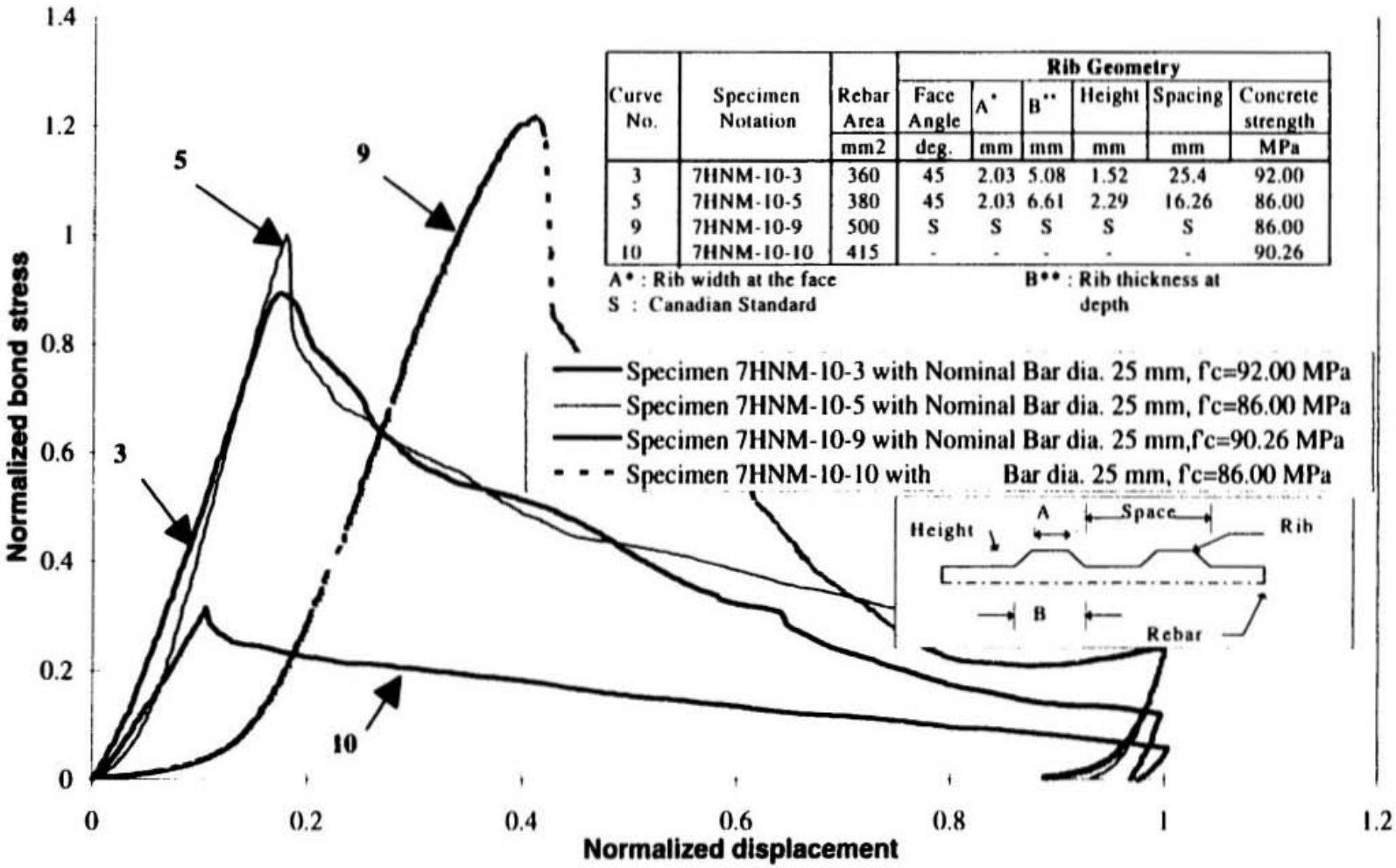

Curve No.	Specimen Notation	Rebar Area	Rib Geometry					
			Face Angle	A*	B**	Height	Spacing	Concrete strength
		mm2	deg.	mm	mm	mm	mm	MPa
3	7HNM-10-3	360	45	2.03	5.08	1.52	25.4	92.00
5	7HNM-10-5	380	45	2.03	6.61	2.29	16.26	86.00
9	7HNM-10-9	500	S	S	S	S	S	86.00
10	7HNM-10-10	415	-	-	-	-	-	90.26

A* : Rib width at the face
S : Canadian Standard
B** : Rib thickness at depth

Fig. 5.19 Comparison of normalized bond stress-displacement response to LVDT for four different deformation patterns with bar diameter 25 mm

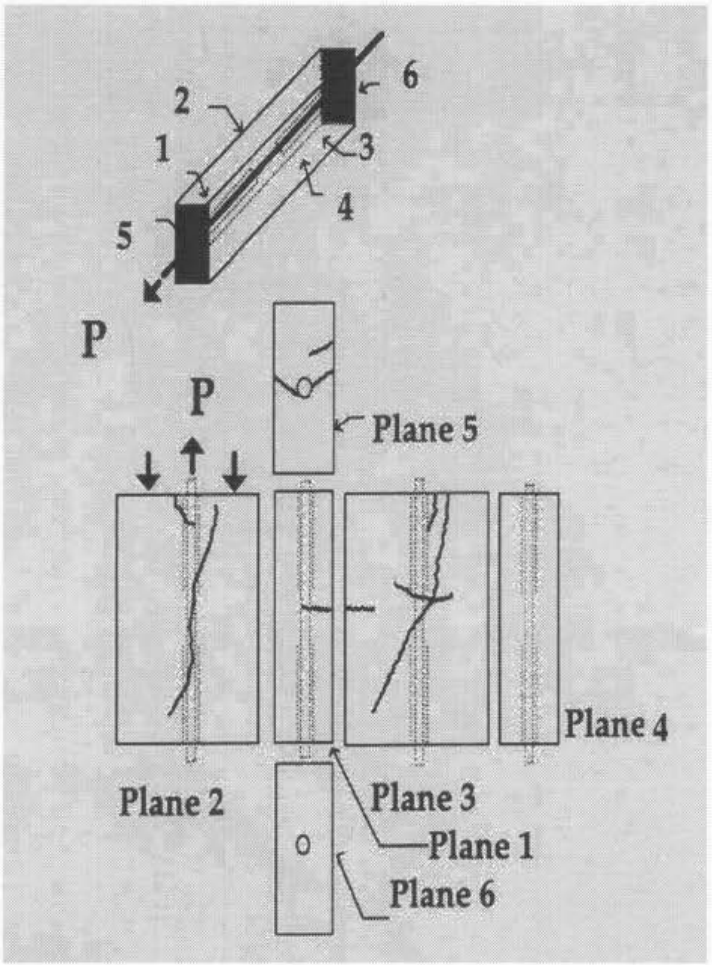

Fig. 5.21 Typical crack propagation of test speciment

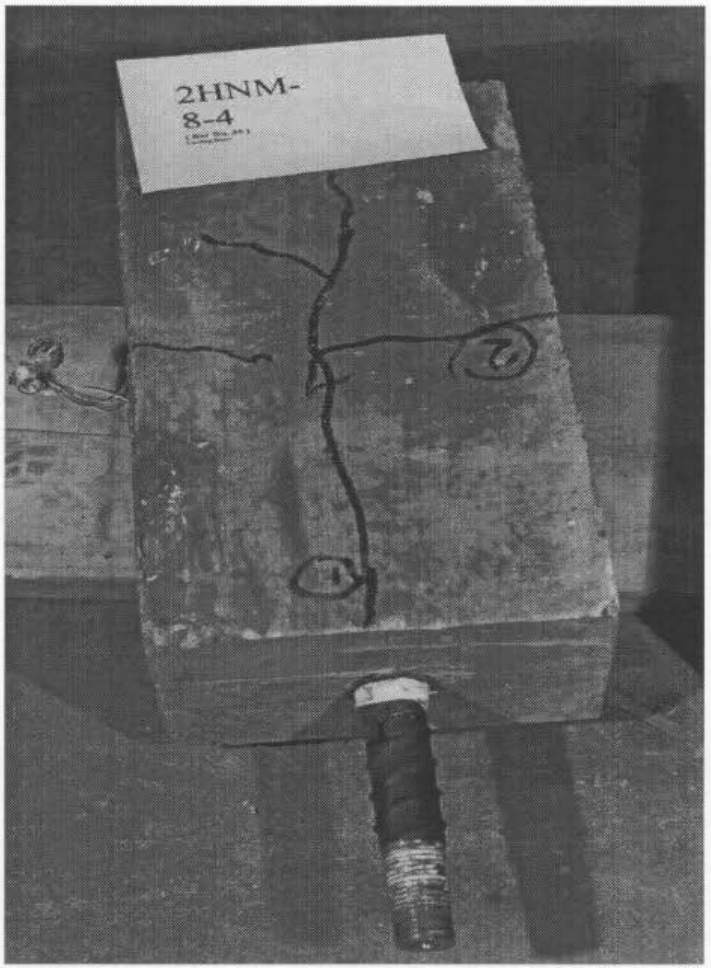

Fig. 5.20 Crack pattern for pull-out test

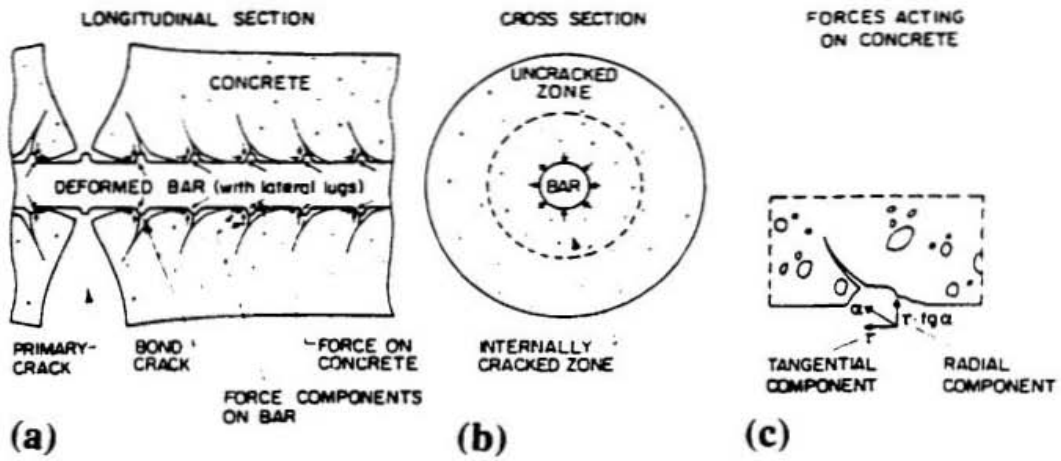

Fig. 5.22- Internal bond cracks and forces acting on concrete [Goto (1971)]

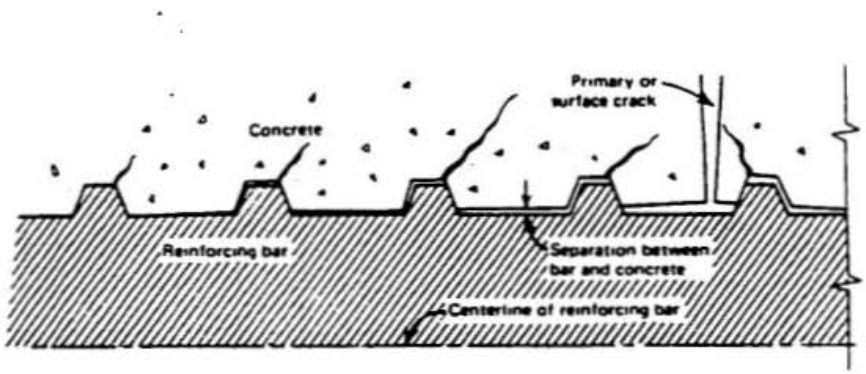

Fig. 5.23- Section through reinforcing bar and concrete, showing separation that occurs near a primary crack

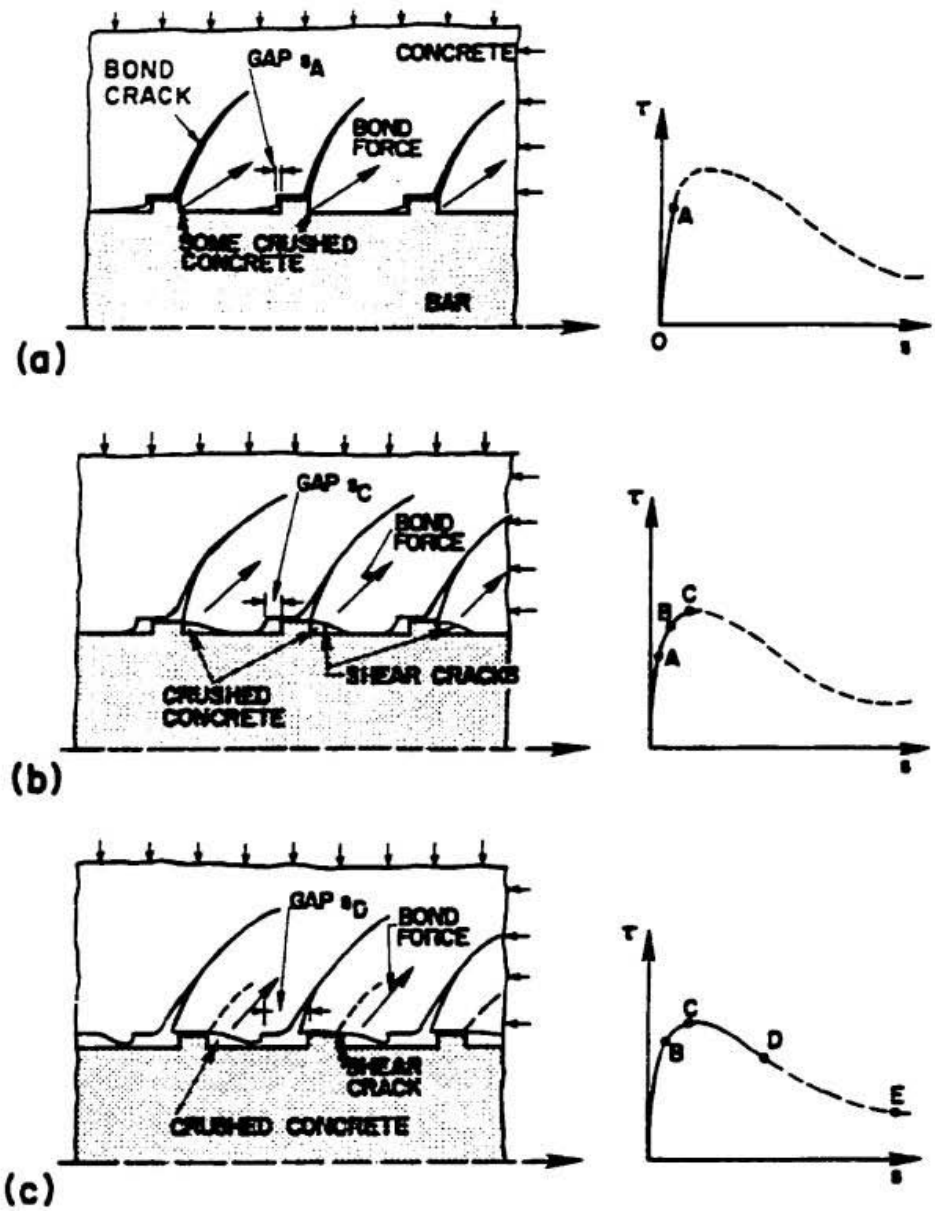

Fig. 5.24- Mechanism of bond resistance, monotonic loading

[Eligehausen, Popov and Bertero (1983)]

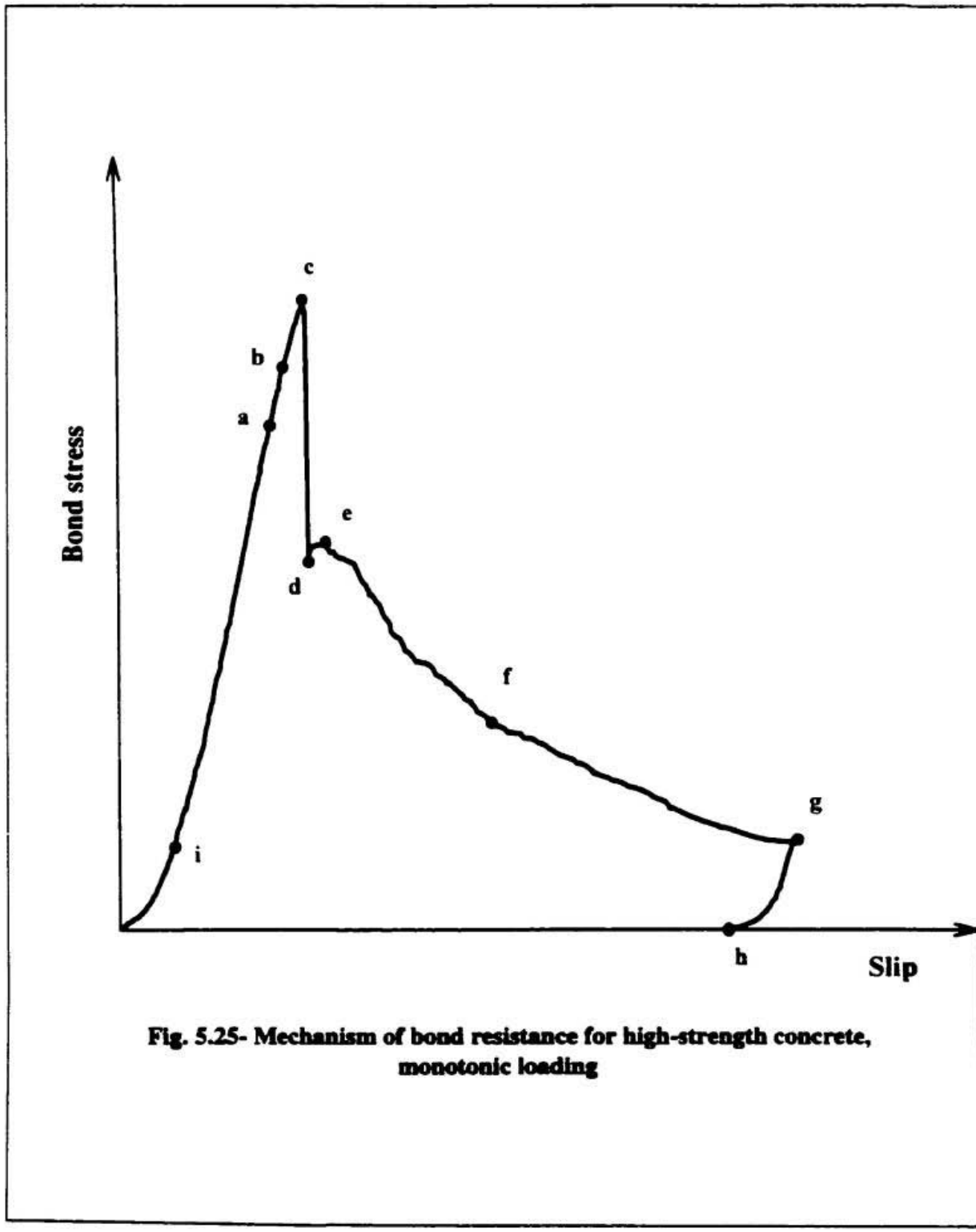

Fig. 5.25- Mechanism of bond resistance for high-strength concrete, monotonic loading

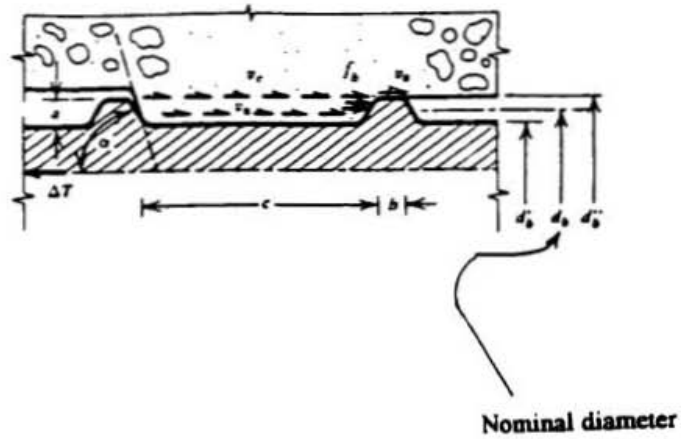

Fig. 5.26- The stresses between two ribs of a deformed bar

Eligehausen, Popov and Bertero (1983)

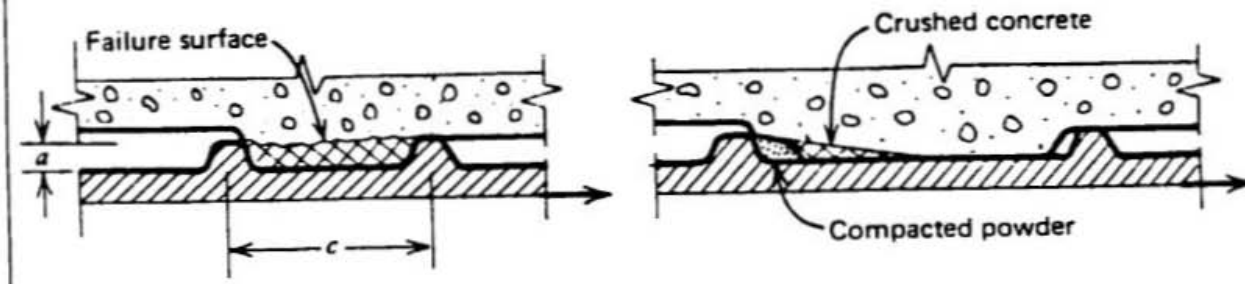

Fig. 5.27- Failure mechanisms at the ribs of deformed bars
(a) a/c > 0.15 (b) a/c < 0.10

Eligehausen, Popov and Betero (1983)

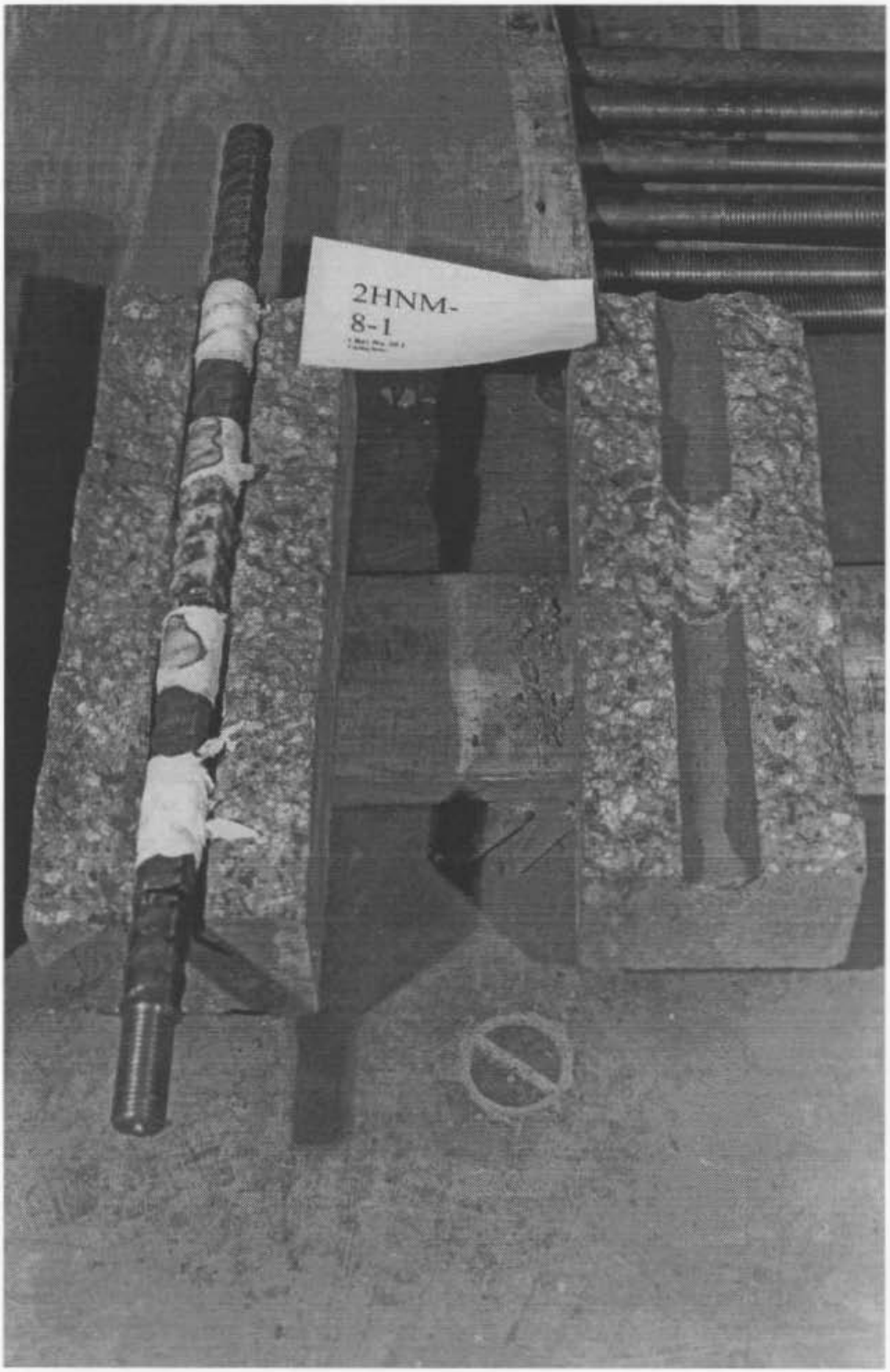

Fig. 5.28 High strength concrete specimen without confinement after pull out test

Chapter 6

Bond Strength of High Strength Concrete Subjected to Reversed Cyclic Loading

6.1 Introduction

The use of high strength concrete in developing strength of bridges, tall buildings and marine structures in seismic zones can offer many advantages. These structures are subjected to severe earthquake motions and will undergo several reversals of loading during an earthquake. As a result, joints in these structures are subjected to repeated forces such as compression and tension. The gradual loss of bond can result in penetration of yielding into the bond anchorage zone, drastically diminishing the effective development length available to absorb the yield strength of the rebar.

In general, limited information exists on high strength concrete behavior under excitation loading conditions and in particular, for the bond behavior between high strength concrete and rebar. However, the lack of sufficient research data for the development of seismic design guidelines leads to over-design of these structures. In

addition, a study an the loading and unloading experiments will help in exploring the residual tensile strength and the associated stiffness. Therefore, in this phase of the research program, the influence of earthquake loading was modeled by cyclic loading and the bond strength between high strength concrete and rebar was studied experimentally.

The aim of this chapter is to present the experimental results of the investigation of the bond strength under cyclic load. The influences of tensile versus compressive loading, amount of confined reinforcement, rebar diameter, concrete strength, and rebar space under cyclic load were investigated. Representative samples of the typical bond stress-displacement curves of different specimens are presented. The results are analyzed and some conclusions are made.

6.2 Test Program

Fifty five specimens were tested and the details of the specimens are described in Table 4-3 to 4-6 for different study parameters under cyclic load. The specimens were tested in the designed steel frame as described in Chapter 4. The test set-up includes a MTS testing machine, which permitted the application of a cyclic load. The bond length of the rebars was 75 and 100 mm for rebars with diameter of 25 and 35 mm, respectively. The high strength concrete surrounding the bond area was well confined by stirrups and vertical rebars. In addition, the size of specimen compared with the bond length was adequate. Further, since the length of the rebar in the contact zone with concrete is short, the recorded average bond stress may be considered as representative of a local bond stress. The loading history was the displacement-controlled cycles.

The level of displacement at two steps affected the specimen. The larger displacement provides more severe damage in the tested specimen. Firstly, the level of assigned displacement was less than the damage level of bond strength to study initial response of the bond strength. Secondly, the specimen has been tested again for the level of displacement close to the maximum slip response to maximum bond stress, to study the strength degradation and loss of bond strength. Since the applied load was controlled by displacement, the recorded displacements were identical to those of the controlling actuator at the column tips. Furthermore, the load corresponding to displacements was not equal at both half cycles. Emam (1995), Osman (1998) and Popov (1984) observed the same phenomenon earlier under cyclic loading. Typical values for maximum average bond stresses are compared with ACI 318-(1995) Building Code and the results are summarized in Table 6.1.

6.3 The Test Results of Cyclic Loading

6.3.1 General

The behavior of bond strength between the rebar and the surrounding confined concrete under cyclic load are plotted in Fig. 6.1 to 6.20. Most specimens are tested under small and large cyclic displacements. Several aspects of this investigation can be observed from these graphs as follow: significant deterioration in the bond capacity takes place during the cyclic loading. Also, after one full cycle, the bond was not damaged under small displacement. In addition, the bond damage was continuous under larger displacement due to further application of cyclic loading. Finally, the maximum bond stress after the first cycle under the large displacement was significantly decreased, then

the average bond stress reached roughly a constant value.

The mechanism of bond under cyclic load can be described as follows: when the tensile force in a rebar is increased and the adhesive bond between steel and concrete is broken, some frictional slip takes place before the full bearing capacity at a rib is mobilized. After dislodging from the rebar, negative frictional resistance is developed, accounting for some residual tension in the rebar and corresponding compression in the surrounding concrete. Inelastic deformation in the vicinity of the ribs, microcracking in concrete, and release of shrinkage strains result in some permanent slip, its magnitude primarily depending on the intensity of the previously applied load. For this reason cracks formed during the tensioning of a rebar do not close completely after the removal of the load. With repeated loading, the frictional resistance diminishes, resulting in a deterioration of the stiffness of the bond mechanism. It should be mentioned that the behavior of high strength concrete under cyclic load is slightly different from normal strength concrete as reported by Eligehausen, Popove and Bertero (1983).

6.3.2 Cyclic Plots for Load History Parameter

Fig.6.1 to 6.2 show the recorded bond stress-displacement response plotted for evaluating the effect of load history. At the beginning the Specimen 1HND-19-5 was under cyclic load with displacement of +/-3.75 mm for loading and unloading conditions, then the range of loading was changed to +/-7.5 mm. The value of 12.6 MPa as maximum bond stress for this specimen was recorded. After several cycles the level of bond stress dropped. Since the test was run under displacement control when the displacement changed form +/-3.75 to +/-7.50 mm, more severe damage was observed. During the

reversal part of the cycle, the lugs press against the concrete whose resistance has been lowered by the inclined cracks created during the previous half cycle loading. Moreover, the inclined cracks coupled with splitting cracks along the concrete result in degradation and reduction in bond capacity. Figure 6.2 represents the behavior of the bond under cyclic load for specimen 1HND-19-8 with an embedded rebar diameter of 35 mm with a cyclic displacement of +/-4.2 mm. This figure indicates that at loading phase the maximum bond capacity was realized after the bond resistance reached peak slip due to the increase number of cycles. As a result, it is indicated that the unloading and reloading branches of these curves as well as the reduced envelopes depend on damage parameters and it is a function of the load history.

6.3.3 Cyclic Plots for Confining Reinforcement Parameter

The effects of confining reinforcement are examined by testing of nine specimens. Four of them have an embedded rebar diameter of 35 mm and the rest 25 mm, respectively. The measured bond stress-displacement response is plotted as shown in Figures 6.3 to 6.11. The confinement of high strength concrete offers many advantages with respect to control of the splitting of concrete under the load bearing capacity. The test results showed that both confined and unconfined specimens reached the highest possible bond level. The observed difference indicated that in the case of unconfined specimens the failure is of the splitting type, associated with a huge amount of released energy and a few number of cycles are recorded. While, for confined specimens the frictional pull out failure type was observed with a greater number of cycles. In addition, it can be concluded that the confining rebar diameter also has an effect on the strength of

the bond during the cyclic test. The result of these experiments indicates that there should be some kind of rule for selecting the adequate rebar diameter as confinement. It has been observed that the main damage was recorded at the peak value of large cyclic displacement. The interlocking and frictional resistance of concrete are greatly reduced at the failure surface with respect to successive cycles. The behavior shown on this section of tests is notably different from that shown by other researchers for normal strength concrete.

6.3.4 Cyclic Plots for Rebar Diameter Parameter

In Figure 6.12 the behavior of bond strength for specimen 3HND-12-5 with embedded rebar diameter of 20 mm is shown. The range of cyclic displacement was +/- 3.75 mm and the maximum bond stress in the first half cycle was recorded to be 26 MPa with sharp slope. The moving of rebar at peak load can be seen as a result of deterioration of bond strength due to adhesion and friction. Also, it can be seen that the bond stress is decreased due to further cyclic loads.

6.3.5 Cyclic Plots for Concrete Strength Parameter

The behavior of bond stress-displacement response for specimen 4HND-12-5, 4HND-12-6, 4HND-12-7, 4HND-12-8 with embedded rebar diameter of 25 and 35 mm, and the concrete strengths of 50, 80, 90 and 95 MPa, respectively are shown in Fig. 6.13 to 6.16. The influence of concrete strength in load carrying capacity of local bond are examined and the results indicate that the bond resistance of high strength concrete under cyclic load is more than normal strength concrete. This result is evident, comparing the

test results of the above specimens. Specimen 4HND-12-6, 7 and 8 has compressive strength of 80, 90 and 95 MPa, respectively. These specimens were subjected to several cycles of loading, while specimen 4HND-12-5 with compressive strength of 50 MPa, after the first half cycle the bond resistance was reduced drastically with the increase number of cycles. In addition, these figures showed that a considerable reduction in bond strength is observed when the displacement reached a maximum value. In general for cyclic loading the compressive strength has a major effect on the bond strength. The value of bond strength was affected by the increases of the concrete compressive strength. The maximum bond strength increase with the increase of the concrete strength. It is suggested that in the recommended bond model in Chapter five, this effect should be considered by a modification factor for influence of dynamic load. Furthermore, cyclic loading does not affect the bond strength of high strength concrete as long as the cyclic slip is less than the measured maximum cyclic slip for monotonic loading. However, for normal strength concrete, cyclic slip always results in a degradation of the bond strength at any slip.

6.3.6 Cyclic Plots for Rebar Spacing Parameter

The behavior of bond stress-displacement for specimen 6HND-6-5 with embedded rebar diameter of 25 mm and rebar space of 50 mm is shown in Figure 6.17. The specimen is tested under cyclic displacement of +/-4 mm. The concrete compressive strength of tested specimen was 94 MPa. The reduction of bond resistance is observed gradually after the first cycle.

6.3.7 Cyclic Plot for Rate of Loading Parameter

The result of investigation for examining the influence of rate of loading is shown on Figures 6.18, 6.19, and 6.20 for embedded rebar diameter of 35 mm. All the specimens were subjected to two cyclic displacements at +/-4 mm and +/-8 mm. It is evident that the bond stiffness for the case of low number of cycles the recorded displacement are stable. On the contrary, there was a gradual reduction in bond stiffness for the case of small number of cycles at large displacement for all the three specimens. It can be concluded that a change in the rate of loading does not have any significant effect on the bond strength for slip less than the maximum slip recorded at static test. The results show that the loading rate does significantly influence the bond behavior of deformed rebar.

6.3.8 Comparison of Test Results with Code

Local bond stress displacement response has been studied under cyclic loading. The maximum bond stress, normalized bond stresses with respect to the cubic root of compressive strength of concrete and also with ACI 318-(1995) are illustrated in Table 6.1. The result of a comparison between normalized test results and ACI Building Code indicates that in most of the cases a good agreement was realized between the experimental and theoretical results. Therefore, taking into consideration a normalized bond stress with respect to the cubic root of concrete compressive strength for high strength concrete is highly recommended.

6.3.7 Failure Mechanism

Several parameters such as the concrete strength, bond length, and the relative rib area have significant effects on the growth of the crack. In the majority of specimens tested, the development of cracking was found to follow a similar pattern, as shown in Figure 6.21. Cracking becomes first visible near the peak load after a large displacement. Typically, at the maximum displacement of the first cycle, cracks were formed along the line of the reinforcing bars, and the bond stress dropped significantly. As the number of cycles was increased, additional cracks were formed across the width of the specimen, and the existing cracks widened. At the low bond stresses, inclined cracks were propagated from tip of the ribs. Transfer of forces across the interface between concrete and steel occur and are caused by bearing and adhesion. The loading and unloading pattern was repeated until severe degradation occurs. The type of failure for all specimens, which had confining reinforcement, was a pull out from the concrete prism while the prism remains together. As ultimate bond stress was reached, shear cracks in concrete between ribs were formed and propagated until the concrete was sheared.

The splitting type failure occurs when the cracks flow from the contact area of the rebar reach the surface of the high strength concrete prism, and in the absence of crack confinement split the prism in several parts with the release of a huge amount of energy. The splitting failure is initiated by the wedging action of the ribs as the rebar moves with respect to the concrete. The ribs create sufficient radial force components that split the concrete. Splitting is characterized by planar like cracks in planes radial to the axis of the rebar.

6.5 CONCLUSIONS

It can be concluded that strength and deformation characteristics of high strength concrete structures are highly dependent on bond slip behavior between rebar and concrete under cyclic load. It has been shown that significant deterioration in the bond capacity takes place during the cyclic loading. The test result indicates that an increase in cyclic displacement will lead to more severe damage. The slope of the cyclic bond stress-displacement curve could describe the influence of bond strength. It is revealed that the maximum bond strength increases with the increase of the concrete strength. Cyclic loading does not affect the bond strength of high strength concrete as long as the cyclic slip is less than the maximum cyclic slip for monotonic loading. The average bond stress reached roughly a constant value that can be associated with an internal frictional force. The behavior of high strength concrete under cyclic load is slightly different from that of normal strength concrete. The influences of several parameters such as the load history, confining reinforcement, rebar space, concrete strength, rebar size and rate of loading were investigated. It is concluded that these parameters have a significant role in the bond strength. It has been concluded that strength of concrete, rib area and bond length have notable effects on the crack growth. In the majority of specimens tested, the development of cracking was found to follow a similar pattern. The type of failure was pull out for specimens with confining reinforcement under a considerable number of cycles. The split type for unconfined specimens includes a low number of cycles.

Table 6.1- Comparison of Results

Series	Investigation Parameter	Loading History	Specimen Notation	Rebar Diameter	Concrete Strength f'c	Vertical Confing Rebar	Min Number of Cycle	Rate of Loading		Test Result Max Bond Stress	Normalized Bond Stress Due to Cubic Root of f'c	Nominal Bond Stress (ACI*)	Bond Stress Ratio *Test / Nominal*
								First Cycles	Last Cycles				
				mm	MPa	mm		S +/-(mm)	S +/-(mm)	MPa		MPa	
M1	**Load History**	Cyclic	1HND-19-5	35	93.67	10	10	3.75	7.50	21.42	4.73	5.04	0.938
			1HND-19-8	35	86.00	10	10	4.20	4.20	22.79	4.88	4.83	1.010
M2	**Confining Rein.**	Cyclic	2HND- 8-5	35	89.00	10		3.10	6.20	21.6	4.84	4.91	0.986
			2HND- 8-6	35	86.20	No Conf.	10	3.10	6.40	23.62	5.35	4.83	1.108
			2HND- 8-7	35	86.20	20		4.00	9.00	21.31	4.82	4.83	0.998
			2HND- 8-8	35	86.20	25		5.50	5.50	18.84	4.27	4.83	0.884
			2HND- 8-5	**25**	88.10	No Conf.		2.50	2.50	17.67	3.97	4.88	0.814
			2HND- 8-6	**25**	88.62	10	10	2.50	2.50	18.67	4.19	4.91	0.853
			2HND- 8-7	**25**	88.62	20		4.30	6.25	21.27	4.77	4.91	0.971
			2HND- 8-8	**25**	88.62	25		5.50	10.00	23.23	5.21	4.91	1.061
			2HND- 8-9	**25**	88.62	No Conf.		5.50	5.50	22.05	4.95	4.91	1.008
M3	**Rebar Diameter**	Cyclic	3HND-12-5	20	87.45	10	10	3.75	3.75	21.32	4.80	4.87	0.986
M4	**Concrete Strength**	Cyclic	4HND-12-6	35	83.3			3.75	7.50	18.91	4.33	4.75	0.912
			4HND-12-7	35	92.65			3.75	7.50	23.93	5.28	5.01	1.054
			4HND-12-8	35	90.00	10	10	4.00	19.00	23.57	5.26	4.94	1.065
			4HND-12-5	**25**	50.61			3.75	3.75	14.63	3.95	3.71	1.065
M5	**Bar Spacing**	Cyclic	5HND- 4-4	**25**	93.40	10	10	4.00	4.00	22.80	5.03	5.03	1.000
M6	**Rate of Loading**	Cyclic	6HND- 6-4	35	86.59			4.00	8.00	19.20	4.34	4.85	0.895
			6HND- 6-5	35	94.64	10	10	4.00	8.00	25.28	5.55	5.07	1.095
			6HND- 6-6	35	94.64			4.00	8.00	22.47	4.89	5.07	0.964

(*) ACI-318M-95/318RM-95

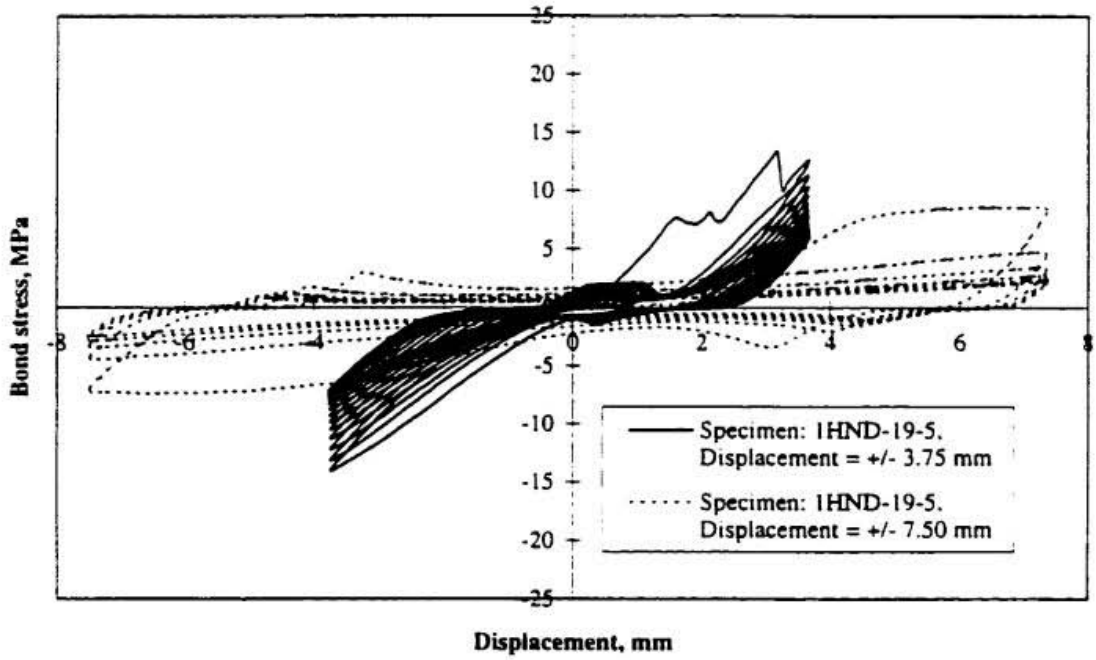

Fig. 6.1 Bond stress-displacement response curve for specimen 1HND-19-5 with embedded rebar diameter of 35 mm under cyclic load

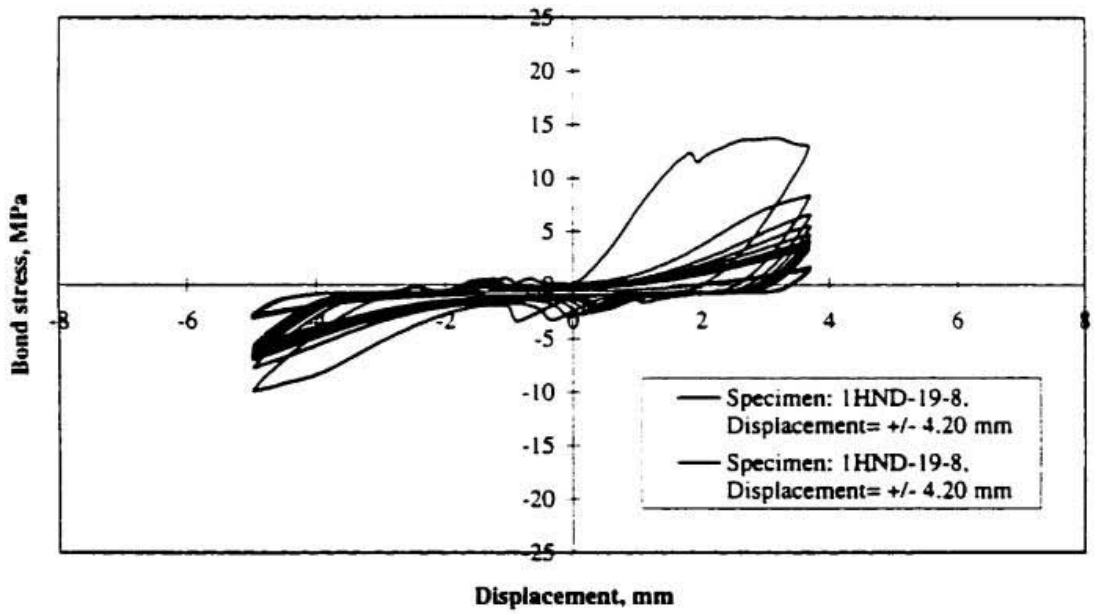

Fig. 6.2 Bond-displacement response curve for specimen 1HND-19-8 with an embedded rebar diameter of 35 mm under cyclic load

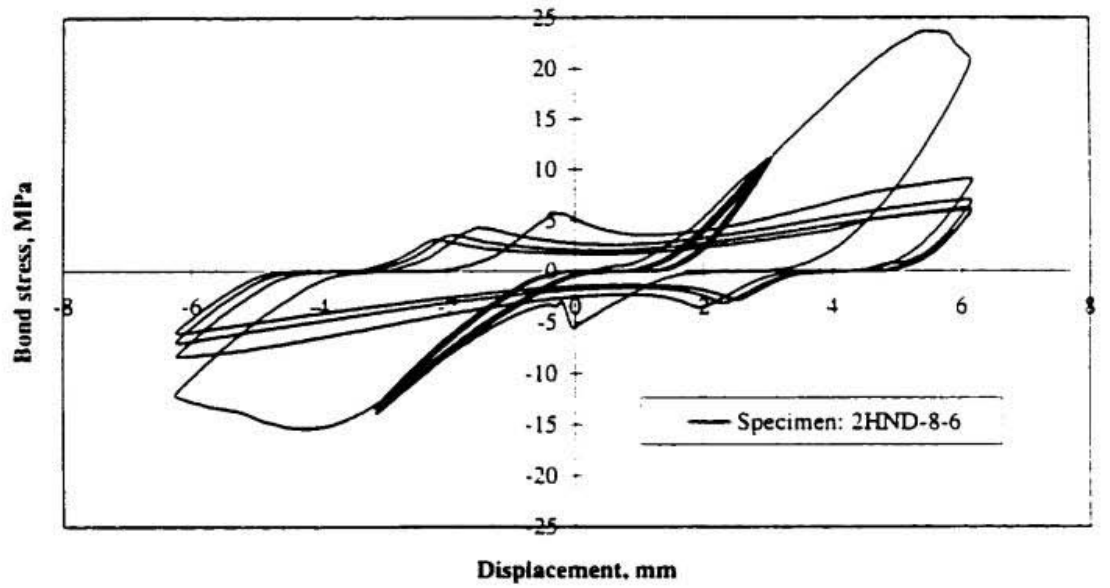

Fig. 6.3 Bond stres-displacement response curve for specimen without confining rebar and embedded rebar diameter of 35 mm

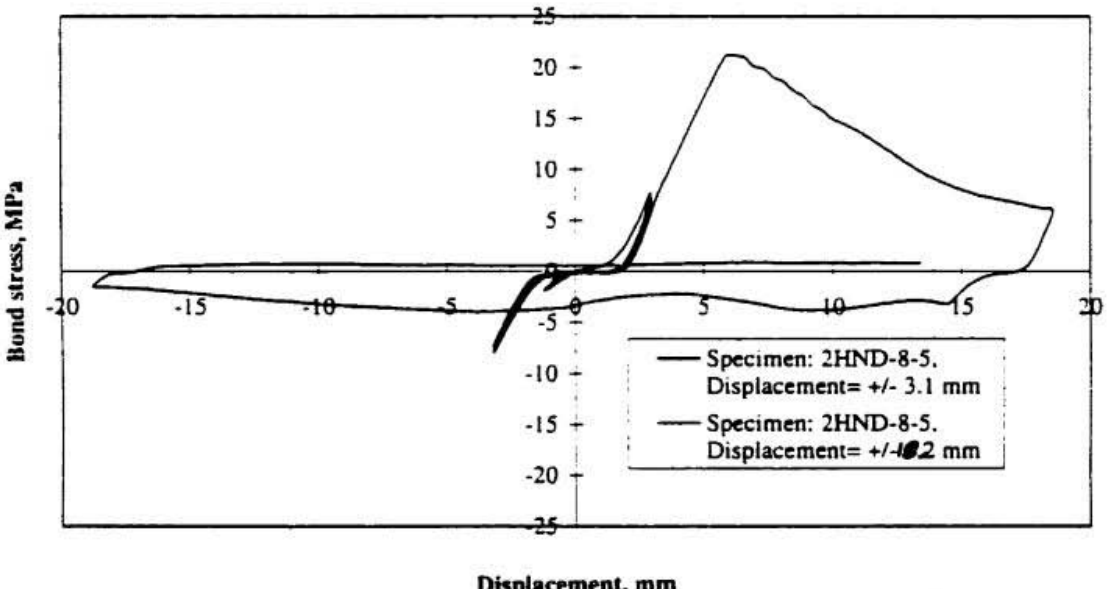

Fig. 6.4 Bond stress-displacement response curve for specimen 2HND-8-5 with confining rebar diameter of 10 mm and embedded rebar diameter of 35 mm under cyclic load

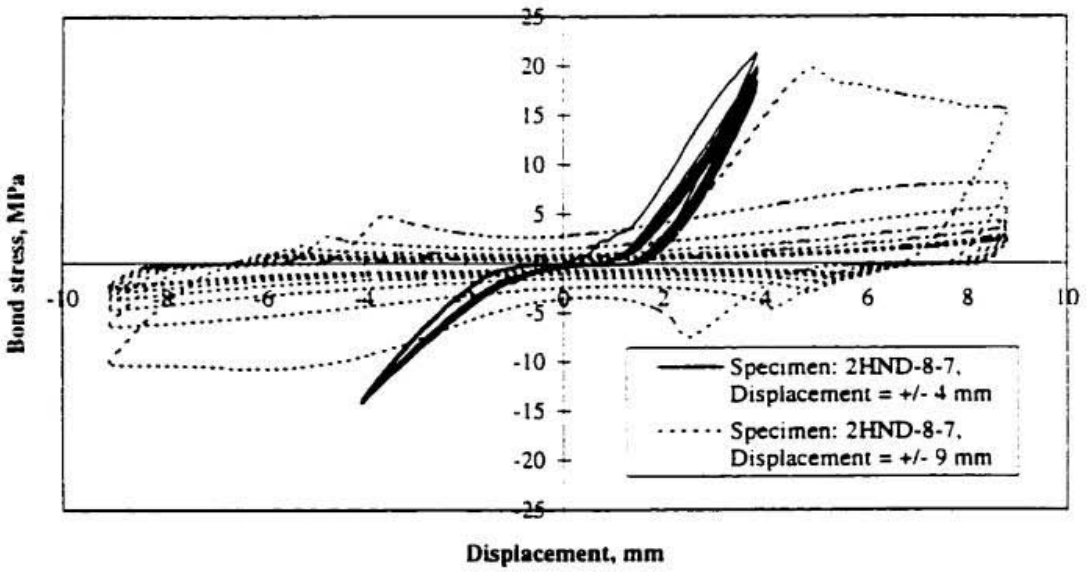

Fig. 6.5 Bond stress-displacement response curve for specimen with confining rebar diameter of 20 mm and an embedded rebar diameter of 35 mm

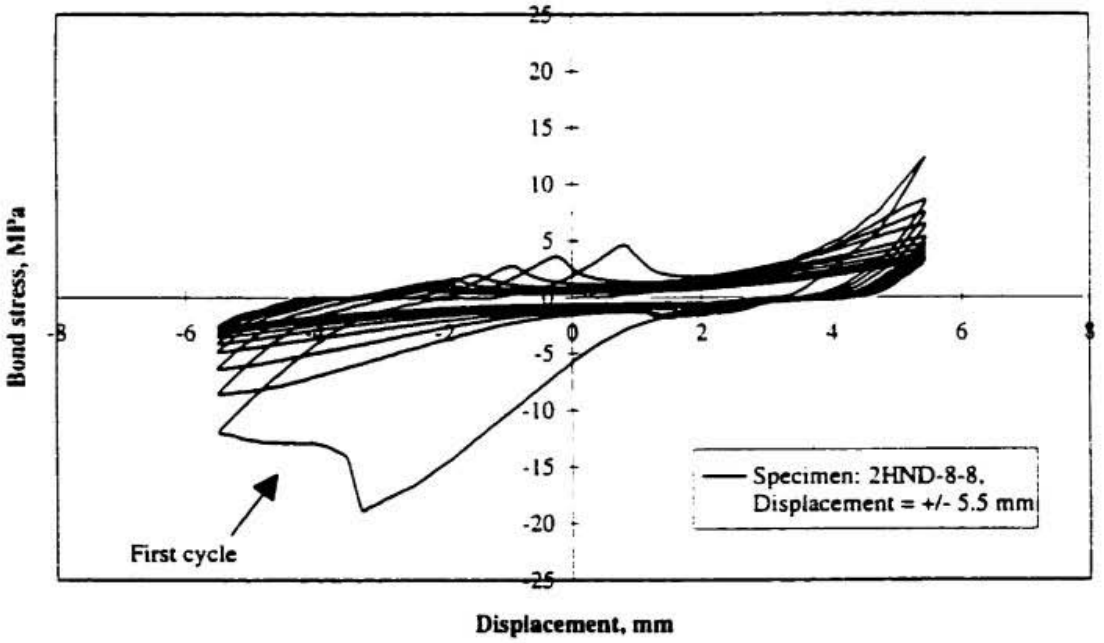

Fig. 6.6 Bond stress-displacement response curve for specimen 2HND-8-8 with confining rebar diameter of 25 mm and embedded rebar diameter of 35 mm under cyclic load

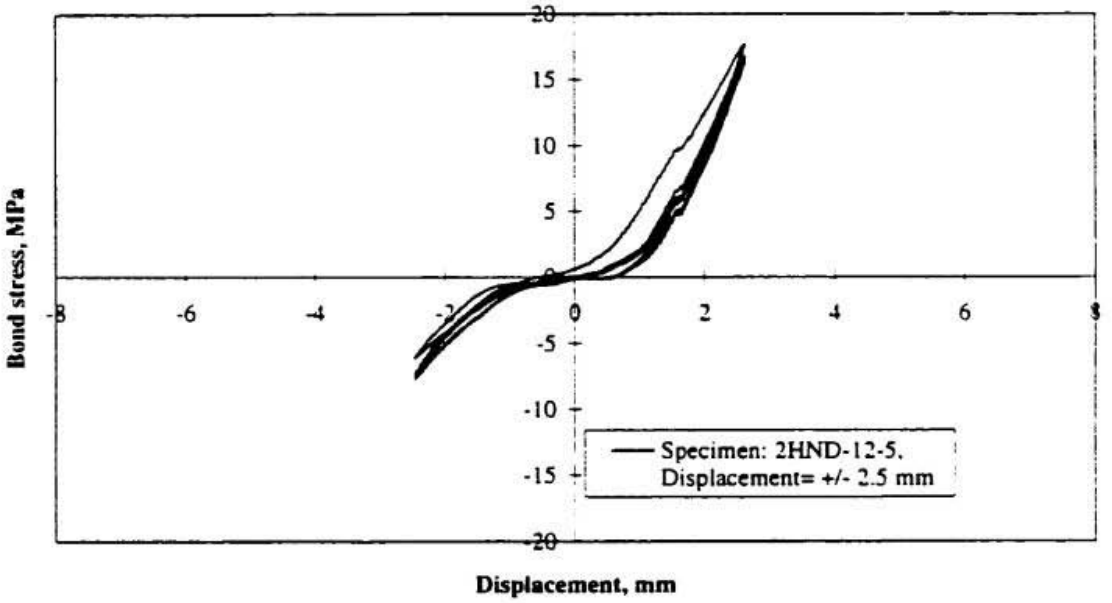

Fig. 6.7 Bond stress-displacement response curve response curve for specimen without confining rebar and an embedded rebar diameter of 25 mm

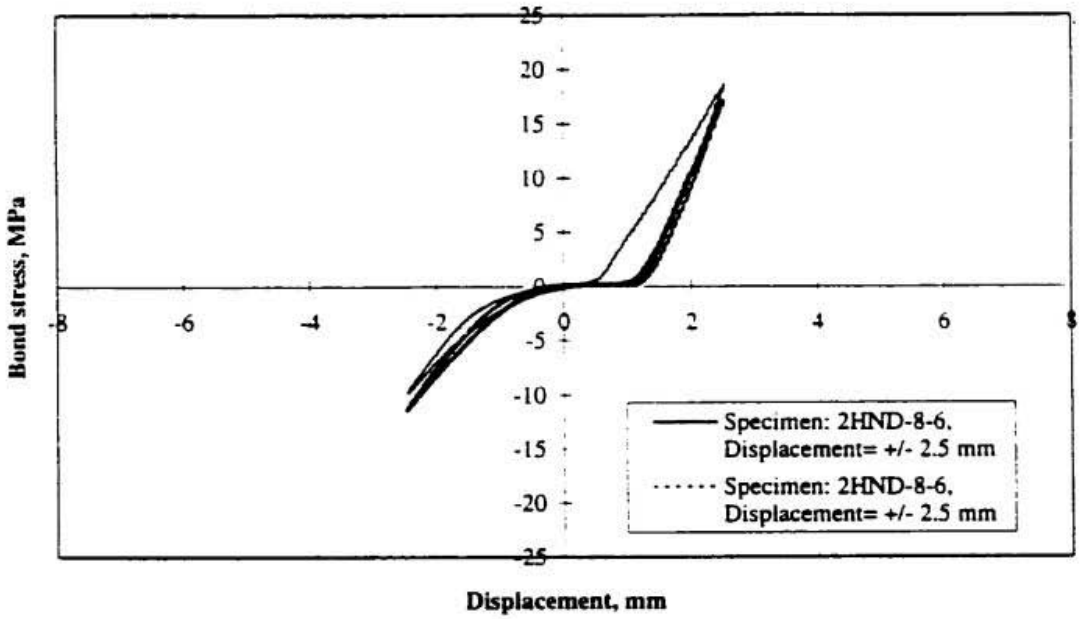

Fig. 6.8 Bond stress-displacement response curve for specimen with confining rebar diameter of 10 mm and embedded rebar diameter of 25 mm under cyclic load

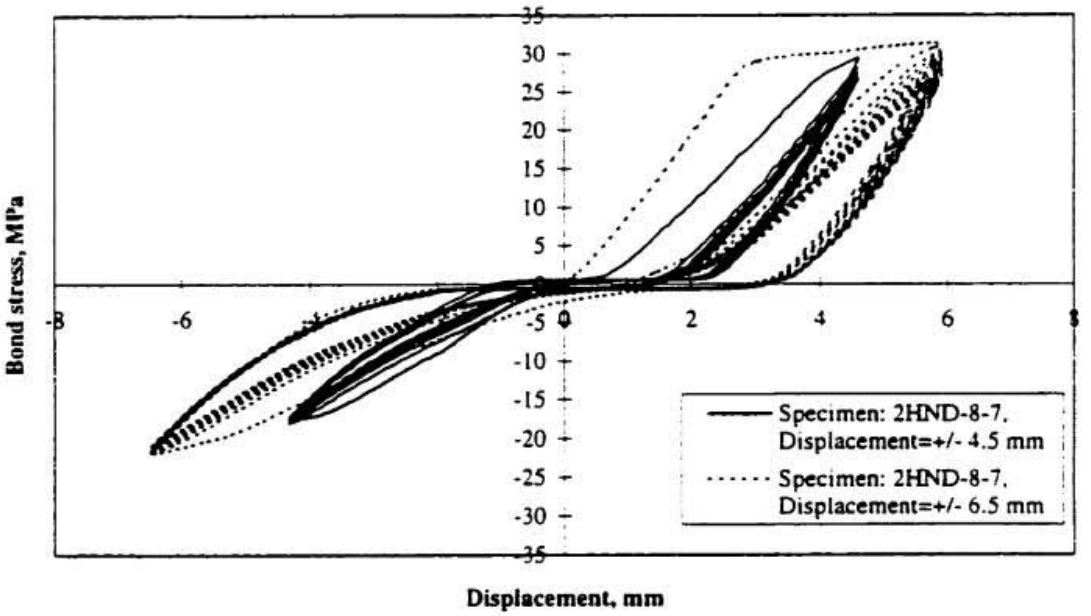

Fig. 6.9 Bond stress-displacement response curve for specimen with confining rebar diameter of 20 mm and embedded rebar diameter of 25 mm under cyclic load

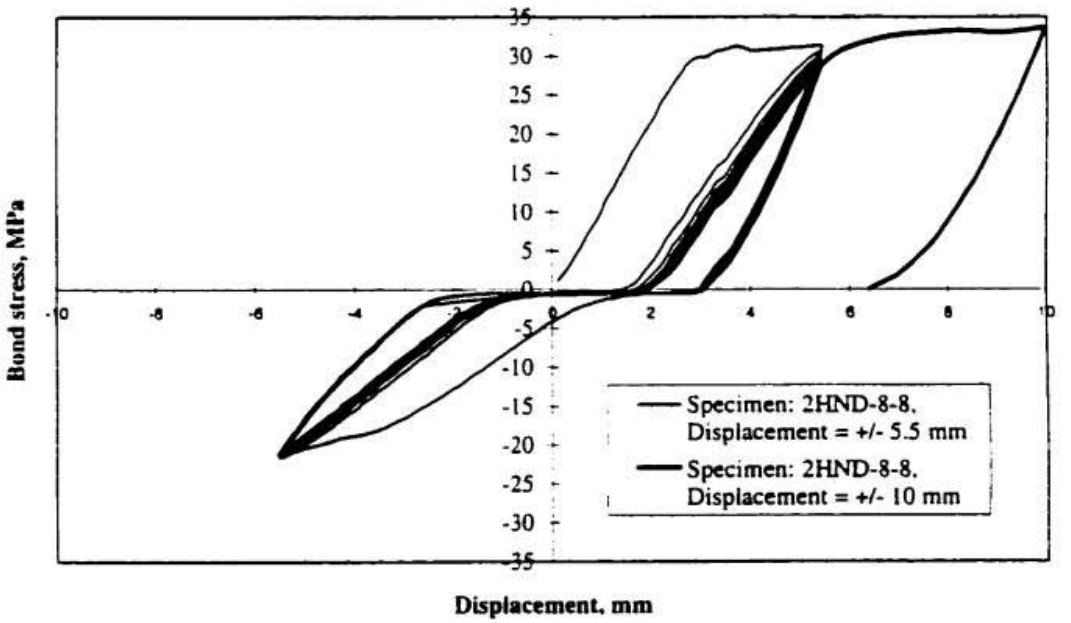

Fig. 6.10 Bond stress-displacement response curve for specimen with confining rebar diameter of 25 mm and embedded rebar diameter of 25 mm under cyclic load

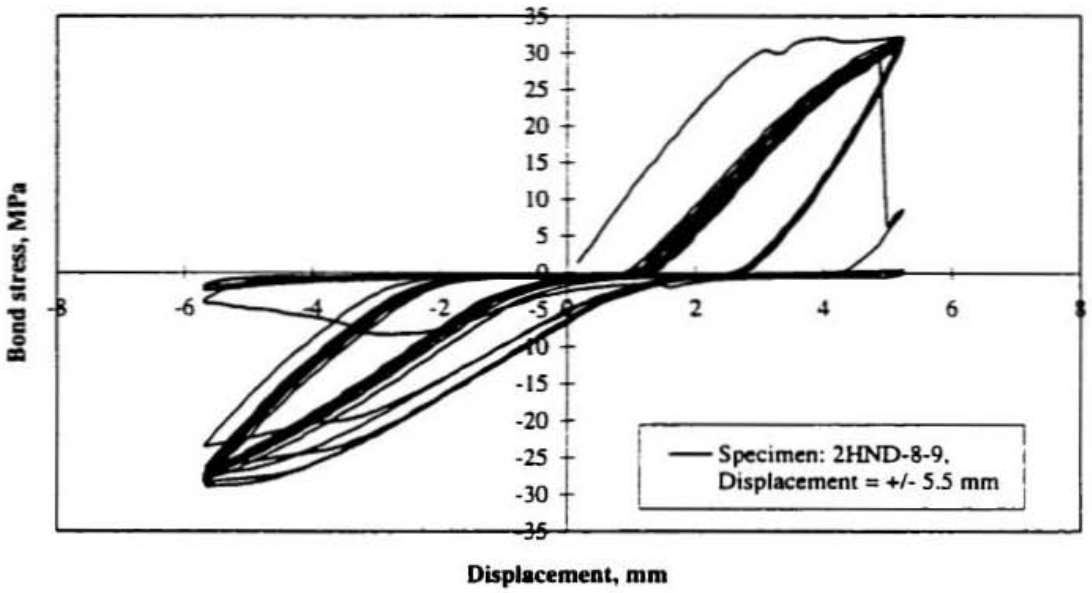

Fig. 6.11 Bond stress-displacement response curve for specimen without confinement and embedded rebar diameter of 25 mm under cyclic load

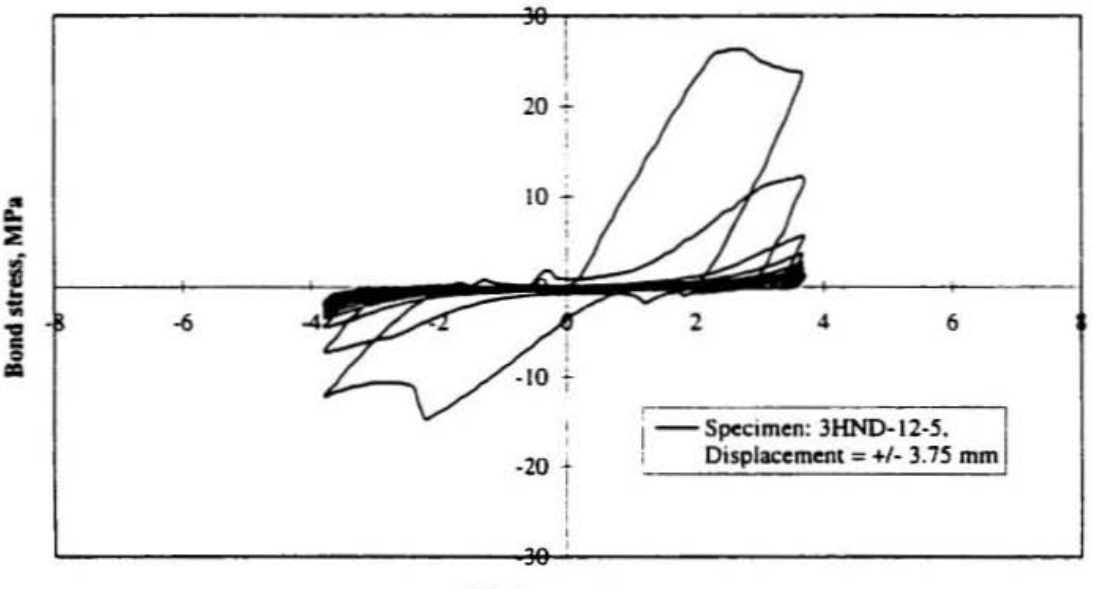

Fig. 6.12 Bond stress-displacement response curve for specimen 3HND-12-5 with embedded rebar diameter of 20 mm under cyclic load

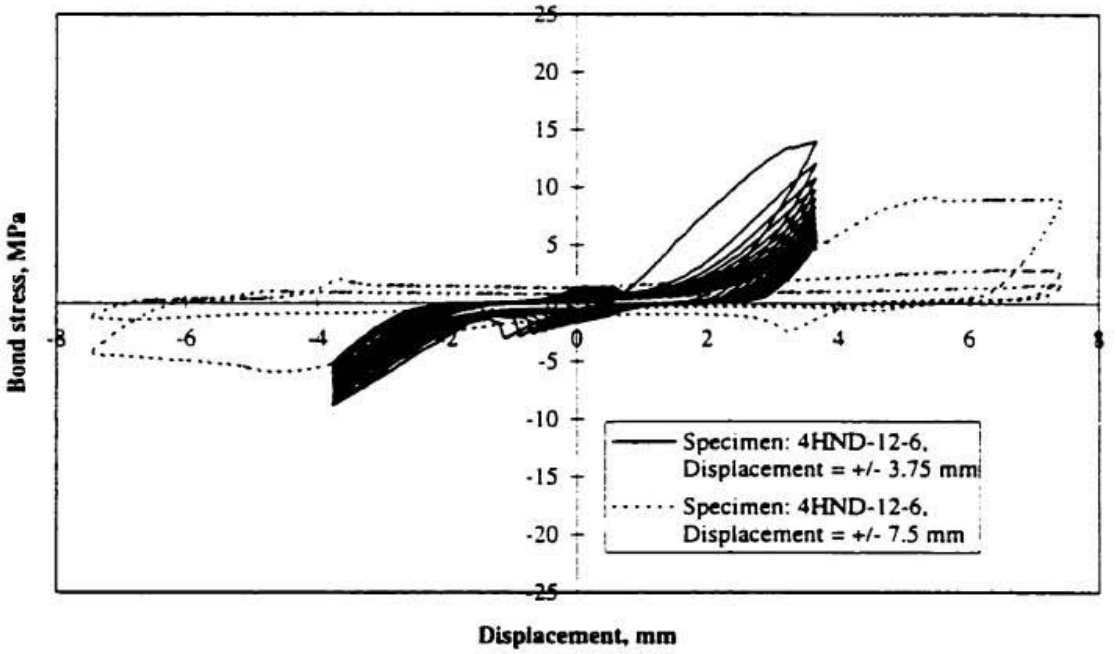

Fig. 6.13 Bond stress-displacement response curve for specimen 4HND-12-6 with embedded rebar diameter of 35 mm under cyclic load

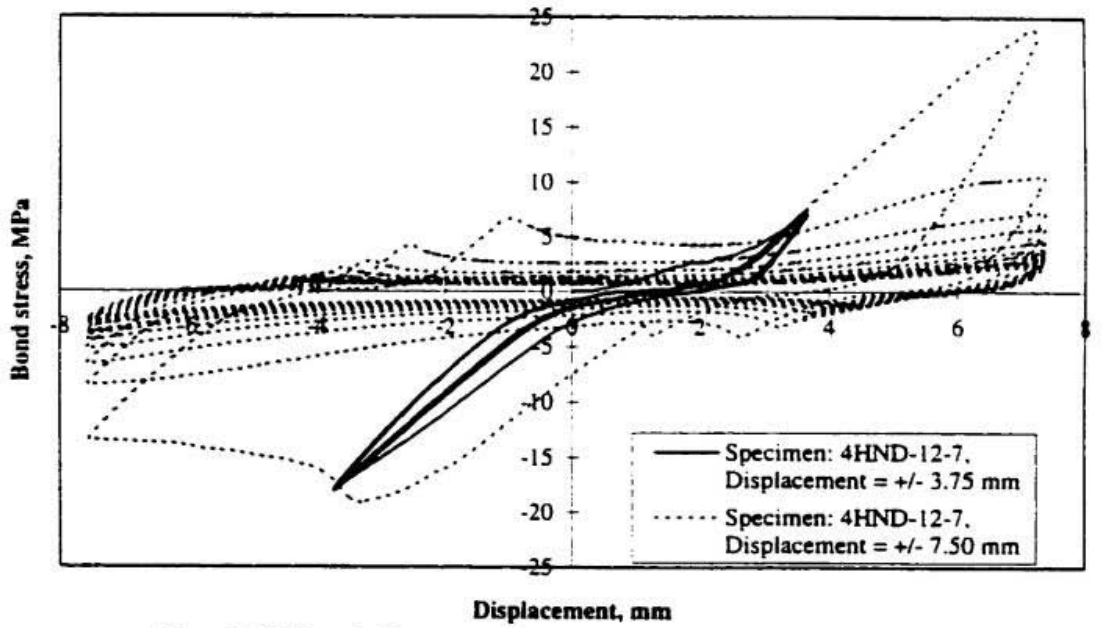

Fig. 6.14 Bond-displacement response curve for specimen 4HND-12-7 with concrete strength 0f 93 MPa and embedded rebar diameter of 35 mm under cyclic load

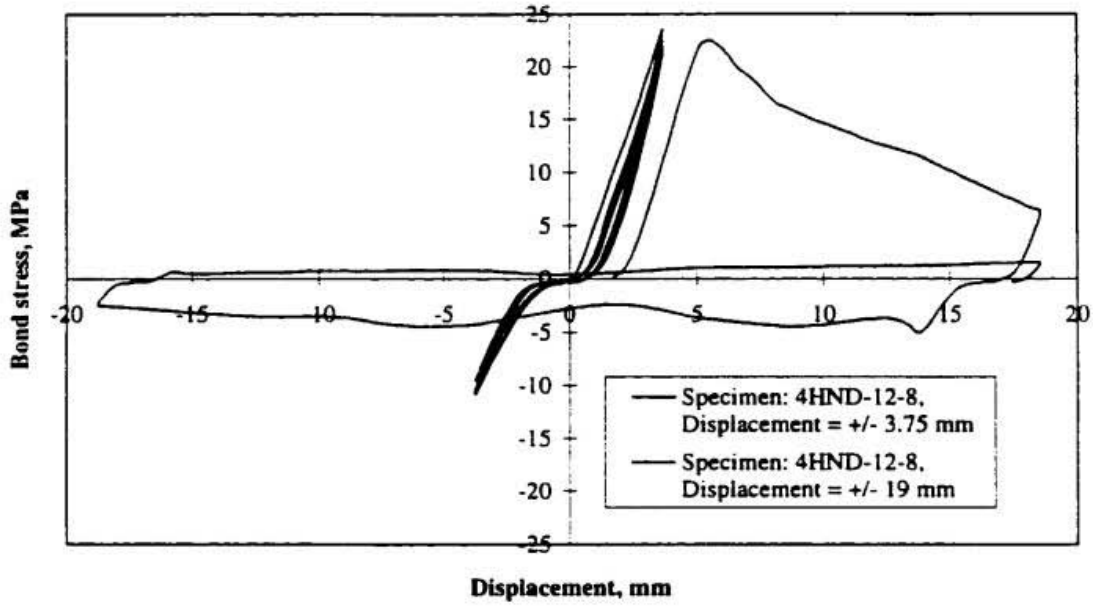

Fig. 6.15 Bond stress-displacement response curve for specimen 4HND-12-8 with compression strength of 90 MPa and an embedded rebar diameter of 35 mm

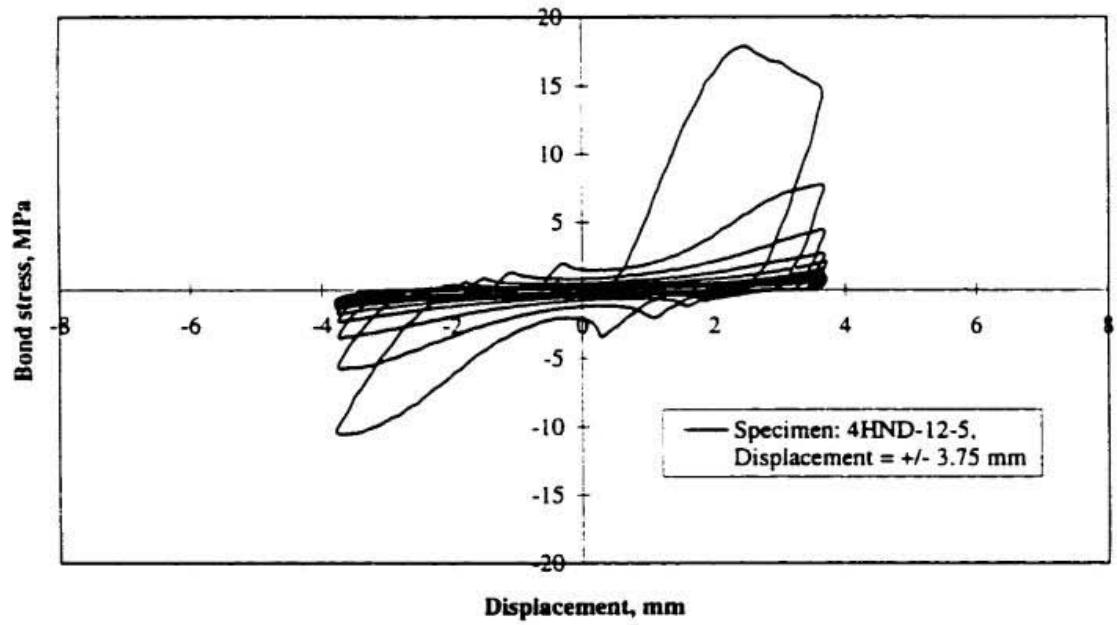

Fig. 6.16 Bond stress-displacement response curve for specimen 4HND-12-5 with concrete strength of 50 MPa and an embedded rebar diameter of 25 mm

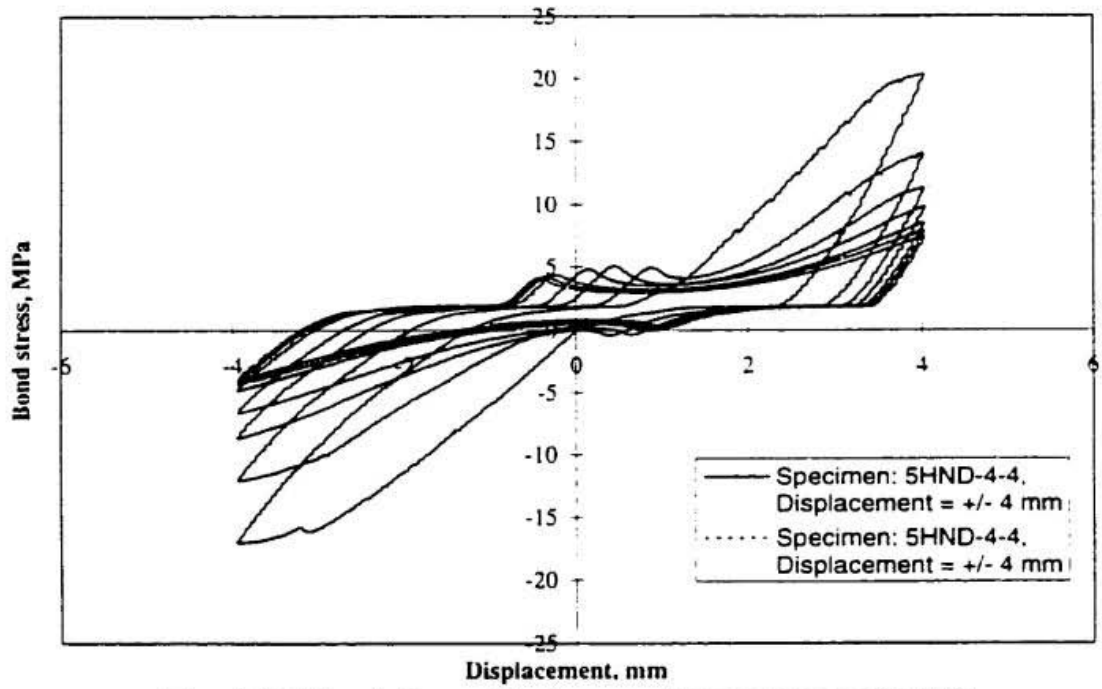

Fig. 6.17 Bond stress-displacement response curve for specimen 5HND-4-4 with embedded rebar diameter of 25 mm

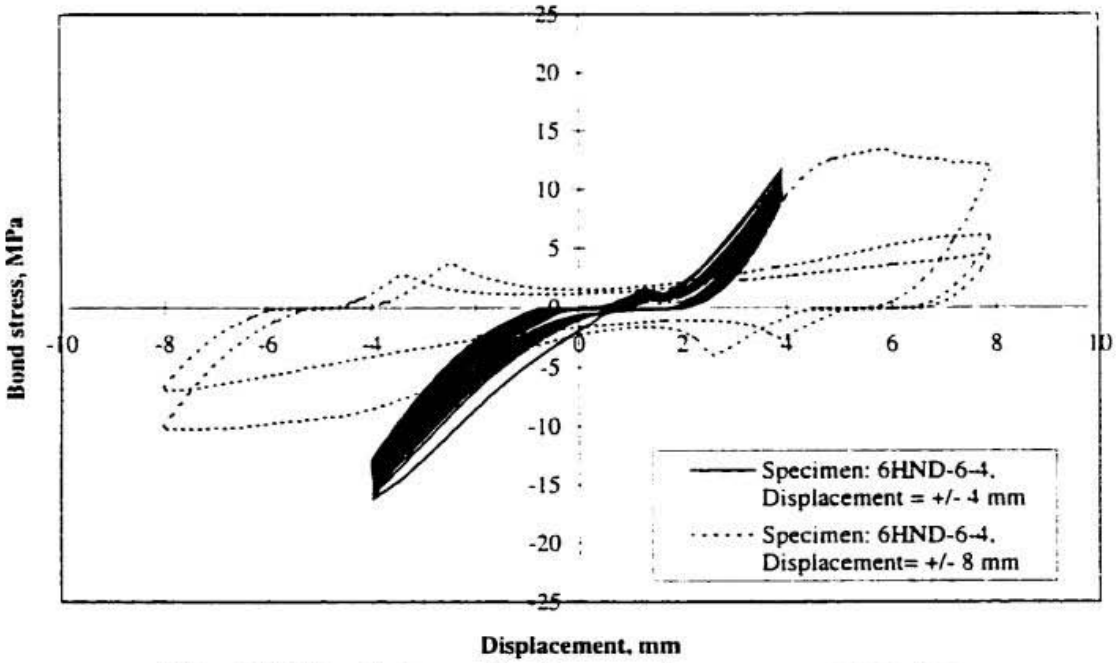

Fig. 6.18 Bond stress-displacement response curve for specimen 6HND-6-4 with embedded rebar diameter of 35 mm under cyclic load

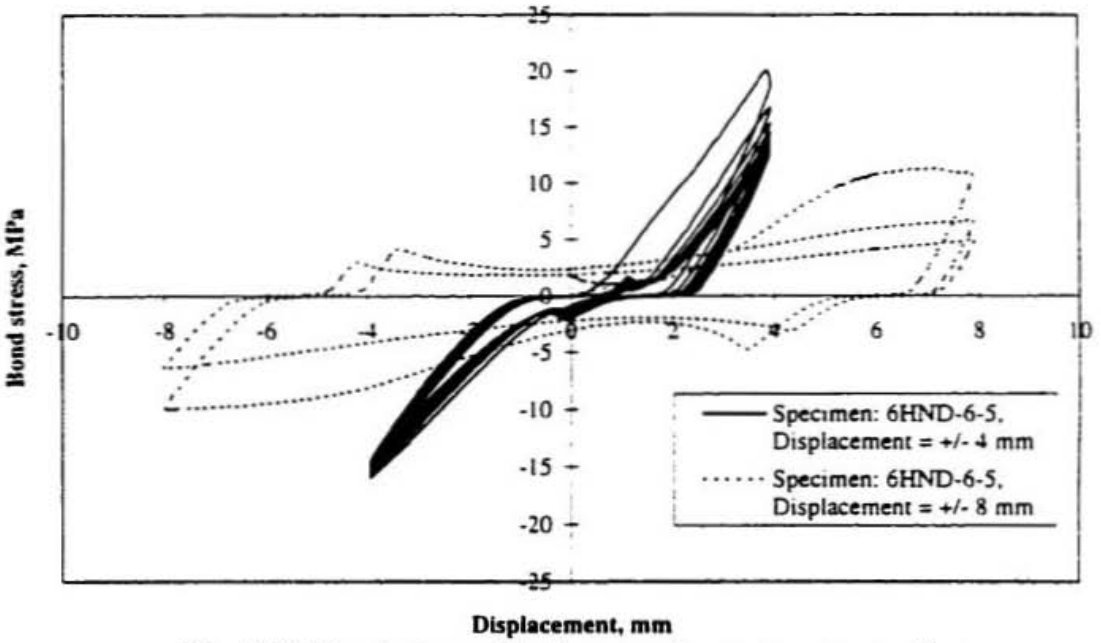

Fig. 6.19 Bond stress-displacement response curve for specimen 6HND-6-5 with embedded rebar diameter of 35 mm under cyclic load

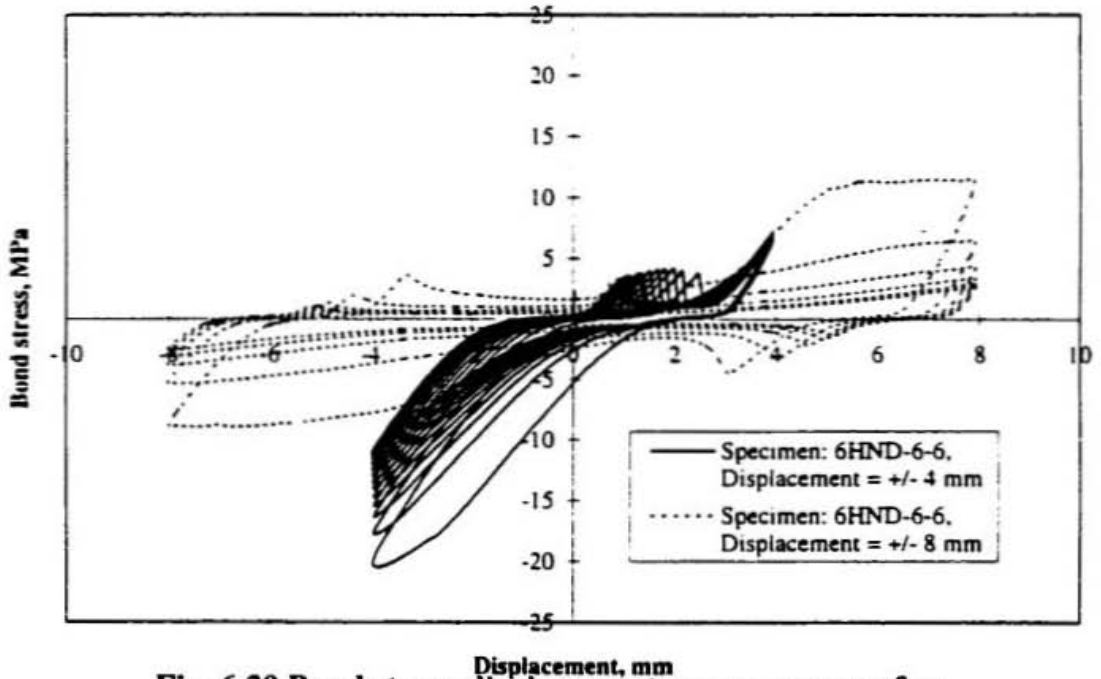

Fig. 6.20 Bond stress-displacement response curve for specimen 6HND-6-6 with embedded rebar diameter of 35 mm under cyclic load

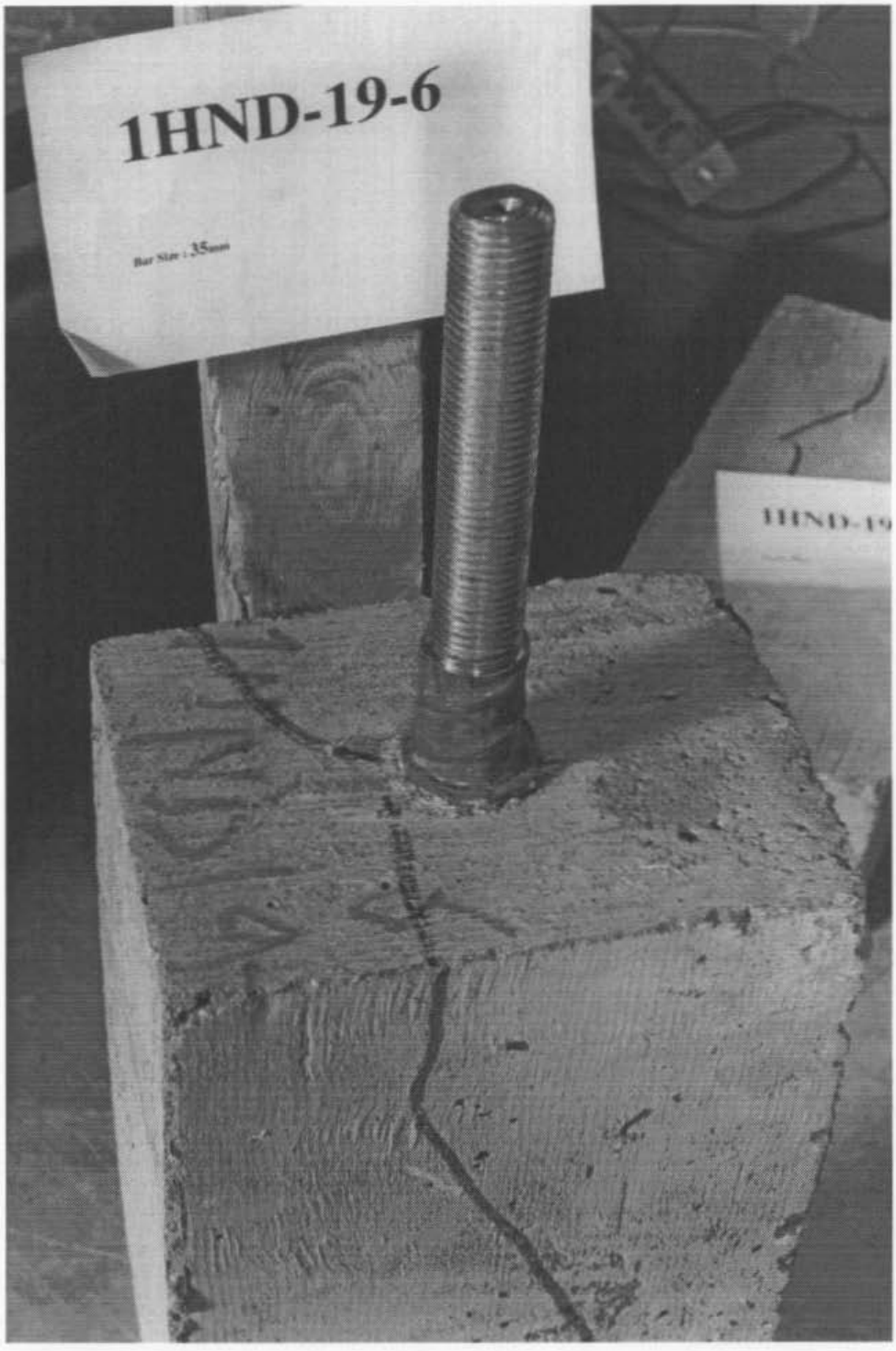

Fig. 6.21 Specimen 1HND-19-6 after cyclic test

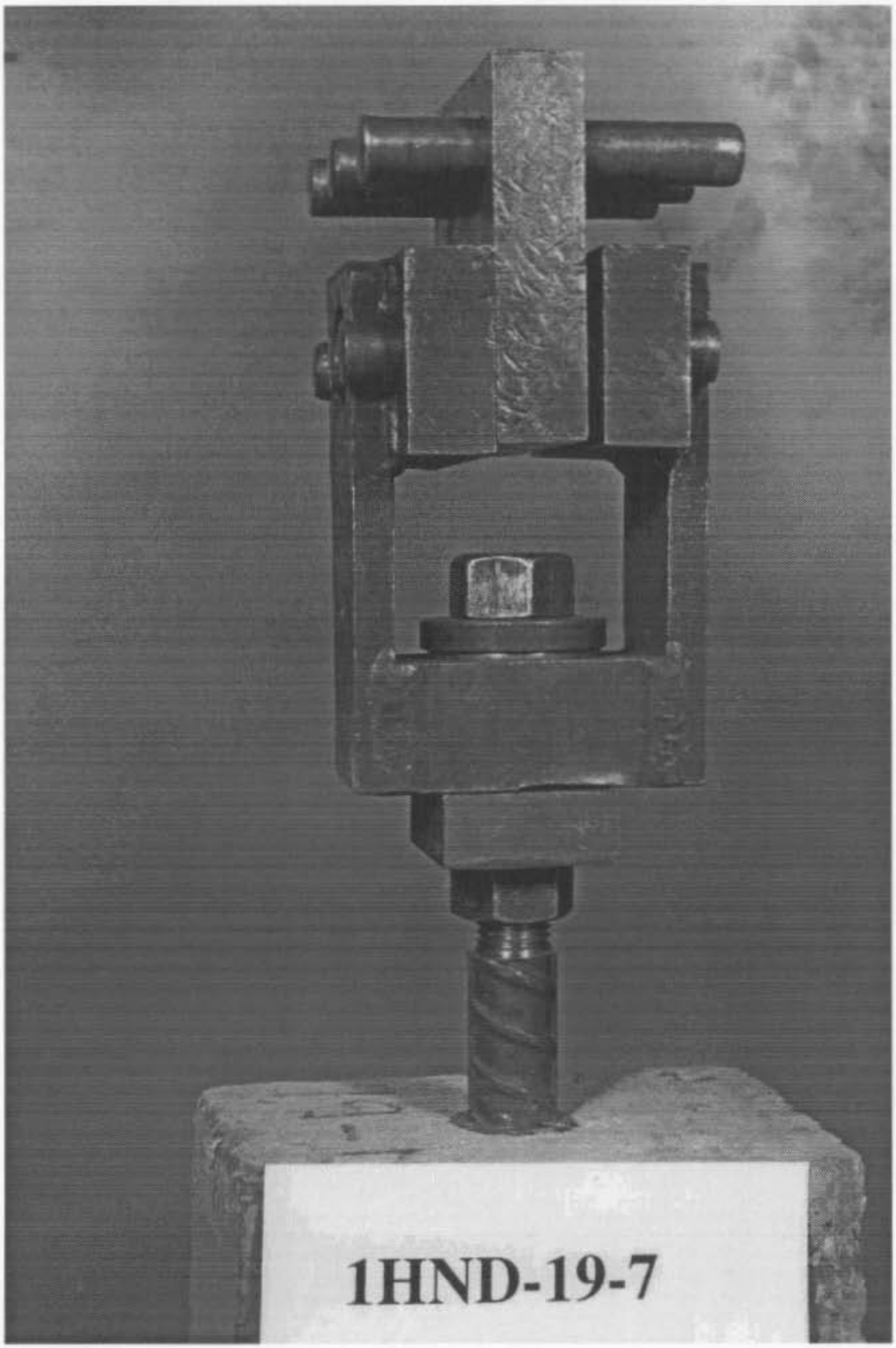

Fig. 6.22 Apparatus for cyclic test

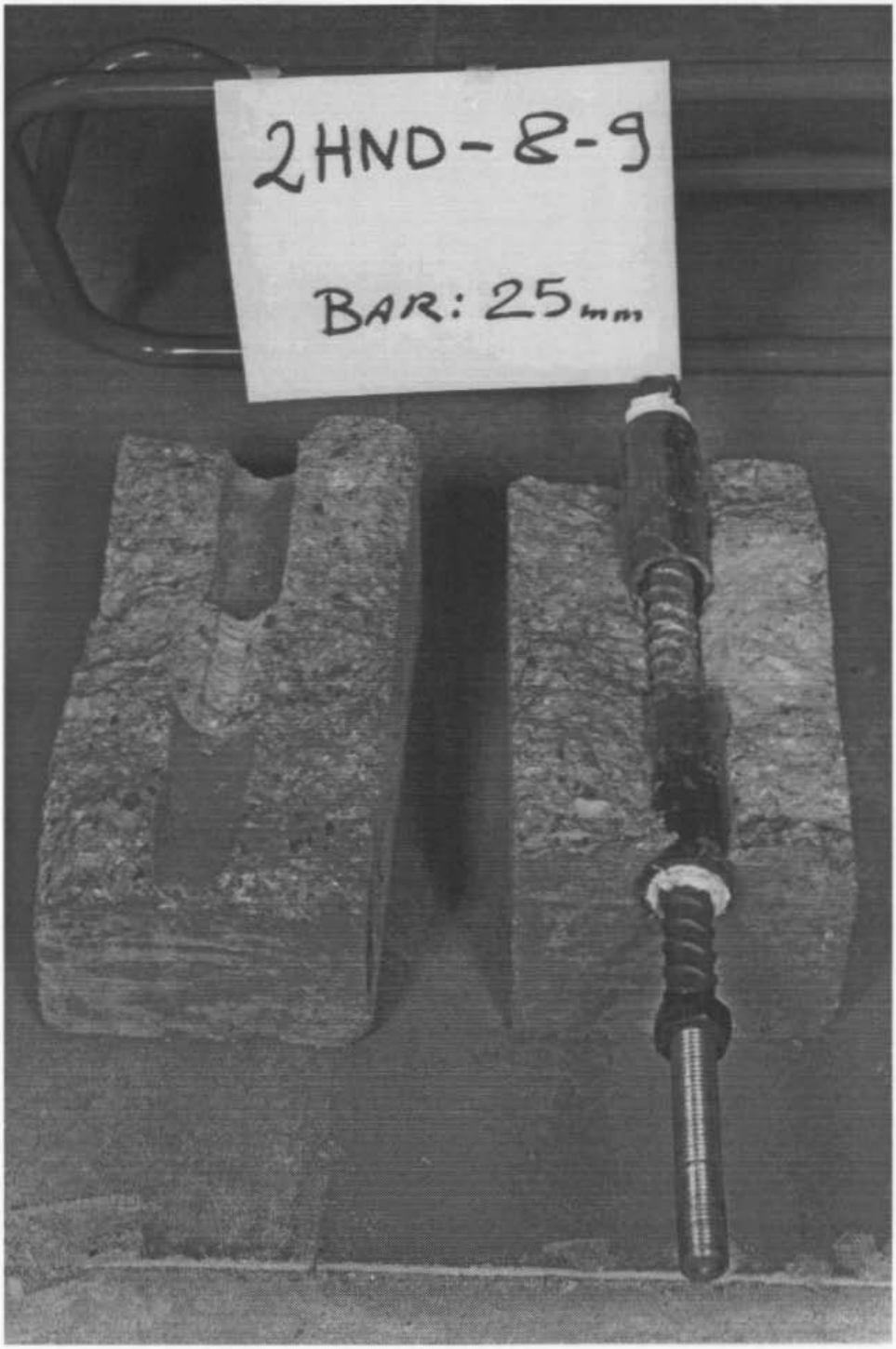

Fig. 6.23 A specimen without reinforcement as confinement after cyclic test

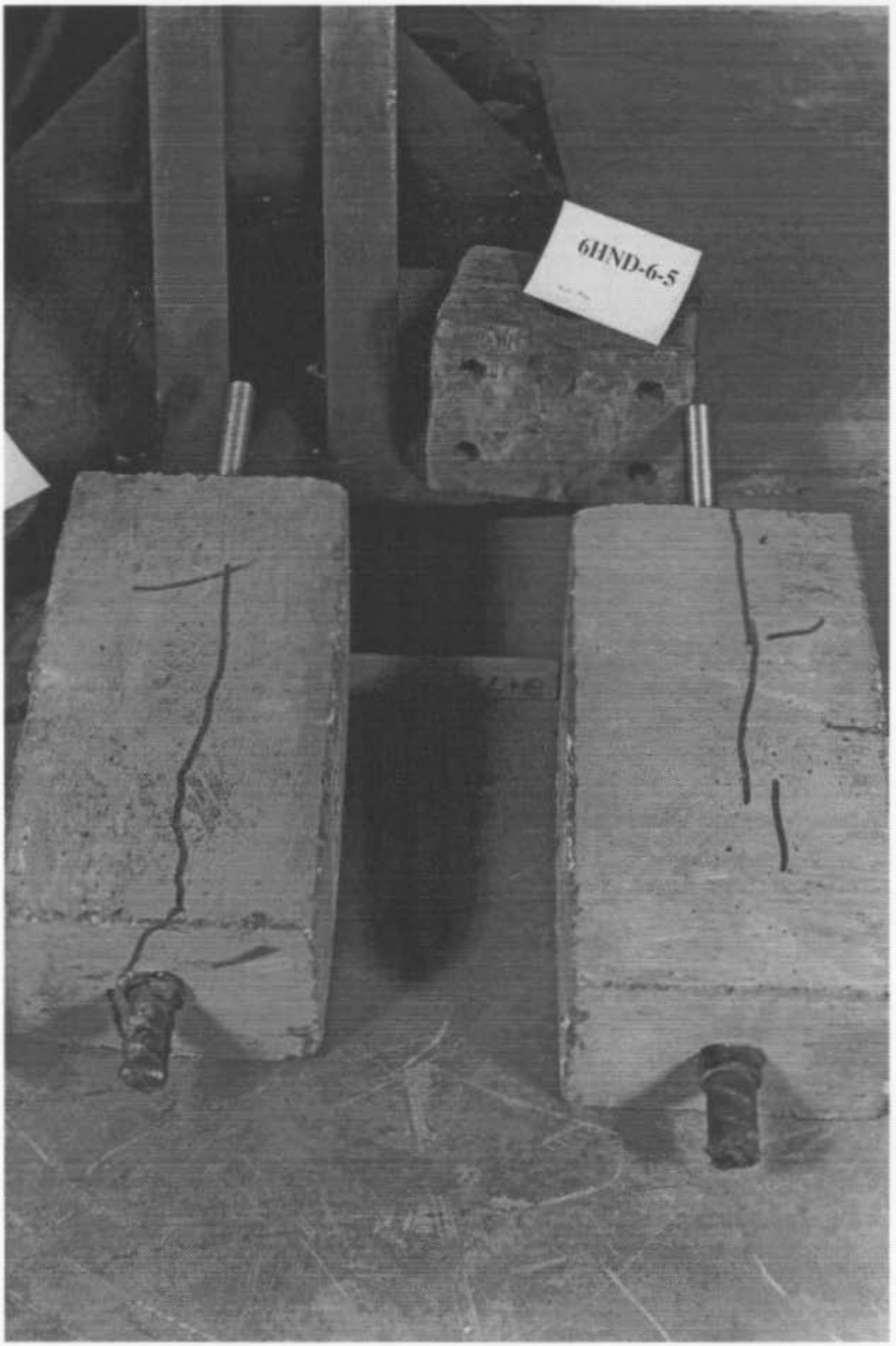

Fig. 6.24 Specimen 6 HND-6-5 after testing and crack pattern

Fig. 6.25 Specimens with rebar diameter of 35 mm after cyclic test

Fig. 6.26 Specimens and set up

Chapter 7

Effect of Bond on the Tension Stiffening of High Strength Concrete

7.1 Introduction

Failure of reinforced high strength concrete structures is initiated in many instances by cracking of plain concrete through the aggregates, resulting in a smooth fracture surface, bond resistance, crushing and rebar yielding. However, for rational calculations using nonlinear finite element analysis, it is necessary to include post-cracking resistance of high-strength concrete for accurate predictions of deflection, crack width, bond transfer and shear transfer phenomena, and tensile stiffening of concrete between cracks.

In developing a useful numerical model, it is essential to provide not only the constitutive relationships to describe the behavior of the steel and high strength concrete material, but also to establish the model and relationship for bond-slip to reflect the real interaction between the two materials. The ABAQUS finite element concrete model is

based on the assumption that the strain of the concrete and the steel are the same at sections under the maximum load. Good bond between the steel and the concrete is required to ensure that the assumption of strain compatibility is reasonably accurate. However, the experimental phase of this study showed that relative displacements do occur between the steel and the surrounding high strength concrete, i.e. the bond between reinforcement and concrete is inelastic. It is also indicated that high strength concrete is brittle in tension, hence, cracking is expected when significant tensile stress is induced in a member. Reasonable steel reinforcement ratios can be used to provide the necessary tensile strength to the concrete member. The behavior of the bond between steel and concrete is inelastic and also brittle at peak loading condition and it is necessary to couple both material components in the best possible way. Numerous kinds of constitutive laws exist to model the bond between concrete and steel. The influence of the bond on the global stiffness of the structure has to be considered for analyzing a structural problem. Also, the influences of bond stresses and cracks can be determined indirectly from the state of strains of concrete. However, for modeling the bond between reinforcement and high strength concrete, the fracture energy approach in conjunction with bond energy, biaxial failure envelope and tension softening were applied to investigate the high strength reinforced concrete model.

In the early study, Gerstle, Ingraffea, and Gergely (1982), the finite element method was combined with nonlinear fracture mechanics concept to study the tension stiffening effect in tension members. Since the finite element modeling of concrete must consider the effect of the rebar/concrete interface, the present investigation adopted a new material model for plain high strength concrete introduced by Hussein (1998), the bond

energy approach that is defined in the early chapter and also the fracture energy concept to improve the material model to represent the tension stiffening effect of high strength concrete. The new material model is implemented in the UMAT subroutine for use with the ABAQUS finite element program.

In this chapter the material model used in the ABAQUS finite element program for concrete is reviewed. The new concept of material model for high strength reinforced concrete is explained. It will be followed by the implementation of the new material model for high strength reinforced concrete in the UMAT subroutine for use in the ABAQUS finite element program. A sensitivity analysis of bond strength with respect to the selected study parameters was used to determine the share of each parameter to the total capacity of the bond strength. The influences of the study parameters on the calculation of tension stiffening are evaluated. The parametric study will be used to improve the numerical model for the bond between reinforcement and high strength concrete.

7.2 Fracture Energy and High Strength Concrete Model

Several researchers have reported that the failure of the bond between rebar and concrete is splitting type. Clark (1949), Hadje-Ghaffari et al. (1991), Darwin and Graham (1993). Since the bond failure is splitting type, fracture mechanics can be applied to study the problem of splitting of high strength concrete which leads to a loss of bond in reinforced high strength concrete members. The micro-crack and the crack propagation phenomena in the case of a uniaxial test are well described by Hillerborg (1985), and it is extended for high strength concrete by Marzouk and Chen (1995).

7.2.1 Fracture Energy

The softening response is initiated when the concrete starts cracking, due to increasing loading, in tension or low confined compression in triaxial tests. In direct tension, (Mode I type cracking), the postcrack behavior was treated with a brittle fracture concept proposed by Hillerborg (1985). The fracture energy required to form a unit area of crack surface, G_f, is assumed to be the material property. This value can be calculated from integrating the complete stress-displacement curve, as follows:

$$G_f = \int_0^{\delta_{max}} f_t \, d\delta_t \tag{7.1}$$

where f_t is a function of tensile displacement tensile stress δ_f, δ_{max}, is maximum tensile effective (cracking) displacement when f_t reaches zero at the end of the tension softening branch. The expression for G_f can be rearranged and expressed as a function of a stress-strain law, which is more common in the description of engineering materials. Thus, W_f is defined as the fracture-energy density (or work per unit of volume) dissipated by cracking, expressed as follows:

$$W_f = \frac{G_f}{\omega_c} = \int_0^{\varepsilon_{max}} f_t \, d\varepsilon_t \tag{7.2}$$

where the tensile stress f_t is expressed in terms of tensile strain ε_t ; ε_{max} is maximum tensile effective (cracking) strain when f_t reaches zero at the end of the tension softening branch; to remain constant before and after cracking. The variable W_f represents the area under a stress-strain curve of concrete in tension. Hillerborg (1985) pointed out that,

unlike metallic materials, the energy absorbed by plain concrete members in tension is mainly associated with the descending branch in tension. Concrete damage consists mainly of cracks perpendicular to the principal tensile stress and the tensile stress-displacement curve is not dependent on stresses in any other directions. In addition, the independence of the tensile stress-displacement curve with respect to specimen shapes allows one to use G_f for any type of structure, Marzouk and Chen (1995). In addition, it is concluded that the softening behavior of high strength concrete is unique and it is more brittle. Also, the fracture energy of high strength concrete was estimated to be about five times the area under the ascending portion of the stress-deformation curve, compared to a corresponding value of 10 estimated for normal strength concrete.

During the tensile test, energy is absorbed inside and outside the fracture zone. The fictitious crack model defines the energy absorbed in the fracture zone or fictitious crack as

$$G_f = \int_0^{w_c} \sigma_t du_f \tag{7.3}$$

Thus, σ_t is tensile stress, u_f is additional deformation and G_f is the absorbed energy per unit crack area for complete separation of the crack surfaces. This absorbed energy is constant for different specimen heights in the $\sigma_t - u_f$ space. It is natural to monitor the softening in terms of the fracture modulus E_d, which is the slope of $\sigma_t - u_f$, Figure 7.1. The mapping between the crack opening displacement rate, du_f, and the equivalent tensile fracture strain rate, $d\varepsilon_f$, leads to the definition of h_t. The value of h_t denotes the height of the elementary volume normal to the crack band as shown in Figure 7.1. The

degradation of the tensile strength, σ_t, is then controlled by the fracture strain, ε_f, which is expressed in terms of $du_f = h_t d\varepsilon_f$.

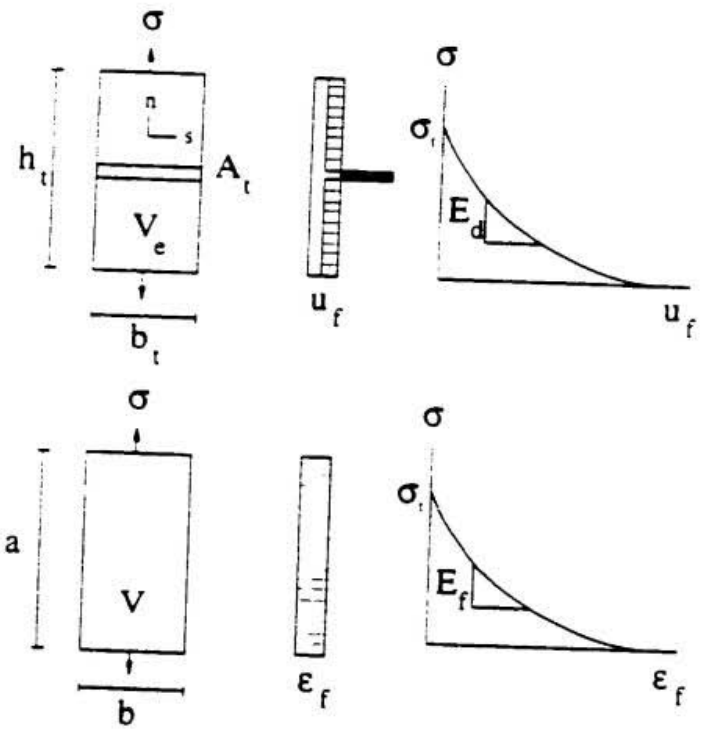

Fig. 7.1 Composite fracture model for tensile cracking (Hussein 1998)

The definition of the fracture energy based strain-softening modulus is:

$$E_f = \frac{\partial \sigma_t}{\partial u_f} \frac{\partial u_f}{\partial \varepsilon_f} \| m \| \tag{7.4}$$

In this case, h_t is used for the evaluation of the softening modulus:

$$E_f = E_d h_t \quad \text{where} \quad E_d = \frac{\partial \sigma_t}{\partial u_f}, \quad h_t = \frac{\partial u_f}{\partial \varepsilon_f} \tag{7.5}$$

Consequently, the definition of the strain softening modulus, E_f, depends on the

geometry of the elementary volume. There are different types of description for the uniaxial strength degradation in the post peak zone, including linear and bi-linear expressions. In all expressions, the area underneath the stress versus crack opening displacement curve, in direct tension, is constant and it is referred to as the fracture energy, G_f^1. The fracture energy, in direct tension, was established as a material property.

In the Etse and Willam model (1994), an exponential expression is adopted with a best fit of the Hurlbut (1985) direct tension test. The expression related the crack defined as total change of length in the crack process zone, to the crack width at complete rupture

$$\sigma_t = f_t \exp\left(-5\frac{u_f}{u_r}\right) \tag{7.6}$$

where u_r is the rupture displacement and u_f is the crack opening displacement.

7.2.2 Biaxial Failure Envelope for High Strength Concrete

The softening response is initiated when the concrete starts cracking, due to increasing loading, in tension or low confined compression in biaxial tests. At this stage, the material can no longer be assumed intact. This mechanism, at low confining pressure, can be assumed to be controlled by the degradation of the cohesion parameter, c, where $-1 \le c \le 1$. When $c = 0$, the material is considered to be completely fractured and it exhibits only residual friction similar to cohesionless material. Etse and Willam (1994) used the model proposed by Willam et al. (1984) to model the post-peak behavior of concrete.

The model that is used in the current work is based on the biaxial failure envelope

developed by Hussein (1998) and is based on the experimental testing conducted at Memorial University of Newfoundland. It has been proved that the strength of concrete under biaxial compression is higher than under uniaxial compression. The biaxial strength envelopes were determined for four types of concrete including normal strength concrete, high-strength concrete, ultera high-strength concrete and high-strength light weight concrete. Figure (7.2) shows biaxial strength envelopes for the four different types of concrete under combined tension and compression, biaxial tension and biaxial compression. The relationships between the normalized principal stresses and strains at failure for high strength concrete were given by Hussein (1998) and are shown on Figure 7.3. It was also proved that the strength increase under biaxial compression was dependent on the biaxial stress ratio. The ratio of 0.5 for a biaxial stress for the maximum biaxial strength has been specified for high strength concrete. Furthermore, it is noted that in biaxial compression, as the minor principal stress is increased, the proportional limit is also increased. A major case for the nonlinearity of the stress strain curve for concrete is internal micro cracking. The micro cracks begin as bond cracks at the aggregate-mortar interface, and propagate through the mortar mix to cause failure.

In the biaxial compression-compression tests, it was observed that failure of the specimen was due to formation of tensile splitting cracks in a plane parallel to the unconfined planes of the specimen. Moreover, it is indicated that under different biaxial compression loading combinations, the results show that the introduction of a second principal stress significantly affects the effective elastic modulus of a concrete specimen in the direction of the first principal stress. The strain, at a given stress, in the major principal stress is induced by the presence of a minor principal stress. This indicates that

the stiffness of the concrete specimen increases in the major principal direction as the minor principal stress is applied. It is important to emphasize that the change in the elastic module is not solely due to the Poisson's effect; it is also related to microcrack confinement. This was observed for four different types of concrete. Also, in the direction of the larger principal stress, the strain at ultimate load increases as the failure stress increases.

7.2.3 Relationship between Tension and Shear Fracture Energy Release Rate

The applied material model for plain high strength concrete is based on Hussein (1998). The model assumes that the failure mode is strongly dependent on the level of confinement. For example, the case of the direct tension test produces a single discrete crack with a fairly brittle post-peak response with the strength dropping to zero at the end of the load displacement curve. On the other hand, triaxial compression tests with a high level of confinement [Hurlbut (1983), and Xie et al. (1994)] develop distributed micro-cracks within the specimen and the strength does not drop to a zero level. Thus, the specimen exhibits ductile hardening or, in the limit, perfectly plastic response. Therefore, we can assume that there is a zone in stress space which defines the transition between brittle and ductile failure behavior.

It should be noted that in the triaxial loading cases, the strain softening becomes more complicated. However, there are still common features in the strength degradation. Based on the triaxial test results of high strength concrete conducted by Xie et al. (1994), the concrete under triaxial compression experiences strain-softening after the minor stress reach the peak. The slope of the descending curve becomes smaller and smaller as the

strain increases. There is a stress level at which the slope of the descending curve becomes insignificant. It is called the residual strength. Etse and Willam (1994) assumed that the residual strength is reached when a purely frictional resistance, which corresponds to a zero residual value of the cohesive parameter, dominates the strength $c_r = 0$. Thus the residual strength envelope becomes:

$$F(\sigma, \rho, \theta, c) = \frac{3}{2}\left[\frac{\rho\, r(\theta)}{f_c}\right] + \frac{m_r}{f_c}\left[\sigma + \frac{\rho\, r(\theta)}{\sqrt{6}}\right] = 0 \tag{7.7}$$

The governing mechanism that controls the degradation of strength, is the decohesion measure that is an independent strength parameter, which is accompanied by the friction hardening as a dependent strength parameter. The relation between the decohesion and the uniaxial tensile strength f_t is expressed as:

$$c_t = \frac{\sigma_t}{f_t} \tag{7.8}$$

where σ_t is the degrading tensile strength. The associated frictional hardening parameter is related to the value of decohesion as:

$$m = m_r - (m_r - m_o)c_t \tag{7.9}$$

This expression is derived from the condition that for $c = 1 \rightarrow m = m_o$, and for $c = 0 \rightarrow m = m_r$. As a result, the intermediate softening surface is defined by

$$F(\sigma, \rho, \theta, c) = \frac{3}{2}\left[\frac{\rho\, r(\theta)}{f_c}\right]^2 + \frac{m_t}{f_c}\left[\sigma + \frac{\rho\, r(\theta)}{\sqrt{6}}\right] - c_t = 0 \tag{7.10}$$

In order to capture the pronounced softening response at low compression, the fracture model for Mode I type tensile cracking is extended to the Mode II type shear

fracture. From experiments, it is known that tensile splitting in compression as well as shear is preceded by distributed microcracking, and that this microcracking is more important for Mode II than for Mode I. Hence, the crack surface in mode II can be interpreted as a multiple of the one in the direct tensile case. Fracture energy similar to the one developed for tensile cracking can be used in order to maintain constant fracture energy release between the surface and volume of the failure process:

$$du_f = \frac{V}{A_c} d\varepsilon_f = h_c d\varepsilon_f \tag{7.11}$$

where the fraction A_c / V represents the microcrack density in compression. Here, h_c is called "gauge length" or the "equivalent crack spacing" for cases other than direct tension. ε_f is called the "equivalent tensile fracture strain", and is used to monitor the degradation of the triaxial strength envelopes. The measure of the incremental equivalent tensile fracture strain is suggested as

$$d\varepsilon_f = \sqrt{<d\bar{\varepsilon}_f>^T \bullet <d\bar{\varepsilon}_f>} \tag{7.12}$$

The McCauley brackets < >, extract the tensile components of the principal fracture strain increments $d\bar{\varepsilon}_f$.

The crack spacing, h_c can be evaluated approximately in terms of the ratio between the fracture energy release rate in tension G_f^I and that in shear G_f^{II}. From the equivalence of strain energy in splitting compression it can be assumed that

$$G_f^I \Delta A_t = G_f^{II} \Delta A_c \qquad \text{or} \qquad \Delta A_t = \frac{G_f^I}{G_f^{II}} \Delta A_t \tag{7.13}$$

The crack spacing in compression and in tension h_c and h_t can thus be related by:

$$h_c = \frac{V}{A_c} = \frac{G_f^I}{G_f^{II}} \frac{V}{A_t} = \frac{G_f^I}{G_f^{II}} h_t \tag{7.14}$$

The ratio G_f^I / G_f^{II} represents the ratio between equivalent compressive crack surface and the direct tensile test crack surface. As adopted by Etse and Willam (1994), this ratio can be described with a quadratic polynomial in terms of the hydrostatic stress as

$$\frac{G_f^{II}}{G_f^I} = A\left[\frac{\sigma - f_t / 3}{f_c}\right]^4 + B\left[\frac{\sigma - f_t / 3}{f_c}\right]^2 + 1 \tag{7.15}$$

where A and B are calibrated from the low and high confined compression tests.

According to the non-associated flow rule, the failure potential Q_t is obtained by volumetric modification of the yield surface in the softening regime in Equation 7.9.

$$Q(\sigma, \rho, \theta, c_t, m_Q) = \frac{3}{2}\left[\frac{\rho\, r(\theta)}{f_c}\right]^2 + \frac{1}{f_c}\left[m_Q + m\frac{\rho\, r(\theta)}{\sqrt{6}}\right] - c_t = 0 \tag{7.16}$$

where the derivative of the dilatancy measure m_Q is defined by

$$\frac{\partial m_Q}{\partial \sigma} = D\exp(E\,x^2) + G \;: \qquad \text{where} \qquad x = \frac{-\sigma + f_t / 3}{f_c} \tag{7.17}$$

D, E, and the material parameters come from experimental investigation. These material and G parameters are calibrated for the current model based on experimental results of Hussein (1998).

7-3 Principal Features of Tension Stiffening Behavior for High strength Concrete

The stiffness of a reinforced concrete member depends on the capacity of the intact concrete to resist any internal tensile forces between adjacent cracks. This effect known as tension stiffening, has been considered to improve for high strength concrete. The following objectives were contributed with the development of tension stiffening effect for high strength reinforced concrete.

(i) Bond energy concept

(ii) Tension softening of high strength concrete, Marzouk and Chen (1995)

(iii) New material model for high strength concrete that was implemented by Hussein (1998).

7-3-1 The Effect of Bond Energy on Tension Stiffening

The load history, confining reinforcement, rebar diameter, rate of loading, rebar spacing, concrete strength, and rebar deformation pattern are the main study variables regarding the bond strength that have been investigated experimentally and the results are summarized in the early chapters. The relationship between tension stress and strain for plain high strength concrete, known as tension softening has been reported by Marzouk and Chen (1995). The complete curve of bond stress slip for high strength concrete has been captured in the experimental phase of this study and the results are reported in earlier Chapters. The concept of bond energy has been defined as the area under the curve of bond stress-slip. This is the basis for the tension stiffening concept of high strength concrete. In the analytical study the area under the curve for both plain concrete and bond

stress-slip are calculated for each test specimen. The rates of increase of the strength of concrete due to the study parameters are found and the results are summarized in Tables 7.1 to 7.3.

Furthermore, the percentage of contribution of each study parameter to the total bond resistance has been calculated by sensitivity analysis. The sensitivity analysis will show the degree of sensitivity of bond strength to the study parameters. This type of analysis provides a good look at the investigation of bond evaluation for high strength concrete. It may provide the motivation and the justification of the study parameters to obtain more accurate estimates of bond strength. In this part of the investigation, the sensitivity of the parameters used in the calculations of tension stiffening that reflects in the bond strength of high strength concrete is evaluated. The results of analyses have been displayed on sensitivity tables that show the effects of percentage variations for each parameter.

Sensitivity analyses will assess the degree of sensitivity of results to the study parameter as a variable. A sensitivity assessment will help to identify the most characteristic parameters of bond strength. It will be used to improve the numerical model for bond between reinforcement and high strength concrete. In this part, formal procedures for evaluating deviations from basic data are discussed and shown on Tables 7.4 to 7.8. The use of this type of analysis is new in this field, so that some assumptions had to be made. Therefore, the present study is mainly concerned with outlining the numerical procedure and demonstrating the functioning of the model.

The compact results of sensitivity analysis due to influence of rebar diameter are shown in Tables 7.7 to 7.8. It has been found that the share of load history confining

reinforcement, rebar diameter, rate of loading, bar spacing, concrete strength, and deformation pattern in the total bond energy is 8%, 5%, 14%, 10%, 20%, 10%, 33%, respectively. Then multiplying the related percentage by total area of tension stiffening was specified as share of each parameter on total capacity of bond energy. However, this sensitivity analyses has been tested for one-parameter at a time. It is possible to conduct a study in somehow that considers more than one-parameter at a time.

The main objective of this numerical investigation was focused on the evaluation of the influence of different bond parameters on the bond energy between rebar and high strength concrete using experimental test results. The objectives were: to develop sensitivity tables that show the effects of percentage variations for each parameter on the bond strength, to identify the most important parameters numerically for further consideration for improvement in order to get better bond resistance and to implement the effect of the parameters numerically in the assessments of the tension stiffening in the finite element program.

7-3-2 The Effect of Tension Stiffening on High Strength Concrete

Etse and Willam (1995) applied the following expression for fracture energy release rate for tensile cracking, G_f^I.

$$G_f^I = f_t \frac{u_r}{5}[1 - \exp(-5\frac{u_f}{u_r})] \tag{7.18}$$

where

f_t : Tension strength

u_f : Crack opening displacement

u_r : Crack opening displacement at residual level

The relation between the fracture energy release for tensile cracking, G_f^I, and that in shear, G_f^{II}, is defined by Equation 7.14. In addition, the fracture energy depends on the degradation of tensile strength as well as the effect of bond capacity. Therefore, any change in the tensile strength of concrete affects the fracture energy release because there is a direct relationship between them.

For the present research, the biaxial stress-strain relationships for high strength concrete, proposed by Hussein (1998), and the tension softening investigation of Marzouk and Chen (1995) in associating the concept of bond energy of experimental phase of this investigation that is explained in the previous section are applied to consider tension stiffening effect of high strength concrete. Also, the discontinuous macrocrack brittle behavior of high strength concrete is modeled by a smeared cracking approach. It is assumed that the presence of cracks enters into calculations by the way the cracks affect the stress and material stiffness associated with each material calculation point. Depending on the state of strain at an integration point of a finite element, the concrete of the proportionate sub-domain of this element is considered either as intact or as crushed or as cracked with equidistant parallel cracks in one or two directions. For simplicity, the second crack band is assumed to be orthogonal to the first one. The possibilities of more than two crack bands are disregarded. The smeared crack approach permits identification of sub-regions of the panel where fracture has occurred. Consequently, it does not permit determination of exact states of strain and stress outside of the region where fracture has occurred.

The direction of the crack in the model follows the fixed orthogonal cracks model. In this model the direction normal to the first crack is aligned with the direction of maximum tensile principal stress at the time of crack initiation. The model has memory of this crack direction, and subsequent cracks at the point under consideration can only form in directions, orthogonal to the first crack. Meanwhile, the maximum number of cracks at a material point is limited by the number of direct stress components present at the material point of the finite element model. Once cracks exist at a point, the component forms of all vector and tensor valued quantities are rotated so that they lie in the local system defined by the crack orientation vectors (the normal to the crack faces). The model ensures that these crack face normal vectors are orthogonal so that this local system is rectangular Cartesian. Crack closing and reopening can take place along the directions of the crack surface normal. The model neglects any permanent strain associated with cracking; that is, it is assumed that the cracks can close completely when the stress across them becomes compressive.

Finally, the results of numerical investigation that presented in Section 7.5 are compared with the experimental investigation of Marzouk and Chen (1995) for different high strength concrete slabs. The conclusions of the work indicate that the tension stiffening values for slab with low steel reinforcement ratio can be varied as follows:

$$A_w = 2\ A_{w1} \quad \text{to} \quad 2.5\ A_{w1} \tag{7.19}$$

and the tension stiffening values for slab with moderate steel reinforcement ratio can be represented as

$$A_w = 1.5\ A_{w1} \quad \text{to} \quad 2.0\ A_{w1} \tag{7.20}$$

Also, the tension stiffening values for slab with high steel reinforcement ratio can be indicated as

$$A_{c} = 1.25\,A_{cf} \quad \text{to} \quad 1.5\,A_{cf} \tag{7.21}$$

where

A_{c} = fracture energy of high strength reinforced concrete

A_{cf} = fracture energy of plain high strength concrete

These results provide more accurate estimation for tension stiffening than those suggested by previous researchers.

7.4 Implementation of Bond Model into ABAQUS

In the present work, the finite element program, ABAQUS/Standard, is used. The material model is introduced by the user subroutine UMAT. The subroutine UMAT was modified to take into consideration the tension stiffening effect of high strength concrete. The subroutine UMAT is programmed in FORTRAN 77 based on the Etse and Willam (1994) material model and its modification by Hussein (1998) for plain high strength concrete.

The user subroutine is called at each material integration point at every iteration of each increment. When it is called, it is provided with the material state, i.e. stress, solution dependent state variables, at the start of the increment and with the strain increment and the time increment. The subroutine updates the stresses to their values at the end of the increment and calculates the Jacobian matrix, i.e. $\partial \Delta\sigma_{v} / \partial \Delta\varepsilon_{ij}$. Since most constitutive models require the storage of solution dependent state variables, ABAQUS

provides possibilities to allocate storage for any number of such variables for each integration point. The non-linear equations are solved numerically, using additional routines. The bond strength is treated by considering the degradation of biaxial tensile strength of Hussein (1998) and tension softening of Marzouk and Chen (1995) for high strength concrete. This effect is well known as tension stiffening. It is updated in the user subroutine during each increment.

In the present work UMAT is formulated strictly for three dimensional continuum elements; plane stress elements, axisymmetric elements and 3-D solid elements. Two or three-dimensional elements can contain rebars. Rebars are defined as single bars or in layers. In the latter case the layer is a surface in each element; the user gives the rebar orientation in the surface. Moreover, the first step is a purely elastic step and the following steps are incremental phase. A number of benchmark tests were analyzed for verification.

7.4.1 Rebar Modeling in Three Dimensions

This part is largely based on the concept which is used for the ABAQUS program. Let g_i, i= 1,2,3, be the isoparametric coordinates of the basic finite element in which the rebars are placed. Let $r_\alpha, \alpha=1,2$, be isoparametric coordinates on the surface of reinforcement, with $-1 \le r_\alpha \le 1$. Let t be a material coordinate along the rebar direction, See Figure 7.4.

The rebar is integrated using 2x2 or 1x1 Gauss points, depending on the order of the underlying element. The volume of integration at a Gauss point is

$$\Delta V = \frac{A_r}{S_r}\left|\frac{\partial X}{\partial r_1}\times\frac{\partial X}{\partial r_2}\right| W_s \tag{7.22}$$

where A_r is the cross-section area of each rebar, S_r is the rebar spacing, W_s is the Gauss weighting associated with the integration point, X is the position of the Gauss point, and

$$\frac{\partial X}{\partial r_\alpha} = \frac{\partial X}{\partial g_i}\frac{\partial g_i}{\partial r_\alpha} \tag{7.23}$$

In these expressions all quantities are taken in the reference configuration, and so ABAQUS ignores changes in the rebar cross-sectional area due to straining of the rebar and changes in the rebar spacing due to straining of the finite element in which the rebar is placed. The strain in the rebar is

$$\varepsilon = \frac{1}{2}\ln\left(\frac{g}{G}\right), \tag{7.24}$$

where

$$g = \frac{\partial x}{\partial t}\cdot\frac{\partial x}{\partial t} \quad \text{and} \quad \frac{\partial x}{\partial t} = \frac{\partial x}{\partial r_i}\cdot\frac{\partial r_i}{\partial t} \tag{7.25}$$

and G is the value of "g" in the original configuration. For convenience "s" is defined as a material coordinate that is distance measuring along the rebar in the current configuration:

$$ds = \sqrt{g}\,dt \tag{7.26}$$

The first variation of strain is

$$\delta\epsilon = \frac{\partial x}{\partial s}\cdot\frac{\partial \delta u}{\partial s} \tag{7.27}$$

and the second variation of strain is

$$d\delta\epsilon = \frac{d\delta u}{\partial s}\cdot\frac{\partial \delta u}{\partial s} - 2\frac{d\delta u}{\partial s}\cdot\frac{\partial x}{\partial s}\frac{\partial x}{\partial s}\cdot\frac{\partial \delta u}{\partial s} \tag{7.28}$$

7.5 Verification Example

In order to check the validity of the new high strength concrete model, after the implementation of the rebar element and the tension stiffening contribution, a few reinforced high strength concrete cases were checked as follows:

7.5.1 Case I- High Strength Concrete One-Way Slab

The first verification example, a one-way reinforced concrete slab was considered. It is supported in the vertical direction at the edges and loaded by two lines load at distance of 152 mm from each support line. The geometry of this problem is defined in Figure 7.5. The slab is reinforced in one direction. The assumed compression strength of concrete is 78 MPa. The slab was tested and has been analyzed by a number of researchers including Gilbert and Warner (1978) and Crisfield (1982).

7.5.1.1 Geometric Modeling

Figure 7.5 shows half of the high-strength reinforced concrete one-way slab that is modeled with the plain stress element type CPS8 from the element library of ABAQUS. Nine integration points are used through the thickness of the concrete to ensure that the development of plasticity and failure through the thickness of the concrete is adequately modeled. The one-way reinforcement is modeled using the REBAR element option. The boundary conditions are symmetric around the center of the slab.

7.5.1.2 Material Properties

The material data assumed are given in Table 7.9. The assumed values are taken from previous test results on high strength concrete. The modeling of the concrete-rebar

interaction and the energy release at cracking are critical to the response of a structure such as this once the concrete starts to crack. These effects are modeled in an indirect way by including, "tension stiffening" to the plain concrete model. Usually tension stiffening is added as a linear loss of strength beyond cracking failure of the concrete. In this example three different values are used for the strain beyond failure at which all the strength is lost to illustrate the effect of the tension stiffening assumption on the response. The values range from $5x10^{-4}$ to $2x10^{-3}$ for high strength concrete, [Marzouk and Chen (1995)].

In this example full shear retention is used after cracking: It is assumed that there is no loss of shear stiffness in the plane of the cracks once they have formed. For problems like this one the response is controlled by the material behavior normal to the crack planes, whereas the material behavior in the plane of the cracks is not important. As a result the choice of shear retention has no influence in the results. Full shear retention has been chosen because it provides a more efficient numerical solution. In addition, the material properties that are used in the UMAT subroutine are shown in Table 7.10.

Since considerable nonlinearity is expected in the response, including the possibility of unstable regimes at the concrete cracks, the modified Riks algorithem is used with automatic incrementation. With the Riks method the load data and solution parameters serve only to give an estimate of the initial increment of load. In this case it seems reasonable to apply an initial load of 44.44 kN on the half-model. The analysis is terminated when the central displacement reaches 25.4 mm.

7.5.1.3 Result and Discussion

The numerical results of different material models are compared in Figure 7.6 on the basis of load versus deflection at the center of the slab. The strong effect of the tension stiffening assumption with the use of the UMAT subroutine is very clear in that graph. The analysis with tension stiffening using the modified high strength concrete model concept for low, moderate and high ratio of reinforcement are compared with the material model that is used in the ABAQUS concrete model. The comparisons of the results are shown on the Figures 7.7, 7.8, 7.9. This analysis provides useful information from a design viewpoint.

7.5.2 Case II- High Strength Reinforced Concrete Two-Way Slab

This example is used to verify the effectiveness of the recommended tension stiffening in three different high-strength reinforced concrete two-way slabs that were tested previously at Memorial University of Newfoundland by Hussein (1991). The ratio of reinforcement for the above slabs was varied from low, moderate and high ratio of reinforcement. The purpose of this example is to compare the results obtained by use of the new concrete model in the UMAT subroutine with the ABAQUS concrete model and actual experimental results.

7.5.2.1 Geometry and Model

The problems were three high-strength reinforced concrete two-way slabs subjected to a vertical load at the center of each slab. A thick shell element (S8R) from the element library of ABAQUS is used for the finite element mesh of these problems. The reason for using reduced integration points is the accuracy of the result. Reduced

integration usually provides more accurate results (provided the elements are not distorted or loaded in in-plane bending) and significantly reduces running time, especially in three dimensions. Also a beam element type B32 at the center of the slab is used as shown in Figure 7.10. The finite element meshes are assumed to have four roller supports and 20 hinged supports at the boundaries. The dimensions of the slabs were 1500x1500x120 mm, 1830x1830x150 mm and 1500x1500x120 mm. The reinforcement ratios of the slabs were 0.00491, 0.01093 and 0.0237 for low, moderate and high ratio of reinforcement, respectively. The analyses are run three times for recommended tension stiffening for low, moderate and high ratio of reinforcement. The values of 2.5, 2 and 1.25 times fracture energy of high strength plain concrete are considered as the tension stiffening values for slabs with low, moderate and high steel reinforcement ratio as explained in the section 7.3.2 of this chapter.

7.5.2.2 Results and discussions

Figure 7.11 shows the deformed shape of the slab. The ultimate deflection for the central point of the tested slabs were 25.45, 23.43 and 14.74 mm while the result after implementing the new bond model were 25.62, 23.31 and 14.82 mm. Comparison of the experimental result and recommended bond model for high strength two-way slab with low, moderate and high reinforcement ratios are shown in the figures 7.12, 7.13, and 7.14. A close agreement between experimental results and numerical results are evident with the use of recommended bond model. The slight difference between the two curves could be as a result of an error in the evaluation of the rigidity of the supports. Finally, the Figures 7.15, 16 and 17 show contour of stress for the slabs with moderate steel ratio.

7.6 Summary and Conclusions

The material model of the UMAT subroutine, developed previously for plain high strength concrete at Memorial University of Newfoundland was reviewed in detail. Several examples to test the subroutine have been solved. The material model was useful for plain high strength concrete, therefore, an attempt has been made to consider the effect of tension stiffening instead of tension softening of high strength concrete.

The concepts of bond energy, fracture energy, tension softening of Marzouk and Chen (1995), and biaxial failure envelope of high strength concrete of Hussein (1998) are applied in the development of a new material model for high strength reinforced concrete. The new model is implemented in the UMAT subroutine for use with the ABAQUS finite element program. Furthermore, a three-dimensional rebar element is added to the program in order that the new model will be able to analyze reinforced high strength concrete structures. The model has been checked by solving several problems.

A new parametric study based on the effect of bond energy on the fracture energy was introduced. Based on sensitivity analysis, the results were applied for analysis of slabs with low, moderate and high steel ratio. The study parameters are considered as the main variables for the bond strength. A sensitivity analysis is conducted to provide justification of the study parameters and to obtain more accurate estimates of bond strength. The most characteristic parameter and the share of each study parameters on the strength of bond between high-strength concrete and reinforcement through sensitivity analysis is found. Finally, the results of two analyzed examples are demonstrated to show the effectiveness of recommended model. The results of the analyses are compared with experimental results and a good agreement is found between them.

Table 7.1- Test results for Series M1, M2

Series	Investigation Parameter	Loading History	Specimen Notation	Rebar Diameter	Concrete Strength f'_c	Tensile Stresses f_t	Peak Load Pmax	Bond Stress Umax	Slip at Peak S	Area Under the Normalized Curve	Area Under the Normalize Curve	Total Tensile Stress Energy		Difference	Increase Rate	Comments
												I1	I2			
				mm	MPa	MPa	kN	MPa	mm	T Softng	I Stdng	T Softng	I Stdng	D I2 I1	%	
M1	Load History	Monotonic in Tension	1HNM-19-1	35	85.00	3.83	278.00	24.80	7.71	0.301582 when f'c 74.152 MPa	0.353	1.154	1.350	0.196	16.999	
			1HNM-19-1A	35	81.00	3.65	218.00	19.47	6.53		0.348	1.099	1.268	0.169	15.352	
			1HNM-19-1B	35	81.00	3.65	167.80	14.98	5.24		0.331	1.099	1.207	0.108	9.818	
			1HNM-19-1C	35	81.00	3.65	210.35	18.78	6.06		0.383	1.099	1.395	0.296	26.935	
		Monotonic in Compression	1HNM-19-2A	35	81.00	3.65	218.65	19.52	6.71		0.421	1.099	1.535	0.435	39.601	
			1HNM-19-2B	35	85.12	3.831	217.54	19.42	6.69		0.429	1.155	1.644	0.488	42.279	
			1HNM-19-2C	35	83.16	3.742	191.08	17.06	5.72		0.448	1.129	1.676	0.548	48.548	
		Monotonic in Tension	1HNM-19-1	**25**	81.70	3.676	180.14	30.19	8.19	0.301582 when f'c 74.152 MPa	0.317	1.109	1.166	0.058	5.199	
			1HNM-19-1A	**25**	86.00	3.870	157.65	27.34	9.67		0.409	1.167	1.583	0.416	35.641	
			1HNM-19-1B	**25**	85.12	3.830	137.43	23.82	5.92		0.381	1.155	1.460	0.305	26.397	
			1HNM-19-1C	**25**	85.12	3.830	146.23	25.35	5.08		0.402	1.155	1.540	0.385	33.317	
		Monotonic in Compression	1HNM-19-2	**25**	83.60	3.762	135.91	23.42	5.52		0.402	1.135	1.512	0.377	33.266	
			1HNM-19-2A	**25**	83.67	3.765	139.08	24.05	5.12		0.479	1.135	1.805	0.669	58.939	
			1HNM-19-2B	**25**	83.67	3.765	150.67	25.89	3.86		0.374	1.135	1.407	0.271	23.883	
			1HNM-19-2C	**25**	83.67	3.765	178.38	30.93	5.29		0.384	1.135	1.447	0.312	27.458	
M2	Confining Reinforce.	Monotonic in Tension	2HNM-8-1	35	85.00	3.825	270.64	23.84	7.01	0.301582 when f'c 74.152 MPa	0.246	1.154	0.942	-0.212	-18.363	N/R
			2HNM-8-2	35	85.00	3.825	253.23	22.61	6.43		0.319	1.154	1.222	0.068	5.906	
			2HNM-8-3	35	85.00	3.825	272.54	24.34	7.54		0.333	1.154	1.276	0.122	10.577	
			2HNM-8-4	35	85.00	3.825	190.16	16.98	5.14		0.210	1.154	0.805	-0.348	-30.208	
			2HNM-8-1	**25**	81.70	3.676	168.79	29.14	8.71		0.250	1.109	0.920	-0.189	-17.054	N/R
			2HNM-8-2	**25**	81.70	3.676	171.23	29.65	8.41		0.447	1.109	1.643	0.534	48.193	
			2HNM-8-3	**25**	85.00	3.825	168.23	29.14	8.48		0.550	1.154	2.105	0.951	82.476	
			2HNM-8-4	**25**	85.00	3.825	-	-	N/A		N/A	1.154	N/A	N/A	N/A	
		Monotonic in Compression	2HNM-8-1	**25**	81.70	3.676	193.84	33.45	6.83		0.191	1.109	0.702	-0.407	-36.720	N/R
			2HNM-8-2	**25**	81.70	3.676	185.54	32.05	3.23		0.430	1.109	1.582	0.473	42.672	
			2HNM-8-3	**25**	85.00	3.825	186.37	31.93	5.94		0.485	1.154	1.855	0.701	60.766	
			2HNM-8-4	**25**	85.00	3.825	115.29	19.91	2.32		0.250	1.154	0.956	-0.198	-17.128	

Note: N/R : Not Recommended

Table 7.2- Test results for Series M3, M4, M5

Series	Investigation Parameter	Loading History	Specimen Notation	Rebar Diamete	Concrete Strength f'c	Tensile Stresses ft	Peak Load Pmax	Bond Stress Umax	Slip at Peak S	Area Under the Normalized Curve	Area Under the Normalize Curve	Total Tensile Stess Energy		Difference	Increase Rate	Comments
												I1	I2			
				mm	MPa	MPa	kN	MPa	mm	T Softng	I Stdng	T Softng	I Stdng	D-12-11	%	
M3	**Rebar Diameter**	Monotonic in Tension	3HNM-12-1	20	78.00	3 510	112 67	24 89	7 29	0 301582 when f'c - 74 152 MPa	0 435	1 059	1 526	0 468	44 205	
			3HNM-12-2	25	90 30	4 064	143 55	24 84	6 84		0 407	1 226	1 656	0 430	35 115	
			3HNM-12-3	35	87 45	3 935	220 66	19 69	6 82		0 391	1 187	1 537	0 350	29 492	
M4	**Concrete Strength**	Monotonic in Tension	4HNM-12-1	35	50 61	2 277	168 53	15 05	6 89	0 301582 when f'c - 74 152 MPa	0 256	0 687	0 582	-0 104	-15 185	
			4HNM-12-2	35	87 45	3 935	248 95	22 23	6 95		0 367	1 187	1 445	0 258	21 751	
			4HNM-12-3	35	91 45	4 115	248 85	22 22	6 38		0 368	1 241	1 513	0 272	21 886	
			4HNM-12-4	35	92 70	4 172	273 18	24 39	8 06		0 368	1 258	1 535	0 277	22 018	
			4HNM-12-1	**25**	50 61	2 277	141 19	24 45	6 72		0 293	0 687	0 666	-0 021	-2 991	
			4HNM-12-2	**25**	86 00	3 870	157 65	27 34	9 38		0 355	1 167	1 374	0 207	17 724	
			4HNM-12-3	**25**	92 61	4 167	167 24	28 96	6 92		0 357	1 257	1 486	0 230	18 276	
			4HNM-12-4	**25**	94 96	4 273	141 21	24 45	8 83		0 323	1 289	1 381	0 092	7 135	
M5	**Bar Spacing**	Monotonic in Tension	5HNM-4-1	35	86 59	3 897	203 65	18 18	5 80	0 301582 when f'c 74 152 MPa	0 400	1 175	1 557	0 382	32 519	
			5HNM-4-2	35	94 64	4 259	244 81	21 86	8 78		0 429	1 284	1 828	0 543	42 280	
			5HNM-4-1	**25**	90 30	4 064	143 54	24 85	6 83		0 375	1 226	1 523	0 297	24 224	
			5HNM-4-2	**25**	92 61	4 17	167 24	28 96	7 19		0 355	1 257	1 480	0 223	17 765	

Table 7.3- Test results for Series M6, M7

Series	Investigation Parameter	Loading History	Specimen Notation	Rebar Diameter	Concrete Strength f'_c	Tensile Stresses f_t	Peak Load P_{max}	Bond Stress U_{max}	Slip at Peak S	Area Under the Normalized Curve	Area Under the Normalized Curve	Total Tensile Stress Energy		Difference	Increase Rate	Comments
												I1	I2			
				mm	MPa	MPa	kN	MPa	mm	T Softng	T Stdng	T Softng	T Stdng	D 12-11	%	
M6	Rate of Loading	Monotonic in Tension	6HNM-6-1	35	89.00	4.005	236.73	21.03	6.85	0.301582 when f'_c 74.152 MPa	0.202	1.208	0.809	-0.399	-33.020	
			6HNM-6-2	35	87.45	3.935	248.95	22.23	6.96		-	-	-	-	-	
			6HNM-6-3	35	78.00	3.510	227.67	20.32	5.98		0.167	1.059	0.585	-0.474	-44.733	
			6HNM-6-1	**25**	83.30	3.749	28.25	4.88	5.54		0.140	1.131	0.526	-0.604	-53.463	
			6HNM-6-2	**25**	83.67	3.765	150.16	25.89	5.29		0.236	1.135	0.889	-0.246	-21.685	
			6HNM-6-3	**25**	83.30	3.749	106.89	18.5	7.19		0.184	1.131	0.691	-0.439	-38.851	
M7	Rebar Deformation Pattern	Monotonic in Tension	7HNM-14-1	35	83.15	3.742	270.28	30.75	7.42	0.301582 when f'_c 74.152 MPa	0.309	1.129	1.157	0.029	2.551	
			7HNM-14-2	35	83.15	3.742	234.71	26.71	7.63		0.336	1.129	1.258	0.130	11.476	
			7HNM-14-3	35	83.15	3.742	190.30	21.62	7.46		0.343	1.129	1.285	0.156	13.827	
			7HNM-14-4	35	83.15	3.742	179.35	20.38	5.91		0.415	1.129	1.553	0.424	37.588	
			7HNM-14-5	35	82.93	3.732	197.00	21.62	4.64		0.306	1.126	1.141	0.016	1.384	
			7HNM-14-6	35	82.93	3.732	216.22	23.73	5.23		0.341	1.126	1.274	0.149	13.213	
			7HNM-14-7	35	82.56	3.715	182.36	19.99	5.17		0.488	1.120	1.815	0.694	61.976	
			7HNM-14-8	35	82.56	3.715	166.24	18.21	6.08		0.502	1.120	1.864	0.744	66.413	
			7HNM-14-9	35	89.52	4.028	251.76	26.71	7.93		0.343	1.215	1.381	0.166	13.661	
			7HNM-14-10	35	89.52	4.028	258.62	27.45	7.92		0.323	1.215	1.301	0.086	7.089	
			7HNM-14-11	35	86.23	3.880	206.71	21.87	5.13		0.467	1.170	1.812	0.642	54.827	
			7HNM-14-12	35	86.23	3.880	167.78	17.8	5.64		0.514	1.170	1.996	0.826	70.581	
			7HNM-14-13	35	74.75	3.364	83.18	7.76	3.07		0.244	1.015	0.820	-0.195	-19.189	Plain
			7HNM-14-14	35	81.00	3.645	218.00	19.47	6.53		0.348	1.099	1.268	0.169	15.352	Standard
			7HNM-10-1	**25**	94.64	4.259	66.51	13.18	4.79		0.286	1.284	1.219	-0.066	-5.100	
			7HNM-10-2	**25**	94.64	4.259	76.82	15.48	4.24		0.309	1.284	1.317	0.032	2.526	
			7HNM-10-3	**25**	92.00	4.140	99.12	20.12	4.12		0.379	1.249	1.567	0.319	25.538	
			7HNM-10-4	**25**	86.70	3.902	89.01	17.80	5.15		0.381	1.177	1.487	0.311	26.400	
			7HNM-10-5	**25**	86.00	3.870	113.71	22.55	4.21		0.410	1.167	1.587	0.420	35.950	
			7HNM-10-6	**25**	86.00	3.870	-	-	-		N/A	1.167	N/A	N/A	N/A	
			7HNM-10-7	**25**	86.70	3.902	75.23	15.09	5.07		0.315	1.177	1.227	0.051	4.293	
			7HNM-10-8	**25**	88.79	3.996	98.65	19.61	4.02		0.429	1.205	1.716	0.511	42.366	
			7HNM-10-9	**25**	86.00	3.870	157.65	27.34	6.53		0.449	1.167	1.738	0.571	48.882	Standard
			7HNM-10-10	**25**	90.26	4.062	37.68	7.08	2.49		0.172	1.225	0.699	-0.526	-42.934	Plain

Note Standard is refer to Canadian Standard

Table 7.4- Conclusions (Examination of Rebar Diameter)

Serie	Investigation Parameter	Loading History	Detail of Study Parameter	Increase Rate	Selected Proportio	Influence of Study Parameter	Rosen Approximation
1	Load History	Monotonic in Tension for Bar No. 35		17.276	17.276	0.116	8
		Monotonic in Compression for Bar No. 35		43.476			
		Monotonic in Tension for Bar No. 25		25.138			
		Monotonic in Compression for Bar No. 25		35.887			
2	Confining Reinf.	Monotonic in Tension for Bar No. 35	Without Confinment	N/R	5.906	0.040	3
			Conf. with bar No. 10	5.906			
			Conf. with bar No. 20	10.577			
			Conf. with bar No. 25	N/A			
		Monotonic in Tension for Bar No. 25	Without Confinment	N/R			
			Conf. with bar No. 10	48.193			
			Conf. with bar No. 20	82.476			
			Conf. with bar No. 25	N/A			
		Monotonic in Compression for Bar No. 25	Without Confinment	N/R			
			Conf. with bar No. 10	42.672			
			Conf. with bar No. 20	60.766			
			Conf. with bar No. 25	-			
3	Rebar Diam.	Monotonic in Tension	Bar No. 20	44.205	44.205	0.297	20
			Bar No. 25	35.115			
			Bar No. 35	29.492			
4	Concrete Strength	Monotonic in Tension for Bar No. 35	f'c= 50 MPa	-	21.751	0.146	10
			f'c= 85 MPa	21.751			
			f'c= 90 MPa	21.886			
		Monotonic in Tension for Bar No. 25	f'c= 50 MPa	-			
			f'c= 85 MPa	17.724			
			f'c= 90 MPa	18.276			
5	Bar Spacing	Monotonic in Tension for Bar No. 35	Bar Spacing= 1db	32.519	42.280	0.284	19
			Bar Spacing= 2db	42.280			
		Monotonic in Tension for Bar No. 25	Bar Spacing= 1db	24.224			
			Bar Spacing= 2db	17.765			
6	Rate of Loading	Monotonic in Tension for Bar No. 35	1.51 mm/min	33.297	21.584	0.145	10
			0.0151mm/min	N/A			
			75 mm/min	21.584			
		Monotonic in Tension for Bar No. 25	1.51 mm/min	12.854			
			0.0151mm/min	44.632			
			75 mm/min	27.466			
7	Deformation Pattern	Monotonic in Tension for Bar No. 35	7HNM-14-4	37.588	70.581	0.474	32
			7HNM-14-8	66.413			
			7HNM-14-12	70.581			
			Standard	15.352			
			Without Rib	N/R			
		Monotonic in Tension for Bar No. 25	7HNM-10-4	26.400			
			7HNM-10-8	42.366			
			Standard	48.882			
			Without Rib	N/R			
Note	1-Canadian Standard	2-N/R Not Recommended	3-N/A Not Available	SUM=	223.583	1.500	100

Table 7.5- Conclusions (Examination of the Influnce of Confinment)

Series	Investigation Parameter	Loading History	Detail of Study Parameter	Increase Rate	Selected Proportio	Influence of Study Parameter S.P.	Rough Approximation of S.P.
1	Load History	Monotonic in Tension for Bar No. 35		17.276	17.276	0.121	8
		Monotonic in Compression for Bar No. 35		43.476			
		Monotonic in Tension for Bar No. 25		25.138			
		Monotonic in Compression for Bar No. 25		35.887			
2	Confining Reinf.	Monotonic in Tension for Bar No. 35	Without Confinment	N.R			
			Conf. with bar No. 10	5.906			
			Conf. with bar No. 20	10.577	10.577	0.074	5
			Conf. with bar No. 25	N.A			
		Monotonic in Tension for Bar No. 25	Without Confinment	N.R			
			Conf. with bar No. 10	48.193			
			Conf. with bar No. 20	82.476			
			Conf. with bar No. 25	N.A			
		Monotonic in Compression for Bar No. 25	Without Confinment	N.R			
			Conf. with bar No. 10	42.672			
			Conf. with bar No. 20	60.766			
			Conf. with bar No. 25	-			
3	Rebar Diam.	Monotonic in Tension	Bar No. 20	44.205			
			Bar No. 25	35.115			
			Bar No. 35	29.492	29.492	0.207	14
4	Concrete Strength	Monotonic in Tension for Bar No. 35	f'c= 50 MPa	-			
			f'c= 85 MPa	21.751	21.751	0.153	10
			f'c= 90 MPa	21.886			
		Monotonic in Tension for Bar No. 25	f'c= 50 MPa	-			
			f'c= 85 MPa	17.724			
			f'c= 90 MPa	18.276			
5	Bar Spacing	Monotonic in Tension for Bar No. 35	Bar Spacing= 1db	32.519			
			Bar Spacing= 2db	42.280	42.280	0.297	20
		Monotonic in Tension for Bar No. 25	Bar Spacing= 1db	24.224			
			Bar Spacing= 2db	17.765			
6	Rate of Loading	Monotonic in Tension for Bar No. 35	1.51 mm/min	33.297			
			0.0151mm/min	N.A			
			75 mm/min	21.584	21.584	0.152	10
		Monotonic in Tension for Bar No. 25	1.51 mm/min	12.854			
			0.0151mm/min	44.632			
			75 mm/min	27.466			
7	Deformation Pattern	Monotonic in Tension for Bar No. 35	7HNM-14-4	37.588			
			7HNM-14-8	66.413			
			7HNM-14-12	70.581	70.581	0.496	33
			Standard	15.352			
			Without Rib	N/R			
		Monotonic in Tension for Bar No. 25	7HNM-10-4	26.400			
			7HNM-10-8	42.366			
			Standard	48.882			
			Without Rib	N/R			
Note	1-Canadian Standard 2-N/R Not Recommended		3-N/A Not Available		SUM=	213.540	1.500	100

Table 7.6 Conclusions (Examination of the Influnce of Confinment)

Series	Investigation Parameter	Loading History	Detail of Study Parameter	Increase Rate %	Selected Proportio %	Influence of Study Parameter USP	Reach Approximation Of USP %
1	Load History	Monotonic in Tension for Bar No. 35		17.276	17.276	0.124	8
		Monotonic in Compression for Bar No. 35		43.476			
		Monotonic in Tension for Bar No. 25		25.138			
		Monotonic in Compression for Bar No. 25		35.887			
2	Confining Reinf.	Monotonic in Tension for Bar No. 35	Without Confinment	N.R			
			Conf. with bar No. 10	5.906	5.906	0.042	3
			Conf. with bar No. 20	10.577			
			Conf. with bar No. 25	N.A			
		Monotonic in Tension for Bar No. 25	Without Confinment	N.R			
			Conf. with bar No. 10	48.193			
			Conf. with bar No. 20	82.476			
			Conf. with bar No. 25	N.A			
		Monotonic in Compression for Bar No. 25	Without Confinment	N.R			
			Conf. with bar No. 10	42.672			
			Conf. with bar No. 20	60.766			
			Conf. with bar No. 25	-			
3	Rebar Diam.	Monotonic in Tension	Bar No. 20	44.205			
			Bar No. 25	35.115			
			Bar No. 35	29.492	29.492	0.212	14
4	Concrete Strength	Monotonic in Tension for Bar No. 35	f'c= 50 MPa	-			
			f'c= 85 MPa	21.751	21.751	0.156	10
			f'c= 90 MPa	21.886			
		Monotonic in Tension for Bar No. 25	f'c= 50 MPa	-			
			f'c= 85 MPa	17.724			
			f'c= 90 MPa	18.276			
5	Bar Spacing	Monotonic in Tension for Bar No. 35	Bar Spacing= 1db	32.519			
			Bar Spacing= 2db	42.280	42.280	0.304	20
		Monotonic in Tension for Bar No. 25	Bar Spacing= 1db	24.224			
			Bar Spacing= 2db	17.765			
6	Rate of Loading	Monotonic in Tension for Bar No. 35	1.51 mm/min	33.297			
			0.0151mm/min	N/A			
			75 mm/min	21.584	21.584	0.155	10
		Monotonic in Tension for Bar No. 25	1.51 mm/min	12.854			
			0.0151mm/min	44.632			
			75 mm/min	27.466			
7	Deformation Pattern	Monotonic in Tension for Bar No. 35	7HNM-14-4	37.588			
			7HNM-14-8	66.413			
			7HNM-14-12	70.581	70.581	0.507	34
			Standard	15.352			
			Without Rib	N/R			
		Monotonic in Tension for Bar No. 25	7HNM-10-4	26.400			
			7HNM-10-8	42.366			
			Standard	48.882			
			Without Rib	N/R			
Note	1-Canadian Standard	2-N/R Not Recommended	3-N/A Not Available		SUM=	208.870	1.500	100

Table 7.7- Sensitivity Analyses of Parameters Influencing Bond Strength

Serie	Investigation Parameter	Identification Number for Parameters	Loading History	Detail of Study Parameter	The Influence of Study Parameters (I.S.P.) sensitive to													Suggested Rate of Contribution for I.S.P.(1)
					LH1	LH2	CR2	CR3	RD1	RD2	RD3	CS2	BS1	BS2	RL1	RL3	DP3	DP4	
1	**Load History**	LH1	Monotonic in Tension for Bar No. 35	Load History			8	8	8	8	8	8	8	8	8	8	8	11	**8**
		LH2	Monotonic in Compression for Bar No. 35																
		LH3	Monotonic in Tension for Bar No. 25																
		LH4	Monotonic in Compression for Bar No. 25																
2	**Confining Reinf.**	CR1	Monotonic in Tension for Bar No. 35	Without Confinment	3	3			3	5	5	5	5	5	5	5	5	7	**5**
		CR2		Conf. with bar No. 10															
		CR3		Conf. with bar No. 20															
		CR4		Conf. with bar No. 25															
		CR5	Monotonic in Tension for Bar No. 25	Without Confinment															
		CR6		Conf. with bar No. 10															
		CR7		Conf. with bar No. 20															
		CR8		Conf. with bar No. 25															
		CR9	Monotonic in Compression for Bar No. 25	Without Confinment															
		CR10		Conf. with bar No. 10															
		CR11		Conf. with bar No. 20															
		CR12		Conf. with bar No. 25															
3	**Rebar Diam.**	RD1	Monotonic in Tension	Bar No. 20	14	13	14	14				14	14	14	13	14	14	19	**14**
		RD2		Bar No. 25															
		RD3		Bar No. 35															
4	**Concrete Strength**	CS1	Monotonic in Tension for Bar No. 35	f'c= 50 MPa	10	9	10	10	10	10	10	10	11	10	10	10	10	14	**10**
		CS2		f'c= 85 MPa															
		CS3		f'c= 90 MPa															
		CS4	Monotonic in Tension for Bar No. 25	f'c= 50 MPa															
		CS5		f'c= 85 MPa															
		CS6		f'c= 90 MPa															

Note: (1): Based on Maximum Number of Repetition (2): Canadian Standard

Table 7.8- Sensitivity Analyses of Parameters Influencing Bond Strength

Serie	Investigation Parameter	Identification Number for Parameters	Loading History	Detail of Study Parameter	The Influence of Study Parameters (I.S.P.) sensitive to													Suggessted Rate of Contribution for I.S.P.(1)
					LH1	LH2	CR2	CR3	RD1	RD2	RD3	CS2	BS1	BS2	RL1	RL3	DP3	DP4	
5	**Bar Spacing**	BS1	Monotonic in Tension for Bar No. 35	Bar Spacing= 1db	20	18	20	20	19	19	20	20	16	20	19	20	20	27	**20**
		BS2		Bar Spacing= 2db															
		BS3	Monotonic in Tension for Bar No. 25	Bar Spacing= 1db															
		BS4		Bar Spacing= 2db															
6	**Rate of Loading**	RL1	Monotonic in Tension for Bar No. 35	1.510 mm/min	10	9	10	10	10	10	10	10	11	10	15	10	10	14	**10**
		RL2		0.015 mm/min															
		RL3		75.000 mm/min															
		RL4	Monotonic in Tension for Bar No. 25	1.510 mm/min															
		RL5		0.015 mm/min															
		RL6		75.000 mm/min															
7	**Deformation Pattern**	DP1	Monotonic in Tension for Bar No. 35	7HNM-14-4	34	30	34	33	32	32	33	33	35	33	31	33	33	10	**33**
		DP2		7HNM-14-8															
		DP3		7HNM-14-12															
		DP4		Standard															
		DP5		Without Rib															
		DP6	Monotonic in Tension for Bar No. 25	7HNM-10-4															
		DP7		7HNM-10-8															
		DP8		Standard (2)															
		DP9		Without Rib															

Note: (1): Based on Maximum Number of Repetition (2): Canadian Standard

Table 7.9 Material properties of one-way high strength reinforced concrete slab *

Reinforcement ratio		
(Volume of steel : volume of concrete):	in each direction	7.2×10^{-3}
Steel (rebar) properties:		
- Young's modulus		193 GPa
- Yield stress		435 MPa
Concrete properties:		
- Young's modulus		36.2 GPa
- Poisson's ratio		0.24
Uniaxial compression values:		
- Yield Stress		44.88 MPa
- Failure stress		78.00 MPa
- Plastic strain at failure		1.24×10^{-3}
- Ratio of uniaxial tension to compression failure stress		4.53×10^{-2}
- Ratio of biaxial to uniaxial compression failure stress		1.16
"Tension stiffening" is assumed as a linear decrease of the stress to zero stress, at a strain of 5×10^{-4}, at a strain of 10×10^{-4}, or at a strain of 20×10^{-4}.		

* The Material constants of Jain and Kennedy R.C. Slab of ABAQUS (1997), "Example Manual", include necessary modification for High Strength Concrete material

Table 7.10 Material properties of one-way high strength reinforced concrete slab used in UMAT subroutine *

	1.0
E, Young's modulus (Mpa)	$E = 44159.0$
ν, Poissin's ratio	$\nu = 0.24$
ρ, material density	$\rho = 1.0$
f_c, compressive strength (Mpa)	$f_c = 78.00$
f_t, tensile strength (Mpa)	$f_t = 3.5327$
c_o, cohesion parameter at peak	$c_o = 1.0$
k_o, initial hardening parameter	$k_o = 0.1$
m_r, frictional parameter at residual	$m_r = 12.0$
A_h, B_h, C_h, hardening ductility parameters	$A_h = -0.000425, B_h = -0.00495, C_h = 0.000212$
A_t, B_t, softening parameters for fracture energy ratio	$A_t = 12.517, B_t = 23.753$
$D_{ho}, E_{ho}, F_{ho}, D_{hl}, E_{hl}$, parameters for dilation function m_Q	$D_{ho} = 8.675, E_{ho} = -14.695, F_{ho} = -6.3, D_{hl} = 5.115, E_{hl} = 6.736$
u_r, rupture displacement (mm)	$u_r = 0.1300$
$u_r = 5.034\, G_f^I / f_t$ *if using exponet softening function* $\sigma_t = f_t \exp(-5u_f / u_r)$	
$u_r = 2.0 G_f^I / f_t$ *if using linear softening function*	
u_k, rupture displacement if exponent softening function is used	$u_k = -0.060$
D_B, ratio of reduced tensile strength at u_k to f_t	$D_B = 0.3333$
H_t, tensile crack spacing or height of tension specimen (mm)	$H_t = 108.0$
H_E, height of finite element (mm)	$H_E = 38.1$
R_v, ratio of total volume to localized damaged volume	$R_v = 1.0$
ξ, ratio of shear band height to finite element height	$\xi = 1.0$

* [Original source of data come from XieJ., Elwi A., and MacGreger, then some parameters were calibrated by Hussain (1998)]

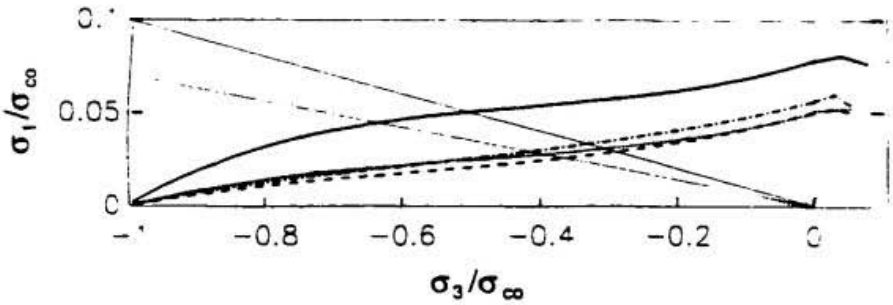

(a) Compression-tension and tension-tension

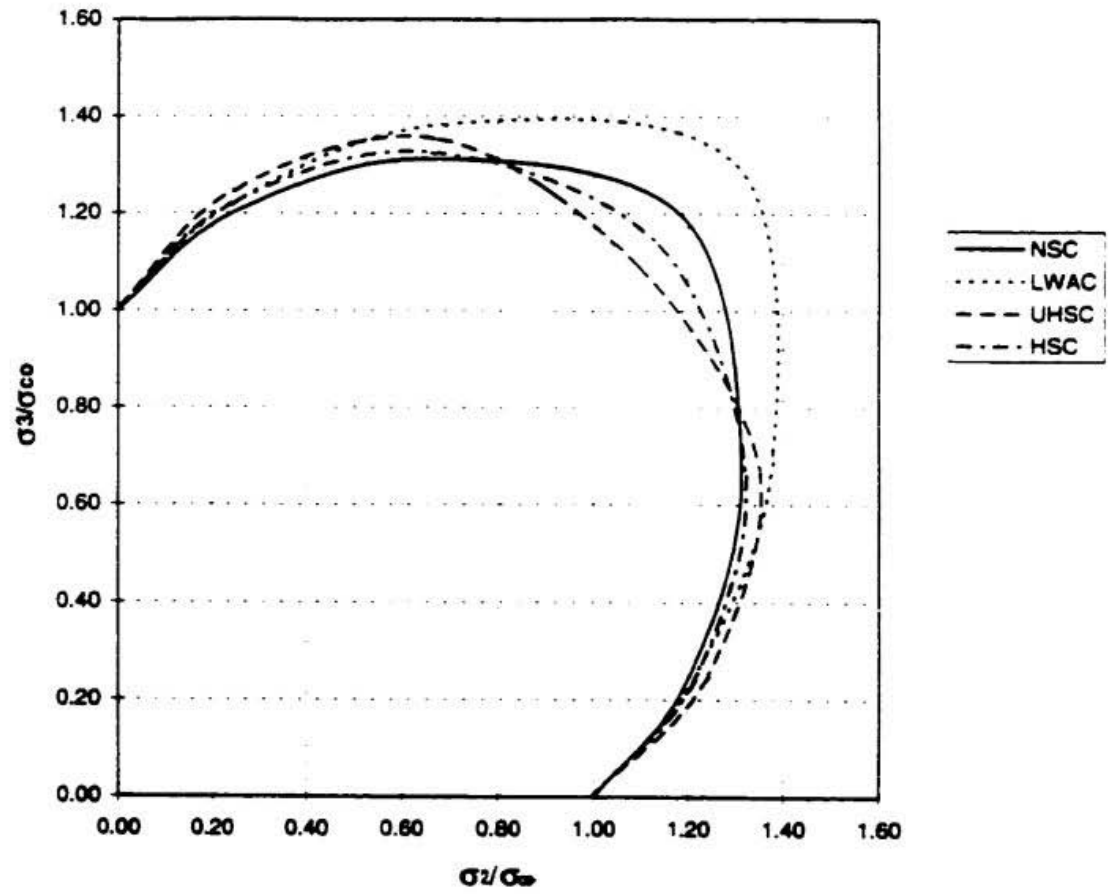

(b) Compression-Compression

Fig. 7.2 Biaxial strength envelopes for four different types of concrete under combined tension and compression, biaxial tension and biaxial compression [Hussein (1998)]

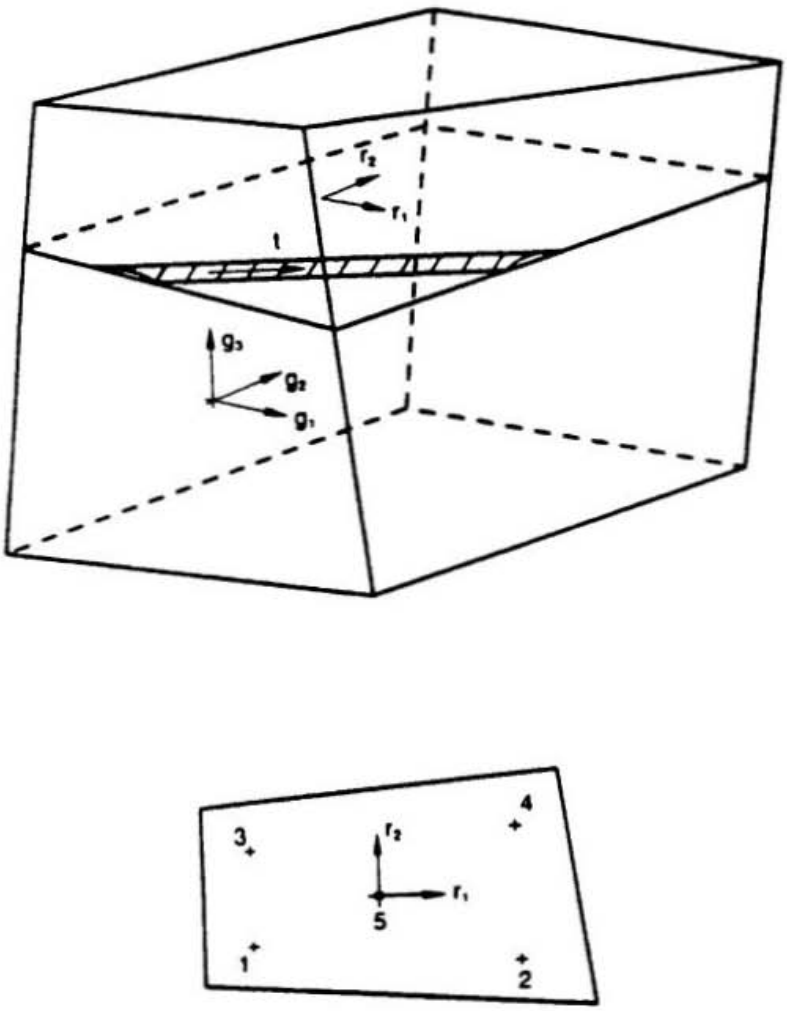

Fig. 7.4 Rebar in a solid. three-dimensional element

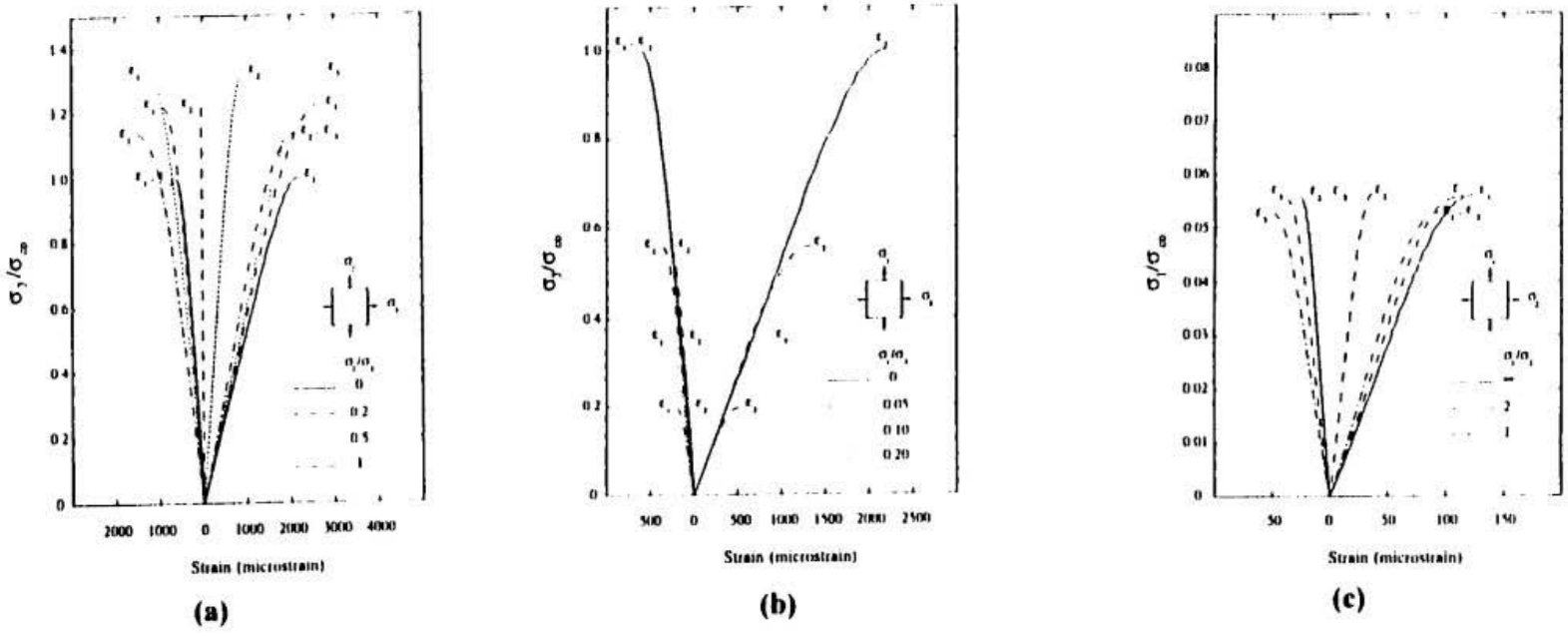

Fig. 7.3 Stress-strain relationships for high strength concrete under
a) biaxial compression, b) combined tension and compression, c) biaxial tension [Hussain (1998)]

ABAQUS

High-Strength R.C. One-way Slab

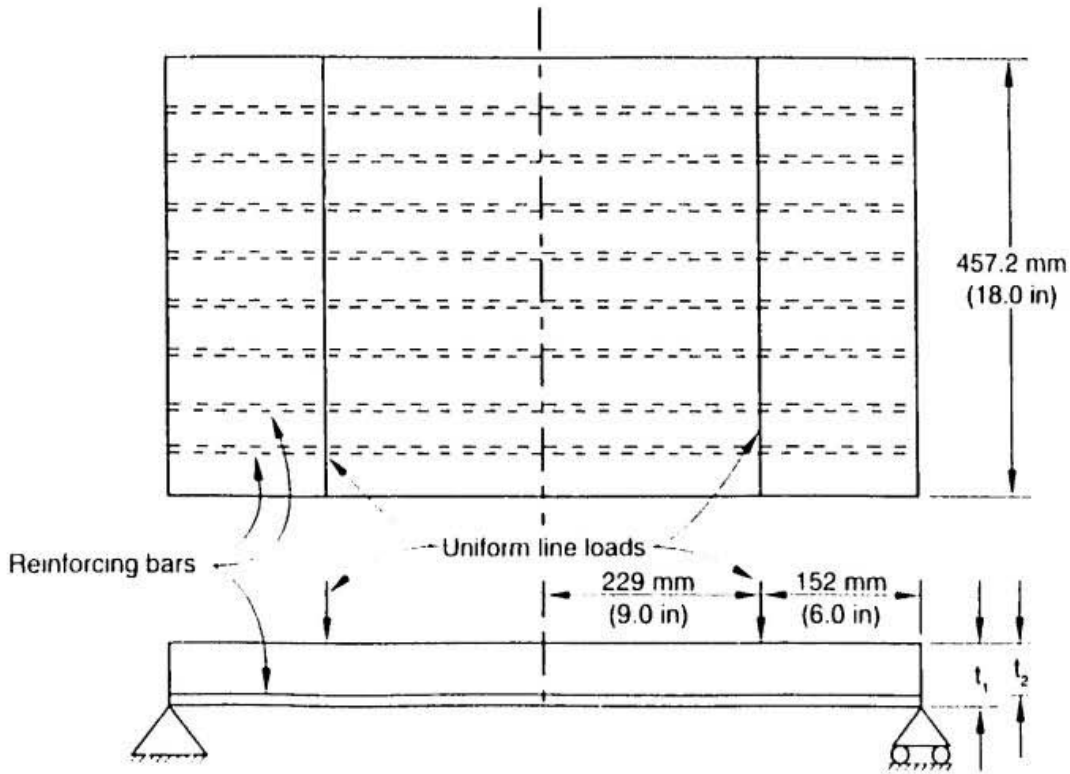

Fig. 7.5 Dimension of one-way slab (the first verification example)

t_1 = 38.1 mm (1.5 in)
t_2 = 31 mm (1.22 in)

Fig. 7.6 Tension Stiffening by Means of Postfailure Stress-Strain Relation

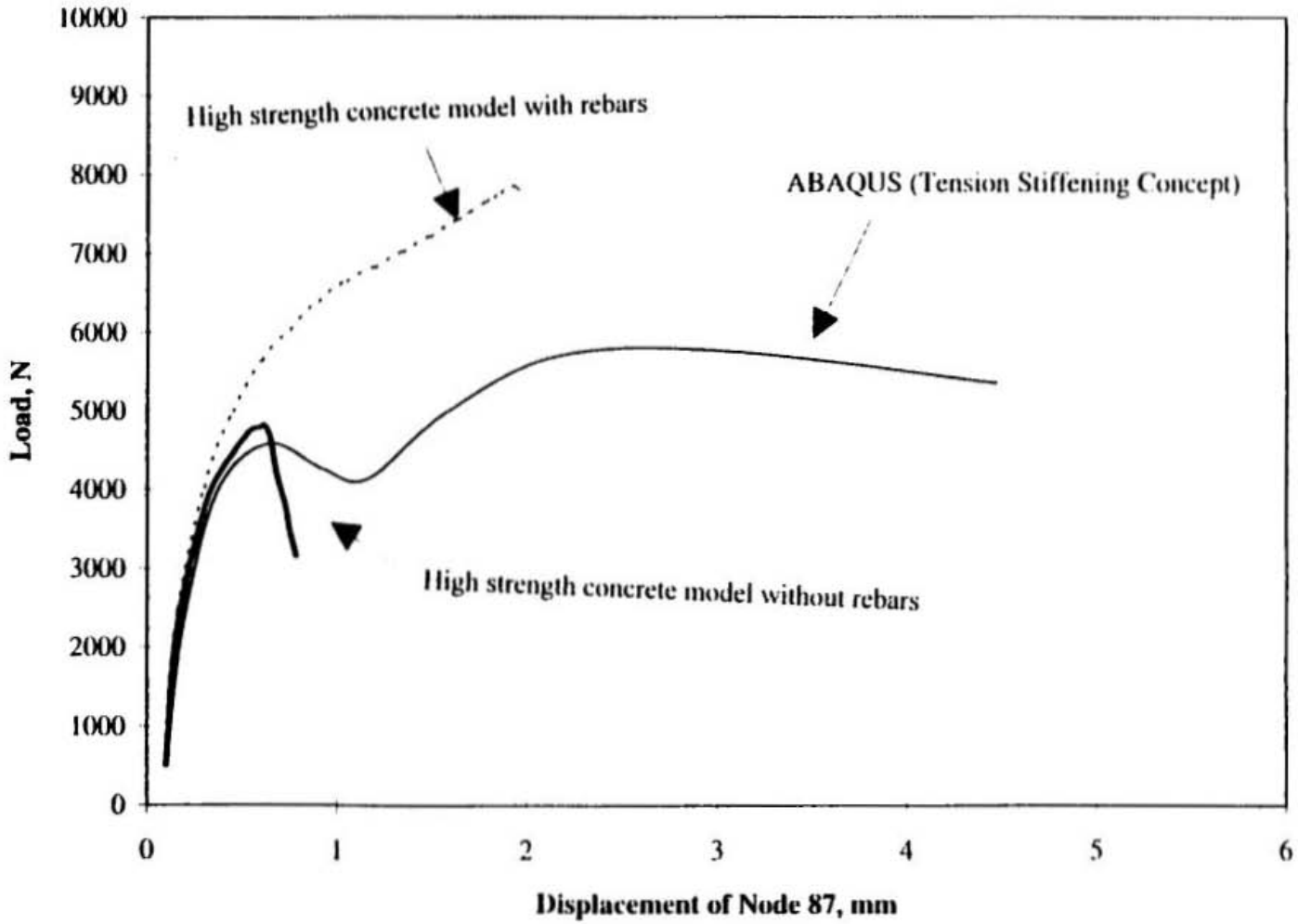

Fig. 7.7 Comparison of the results for one-way slab with low ratio of reinforcement by different material models

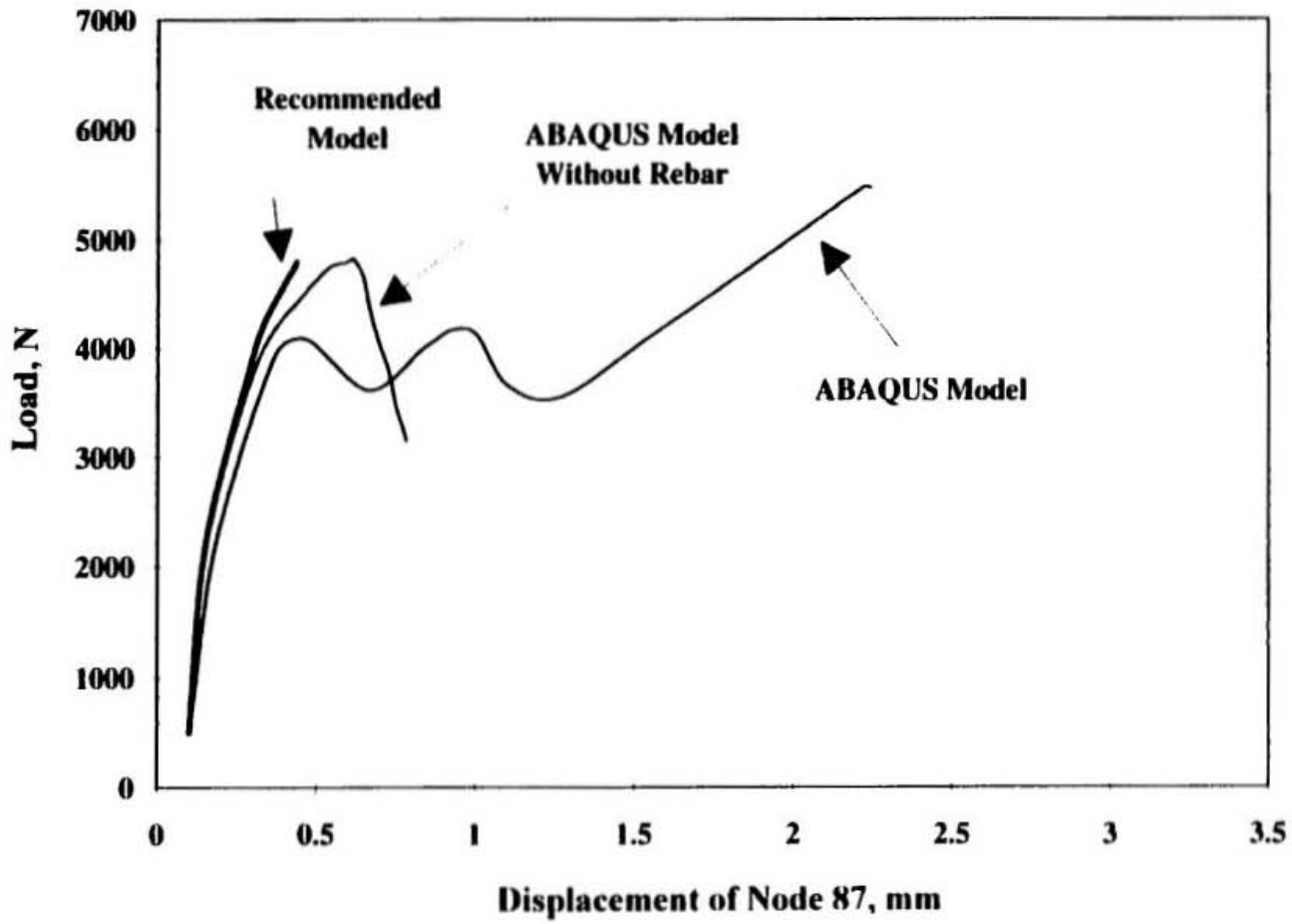

Fig. 7.8 Comparison of the results for one-way slab with moderate ratio of reinforcement by different material models

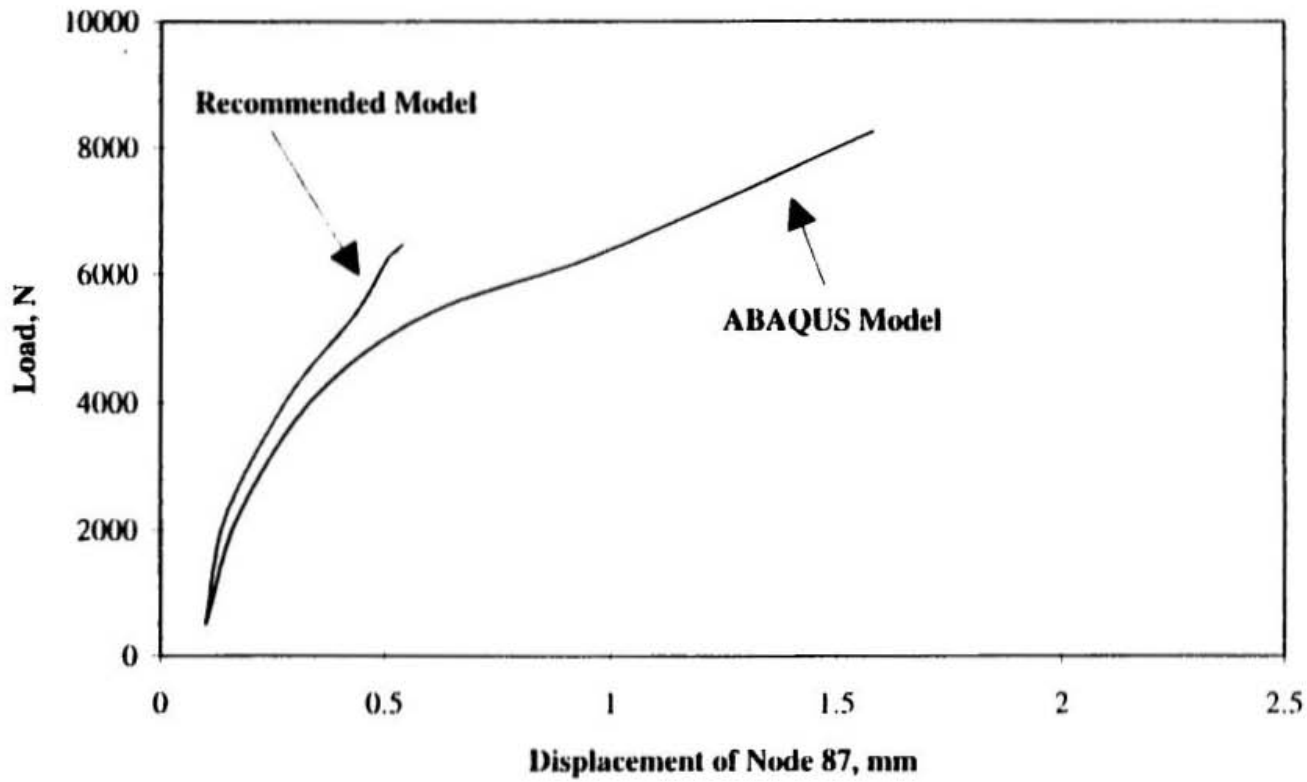

Fig. 7.9 Comparison of the results for one-way slab with high ratio of reinforcement by different material models

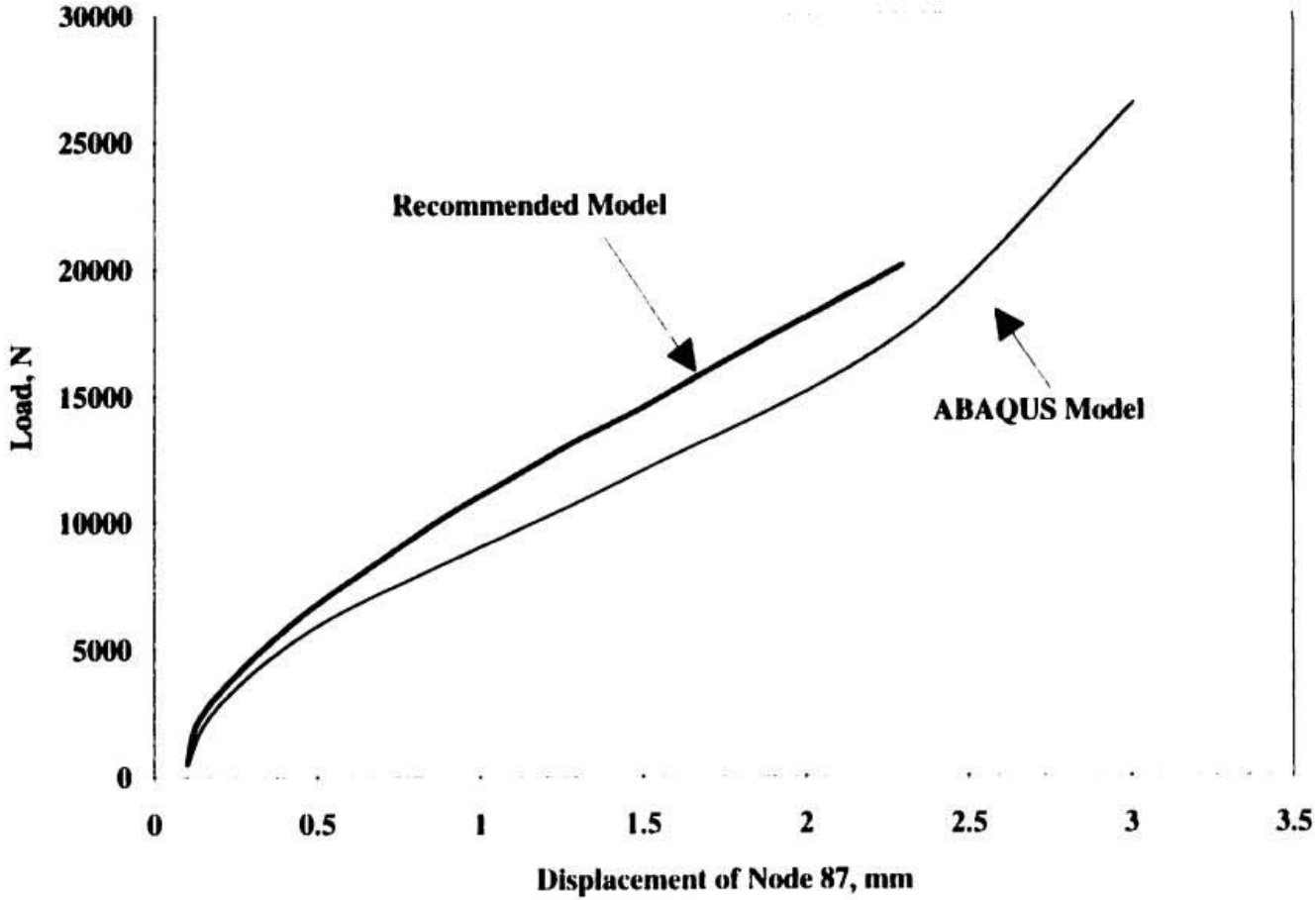

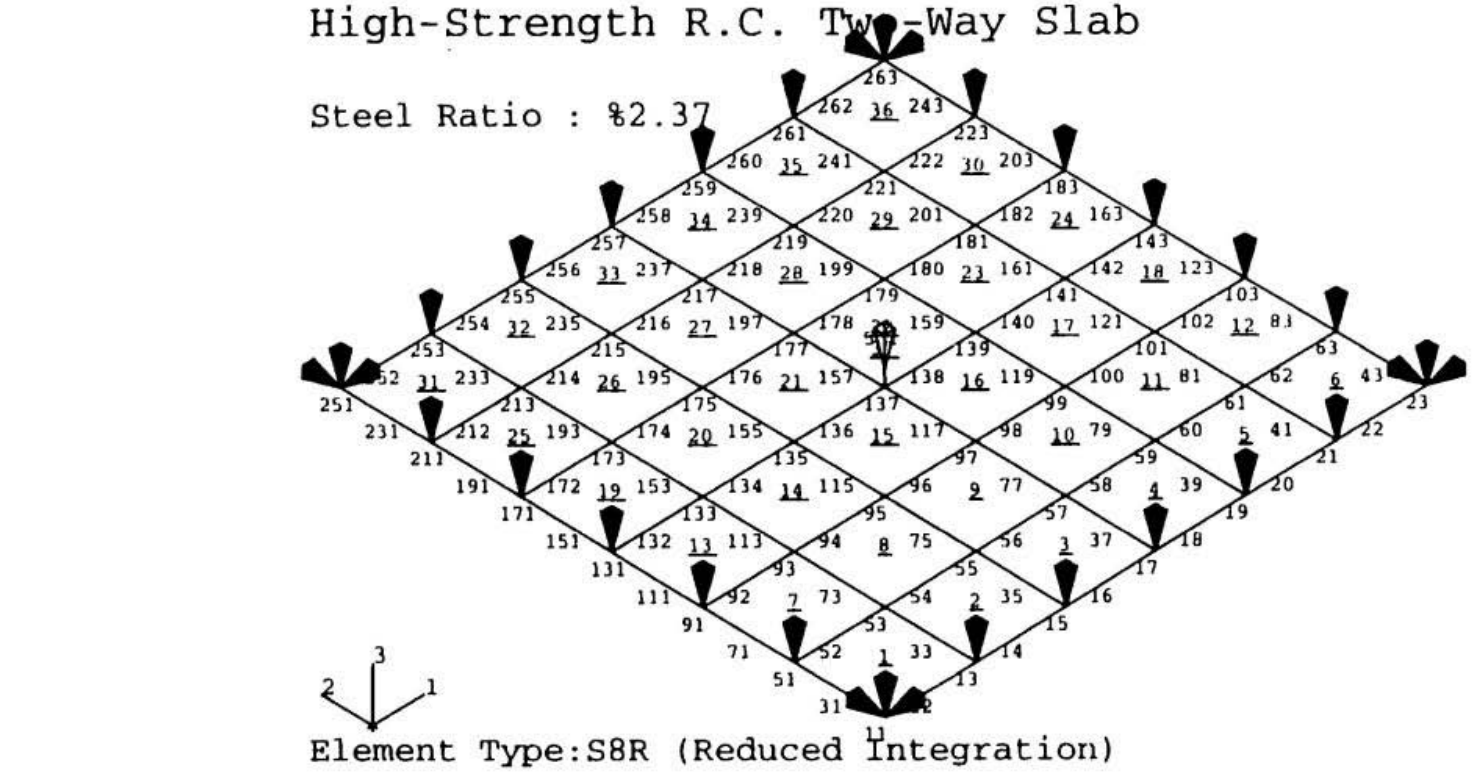

Fig. 7.10 Finite Element Mesh Idealisation for Two-way Slab of Second Verification Example

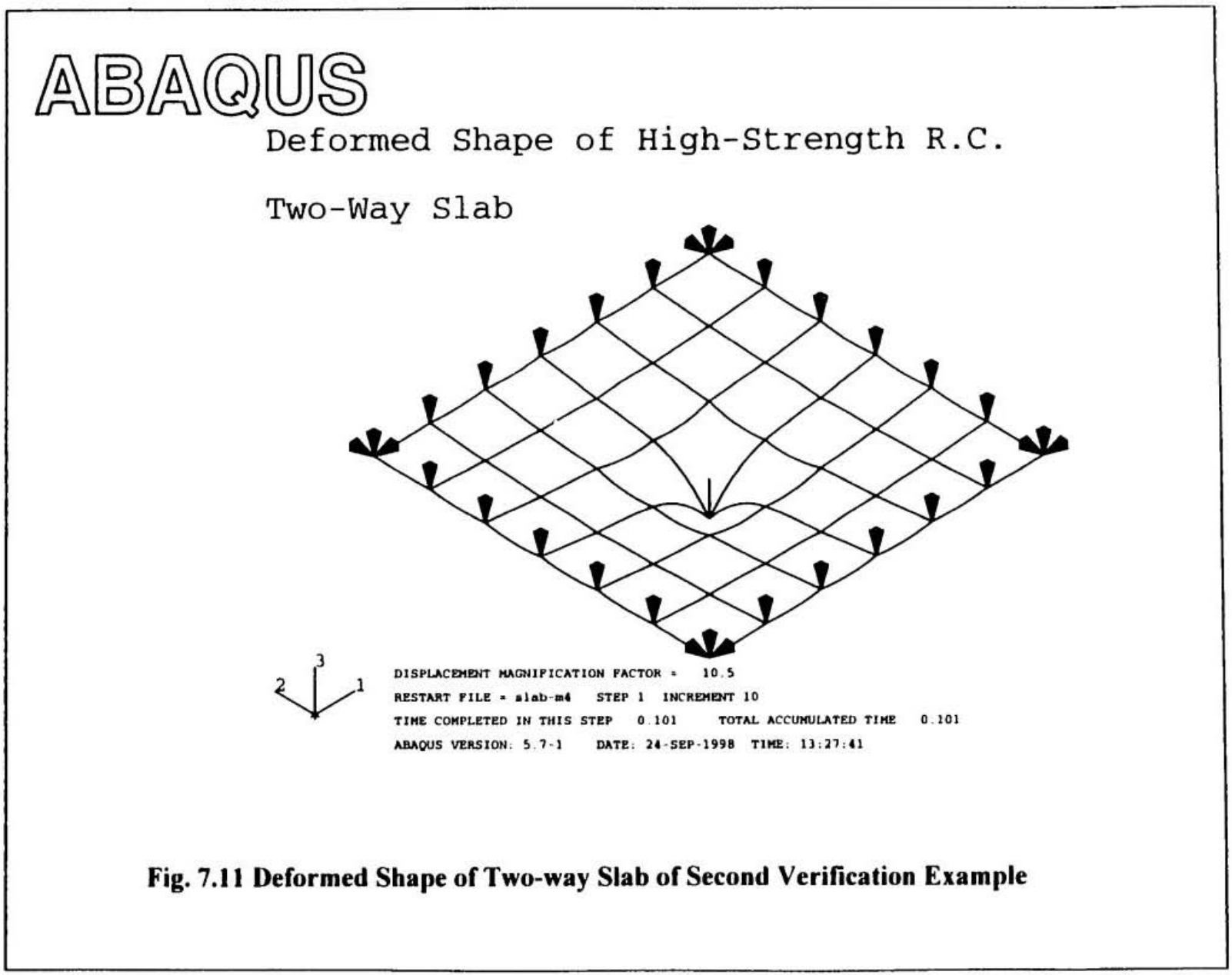

Fig. 7.11 Deformed Shape of Two-way Slab of Second Verification Example

Fig. 7.12 Comparison of the Experimental Result and Recommended Bond Model for High-Strength R.C. Two-way Slab with Low Steel Ratio

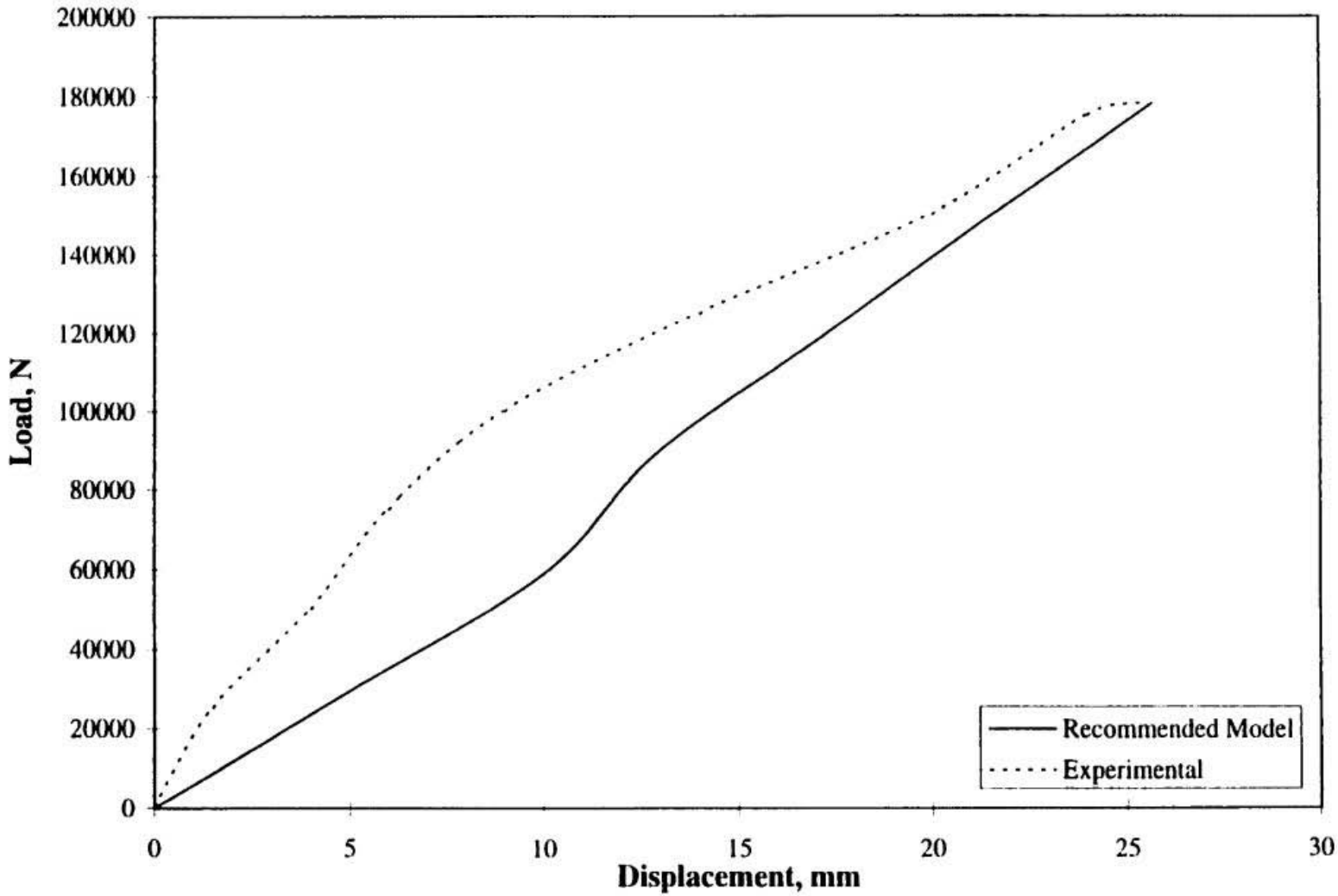

Fig. 7.13 Comparison of the Experimental Result and Recommended Bond Model for High-Strength R.C. Two-way Slab with Moderate Steel Ratio

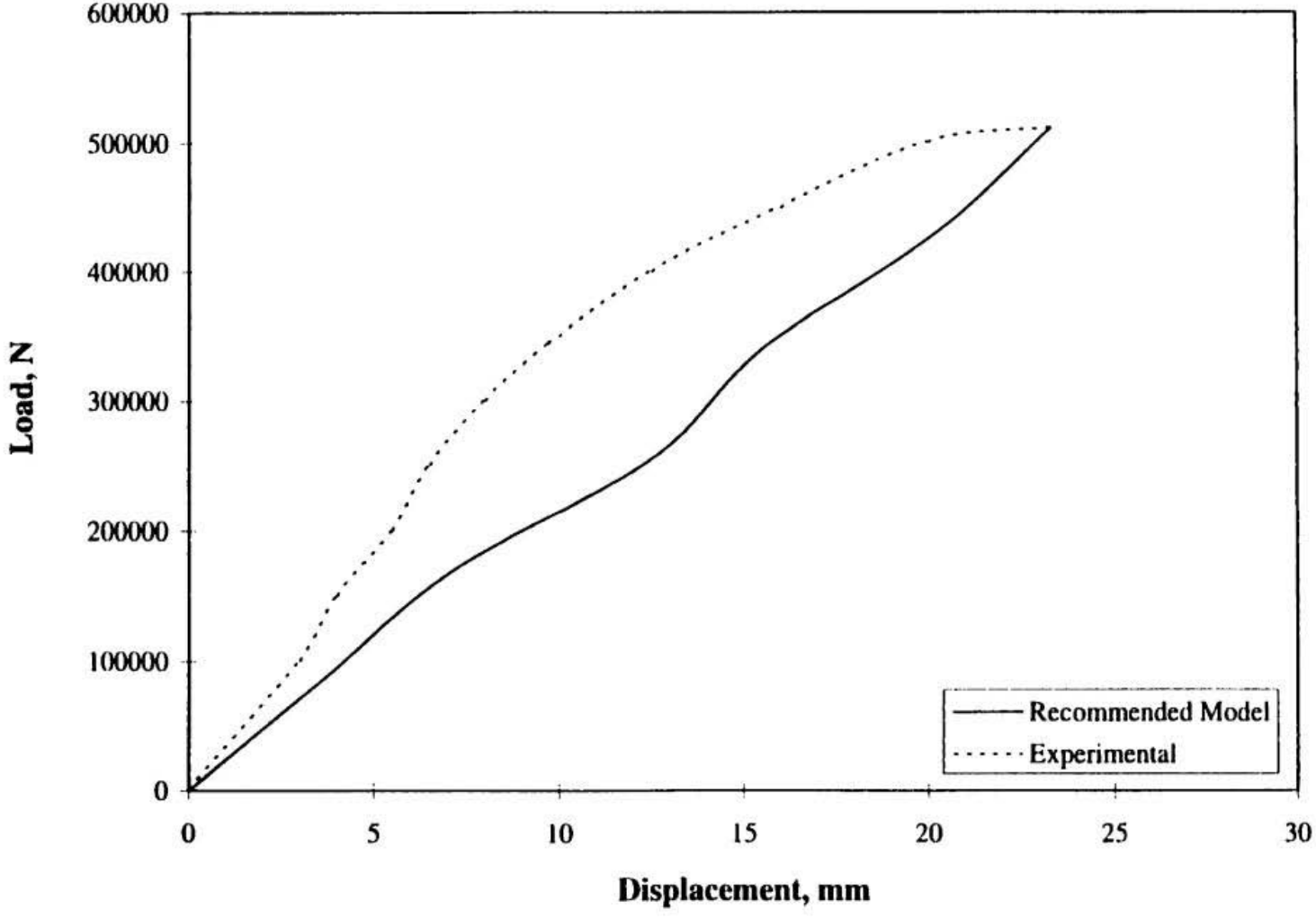

Fig. 7.14 Comparison of the Experimental Result and Recommended Bond Model for High-Strength R.C. Two-way Slab with High Steel Ratio

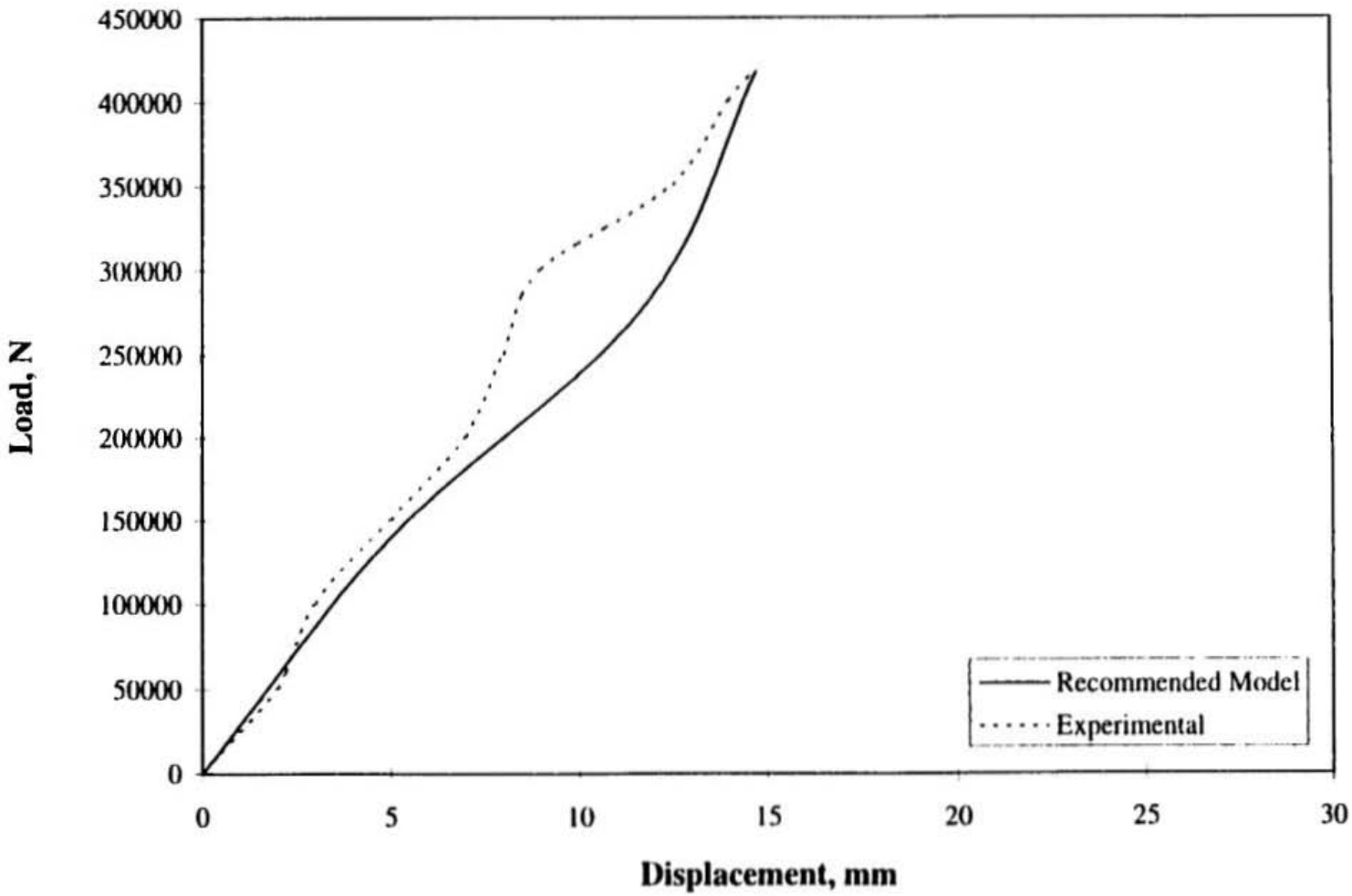

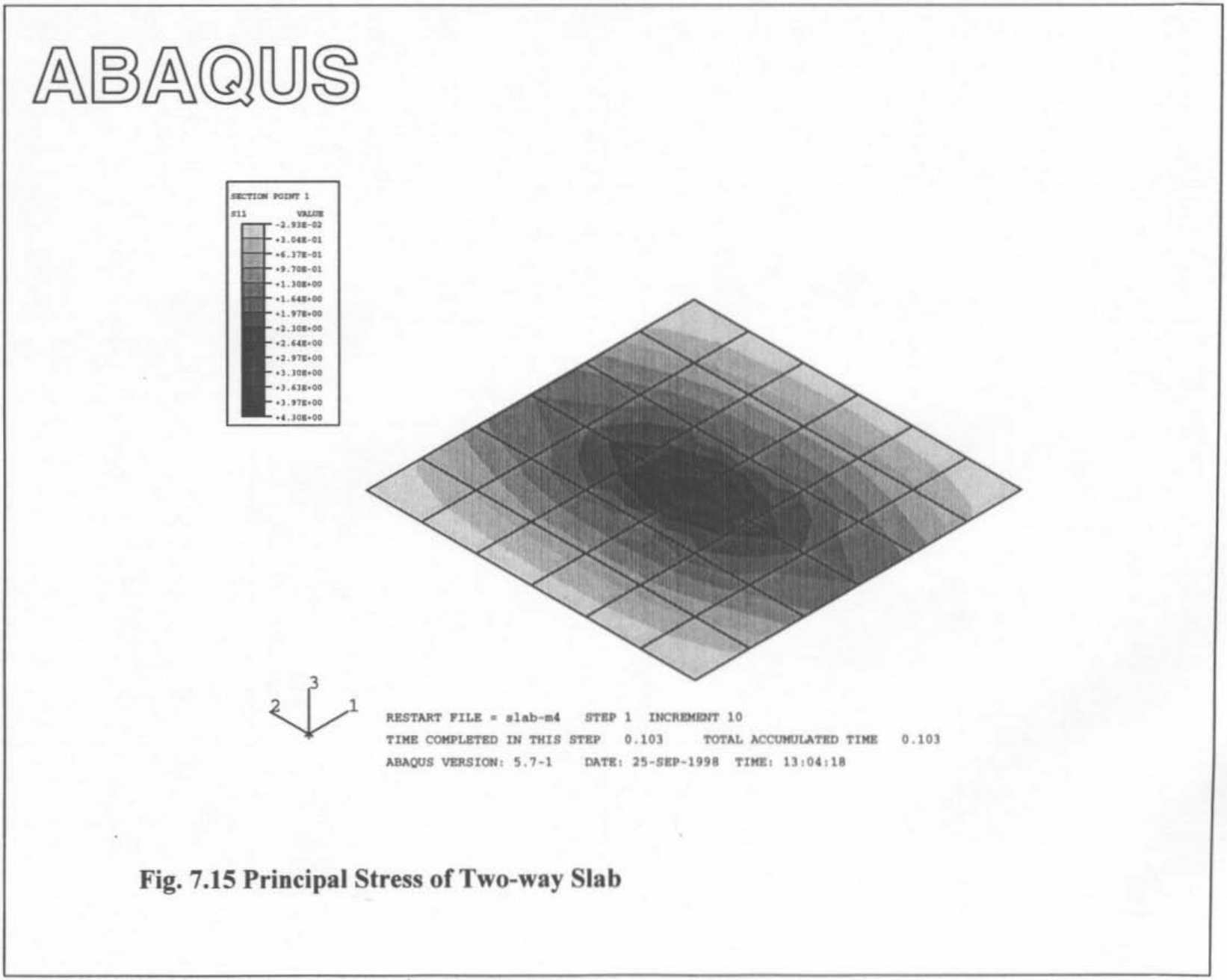

Fig. 7.15 Principal Stress of Two-way Slab

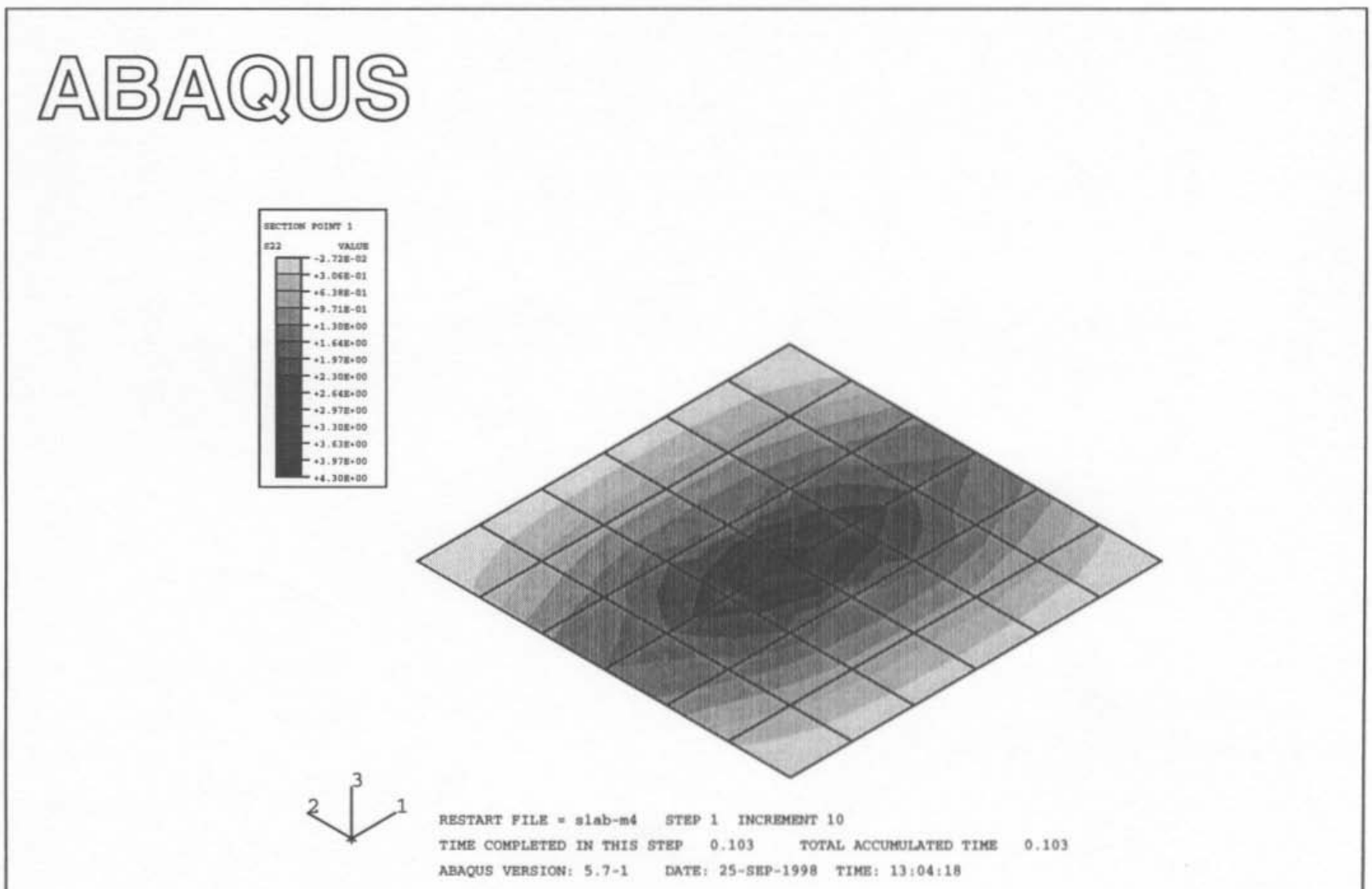

Fig. 7.16 Principal Stress of Two-way Slab

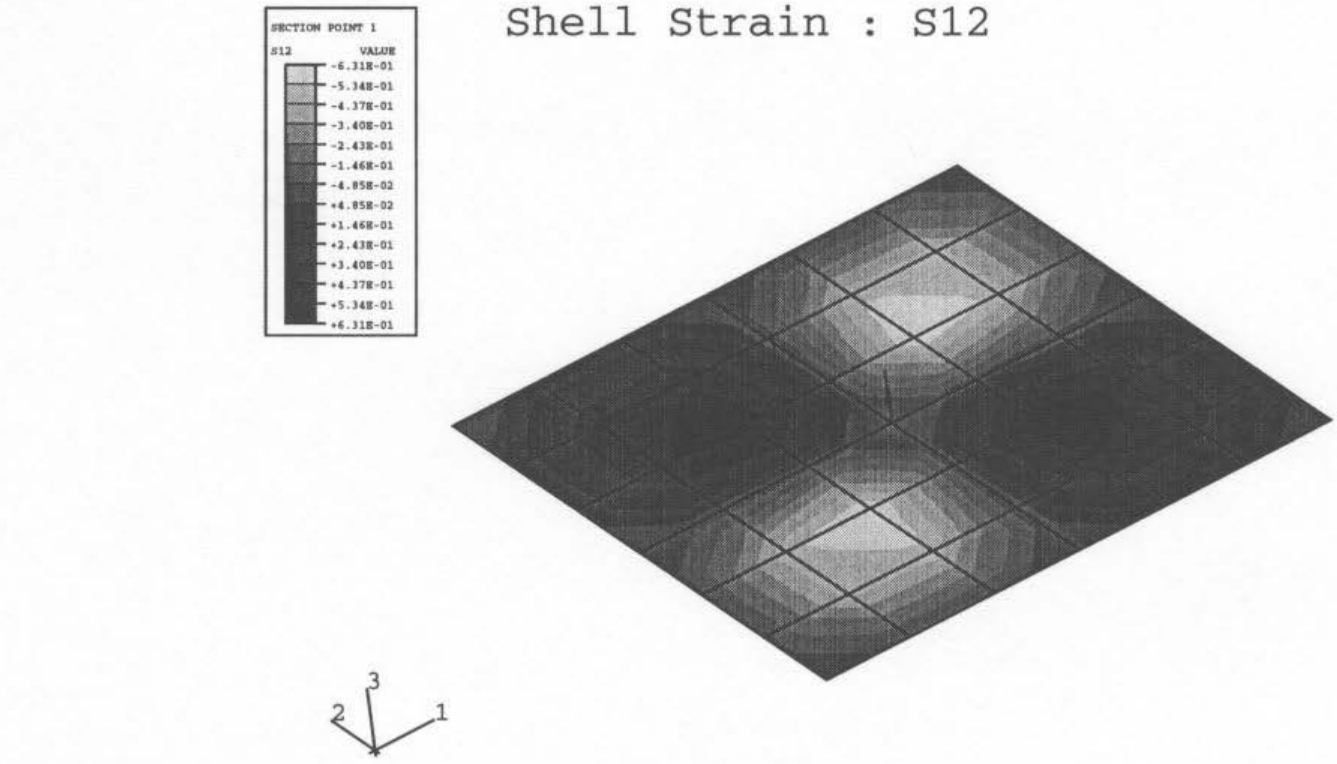

Fig. 7.17 Principal Stress of Two-way Slab

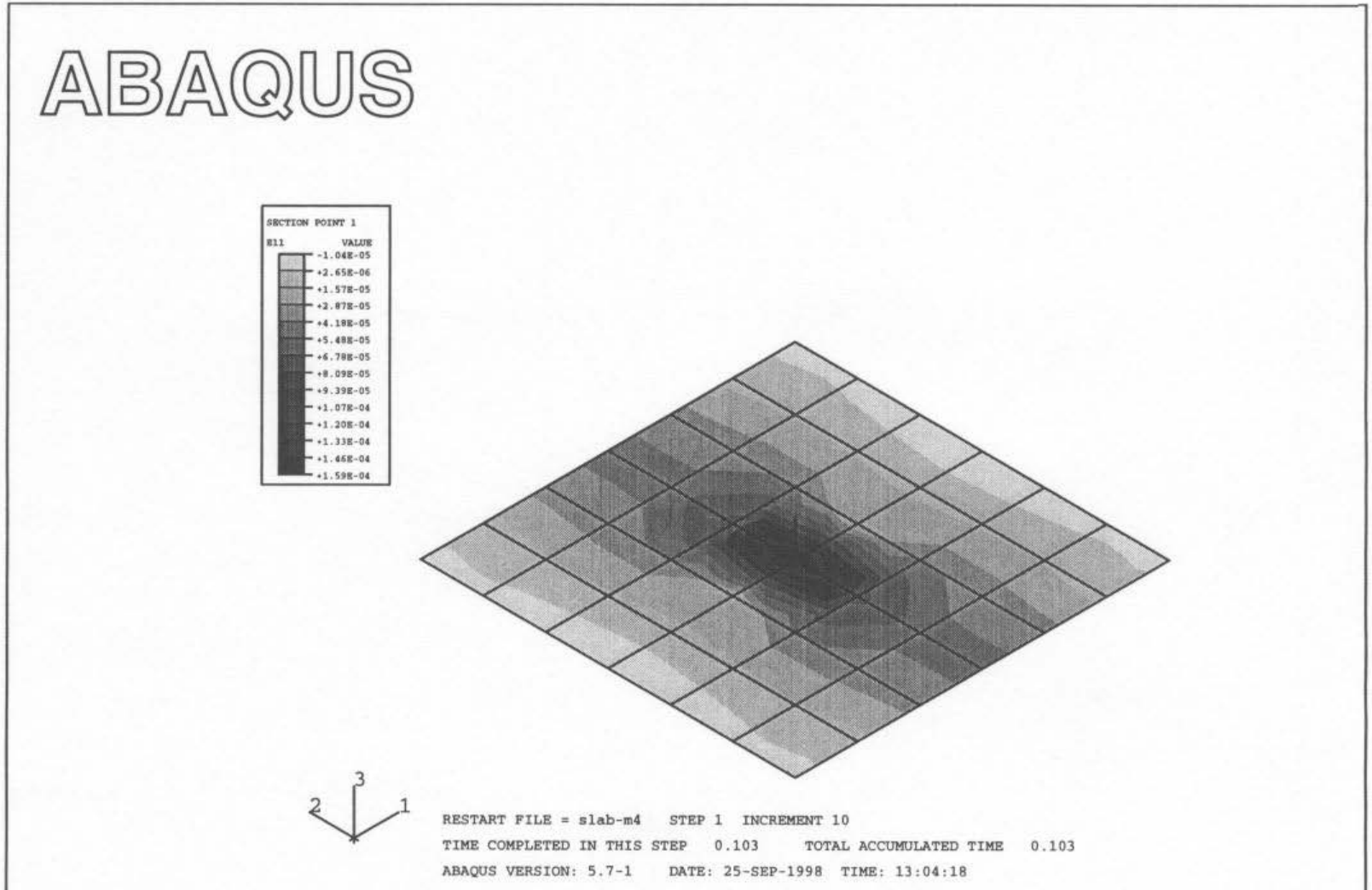

Fig. 7.18 Strain Contour of Two-way Slab

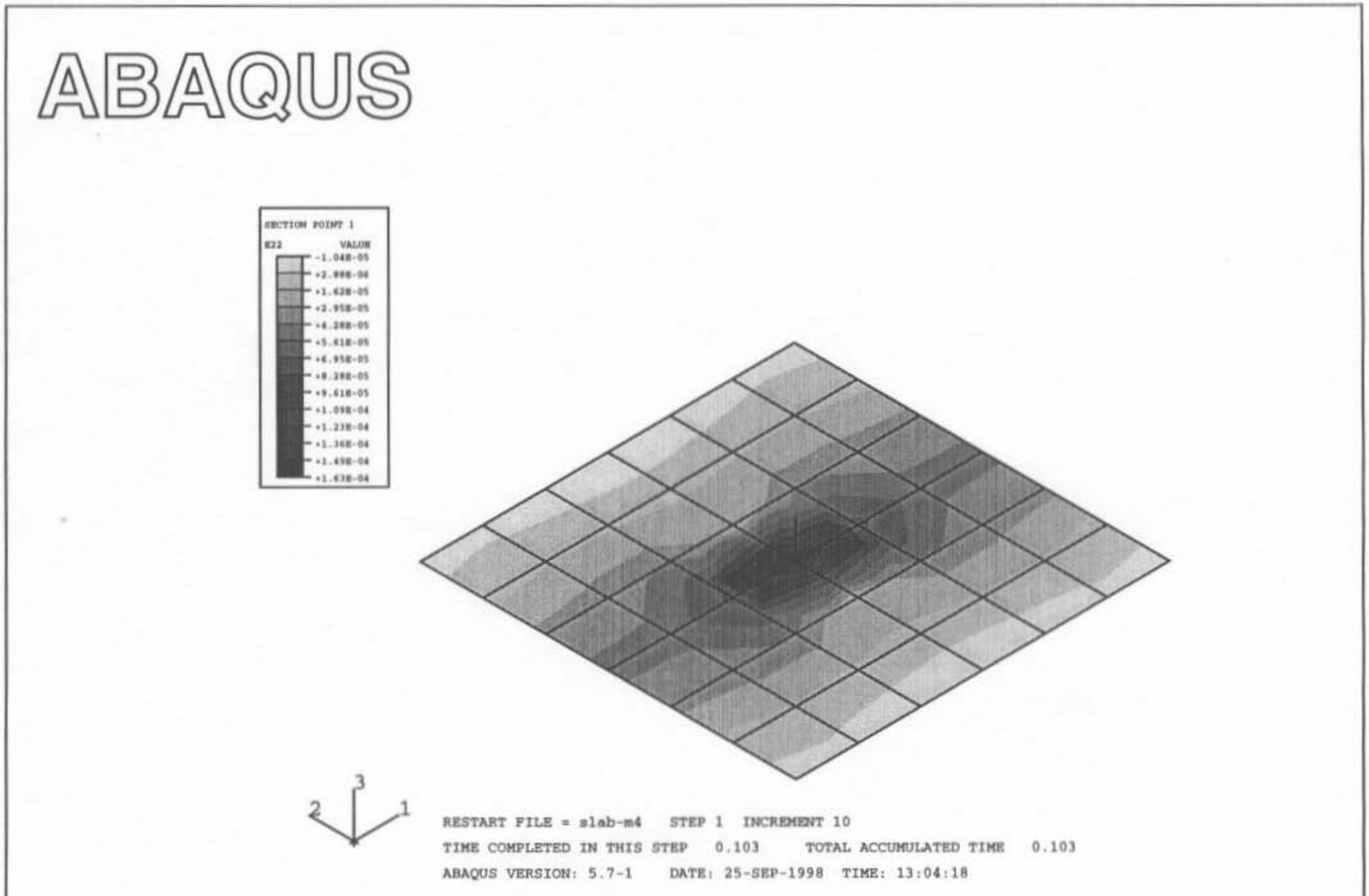

Fig. 7.19 Strain Contour of Two-way Slab

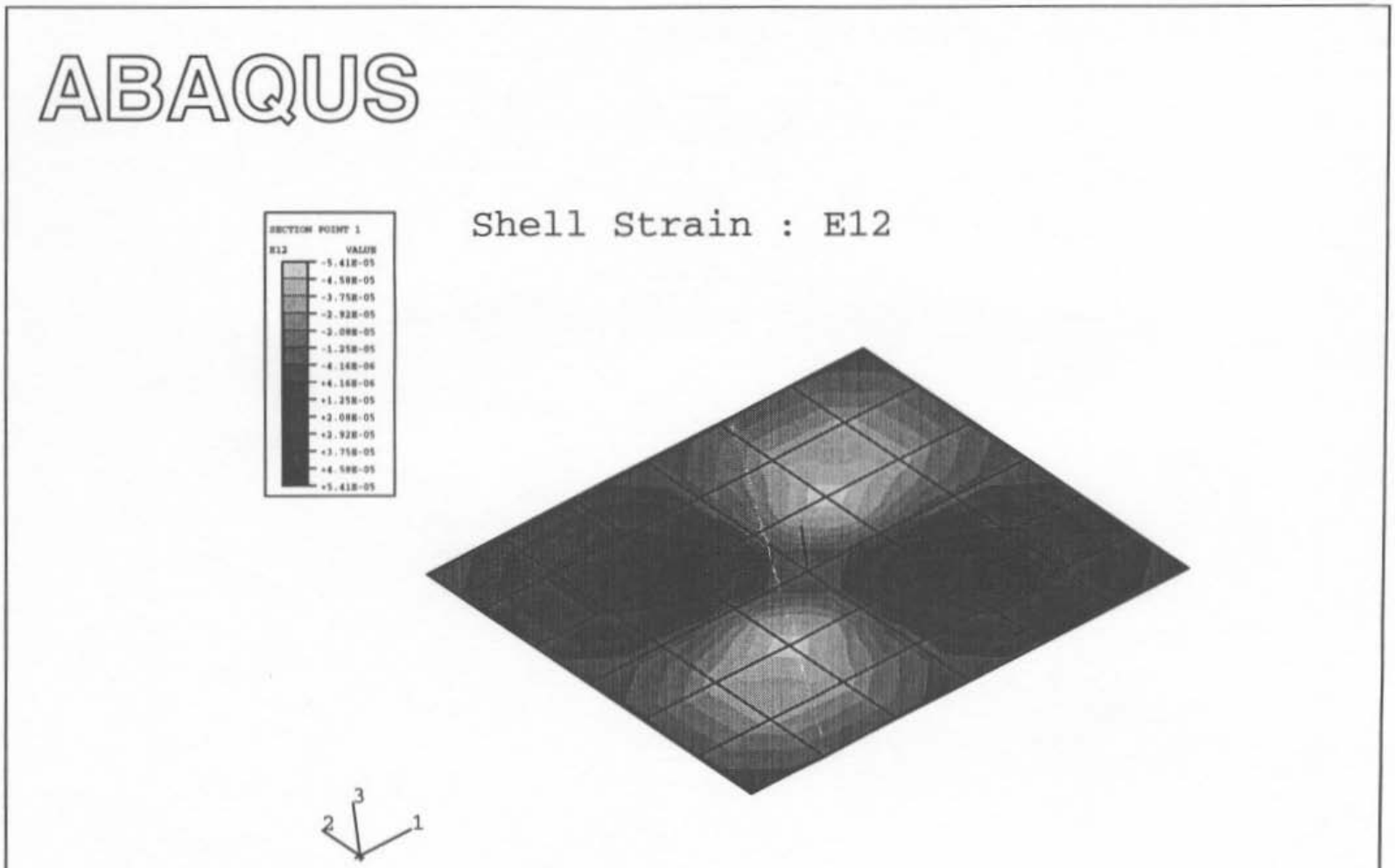

Fig. 7.20 Strain Contour of Two-way Slab

Chapter 8

Conclusions and Recommendations

8.1 Summary

The main objective of investigation is to provide more information regarding the bond performance between reinforcement bar and high strength concrete. An additional objective is to determine the internal distribution of stress and strain along the rebar and the influence of high strength concrete on such strain distribution. The characteristics of the bond under seven selected parameters were studied experimentally and numerically. A total of 150 specimens were tested in the experimental phase of this investigation. The influences of monotonic and cyclic loading conditions on the bond strength were investigated separately for each parameter.

The test results revealed that the maximum bond stress for high strength concrete is higher than the corresponding one for normal strength concrete. However, the behavior of high strength concrete is more nonlinear and brittle and it must be considered in

modeling bond behavior. The measured value for the maximum slip at complete failure of the bond resistance would indicate that the value is estimated by five times the value of the slip corresponding to the maximum bond stress.

The development of a new technique of strain measurement around the steel rebar is unique and it is concluded that by modifying this method it is possible to identify the internal crack pattern and to predict possible failure modes. The internal concrete strain with some degree of accuracy has been measured. The surface crack patterns have been plotted and the mode of failures has been identified.

Furthermore, the effect of the rebar diameter and rib deformation patterns was examined on the bond resistance of high strength concrete. Several specimens with different rebar diameters and rib geometeries were tested. The test concrete compressive strengths for the specimen ranged between 75 MPa and 95 MPa. The deformation patterns were examined for rebar with nominal diameter of 25 mm and 35 mm. All the deformation patterns on the tested rebars were machined.

An equation for calculating average bond stress for high strength concrete is recommended. The result is compared with different Codes and other expressions from the literature. It is suggested that, in the case of high strength concrete, bond stress has direct relation with the cubic root of compressive strength of concrete. In addition, the effect of dynamic loading was modeled by cyclic loading. The influence of several parameters on bond strength between high strength concrete and rebar was investigated under this condition of loading. The test result indicates that an increase in cyclic displacement will lead to more severe damage in a high strength concrete member as compared with normal strength conrete.

An attempt was made to apply the results of these experiments to improve the material model using the tension stiffening effects on high strength concrete. Therefore, a new material model based on biaxial test results of high strength concrete, bond energy and fracture mechanics was developed to evaluate the tension stiffening effects of high strength concrete. The influence of individual parameters was considered in the theoretical analysis and a new parametric evaluation to the tension stiffening effects was recommended.

8.2 Experimental Investigation

A summary of the test results of the experimental investigation can be given as follows:

1. The bond stress-slip curve of high strength concrete is characterized by a sharp drop of the level of stress at the beginning of the descending portion of the bond stress-slip curve.
2. The area under the curve of the bond stress-slip curve can define the bond energy. The bond energy should be used to evaluate the bond behavior rather than the maximum bond stress.
3. The influence of confinement on bond is significant, especially after reaching the ultimate bond strength. The mode of failure has been explained for each tested specimen. A method for selecting a suitable size of rebar confinement is recommended.
4. The result of tests examining the effect of varying rebar diameter embedded in high strength concrete indicates that the bond is higher for the smaller rebar diameter than for the bigger one. The ultimate bond strength for 25 mm rebar diameter is

approximately 15 percent higher than 35 mm rebar diameter. A sharp drop of bond stress at the beginning of the descending portion of the bond stress-slip curve for high strength concrete is confirmed for all rebar diameters. The level of bond stress decreases by about 30 percent of total bond stress-slip at the beginning of the descending branch of the bond stress-slip curve.

5. Results of the investigation regarding the influence of rebar spacing revealed that the bond strength could be improved by selecting proper rebar spacing.
6. An investigation into the bond resistance subjected to the effect of the concrete strength concluded that the ultimate bond stress for high strength concrete is higher than the corresponding one for normal strength concrete. However, the behavior of high strength concrete is more nonlinear-brittle and it must be reflected in the bond model.
7. The relative rib area approach concept can only reflect the effect of rib in the ascending portion of the bond stress-slip curve and more attention should be given to the descending portion. The rib face angle, rib height and rib spacing combined with the area under the curve approach are more suitable to express the effect of rib on the bond behavior.
8. It is recommended to consider the total behavior of the bond stress-slip curve for evaluating the bond resistance of the high strength concrete with respect to deformation pattern. In this case, the effect of concrete strength will be considered automatically.
9. The most effective deformation pattern for 25 mm rebar diameter is the standard deformation pattern adopted by the Canadian code. For rebar with diameter of 35

mm a new deformation pattern is recommended for high strength concrete.

10. The bond resistance increased approximately proportional to $\sqrt[3]{f_c'}$.

11. A new expression for calculating bond stress based on the cubic root of concrete strength is suggested and the results are compared with similar equations from different codes.

12. The proposed bond stress expression can be used to improve the development length in reinforced high strength concrete.

13. The influences of several parameters such as the load history, confining reinforcement, rebar space, concrete strength, rebar size and rate of loading were investigated under cyclic loading.

14. It is concluded that strength and deformation characteristics of high strength concrete structures are highly dependent on bond slip behavior between rebar and concrete under cyclic load.

15. The results of cyclic tests indicate that an increase in cyclic displacement will lead to more severe damage compare to normal strength concrete.

16. The influence of bond strength in a cyclic test could be described by the slope of the cyclic bond stress-displacement curve.

17. It is also revealed that the maximum bond strength increases with the increase of the concrete strength.

18. Cyclic loading does not affect the bond strength of high strength concrete as long as the cyclic slip is less than the maximum slip for monotonic loading.

19. The behavior of high strength concrete under cyclic load is slightly different from that of normal strength concrete.

20. It has been concluded that strength of concrete, rib area and bond length have notable effect on the crack growth.

21. It is concluded that these parameters have a significant role in the bond strength. Also, in a majority of specimens tested, the development of cracking was found to follow a similar pattern.

8.3 Application of the Bond Model to Tension Stiffening

The new high strength concrete plasticity model of the UMAT subroutine developed at Memorial University of Newfoundland previously was studied and applied. The material model can analyze plain high strength concrete members only, without any steel reinforcement. Complete fracture behavior of high strength concrete was theoretically analyzed by means of a model, where the softening of the material due to the damage within the fracture zone was taken into account. The softening is described as a relation between the additional deformation within the fracture zone, and the stress, which can still be transferred in spite of the damage. In the present investigation the material model of the UMAT subroutine was modified for taking into consideration the tension stiffening effect of high strength concrete. In this model the bond strength is treated by considering tension softening of Marzouk and Chen (1995), biaxial tensile strength of Hussein (1998), concept of fracture energy and bond energy for high strength concrete. In addition, a three-dimensional rebar element is added to the program in order that the new model will be able to analyze reinforced high strength concrete structures rather than plain high strength concrete elements.

A new parametric study based on the effect of fracture and bond energies was conducted. The most characteristic parameter and the share of each study parameter on the bond energy through sensitivity analysis was evaluated. Furthermore, the result of a sensitivity analysis was applied to analyze some slabs with low, moderate and high steel ratio. The results of the analyses are compared with the experimental results. It is found that there is good agreement between them.

8.4 Contribution of Present Thesis

The contribution of present investigation can be summarized as below:

- It is the first time that the complete bond stress-slip curve for high strength concrete has been studied. It is also the first time that the concept of bond energy has been introduced and it is recommended that this concept be used to evaluate the bond behavior. Also, the bond stress-slip curve is characterized by a sharp drop of the level of stress at the beginning of the descending portion of the curve.
- A new design formula for calculation of bond strength for high strength concrete based on the cubic root of the concrete compressive strength is developed.
- The possibility of measuring internal bond strain in the surrounding high strength concrete has been shown.
- A design formula for selecting the rebar size as confinement for high strength concrete is recommended.
- The investigation on deformation pattern of rebar indicates that the evaluation of rib geometries by rib face angle, rib height and rib spacing approach are more suitable

than the relative rib area approach that is used by the German Specification Din 488 and some other researchers.

- It is suggested to develop a formula for evaluation of deformation pattern by taking into consideration the effect of the rib on both the ascending and descending portion of the curve using the concept of bond and fracture energies.
- It is found that for rebar with diameter of more than 25 mm a new deformation pattern is recommended.
- It is concluded that significant deterioration in the bond capacity takes place during the cyclic loading and the influence of bond strength could be described by the slope of the cyclic bond stress-displacement curve for high strength concrete.
- Failure mechanisms for both monotonic and cyclic test specimens have been investigated.
- A three dimensional rebar element was added to the program.
- The share of each study parameter in the bond energy of high strength reinforced concrete with use of a new parametric study has been evaluated.
- Further attention to use of the concept of bond energy and determination of the share of each study parameter is highly recommended.
- The high strength material model of the UMAT subroutine developed at Memorial University of Newfoundland previously was studied in detail and improved to include the high strength reinforced concrete with special consideration to the tension stiffening effect.

8.5 Recommendations for Future Study

The author would recommend studying the influence of other parameters such as casting position, size of cover, specimen dimension, transverse pressure, aggregate size, reinforcement coating and creeping of bond stress for high strength concrete. It is interesting to change the type of specimen and consider the double-ended pullout testing, beam testing and different full-scale structural members testing on the bond stress.

It is valuable to investigate crack width opening with time and creep deflection of highly cracked elements in conjunction with bond. It is suggested that the effect of bond relaxation under imposed constant slip, as well as the increase of slip under constant bond stress be investigated. This information would lead to better understanding of the long term deformation bond behavior of high strength concrete, especially in the case of prestress/precast members.

Finally, it is suggested that another experimental program should be conducted to investigate the effect of bond characteristic's parameters for lightweight high strength concrete.

REFERENCES

ABAQUS. (1997). "Users Manual." Hibbitt. Karlsson and Sorensen Inc., Providence. R.I., Version 5.7.

Abrams. D.A. (1913). "Test of Bond Between Concrete and Steel." *University of Illinois bulletin*. Vol. 11. no. 15. pp.238.

Abrishami H.H., and Mitchell D. (1992). "Simulation of Uniform Bond Stress." *ACI Materials Journal*. Vol. 89. no. 2. pp. 161-168.

Abrishami H.H., and Mitchell D. (1993). "Bond Characteristics of Pretensioned Strand." *ACI Materials Journal*. Vol. 90. no. 3. pp. 228-235.

ACI Committee 318-(1981). "Development and Splices of Reinforcement." *Chapter 12 of ACI Building Code. Commentary*. American Concrete Institute. Detroit. MI. USA.

ACI Committee 363-(1984). "State of the Art Report on High Strength Concrete." American Concrete Institute. Detroit. MI. USA. 48 p.

ACI Committee 363-(1992). "State of the Art Report on High Strength Concrete." American Concrete Institute. Detroit. MI. USA. 55 p.

ACI (1993). "Guide for Selecting Proportions for High Strength Concrete with Portland Cement and Fly Ash." *ACI Material journals*. Vol. 90. no. 3. pp. 272-283.

ACI Committee 318-(1995). "Building Code Requirements for Reinforced." American Concrete Institute. Detroit. MI. USA. 55 p.

ACI Committee 408-(1996). "State of the Art Report." American Concrete Institute. Detroit. MI. USA. 55 p.

Aitcin P.C., Mioo B., Cook W.D., and Mitchell D. (1994). "Effects of Size and Curing on Cylinder Compressive Strength of Normal and High Strength Concrete." *ACI Materials Journal*. Vol. 91. no. 4. pp. 349-305.

Aitcn P.C., Jolicoeur C., and MacGregor J.G. (1994). "Superplasticizers: How They Work and Why They Occasionally Don't." *Concrete International*, pp. 45-52.

Aitcin P.C., and Lessard M. (1994). "Canadian Experience with Air-Entrained High Performance Concrete." *Concrete International*, pp. 35-38.

Allwood R.J., and Bajarwan A.A. (1989). "A New Method for Modeling Reinforcement and Bond in Finite Element Analysis of Reinforced Concrete." *International Journal for Numerical Method in Engineering*, Vol. 28, pp. 883-844.

ASTM C127-88 (1993). "Test Method for Specific Gravity and Absorption of Coarse Aggregate." *Annual Book of ASTM Standard*, Vol. 04.02, 04.03, pp. 97-104.

ASTM C128-88 (1993). "Test Method for Specific Gravity and Absorption of Fine Aggregate." *Annual Book of ASTM Standard*, Vol. 04.02, 04-03, pp. 36-38.

ASTM C135-86 (1993). "Standard Test Method for True Specific Gravity of Refractory Materials by Water Immersion." *Annual Book of ASTM Standard*, Vol. 15.01, pp. 58-59.

ASTM C192-88 (1993). "Test Method of Making and Curing Concrete Test Specimens in the Laboratory." *Annual Book of ASTM Standard*, Vol. 04.02, pp. 188-189.

ASTM C494-86 (1993). "Specification for Chemical Admixtures for Concrete." *Annual Book of ASTM Standard*, Vol. 04.02, pp. 297-304.

Austin S., Robins P., and Pan Y. (1995). "Tensile Bond Testing of Concrete Repairs." *Materials and Structures*, Vol. 28, no. 1, pp. 249-259.

AS 3600-(1994). "Australian Standard for Concrete Structures." North Sydney, 255 pp.

Avi Mor. (1992). "Steel-Concrete Bond in High Strength Lightweight Concrete." *ACI Materials Journal*, Vol. 89, no. 1, pp. 76-82.

Azizinamini A., Stark M., Roller J.J., and Ghosh S.K. (1993). "Bond Performance of Reinforcing Bars Embedded in High Strength concrete." *ACI Structural Journal*, Vol. 90, no. 5, pp. 554-561.

Azizinamini A., Chisala M., and Ghosh S.K. (1995). "Tension Development Length of Reinforcing Bars Embedded in High Strength Concrete." *Steel Structure journal*, Vol. 1, no. 8, pp. 512-522.

Baalbaki W., Aitcin P., and Ballivy G. (1992). "On Predicting Modulus of Elasticity in High Strength Concrete." *ACI Materials Journal*, Vol. 89, no. 5, pp. 517-520.

Barenblatt G.I. (1962). "The Mathematical Theory of Equilibrium Cracks in Brittle Fracture." *Advances in Applied Mechanics*, Academic Press, Vol. 7, pp. 55-129.

Bazant Z.P., and Kim S. (1979). "Plastic-Fracturing Theory for Concrete." *ASCE, The Journal of Engineering Mechanics Division*, Vol. 105, no. 3, pp. 407-426.

Bazant Z.P., and Kim S. (1979). "Nonlinear Creep of Concrete, Adoption and Flow." *ASCE, The Journal of Engineering Mechanics Division*, Vol. 105, no. 3, pp. 429-446.

Bazant Z.P., Oh, B.H., and Byung H. (1983). "Crack Band Theory for Fracture of Concrete." *Materials and Structures*, Vol. 16, no. 93, pp. 155-177.

Bazant Z.P., and Kazemi, M.T. (1989). "Size Effect on Diagonal Shear Failure of Beams without Stirrups." *Report no. 89-8/498S*, Center of Advanced Cement-Based Materials, Northwestern University, Evanston, USA, 365 p.

Bazant P.Z., and Schell W.F. (1993). "Fatigue Fracture of High Strength Concrete and Size Effect." *ACI Materials Journal*, Vol. 90, no. 5, pp. 472-478.

Bilodeau A., Malhotra V.M., and Hoff G.C. (1998). "Hydrocarbon Fire Resistance of High Strength Normal and Lightweight Concrete Incorporating Polypropylene Fires." *International Symposium on High-Performance and Reactive Powder Concrete*, Sherbrooke, Quebec, Canada, Vol. 4, pp. 271-296.

Bolander Jr. J., Satake M., and Hikosaka H. (1992). "Bond Degradation Near Developing Cracks in Reinforced Concrete Structures." Faculty of Engineering, Kyushu University, Vol. 52, no. 4, pp. 379-395.

Bouzoubaa N., M.H. Zhang, and Malhotra V.M (1998). "Superplasticized and Portland Cement: Production and Compressive Strength of Mortars and Concrete." *International Symposium on High-Performance and Reactive Powder Concrete*, Sherbrooke, Quebec, Canada, Vol. 4, pp. 435-444.

Broms B.B. (1965). "Stress Distribution in Reinforced Concrete Members with Tension Cracks." *Proceedings, Journal of the ACI*, Vol. 62, no. 9, pp. 1095-1108.

Buyukozturk O., and Shareff S. (1985). "Constitutive Modeling of Concrete in Finite Element Analysis." *Computers and Structures*, Vol. 21, no. 3, pp. 581-610.

Budan Y., and Murray W. (1994). "Study of Concrete Cracking and Bond Using a Distributed Discrete Crack Finite Element Model." *ACI Materials Journal*, Vol. 92, no. 1, pp. 93-104.

Cairns J., and Jones K. (1996). "An Evaluation of the Bond-Splitting Action of Ribbed Bars." *ACI Materials Journal*, Vol. 93, no. 1, pp. 10-19.

Cairns J., and Abdulah R. (1994). "Fundamental Tests on the Effect of an Epoxy Coating on Bond Strength." *ACI Materials Journal*, Vol. 91, no. 4, pp. 331-338.

Cao H.C. and Evans A.G. (1989). "An Experimental Study of the Fracture Resistance of Bimaterial Interface." *Mechanics of Materials*, Vol. 12, no. 1, pp. 24-36.

Cervenka V. (1985). "Constitutive Model for Cracked Reinforced Concrete." *ACI Journal*, Vol. 82, no. 6, pp. 877-882.

Chan H.C., Cheung Y.K., and Huang Y.P. (1994). "Nonlinear Modeling of Reinforced Concrete Structures." *Computer and Structures Journal*, Vol. 53, no. 5, pp. 1099-1107.

Chen E.S., and Buyukozturk O. (1985). "Constitutive Model for Concrete in Cyclic Compression." *ASCE. Engineering Mechanics*, Vol. 111, no. 6, pp. 797-814.

Chen W.F. (1982). "Plasticity in reinforced concrete". McGraw-Hill Book Co. Inc., New-York, USA, 476 p.

Chen Z. (1993). "Nonlinear Analysis of High Strength Concrete Slabs." *M.Eng. thesis*, Memorial University of Newfoundland, St. John's, Newfoundland, Canada, 185 p.

Choi O. C., Hadje-Ghaffari H., Darwin D., and McCabe S.L. (1990). "Bond of Epoxy-Coated Reinforcement: Bar Parameters." *ACI Materials Journal*, Vol. 88, no. 2, pp. 207-217.

Clark, A.P. (1946). "Comparative Bond Efficiency of Deformed Concrete Reinforcing Bars." *Proceedings, ACI Journal*, Vol. 43, no. 4, pp. 381-400.

Cohen M.D., Zhou Y., and Dolch W.L. (1992). "Non-Air Entrained High Strength Concrete- Is It Frost Resistant?" *ACI Structural Journal*, Vol. 89, no. 2, pp. 406-415.

Cope, R.J. (1984). "Material Analysis of Reinforced Concrete Slab." *Computational Modeling of Reinforced Concrete Structures*, ed. E. Hinton, and R. Owen, Pineridge Press, Swansea, U.K., pp. 3-43.

Cox J.V., and Hermann L.R. (1992). "Confinement Stress Dependent Bond Behavior. Part II: A Two Degree of Freedom Plasticity Model." *International Conference on bond in Concrete*, Rigina, Canada, pp. 11-11,11-20.

CSA A23.3-1994. "Design of Concrete Structures." *Standard*, Canadian Portland Cement Association, Rexdale (Toronto), Ontario, Canada.

Darwin D. (1977). "Analysis of Cyclic Loading Plane R/C Structures." *Computers and Structures*, Vol. 7, pp. 137-147.

Darwin D., J. Zuo, M.L.Tholen, and E.K. Idun (1996). "Splice Strength of High Relative Rib Area Reinforcing Bars." *ACI Structural Journal*, Vol. 93, no. 1, pp. 95-107.

Darwin D. and Graham E.K. (1993) "Effect of Deformation Height and Spacing on Bond Strength of Reinforcing Bars." *ACI Structural Journal*, Vol. 90, no. 6, pp. 646-657.

Darwin D., Zuo J., Tholen M., and Idun E.K. (1995). "Development Length Criteria for Conventional and High Relative Rib Area Reinforcing Bars." *Structural Engineering and Engineering Materials, SL Report*, University of Kansas Center for Research, Inc. Lawrence, Kansas, USA, no. 95-4, 69 p.

Darwin D., Zuo J., Tholen M., and Idun E.K. (1995). "Splice Strength of High Relative Rib Area Reinforcing Bars." *Structural Engineering and Engineering Materials, SL Report*, University of Kansas Center for Research, Inc. Lawrence, Kansas, USA, no. 95-3.

Darwin D., Zuo J., Tholen M., and Idun E. (1995). "Reliability-Based Strength Reduction Factor for Bond." *Structural Engineering and Engineering Materials, SL Report*, University of Kansas Center for Research, Inc. Lawrence, Kansas, USA, no. 95-5.

Darwin D., Brown C.J., and McCabe S.L. (1993). "Finite Element Fracture Analysis of Steel-Concrete Bond." *Structural Engineering and Engineering Materials, Report no. 36*, University of Kansas Center for Reset, Lawrence Inc., Kansas, USA, 99 p.

De Larrard F., D. Schaller, and J. Fuchs (1993). "Effect of Bar Diameter on the Bond Strength of Passive Reinforcement in High-Performance Concrete." *ACI Materials Journal*, Vol. 90, no. 4, pp. 333-339.

DIN 488-(1986). "Reinforcing Steel." (DIN 488), (English Translation), 29 pp.

Doerr K. (1981). "Ein Beitrag Zur Berechnung von Stahlbetonscheiben unter besonderer Berucksichtigung des Verbundverhaltens." *Ph.D. thesis*, Darmstadt, Germany, 145 p.

Drucker, D.C. (1959). "A Definition of Stable Inelastic Material." *Journal of the Applied Mechanics*, Vol. 26, no. 1, pp. 101-106.

Dugdale D.S. (1960). "Yield of Steel Sheets Containing Slits." *Journal of the Mechanics and Physics of Solids*, no. 8, pp. 100-104.

Eligehausen R., Popov E.P., and Betero V. (1983). "Local Bond Stress-Slip Relationships of Deformed Bar Under Generalized Excitations." *Report no. UCB/EERC-83/23, Earthquake Engineering*, Research Center, Berkeley, California, USA, 185 p.

Eligehausen R., "Anchorage to Concrete (1989)." RILEM, *Chapter 13 of Fracture Mechanics of Concrete from Theory to Application*, Report to the Technical Committee 90 FMA, Fracture Mechanics to Concrete/Applications, Chapman and Hall, pp. 263-311.

Elwi A.A., and Murray W. (1979). "A 3D Hypoelastic Concrete Constitutive Relationship." *Proceedings of ASCE, The Journal of Engineering Mechanics division*, Vol. 105, no. EM4, pp. 623-641.

Emam M. (1995). "Effect of Concrete Strength on the Behavior of Flat Plate-Column Connections Under Static and Cyclic Loads." *Ph.D. thesis*, Civil Engineering Department, Cairo University, Egypt, 267 p.

Esfahani M.R., and Rangan B.V. (1998). "Local Bond Strength of Reinforcing Bars in Normal Strength and High-Strength Concrete (HSC)." *ACI Structural Journal*, Vol. 95, no. 2, pp. 96-106.

Esfahani M.R., and Rangan B.V. (1998). "Local Bond Strength of Reinforcing Bars in Normal Strength and High Strength Concrete (HSC)." *ACI Structural Journal*, Vol. 95, no. 3, pp. 272-280.

Esfahani M.R., and Rangan B.V. (1998). "Reinforcing Steel-Concrete Bond in Normal and High Strength Concrete." *International Conference on HPHSC, Perth, Australia*, pp. 367-378.

Etse G., and Willam K. (1994). "Fracture Energy Formulation for Inelastic Behavior of Plain Concrete." *ASCE, Journal of Engineering Mechanics*, Vol. 120, no. 9, pp. 1983-2011.

Ezeldin A.S., and Balaguru P.N. (1989). "Bond Behavior of Normal and High Strength Fiber Reinforced Concrete." *ACI Materials Journal*, Vol. 86, no. 5, pp. 515-524.

Farny J.A. and Panarese W.C. (1994). "High Strength Concrete." *PCA. Portland Cement Association*. Engineering Bultin. USA. 48 p.

Farrow C.B., Frigui I., and Klingner E. R. (1995). "Tensile Capacity of Single Anchors in Concrete: Evaluation of Existing Formulas on an LRFD Basis." *ACI Material Journal*. Vol. 91. no. 2. pp. 128-137.

Floegl H., and Mang H.A. (1982). "Tension Stiffening Concrete Based on Bond Slip." *ASCE. Journal of Structural Engineering*. Vol. 108. no. ST12. pp. 2681-2701.

Gambarova P.G., Paolorosati G., and Zasso B. (1989). "Steel to Concrete Bond After Concrete Splitting: Test Result." *Materials and Structures*. Vol. 22. pp. 35-47.

Gambarova P.G., Paolorosati G., and Zasso B. (1989). "Steel to Concrete Bond After Concrete Splitting: Constitutive Laws and Interface Deterioration." *Materials and Structures*. Vol. 22. pp. 347-356.

Giaccio G., Rocco C., Violini D., Zappitelli Z., and Zerbino R. (1992). "High Strength Concrete Incorporating Different Coarse Aggregates." *ACI Materials Journal*. Vol. 89. no. 3. pp. 242-246

Giaccio G., Rocco C., and Zerbino R. (1993). "The Fracture Energy (G_f) of High Strength Concrete." *RILEM. Materials and Structures. Research and Testing*. Vol. 26. pp. 381-386.

Gilbert R.I., and Warner. R.F. (1978). "Tension Stiffening in Reinforced Concrete Slabs." *ASCE. Journal of the Structural Division*. Vol. 104. no. ST12. pp. 1885-1900.

Gilkey H.J., Chamberlain S.J., and Beal R.W. (1940). "Bond Between Concrete and Steel." *Iowa Engineering Experimental Station*. Vol. 39. no. 29. Bulletin no. 147. 120 pp.

Giuriani E., Plizzari G., and Schumm C. (1991). "Role of Stirrups and Residual Tensile Strength of Craked Concete on Bond." *ASCE. Journal of Structural Engineering*. Vol. 117. no. 1. pp. 1-19.

Glanville W.H. (1930). "Studies in Reinforced Concrete Bond Resistance." *Building Research Technical paper 10*. USA. 87 p.

Goldman A., and Bentur A. (1989). "Bond Effects in High Strength Silica-Fume Concrete." *ACI Materials Journal*. Vol. 86. no. 5. pp. 440-447.

Goto Y. (1971). "Cracks Formed in Concrete Around Deformed Tension Bars." *ACI-Journal*, Detroit. MI. USA. pp. 244-251.

Hadje-Ghaffari H., Darwin D., Choi O.C., and McCabe S.L. (1994). "Bond of Epoxy-Coated Reinforcement: Cover, Casting Position, Slump, and Consolidation." *ACI Structural Journal*, Vol. 91, no. 1, pp. 59-68.

Hamad B.S. (1995). "Bond Strength Improvement of Reinforcing Bars with Specially Designed Rib Geometries." *ACI Structural Journal*, Vol. 92, no. 1, pp. 3-13.

Hamad B.S. (1995). "Comparative Bond Strength of Coated and Uncoated Bars with Different Rib Geometries." *ACI Materials Journal*, Vol. 92, no. 6, pp. 579-590.

Hamoush S.A.and Salami M.R. (1990). "Interfacial Strain Energy Release Rate of Fiber Reinforced Concrete Based on Bond Stress-Slip Relationship." *ACI Structural Journal*, Vol. 87, no. 6, pp. 678-686.

Han D.J., and Chen W.F. (1985). "A Nonuniform Hardening Plasticity Model for Concrete Materials." *Proceedings Inelastic Deformation and Failure Modes*, ed. S. Nemat Nasser, pp. 238-308.

Hawkins N.M., Lin I., and Ueda T. (1987). "Anchorage of Reinforcing Bars for Seismic Forces." *ACI Structural Journal*, Vol. 84, no. 5, pp. 407-418.

Hawkins N.M., Lin I.J., and Jeang F.L. (1982). "Local Bond Strength of Concrete for Cyclic Reversed Loading." *Proceedings of the International Conference on Bond in Concrete*, Scotland, UK, pp. 151-161.

Hill, R. (1950). "The Mathematical Theory of Plasticity." Clarendon press, Oxford.

Hillerborg A, Modeer M., and Petersson P.E. (1976). "Analysis of Crack Formation and Crack Growth in Concrete by Means of Fracture Mechanics and Finite Elements." *Cement and Concrete Research*, Vol. 6, pp. 773-782.

Hillerborg A. (1976). "The theoretical basis of a Method to Determine the Fracture Energy *G* of Concrete." *RELEM Technical Committees*, Materials and structures, Vol. 18, no. 106.

Hillerborg A. (1985). "Numerical Methods to Simulate Softening and Fracture of Concrete." Martinus Nijhoff Publication, Dordrecht, Netherlands, pp. 141-170.

Hoff, G.C. (1988). "Resistance of Concrete to Ice Abrasion-Areview." *Proceedings of Second International Conference on Concrete in a Marine Environment*. St. Andrews by-the-Sea. New Brunswick. Canada. pp. 427-455.

Hoff, G.C. (1991). "Durability of Offshore and Marine Concrete Structures." ACI. SP-126. *Second International Conference*. Montreal. Canada. Vol. 1. pp. 33-64.

Hoff, G.C. (1992). "High Strength Lightweight Aggregate Concrete for Arctic Applications." ACI SP 136 1-3. *Structural Lightweight Aggregate Concrete Performance*. 28 p.

Hota S., and Naaman A.E. (1997). "Bond Stress-Slip Response of Reinforcing Bars Embedded in FRC Matrices under Monotonic and Cyclic Loading." *ACI Structural Journal*. Vol. 94. no. 5. pp. 525-537.

Hurlbut B. (1983). "Experimental and Computation Investigation of Strain-Softening in Concrete." *M.Sc. thesis*. University of Colorado. Boulder. USA. 128 p.

Hussein A.A. (1998). "Behavior of High Strength Concrete Under Biaxial Loading Conditions." *Ph.D. thesis*. Memorial University of Newfoundland. St. John's. Canada. 242 p.

Hwang S.J., Leu Y.R., and Hwang H.L. (1996). "Tensile Bond Strengths of Deformed Bars of High Strength Concrete." *ACI Structural Journal*. Vol. 93. no. 1. pp. 11-20.

Ilyushin. A.A. (1948). "Plasticity." Moscow. Gosstroizdat. Leningrad.

Jenq Y., and Shah S.P. (1985). "Two Parameter Fracture Model." *Journal of Engineering Mechanics*. Vol. 111. no. 10. pp. 1227-1238.

Jiang D.H., Shah S.P., and Andonian A.(1984). "Study of the Transfer of Tensile Forces by Bond." *ACI Journal*. Vol. 81. no. 2. pp. 251-258.

Kashiwazaki T., and Noguchi H. (1994). "Nonlinear Finite Element Analysis on Shear and Bond of RC Interior Beam-Column Joints with Ultra High Strength Materials." *Trans. of The Japan Concrete Institute*. Vol. 16. pp. 509-516.

Kupfer H., and Hilsdorf. H.K. and Rusch. H. (1969). "Behavior of Concrete Under Biaxial Stresses." *ACI Journal*. Vol. 66. pp. 656-666.

Kupfer H., and Gerstle K.H. (1973). "Behavior of Concrete Under Biaxial Stresses." *ASCE. Journal of Engineering Mechanics Division*. Vol. 99. pp. 853-866.

Leon. A. (1935). "Uber die Scherfestigkeitdes Betons." *Beton und Eisen*. Berlin. Germany. Vol. 34. no. 8. pp. 100-104.

Li Z., Kuikarni S. M., and Shah S.P. (1993). "New Test Method for Obtaining Softening Response of Unnotched Concrete Specimen Under Uniaxial Tension." *Experimental Mechanics*. Vol. 33. no. 1. pp. 181-188.

Li Z., and Shah S.P. (1994). "Localization of Microcracking in Concrete Under Uniaxial Tension." *ACI Materials Journal*. Vol. 91. no. 4. pp. 372-381.

Lin. C.S., and Scordelis. A.C. (1975). "Nonlinear Analysis of Reinforced Concrete Slabs by Finite Element Method." *Technology Reports of the Osaka University*. Faculty of Engineering. Osaka University. Vol. 26. no. 1333. pp. 595-604.

Losberg A., and Olsson P.A. (1979). "Bond Failure of Deformed Reinforcing Bars Based on the Longitudinal Splitting Effect of the Bars." *ACI Journal*. Vol. 76. no. 1. pp. 5-19.

Lubliner J. (1990). "Plasticity Theory." Macmillan Publishing Company.

Lutz A.L. (1966). "The Mechanics of Bond and Slip of Deformed Reinforcing Bars in Concrete." *Ph.D. thesis*. Cornell University. 185 p.

Lucie V. (1992). "Theoretical Prediction of the Ultimate Bond Strength Between a Reinforcement Bar and Concrete." *International Conference on Bond in Concrete*. CEB. Riga Technical University. pp. 1-1.1-18.

Mainz J., Stockl S., and Kupfer H. (1992). "FE-Calculations Concerning the Bond Behavior of Deformed Bars in Concrete." *International Conference on Bond in Concrete*. Riga. Layuia. pp. 12-17.12-26.

Malhotra v., Carette G., and Bremner T. (1988). "Current Status of CANMET's Studies on the Durability of Concrete Containing Supplementary Cementing Materials in Marine Environment." ACI SP-109. *Special Publications*. American Concrete Institute. Detroit. MI. USA. pp. 31-72.

Malvar L.J. (1992). "Bond of Reinforcement Under Controlled Confinement." *ACI Materials Journal*. Vol. 89. no. 6. pp. 593-601.

Marzouk. H. and Chen Z.W. (1993). "Finite Element Analysis of High Strength Concrete Slabs." *ACI Structural Journal*. Vol. 90. no. 5. pp. 505-513.

Marzouk, H. and Chen Z.W. (1993). "Nonlinear Analysis of Normal and High Strength Concrete Slabs." *Canadian Journal of Civil Engineering*, no. 20, pp. 697-707.

Marzouk, H. and Chen Z.W. (1995). "Fracture Energy and Tension Properties of High Strength Concrete." *ASCE, Journal of Materials in Civil Engineering*, Vol. 7, no. 2, pp. 108-116.

Marzouk, H. and Dajiu J. (1994). "Effect of Freezing and Thawing on The Tension Properties of High Strength Concrete." *ACI Materials Journal*, Vol. 91, no. 6, pp. 577-585.

Marzouk, H. (1990). "Durability of High Strength Concrete Containing Fly-Ash and Silica Fume." *ASCE, Proceedings of First Material Engineering Congress*, Material Engineering Division, Denver, USA, pp. 1026-1038.

Marzouk, H. (1991). "Creep of High Strength Concrete and Normal Strength Concrete." *Magazine of Concrete Research*, Vol. 43, no.155, pp.121-126.

Marzouk, H. and Hussein A. (1991). "Experimental Investigation on the Behavior of High Strength Concrete Slabs." *ACI Structural Journal*, Vol. 88, no. 6, pp. 701-713.

Marzouk, H. and Hussein A. (1991) "Punching Shear Analysis of Reinforced High Strength Concrete Slabs." *Canadian Journal of Civil Engineering*, no. 18, pp. 954-963.

Marzouk, H. and Hussein A. (1990) "Properties of High Strength Concrete at Low Temperatures." *ACI Materials Journal*, Vol. 87, no. 2, pp. 167-171.

Marzouk, H. and Hussein A. (1989) "Development of 70 MPa Concrete for Nekton Project," Ocean Engineering Research Group, Memorial University of Newfoundland, St. John's, Canada, 120 P.

Marzouk, H. (1987). "Utilization of Fly Ash and Silica Fume to Produce High Strength Concrete," Conference *Proceedings of International Conference on the Quality and Performance of Cement and Concrete*, Baqgdad, Iraq, pp. 237-254.

Masaki M., Otani S., and Aoyama H. (1991). "Bond Splitting Strength in Reinforced Concrete Members." *Transactions of the Japan Concrete Institute*, Vol. 13, pp. 581-588.

Massicotte, B., Elwi, A.E., and MacGregor, J.G. (1990). "Tension Stiffening Model for Planar Reinforced Concrete Members." *ASCE, Journal of Structural Engineering*, Vol. 116, no. 11, pp. 3039-3058.

McCabe S.L., Darwin D., Choi O.C., and Hadje-ghaffari H. (1992). "Application of Fracture Mechanics to Steel-Concrete Bond Analysis." *Concrete Design Based on Fracture Mechanics*, ACI SP-134, American Concrete Institute, Detroit, MI, USA, pp. 101-114.

Mehlhorn G., and Keuser M. (1985). "Isoparametric Contact Elements for Analysis of Reinforced Concrete," *ASCE, U.S. Japan Seminar on Finite Element Analysis of Reinforced Concrete Structures Analysis*, ed. C. Meyer and H. Okamura, N.Y., USA, pp. 329-347.

Mehlhorn G. and Kollegger J. (1985). "Nonlinear Contact Problems-A Finite Element Approach Implemented in ADINA," *Computers & Structures Journal*, Vol. 21, no. 1/2, pp. 69-80.

Mirza S.A. (1987). "Bond Strength Statistics of Flexural Reinforcement in Concrete Beams," *ACI Structural Journal*, Vol. 84, no. 5, pp. 383-391.

Mishima T. (1995). "Nonelastic Behavior of Axial Reinforcement Subjected to Axial and Slip Deformation at the Crack Surface," *ACI Structural Journal*, Vol. 92, no. 3, pp. 380- 385.

Mitchell D., Abrishami H.H., and Mindess S. (1996). "The Effect of Steel Fibers and Epoxy-Coated Reinforcement on Tension Stiffening and Cracking of Reinforced Concrete," *ACI Materials Journal*, Vol. 93, no. 1, pp. 61-68.

Mitsui K., Li Z., Lange D.A., Shah S.P. (1994). "Relationship between Microstructure and Mechanical Properties of the Paste-Aggregate Interface," *ACI Materials Journal*, Vol. 91, no. 1, pp. 30-39.

Mor A., Gerwick B.C., and Hester W.T. (1992). "Fatigue of High Strength Reinforced Concrete," *ACI Materials Journal*, Vol. 89, no. 2, pp. 197-207.

Murata J., and Kikukawa H. (1992). "Viscosity Equation for Fresh Concrete," *ACI Materials journal*, Vol. 89, no. 3, pp. 230-237.

Nasser K.W. and Marzouk H. (1981) "Creep of Concrete at Temperatures from 70 to 450F Under Atmospheric Pressure," *ACI Journal*, Vol. 63, no. 8, pp. 147-150.

Neven K.O., Watson K.A., and Lafave J.M. (1994). "Effect of Increased Tensile Strength and Toughness on Reinforcing Bar Bond Behavior," *Cement and Concrete Composites*, Vol. 16, pp. 129-141.

Nilson A.H. (1972). "Internal Measurement of Bond Slip." *ACI Journal*, Vol. 24, no. 6, pp. 439-441.

Ngo, D. (1975). "A Network-Topological Approach for the Finite Element Analysis of Progressive Crack Growth in Concrete Members." *Ph.D. thesis*, University of California, Berkeley, USA, 253 p.

Ortiz M. and Popov E., (1985). "Accuracy and Stability of Integration Algorithms for Elastoplastic Constitutive Relations." *International Journal for Numerical Methods in Engineering*, Vol. 21, no. 9, pp. 1561-1576.

Ortiz M., and Simo J. (1986). "An Analysis of a New Class of Integration Algorithms for Elastoplastic Constitutive Relations." *International Journal of Numerical Methods in Engineering*, Vol. 23, no. 8, pp. 353-366.

Osman M. (1998). "Behavior of High Strength Lightweight Concrete Interior Flat-Slab Connections Under Static and Cyclic Loading." *Ph.D. thesis*, Civil Engineering Department, Helwan University, Egypt, 279 p.

Ozbolt J., and Eligehausen R. (1992). "Numerical Simulation of Cycling Bond-Slip Behavior." *CEB, Proceedings, International Conference on Bond in Concrete*, Riga, pp. 12-27 - 12-33.

Panahshahi N., White R.N., and Gergely P. (1992). "Reinforced Concrete Compression Lap Splices Under Inelastic Cyclic Loading." *ACI Structural Journal*, Vol. 89, no. 2, pp. 164-175.

Papadopoulos P. ,and Taylor R.L. (1992). "A Mixed Formulation for the Finite Element Solution of Contact Problems". *Comp. Math. in Appl. Mech. And Eng.*, Vol. 94, pp. 373-389.

Papworth F., and Ratcliffe R. (1994). "High-Performance Concrete-the Concrete Future." *Concrete International*, pp. 39-44.

Peattie K.R., and Pope J.A. (1956). "Effect of Age of Concrete on Bond Resistance." *Proceedings, Journal of the ACI*, Vol. 27, no. 27, pp. 661-672.

Pendyala R., Mendis P., and Patnaikuni I. (1996). "Full-Range Behavior of High Strength Concrete Flexural Members: Comparison of Ductility Parameters of High and Normal Strength Concrete Members." *ACI Structural Journal*, Vol. 93, no. 1, pp. 30-45.

Petersson P.E. (1979). "Fracture Energy of Concrete: Method of Determination." *Cement and Concrete Research*, Vol. 10, no. 1, pp. 78-89.

Petersson P.E. (1981). "Crack Growth and Development of Fracture Zones in Plain Concrete and Similar Materials." *Report TVBM-1006*. Division of Building Materials. University of Lund. Sweden. 174 pp.

Phillips D.V., Al-Manaseer A.A. (1984). "Simple Non-linear Analysis of T-Beams Using Plane Stress Element." *Proceedings of the International Conference on Computer Aided Analysis and design of Concrete Structures*. Split. Yugoslavia. Pineridge Press. Part I. pp. 677-691.

Pijaudier-Cabot G., Mazars J., and Pulikowski J. (1991). "Steel-Concrete Bond Analysis with Non-linear Continuous Damage." *Journal of Structural Engineering*. Vol. 117. no. 3. pp. 862-882.

Plaines P., Tassios T., and Vintzeleou E. (1982). "Bond Relaxation and Bond-Slip Creep Under Monotonic and Cyclic Actions." *Proceedings of the International Conference on Bond in Concrete*. Scotland. UK. pp. 193-205.

Plauk G., and Hees G. (1981). "Finite Element Analysis of Reinforced Concrete Beams with Special Regard to Bond Behavior." *Advanced Mechanics of Reinforced Concrete*. Colloquium. Delft. Netherlands. pp. 655-670.

Pochanart S., and Harmon T. (1989). "Bond-Slip Model for Generalized Excitations including Fatigue." *ACI Materials Journal*. Vol. 86. no. 5. pp. 465-474.

Popov E.P. (1984). "Bond and Anchorage of Reinforcing Bars Under Cyclic Loading." *ACI Journal*. pp. 340-349.

Pramono E., and Willam K. (1989). "Fracture Energy-Based Plasticity Formulation of Plain Concrete." *Journal of Engineering Mechanics*. Vol. 115. no. 6. pp. 1183-1204.

Rehm G. (1961). "Uber die Grunlagen des Verbundes Zwischen Stahl und Beton." *Deutscher Ausschuss fur Stahlbeton*. (C&CA Library Translation no. 134. 1968. "Basic Principle of the Bond between Steel and Concrete). no. 1381. 59 p.

Rehm G., and Eligehausen R. (1979). "Bond of Ribbed Bars Under High Cycle Repeated Loads." *ACI Journal*. Symposium Paper. ACI Annual Convention. San Diego. California. USA. pp. 297-309.

Rice J.R. (1989). "Mechanics and Thermodynamics of Brittle Interfacial Failure in Bimaterial System." *Metal-Ceramic Interfaces*. Proceedings of International workshop. Santa Barbara. California. USA. pp. 269.

RILEM (1957). "Bond Crack Form Reinforced Concrete." Symposium. Stockholm.

RILEM (1990). "Analysis of bond-Slip." *Fracture Mechanics of Concrete Structures from theory to applications*. ed. Elfgren L.. Chapman and hall Book Company. pp. 246-262.

Robins P.J.. and Standish I.G. (1982). "The Effect of Lateral Pressure on the Bond of Round Reinforcing Bars in Concrete." *Proceedings of the International Conference on Bond in Concrete*. Paisley. pp. 262-272.

Sankarasubramanian G.. and Rajasekaran S. (1996). "Constitutive Modeling of Concrete Using a New Failure Criterion." *Computers and Structures Journal*. Vol. 58. no. 5. pp 1003 -1014.

Scanlon. A. (1972). "Time Dependent Deflections of Reinforced Concrete Slabs." *Ph.D. thesis*. University of Alberta. Edmonton. Canada. 265 p.

Scanlon. A.. and Murray. D.W. (1974). "Time dependent reinforced Concrete Slab Deflections." *ASCE. Journal of the Structural Division*. Vol. 100. no. ST9. pp.1911-1924.

Shima H.. and Tetsuji S. (1994). "Local Bond Stress-Slip Relationship of Braided Aramid Fiber Bar Obtained from Pretensioned Bond Test." *Translation of The Japan Concrete Institute*. Vol. 16. pp. 191-196.

Sivasundaram V.. Carette G.G.. and Malhotra V.M. (1989). "Properties of Concrete Incorporating Low Quality of Cement and High Volumes of Low Calcium Fly-Ash." ACI SP-114. *Special Publication*. Vol. 1. pp. 45-71.

Somayaji S.. and Shah S.P. (1981). "Bond Stress versus Slip Relationship and Cracking Response of Tension Members." *ACI Journal*. Vol. 78. no. 3. pp. 217-225.

Song H.. Yupu M.. Zhao L.. and Guofan Y. (1994). "Stress Variation Model of Bond Stress-Slip Relationship Between Steel and Concrete." *Journal of Dalian University of Technology*. Vol. 34. no. 1. pp. 59-67.

Soretz S.. and Holtzenbein H. (1979). "Influence of Rib Dimensions of Reinforcing Bars on Bond and Bendability." *Proceedings. ACI Journal*. Vol. 76. no. 1. pp. 111-127.

Soroushian P.. K. Obaseki. M. Nagi. and M.C. Rojas (1988). "Pull Out Behavior of Hooked Bars in Exterior Beam-Column Connections." *ACI Structural Journal*. Vol. 86. no. 2. pp. 269-276.

Soroushian P., Mirza F., and Alhozaimy A. (1994). "Bonding of Confined Steel Fiber Reinforced Concrete to Deformed Bar." *ACI Materials Journal*, Vol. 91, no. 2, pp. 141-149.

Soroushian P., Obasaki K., and Marikunte S. (1991). "Analytical Modeling of Bonded Bars Under Cyclic Loads." *Journal of Structural Engineering*, Vol. 117, no.1, pp. 48-60.

Stankowski T., and Gerstle K.H. (1985). "Simple Formulation of Concrete Behavior Under Multiaxial Load Histories." *ACI Journal*, Vol. 82, pp. 213-221.

Symposium on Bond and crack Formation in reinforced Concrete (1957). "The Foundation of Law of Bond." Stockholm, Tekniska Hogskolans, pp. 491- 499.

Tachibana D., Kumagai H., Yamazaki N., Suzuki T. (1994). "High Strength Concrete ($f' = 600\ Kg / Cm^2$) for Building Construction." *ACI Materials Journal*, Vol. 91, no. 4, pp. 390-400.

Tassios T.P., and Yannopoulos P.J. (1981). "Analytical Studies on Reinforced Concrete Members Under Cyclic Loading Based on Bond Stress-Slip Relationships." *ACI Journal*, Vol. 78, no. 2, pp. 236-246.

Tedesco J.W., Ross C., and Kuennen S. (1993). "Experimental and Numerical Analysis of High Strain Rate Splitting Tensile Tests." *ACI Materials Journal*, Vol. 90, no. 2, pp. 162-169.

Tianxi T., Shah S.P., and Chengsheng Ouyang (1992). "Fracture Mechanics and Size Effect of Concrete in Tension." *ASCE, Journal of Structural Engineering*, Vol. 118, no. 11, pp. 3169-3185.

Torii K., Mak S.L. and Ho D.W.S. (1994). "Influence of High Hydration Temperature at Early Age on the Strength Development of High Strength Concrete with and without Silica Fume." *Journal Society Material Science*, Japan, Vol. 43, no. 484, pp. 95-100.

Untrauer R.E., and Henry R.L. (1965). "Influence of Normal Pressure on Bond Strength. *Proceedings, ACI Journal*, Vol. 62, no. 5, pp. 577-585.

Valanis K., and Read H.E. (1984). "An End Ochronic Plasticity theory For Concrete." *S-Cube Topic Rep.*, La Jolla, California, USA, 93 p.

Vermeer P., and De Borst R. (1984). "Non-Associated Plasticity for Soils, Concrete and Rock." Heron, Vol. 29, no.3, 1984, 264p.

Willam K.J., Hurlbut B., and Sture S. (1986). "Experimental and Constitutive Aspects of Concrete Failure." *ASCE, Proceedings US-Japan Seminar on Finite Element analysis of Reinforced Concrete Structures*, Tokyo, Special publication, N.Y., USA, pp. 226-254.

Willam K.J., and Warnke E. (1975). "Constitutive Models for Triaxial Behavior of Concrete." *Proceedings, International Association for Bridge Structural Engineering*, Bergamo, Italy, Vol. 19, pp. 1-30.

Wu Z., Falahat M A., and Tanabe T.A. (1994). "Plastic-Fracture Stress Transfer Model for Concrete Discontinuities." *ACI Materials Journal*, Vol. 91, no. 5, pp. 502-508.

Xia Qiu, Plesha M.E., and Meyer D.W. (1991). "Stiffness Matrix Integration Rules for Contact Friction Finite elements." *Computer Method in Applied Mechanics*, Vol. 93, pp. 385-399.

Xie J., Elwi A., and MacGregor J. (1994). "Numerical Investigation of Eccentrically Loaded Tied High Strength Concrete Columns." *Structural Engineering Report no. 204*, Department of Civil Engineering, University of Alberta, Alberta, Canada, 190 p.

Yang, B.L., Dafalias Y.F., and Herrmann L.R. (1985). "A Bounding Surface Plasticity Model for Concrete." *ASCE, Journal Engineering Mechanics*, Vol 111, no. 3, pp. 359-380.

Yannopoulos P.J., and Tassios T.P. (1991). "Reinforced Concrete Axial Elements Analyzed Under Monotonic and Cyclic actions." *ACI Structural Journal*, Vol. 88, no. 1, pp. 3-11.

Yankelevsky D.Z. (1985). "Bond Action Between Concrete and a Deformed Bar-A New Model." *ACI Journal*, Vol. 82, no. 2, pp. 154-161.

Yerex II L., Wenzel T.H., and Davies R. (1985). "Bond Strength of Mild Steel in polypropylene Fiber Reinforced Concrete." *ACI Journal*, Vol. 82, no. 6, pp. 40-45.

Yogendran V., Langan B.W., Haque M.N., and Ward M.A. (1987). "Silica Fume in High Strength Concrete." *ACI Materials Journal*, Vol. 84, no. 2, pp. 124-129.

Zampini D., Jennings H.M., and Shah S.P. (1995). "The Interfacial Transition Zone and Its Influence on The Fracture Behavior of Concrete." *Mat. Res. Soc. Symp. Proc.*, Vol. 370, pp. 357-366.

Zhiming T., Hueizhong L., and Jinping Z. (1992). "A New Bond Model for Finite Element Analysis of RC Structures." *CEB. International Conference on Bond in Concrete*. Riga Technical university, pp. 12-9,12-16.